2018

Uncertainty Quantification for Naval Ships and the Optimal Adaptation of Bridges to Climate Change

Alysson Mondoro
Lehigh University

Uncertainty Quantification for Naval Ships and the Optimal Adaptation of Bridges to Climate Change

by

Alysson Mondoro

Presented to the Graduate and Research Committee
of Lehigh University
in Candidacy for the Degree of
Doctor of Philosophy
in
Structural Engineering

Lehigh University

January 2018

Approved and recommended for acceptance as a dissertation in partial fulfillment of the requirements for the degree of Doctor of Philosophy

_____

Defense Date

_____

Dr. Dan M. Frangopol
Dissertation Advisor
Professor of Civil and
Environmental Engineering
Lehigh University

_____

Approved Date

COMMITTEE MEMBERS:

_____

Dr. John L. Wilson
Committee Chairperson
Professor of Civil and
Environmental Engineering
Lehigh University

_____

Dr. Ben T. Yen
Committee Member
Emeritus Professor of Civil and
Environmental Engineering
Lehigh University

_____

Dr. Spencer Quiel
Committee Member
Assistant Professor of Civil and
Environmental Engineering
Lehigh University

_____

Dr. Mitsuyoshi Akiyama
External Committee Member
Professor of Civil and
Environmental Engineering
Waseda University

ACKNOWLEDGMENTS

"*IT TAKES A VILLAGE*" - *UNKNOWN*

Without the continued support of everyone in my life, I would not have been able to be the individual I am today.

I would like to express my gratitude to my advisor, Prof. Dan M. Frangopol. His support and guidance over the past 5 years has helped shape me into the researcher that I am. I would like to thank my academic advisor and committee chair, Dr. John L. Wilson, for his advice and guidance. I gratefully acknowledge Dr. Mitsuyoshi Akiyama for his sincere support while I was a visiting researcher in his lab and for his role as a committee member; his patience and wisdom while I was in Japan was invaluable. I would also like to thank Dr. Spencer Quiel and Dr. Ben Yen for their insightful comments and conversations regarding my work.

I gratefully acknowledge the support of grants from (a) the National Science Foundation (NSF) Award CMMI-1537926 and OISE-1613391, (b) the U.S. Federal Highway Administration (FHWA) Cooperative Agreement Award DTFH61-07-H-00040, (c) the U.S. Office of Naval Research (ONR) Awards N00014-08-1-0188, N00014-12-1-0023, and N00014-16-1-2299, and (d) the Commonwealth of Pennsylvania, Department of Community and Economic Development, through the Pennsylvania Infrastructure Technology Alliance (PITA) Awards. My research advisor, Prof. Frangopol, served as

the Principal Investigator in these grants and awards. I would also like to acknowledge the support provided to me by the National Science Foundation in the form of the East Asia Pacific Summer Institute (EAPSI) grant OISE-1613391. I would like to thank Lehigh University and the Civil and Environmental Engineering Department for the academic fellowships that supported me for 2 years of my Ph.D. studies. I would like to thank Lehigh's Office of International Affairs for the support of the Doctoral Travel Grant for Global Opportunities (DTG-GO) which allowed me to present a portion of my research at the 12th International Conference on Structural Safety and Reliability in Vienna, Austria.

I would like to recognize and thank the current and former CEE graduate students for (1) broadening my understanding of structural engineering through discussions and (2) dealing with me and my shenanigans. In particular, I would like to thank Dr. Mohamed Soliman, Dr. You Dong, Dr. Samantha Sabatino, and Mr. Liang Liu for their support and advice throughout my Ph.D. career. I would like to thank Frank Artmont, Vasileios Christou, Phillip Keller, Aman Karamlou, Matt Gombeda, and all of the other graduate students in ATLSS for the part they have played during my time at Lehigh. I would like to thank Dr. Akiyama's graduate students for their kindness while I was working at Waseda Univeristy; without them my time in Tokyo would not have been the same. I would also like to thank all of the post-docs, visiting graduate students, and visiting scholars that have brought a broader perspective and made this process more interesting. Also, I would like to thank Peter Bryan, the IT Manager of ATLSS, for providing

technological support and solutions for the times that my solution of “turn it off – then – turn it on again” didn’t work.

Finally and most importantly, I am grateful for the unconditional love and support of my family. I would like to thank my parents for instilling in me the discipline, dedication, and strength that has helped me in my studies and my life. I want to thank them for stressing balance in what I do - without it, I would have missed out on all of the experiences that I have had and the people that I’ve gotten to know. I want to thank my brothers, Chris, Matt, and Jeff, for being there for me my entire life and encouraging me to “be me”. And my sister-in-laws, Lauren and Julia, for their support and kindness. To the rest of my family - thank you for always asking ‘so what do you work on?’ and caring about what I do.

TABLE OF CONTENTS

LIST OF TABLES

LIST OF FIGURES

ABSTRACT

Repairing and adapting existing structures and infrastructure is essential for maintaining the functionality of a transportation network and the flow of people, goods, and ideas across a region. However, structures are vulnerable to extreme events, such as hurricanes and floods, and continuous deterioration, due to exposure to corrosive environments and cyclic loading. The occurrence of extreme events may be nonstationary over the service life of the structures, leading to uncertain future loading conditions on the structure. Continuous deterioration, due to corrosion or fatigue, changes the capacity of the structure to resist loads over time. Repair and adaptation measures may be applied to a structure in order to improve the capacity to resist loads. However, limited economic resources prohibit the immediate repair and adaptation of all structures, thus requiring a systematic methodology be established prioritizing actions. It is because of this need that the field of life-cycle management has emerged. The focus of the research in this dissertation is on enhancing this field and the ability of engineers to (1) quantify uncertainty in the life-cycle management problem, (2) assess the performance of structures and develop effective management strategies, and (3) integrate the uncertainties of climate changes and future loading conditions into the management of structures.

Uncertainty quantification typically involves describing the variability in the loads acting on a structure, the capacity of the structure, and the deterioration over time of the structure. In the design phase, uncertainty quantification is based on observing loads in

the area (traffic, wind, hydraulic loads, etc) and testing materials and connections to characterize their properties. In the operational phase, Structural Health Monitoring (SHM) data can be integrated into the uncertainty quantification process. This research specifically enhances the ability to integrate SHM data into the fatigue life prediction of ship structures and improve uncertainty quantification for naval ships.

Life-cycle management integrates the quantifiable uncertainties into the performance assessment of a structure. For civil structures, hydraulic hazards like hurricanes, floods, and tsunamis may cause extensive damage; and failure may have major economic, societal, and environmental consequences. This research focuses on enhancing the performance assessment methodologies for evaluating the risk associated with the failure of riverine and coastal bridges once the uncertainties are known. The considerations for the multiple failure modes, as well as the multiple hazards, included in this research are shown to be essential when determining the risk level of bridges. Furthermore, this work includes proposed methodologies for determining optimal management strategies that are driven by both performance and cost in order to aid decision makers.

The final thrust area of this research emanates from the uncertainties associated with anticipated climate changes. Natural and anthropogenic changes result in changes to sea level, the intensity of storms, and the intensity of precipitation which leave riverine and coastal bridges increasingly vulnerable. The uncertainties that govern the future variability in climate are currently reported as unquantifiable. This type of uncertainty is referred to as a deep uncertainty and stems from the multiple feasible projections for gas concentrations and the multiple available climate models with which to evaluate them.

This research introduces a systematic decision support framework for determining adaptation strategies in the presence of both the deep uncertainties of climate change and the quantifiable uncertainties of structural performance.

CHAPTER 1

INTRODUCTION

1.1. MOTIVATION

The constant deterioration of structures (due to corrosion and fatigue) and the potential for damage during extreme hydraulic events (such as hurricanes and flooding) leave civil and marine structures vulnerable to failure throughout their service life. In the United States, just over 53% of all bridges failures can be attributed to hydrologic events including flooding and hurricanes (Wardhana and Hadipriono 2003). The degradation of existing structures due to corrosion and fatigue contributes to just over 9% of failures Furthermore, fatigue damage is highlighted as a major concern for naval structures due to the cyclic loading applied to the structure and the ensuant potential for failure (Sielksi et al. 2013).

In order to maintain functionality in civil and marine structures, researchers have focused on developing methodologies to assess the reliability of structures, mitigate life-cycle risk, and identify economically feasible management strategies. All of these methodologies, however, are contingent on first being able to quantify the uncertainties associated with structural performance. This includes the natural variabilities in the environmental and human-induced loads on a structure, as well as in material properties and structural design. The use of SHM data aids uncertainty quantification since it contains information on the as-built characteristics of the structure and the operational loads the structure (Lynch and Loh 2006). However, further attention is needed to

address issues related to uncertain future loading conditions since the observed SHM data may not be able to adequately account for future changes.

When developing optimal management strategies, uncertainties are propagated through a time-variant performance assessment framework in order to estimate future risk profiles. Structural enhancements, such as maintenance and repair measures (i.e. painting of exposed steel, replacement of existing components, etc) and retrofit measures (i.e. the addition of components to a structure to enhance performance), may be applied to a structure in order to reduce life-cycle risk. While managers strive to mitigate risk, they must also accept the financial constraints of their budget. Research has thus be oriented towards supporting decisions in a systematic method that considers both the financial costs and the benefits of a management strategy (Thoft-Christensen 2009; Padgett et al. 2010; Liu and Frangopol 2006). Despite the extensive work on the development of optimal management strategies for bridges, key concepts such as the presence of multiple failure modes, continuous deterioration and extreme events, and post-disaster economic conditions have been omitted.

Furthermore, researchers have developed the life-cycle management frameworks around the assumption of a stationary climate; that future climate will exhibit the same statistical characteristics of the past and current climate. However, the Intergovernmental Panel on Climate Change (IPCC) has noted an unequivocal warming of the climate, changes in sea levels and extreme events have been observed, and future changes in sea level rise, the intensity of hurricanes, and the intensity of precipitation and flooding are predicted. There is no consensus on a single expected future: researchers have identified a

set of Representative Concentration Pathways (RCPs) that define potential scenarios for greenhouse gas trajectories (IPCC 2014), numerous Global Climate Models (GCMs), also denoted as General Circulation Models, exist and use the RCPs as inputs in order to estimate future scenarios. However, no probability can be assigned to an RCP (IPCC 2014), and there is no agreement (at this time) as to which GCM is most accurate (Flato et al. 2013). Therefore, there are uncertainties that cannot be quantified associated with the management of civil infrastructure; presenting a unique challenge to decision makers. The unquantifiable uncertainty in climate change is also referred as deep uncertainty (Hallegatte et al. 2012; Espinet et al. 2017). The field of managing structures under the deep uncertainties of climate change is in its beginning stages. It can be enhanced through the development of a systematic metric for assessing the efficiency of management strategies and the development of a framework with which to make decisions based on the set of future scenarios.

In this way, the field of life-cycle management is a continuously developing effort to integrate quantifiable and unquantifiable (deep) uncertainties into the management process for civil and marine structures. The research developed herein addresses the deficiencies highlighted above and represents advancements made in (1) the use of SHM data to quantify uncertainties in fatigue life predictions, (2) time-variant performance assessment and management methodologies for bridges vulnerable to extreme hydrologic events, and (3) decision support for climate change management considering uncertainties of potential climate changes. Overall, this research fills the gaps in existing methodologies and advances the field of life-cycle management with respect to both civil

and naval structures. The detailed objectives, research approach, and significant contributions are outlined in the following sections.

1.2. OBJECTIVES

The overall objective of this research is to enhance the field of life-cycle management of existing structures. Figure 1.1 summarizes the concepts essential to life-cycle management. Uncertainty quantification involves assessing the variability in loads and structural capacity. These uncertainties are used to estimate the current performance of structures by assessing the risk associated with failure. In structural engineering research, risk is typically defined as the multiplication of the probability of failure by the consequences of failure (Ellingwood and Kinali 2009; Stein et al. 1999). The time-variant, future performance (i.e. future risk) of the structure must then be predicted for the remaining service life. Optimal management strategies may then be developed by formulating and solving optimization problems that consider both the performance requirements and existing economic constraints. Due to the climatological origin of hurricanes and flooding and the evolution of the climate change hazard, future performance prediction and the development of optimal management strategies must also consider the deep uncertainties of future loading conditions.

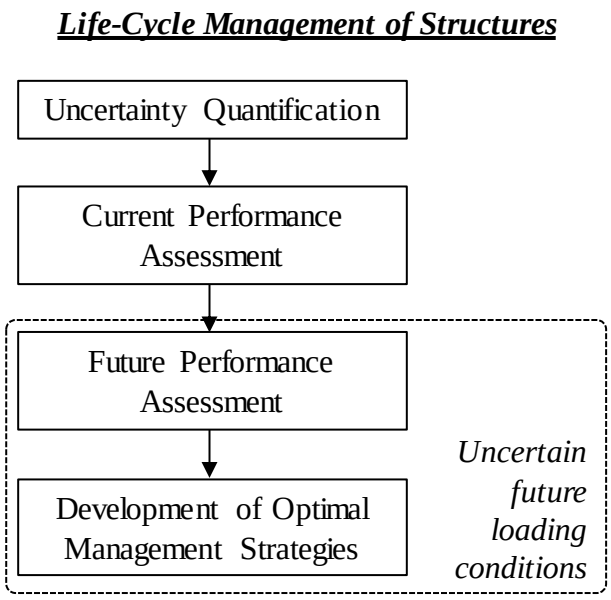

Figure 1.1. Conceptual overview of life-cycle management of civil and naval structures.

This research aims at enhancing the field of life-cycle management of both civil and naval structures. The detailed objectives of the study presented in each chapter are summarized as follows:

Chapter 2. This chapter has the following objectives:

- Address deficiencies in the fatigue life assessment of naval structures that stem from missing SHM data sets and the potential for uncertain future loading conditions.
- Provide a methodology for incorporating observed SHM data into fatigue damage estimates that accounts for both the low and high frequency content of the structural response (since both contribute to fatigue damage).

Chapter 3. This chapter has the following objectives:

- To provide a systematic methodology for determining the optimal management strategies for bridges vulnerable to extreme hydraulic loading based on the benefits and costs; particular emphasis is placed on flooding events.
- Identify site-specific variations for flooding vulnerability and investigate the impact on optimal management strategies.

Chapter 4. This chapter has the following objectives:

- Develop a framework for managing coastal bridges vulnerable to corrosion and coastal storms in order to minimize life-cycle costs and minimize maximum life-cycle risk.
- Investigate the importance of post-disaster economic conditions on the optimal repair and retrofit of coastal bridges.

Chapter 5. This chapter has the following objectives:

- Elucidate the pertinent components of the climate change hazard that impact the performance of bridges and discuss potential adaptation (i.e. management) strategies.
- Identify difficulties associated with managing infrastructure under the uncertainties of climate change. Review current methods employed by researchers and practitioners that try to address these challenges.

Chapter 6. This chapter has the following objectives:

- Develop metrics that address the decision makers desire to delay adaptation until better information is available regarding future scenarios. This desire stems from the deep uncertainties inherent in future climate changes.

- Propose frameworks for identifying optimal management strategies under the deep uncertainties of climate change.

1.3. SUMMARY OF RESEARCH APPROACH

In order to address the research objectives detailed in the previous section and enhance the field of life-cycle management, three specific thrust areas are considered in this research: (1) uncertainty quantification, (2) performance assessment and management, and (3) managing structures under deep uncertainty. Uncertainty quantification is discussed in the context of naval structures, while the other two thrust areas focus on bridges.

Uncertainty quantification: SHM data provides information regarding the response of the structure to the actual loading conditions and the as-built condition of the structure (Lynch and Loh 2006). This can provide vital information to fleet managers that are trying to determine if ships can operate for longer periods of time or if they need to be repaired or taken out of service. This research focuses on cell-based methods for life-cycle performance assessment of ships (Sikora et al. 2002; Hughes 1983). Cell-based methods require the SHM data for a naval vessel to be discretized based on the operational conditions defined with ship speed, heading angle, and wave height. When the operational conditions are constant (i.e. a constant ship speed, heading angle, and wave height) the response of the structure is a stationary ergodic random process (Hughes 1983); the term "cell" is used to describe a constant operational condition. Throughout the operating period of a ship, not all cells are observed; but the response in all cells is

essential for the fatigue life estimation of the ship. The research detailed in Chapter 2 evaluates SHM data for observed cells, quantifies the response, develops a theoretically-based relationship between the response in observed cells and that of unobserved cells, and provides a method for estimating fatigue life based on available SHM data.

Performance assessment and management: The risk associated with a structure considers both the probability of structural failure and its consequences (Ellingwood and Kinali 2009; Stein et al. 1999). Managers strive to maintain as low of a risk level as possible but are by constrained by their budget. The work developed in Chapters 3 and 4 enhance the decision-support tools available to managers that must maintain bridges vulnerable to extreme hydraulic events. In Chapter 3, the focus is on riverine bridges: the multiple failures modes of a bridge due to extreme hydraulic events are integrated into a risk assessment framework and benefit-cost analysis is included as the tool to evaluate the effectiveness of a management strategy. Chapter 4 focuses on the vulnerability of coastal bridges to corrosion damage and failure during hurricanes. An approach for assessing the time-variant risk levels of a coastal bridge is presented, and an optimization framework is established to develop optimal management strategies that minimize costs and minimize maximum life-cycle risk. This work contributes to advancements in the field of life-cycle management considering quantifiable uncertainties.

Managing under deep uncertainty: The deep uncertainties of climate change present a unique problem to bridge managers: there are multiple future scenarios that are possible, but no probability can be objectively assigned to them (IPCC 2014; Flato et al. 2013). When it comes to financial planning, infrastructure management, and other

decisions, decision makers strive to enact the most profitable strategies. But, when they cannot quantify what is possible (i.e. there is deep uncertainty in future scenarios) there is also a desire for flexible options. For bridge management, this means that the decision-makers value delaying adaptation (i.e. the application of repairs or retrofits) until they have a better understanding of which future climate scenario will be realized. The work presented in Chapters 5 and 6 first identify the challenges of managing under the uncertainty of climate change. Then, two metrics are proposed in order to systematically quantify the human desire for flexibility in climate change adaptation strategies. Optimization frameworks are then built around these metrics in order to provide decisions makers with guidance on how to aggregate information across all potential scenarios.

1.4. CONTRIBUTIONS

This study further enhances the life-cycle management of civil and naval structures through concentrated efforts to improve uncertainty quantification methods, performance assessment and management methodologies for bridges vulnerable to extreme hydrologic events, and the management of structures under the deep uncertainty of climate change. A summary of the original contributions is as follows.

In regards to naval vessels: Advancements are made to the field of life-cycle management of naval structures by developing a unique methodology for processing observed SHM data in a manner that can then enable the prediction of unobserved responses. Since it is necessary to have SHM data for all potential operating conditions when estimating fatigue damage, the response in unobserved operating conditions must

be estimated, as shown in the flow chart in Figure 1.2. The gray boxes in Figure 1.2 highlight the significant contributions of this work and are further detailed below.

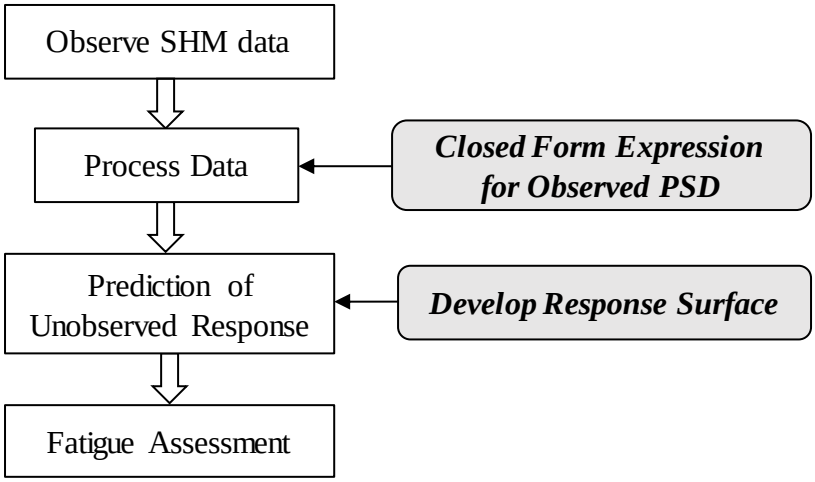

Figure 1.2. Conceptual overview of the contributions to the life-cycle assessment of naval structures through the development of (a) closed form expressions to quantify the observed SHM data and (b) a theoretically based response surface.

- Enhance fatigue damage estimates for in-service ships by developing a methodology for integrating SHM data into lifecycle analysis through the quantification of the low and high frequency content of an observed structural response under known operational conditions.
- Establish a theoretically-based, non-linear prediction surface that can be used to estimate unobserved structural responses based on observed SHM data. The resulting, complete set, includes that available observed SHM data and the predicted response in unobserved cells, fully characterizes the response of a ship under all operating conditions and enables damage prediction under uncertain future loading conditions.

In regards to the management of civil bridges: Changing climate conditions associated with natural and anthropogenic changes present a unique challenge to bridge managers as indicated in Figure 1.3. The multiple future climate scenarios lead to a set of different payoffs for a single adaptation strategy. In order to develop support decision support methodologies for climate change adaptation, this work first makes enhancements to the risk assessment stage (highlighted in light gray in Figure 1.3) and the on the robust optimization methodologies that can address the fact that a strategy has different payoffs based on which future scenario is realized (i.e. the set highlighted in dark gray in Figure 1.3).

A detailed summary of the significant contributions of this work on the management of bridges are further detailed below.

- Develop a framework integrating the predominant failures modes of bridges vulnerable to extreme hydraulic pressures and scour including foundation, pier, and deck failure. An illustrative example demonstrates that there may be adverse effects of retrofitting a structure: while all retrofits may reduce the probability of failure, risk may not be reduced (and may be increased) due to differences in the consequences of failure associated with different failure modes.
- Identify the dependencies of optimal management strategies on the site-specific variations in the hazard. In some instances, it is shown to be optimal to aggressively repair/retrofit a structure, while in others, it may be economically justifiable to do nothing.

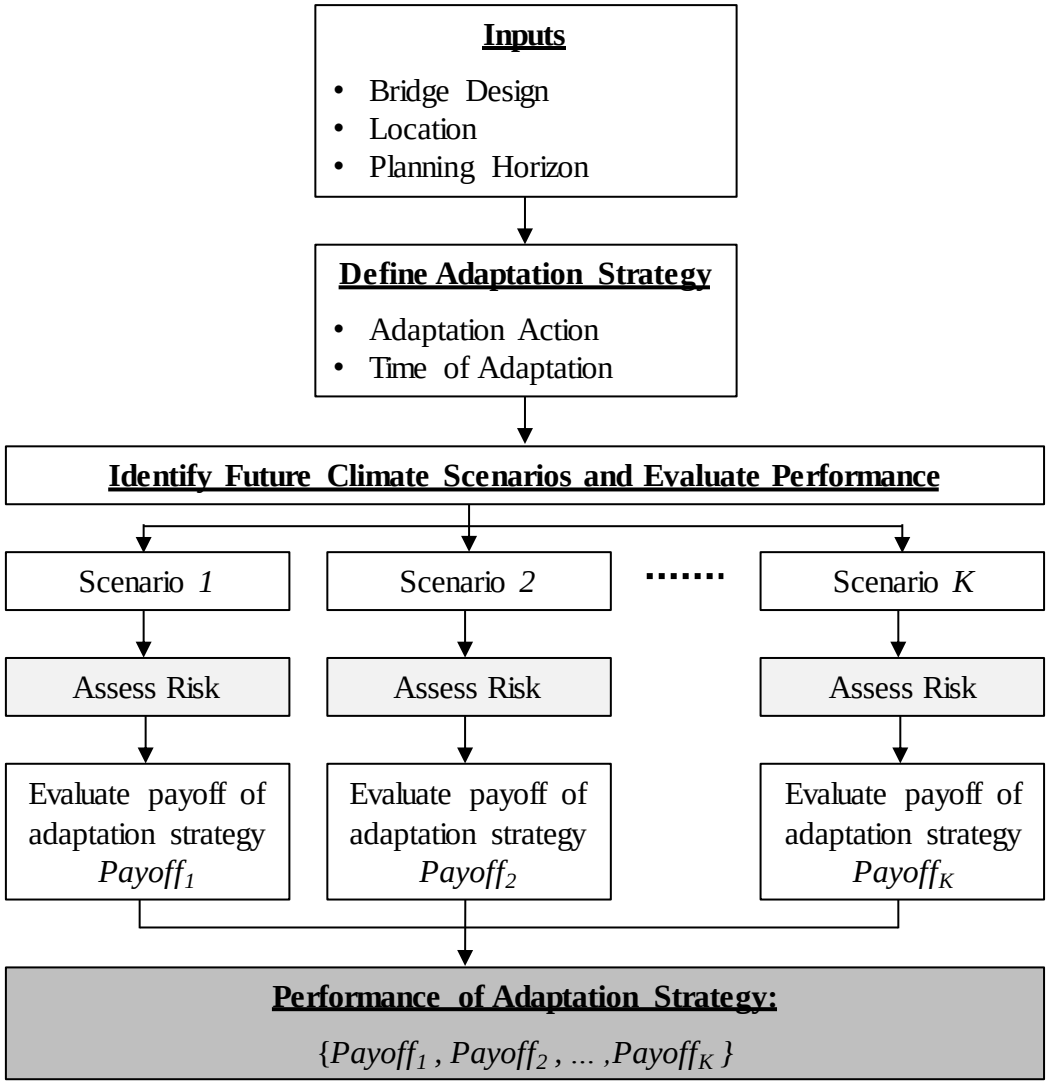

Figure 1.3. Conceptual overview of the evaluation of adaptation strategies under the deep uncertainties of climate change. Contributions of this work lie in the development of risk assessment frameworks (highlighted in light gray) and integration of robust optimization models to account for the multiple payoffs associated with a single adaptation strategy (shown in dark gray).

- Develop an optimization approach that considers the deteriorating effects of corrosion on structural components and the vulnerability of bridges to damage due to coastal storms is developed. It is demonstrated that low-cost high-risk solutions may be drastically improved through minimal investments.
- Address post-disaster economic conditions, which vary significantly from typical economic conditions, in the proposed optimization framework. Since there is an increase in the cost of labor and construction materials after a major hurricane (or other major disaster), optimal strategies tend to include the retrofit options that limit the damage to structures during a hurricane.
- Develop the Gain-Loss Ratio and Regret metrics to aid in decision making process for climate change adaptation.
    - The Gain-Loss Ratio is a metric that systematically quantifies the practicality associated with the desire to delay adaptation until better information regarding the future climate is available.
    - Regret with respect to the Benefit-Cost Ratio is developed as a metric as a means to quantify the desire to not choose a suboptimal solution when planning for multiple future scenarios with no known probability of occurrence.
- Develop single objective and bi-objective stochastic and robust optimization formulations to identify optimal adaptation (i.e. management) strategies. These models aid in decision making under deep uncertainty by providing a systematic method to aggregate the performance of a strategy across the feasible future

scenarios. The bi-objective models include the proposed metrics (GLR and Regret) and existing metrics (the Benefit-Cost Ratio).

- Identify the dependencies of optimal management strategies on the site-specific variations in the climate change hazard. In regions where the climate change scenarios include an overall intensification of the hazard, the desire for flexibility is outweighed by the need to adapt in order to prevent significant losses. However, in regions where there the climate change scenarios include an overall decrease in the intensity of the hazard, the desire for flexibility can lead to optimal adaptation strategies that delay adaptation until additional information is available.

The specific conclusions associated with the contributions are detailed in their subsequent chapters and summarized in the Chapter 7.

1.5. OUTLINE

This dissertation consists of 7 Chapters and is organized as follows:

Chapter 1 presents the motivation, objectives, research approach, and contributions of this work.

Chapter 2 develops a methodology for integrating SHM data into the fatigue life predictions for naval ships that addresses deficiencies stemming from missing data and changes in future operational conditions.

Chapter 3 provides a detailed framework for assessing the risk for bridges vulnerable to extreme hydrologic events and highlights the need to consider all relevant failure

modes when determining optimal management strategies; emphasis is placed on riverine bridges vulnerable to floods.

Chapter 4 addresses the vulnerability of coastal bridges to extreme damage from hurricanes and continuous damage from corrosive marine environments. This work highlights the importance of considering post-disaster economic conditions when assessing risk and determining optimal management strategies.

Chapter 5 reviews the impact of climate change on the vulnerability of civil infrastructure, the potential damage to bridges due to climate change, adaptation options, and the challenges of integrating uncertainty in climate change into the decision-making process.

Chapter 6 develops a framework for managing structures vulnerable to changes in climate by developing metrics to quantify the performance of adaptation strategies and identifying optimization models to support decisions considering multiple future scenarios.

Chapter 7 summarizes the research in this dissertation, provides relevant conclusions, and recommends future research.

CHAPTER 2

USE OF STRUCTURAL HEALTH MONITORING (SHM) DATA TO ESTIMATE SHIP PERFORMANCE

2.1. OVERVIEW

The integration of Structural Health Monitoring (SHM) data is essential for quantifying uncertainties, assessing current performance, and estimating the anticipated fatigue damage for naval ships. It is useful for reducing the epistemic uncertainties arising from inaccuracies in the modeling, including the variations of the as-built structure from the initial design, as well as providing a more appropriate quantification of load. With SHM data, fatigue damage may be predicted through the use of cell-based approaches, such as the lifetime weighted sea method. This method relies on the discretization the operational profile of a ship into cells based on wave height, heading angle, and speed of the ship. The integration of SHM data into the lifetime weighted sea method requires a full set of data that covers the whole operational spectrum. However, technical malfunctions or discrete monitoring practices generate incomplete data sets. Accordingly, there is a need for an approach to predict structural responses in unobserved cells based on limited available monitoring data. The research included in this chapter proposes a methodology to quantify the observed SHM data with a generalized form that captures both the low and high frequency content of the responses. Secondly, it develops a nonlinear prediction surfaces to estimate SHM data in unobserved cells. Expected theoretical variations of the structural response to changes in wave height, heading angle, and ship speed are

accounted for in the development of the non-linear prediction surfaces. The methodology directly enables both spectral and time-domain estimates for fatigue damage. The proposed methodology is illustrated with SHM data from a high speed aluminum catamaran.

2.2. INTRODUCTION

Structural health monitoring (SHM) has recently been integrated into the life-cycle performance assessment program of the U.S. Navy (Sielski 2012) in an effort to monitor the performance of high-speed, high-performance naval vessels. In both civil and naval structures, SHM data is useful for the detection and diagnosis of damage at various locations throughout the structure (Herszberg et al. 2005; Okasha et al. 2011; Reed and Earls 2015; Vanik et al. 2000). Additionally, SHM data can provide information regarding the initial as-built condition of the structure, the actual loads acting on the structure, and, if damage occurs, the current state of the structure. Currently, research efforts have been made to incorporate SHM data into service life predictions of naval ships; with particular emphasis on fatigue life (Soliman et al. 2015; Nichols et al. 2014).

Fatigue damage in aluminum naval vessels is a major concern. This is due to the high propagation rate of cracks in aluminum details and the considerable cost and effort associated with the repair process of damaged hulls. Deficiencies in design stage fatigue damage predictions are addressed, in part, through the use of SHM data. SHM directly contains considerations on the operational loads the ship is subjected to, as well as the as-built design of the ship (Lynch and Loh 2006); thus, aleatoric uncertainties can be further quantified, and epistemic uncertainties associated with load effects can be significantly

reduced. Performance updating (e.g., using the Bayesian approach) has also been employed to integrate SHM data into structural predictions of ship performance parameters, such as vertical bending moments and fatigue life estimates, to account for the stochastic nature of the loads and structural materials (Okasha et al. 2010; Ling et al. 2011; Zárate et al. 2012). The use of observed SHM data in future service life predictions and management strategies dictates the assumption that future loading conditions are similar to past ones (Soliman et al. 2015). This leads to a distinct issue when the operational profile changes. The recent increase in the operational rate and required service life of the vessels operated by the U.S. Navy exemplifies one of these potential changes. Additionally, global climate change may increase the occurrence rate of intense storms (IPCC 2014) and, consequently, exemplifies another potential change in the operational profile. As a result, vessels operated in these future conditions can experience a larger number of annual cycles and may be exposed to rougher and more extreme seas. Thus, the assumption of past data being indicative of future loads and loading sequences is not always valid.

In order to assess the impact of future loading on the fatigue damage state of a vessel, the lifetime weighted sea method may be used (Hughes 1983; Sikora et al. 2002). This method is developed around the assumption that the operational profile of a ship can be discretized into cells, where the response in each cell is stationary (Hughes 1983). A cell is defined by its operational conditions including wave height, ship speed, and heading angle. The lifetime load effect may then computed as the summation of the load effect within each cell, weighted by the probability of operating in that cell (governed by

the travel routes of the ship and the sea conditions of the basin) (Hughes 1983; Kahma et al 2003). Available SHM data may provide information regarding the performance of the structure in some cells, but may not cover all operational conditions necessary to compute the future fatigue damage. This can be attributed to (1) discrete monitoring practices, while useful in limiting financial costs (Kim and Frangopol 2010), can lead to some operational states (i.e., cells) not being recorded, (2) technical malfunctions can result in missing or unreliable data (Iphar et al. 2015), and/or (3) the fact that future operational conditions may not be similar to past ones (ships may be relocated due to the evolving needs of the navy).

In order to address the deficiencies in structural performance assessment that stems from missing data, data prediction techniques for ship response have been developed around cell parameters (i.e., heading angle, ship speed, and sea wave height) and the response parameter of interest (e.g., fatigue damage accumulation). Zhu (2014) proposed a linear interpolation method for identifying the statistical descriptors of vertical bending moments with respect to synthetic data generated using the Large Amplitude Motion Program. The linear surface is useful due to its simplicity of form and ease of implementation. Furthermore, it requires only a minimal amount of parameters to be estimated, thus limiting the variations that arise based on the availability of training data. However, the linear surfaces lack a theoretical foundation.

This chapter presents a methodology for using the SHM data recorded in observed operational cells to estimate the response in unobserved cells. The approach has two objectives: (1) to integrate SHM data from sea keeping trials in order to quantify and

reduce uncertainties in the prediction of fatigue damage and (2) to propose a nonlinear surface for use in predicting unobserved data. In order to address the first objective, a methodology is proposed to capture the low and high frequency content in observed SHM. Fitting functions for the power spectral density (PSD) function of observed SHM are proposed for both the low frequency and high frequency content of the signal based on accepted forms for sea wave spectra. This research investigates the applicability of the proposed functions to the SHM data. For the second objective, a prediction surface is developed around the theoretical relationship between operating conditions and the structural response given as a function of the vertical bending moment. The prediction surface is then used to estimate unobserved SHM data. The proposed methodology is applied to the SHM data from the seakeeping trials of the HSV-2 Swift, a 98 m (322 ft), high-speed, aluminum catamaran and is evaluated for robustness with respect to available training data.

2.3. QUANTIFICATION OF SHIP RESPONSE

A naval vessel is exposed to various loading conditions throughout its lifetime based on its operational theatre and routes. As a result, the time-history response of the ship is a nonstationary random process for which the life-cycle performance is difficult to assess. The nonstationary time-history can be divided into smaller, stationary processes based on operating conditions such as wave height, vessel speed, and heading angle. For a given operational profile, the lifetime sustained loads and load effects can then be built up with additional information on the wave scatter diagram (Sikora et al. 1983). The lifetime

weighted sea method uses the response in each of the stationary cells to evaluate the long term performance (Hughes 1983).

Structural performance assessment can be performed in either the time domain or the frequency domain. For frequency-based methods, the structural time-history response is analyzed in the frequency domain and represented with a response spectrum. The response spectrum is a function of both the loading conditions (i.e., the random sea waves) and the structural response. Linear waves are considered and the loading conditions are defined by the sea wave spectrum, $S_{\xi}(\omega)$, which accounts for the development state of the wave, sea floor topology, fetch limitations, and local currents and swells, among others (Komen et al. 1984). The response spectrum, $S_R(\omega)$, is found through the use of a transfer function applied to the loading spectrum. In the case of the structural response of naval vessels to linear waves, the response amplitude operator $R_A(\omega)$ is used as the linear transfer function, and is different for each cell (Naess and Moan 2012). Accordingly, the response spectrum, $S_R(\omega)$, is expressed as

$$S_R(\omega) = [R_A(\omega)]^2 S_{\xi}(\omega) \tag{2.1}$$

Characterizing the sea surface and wave heights is a highly investigated field with multiple analytical and experimentally developed forms capable of representing the sea wave spectrum $S_{\xi}(\omega)$. Two commonly used spectra, Pierson-Moskowitz and Joint North Sea Wave Observation Project (JONSWAP), are considered. The Pierson-Moskowitz wave spectrum is for fully developed seas wherein the waves have come to equilibrium

with the wind (Pierson Jr. and Moskowitz 1963). The single sided Pierson-Moskowitz spectrum is

$$S_{PM}^{+}(\omega)=\frac{\alpha g^{2}}{\omega^{5}}\exp\left(-\frac{5}{4}\left(\frac{\omega}{\Omega}\right)^{-4}\right) \tag{2.2}$$

where α is 8.10×10^{-3}, g is the gravitational constant (9.81 m/s^2), and Ω is the wave frequency. However, this spectrum fails to fully capture the peak responses for waves that are not fully developed or are fetch limited. The JONSWAP investigated the sea surface in the North Sea, were the waves were either partially formed or experienced wave-wave interactions (Hasselmann et al. 1973). The resulting JONSWAP spectrum modifies the Pierson-Moskowitz spectrum with a peak enhancement factor, γ

$$S_{JONSWAP}^{+}(\omega)=\frac{\alpha g^{2}}{\omega^{5}}\exp\left(-\frac{5}{4}\left(\frac{\omega}{\Omega}\right)^{-4}\right)\gamma^{\exp\left(-\frac{(\omega-\Omega)^{2}}{2\Omega^{2}\sigma^{2}}\right)} \tag{2.3}$$

where

$$\sigma=\begin{cases}0.7 & if\ w\le\Omega\\ 0.9 & if\ w>\Omega\end{cases} \tag{2.4}$$

The response amplitude operator, $R_A(\omega)$, is developed on a cell-by-cell basis as the response of the ship is dependent on the heading angle, sea state, and vessel speed. $R_A(\omega)$ is the structural response (i.e., stress, strain, or accelerations at a given point in the structure) to a unit sinusoid at each frequency. Typically, linear structural analysis methods are employed to determine the stresses, used in fatigue life estimation, due to vertical bending induced by waves. Linear strip theory can be used to quantify vertical bending moment for head seas condition at zero speed, which can be modified for

different heading angles and speeds to generate other $R_A(\omega)$ functions (Sikora 1998). However, in some cells, nonlinear structural analysis may be required either due to the presence of combined wave and slam response (Sikora et al. 2002) or material and geometric nonlinearities. Through the application of nonlinear quadratic strip theory, Jensen and Dogliani (1996) demonstrated that the nonlinear contributions are at least as important as the linear contributions. Commercial analysis tools are available for the bending response to waves but are not readily available to analyze whipping response (Tuitman 2010).

Fatigue life is shown to be dependent on both the low frequency response due to waves and the high frequency response due to slamming. In this way, the lack of commercially available tools represents a limitation in the application of lifetime weighted sea method for fatigue life estimation. This research proposes the use of a fitting function for the spectral response determined from SHM data. The fitting functions are formulated around the sea wave spectrum and quantified for each observed cell of the SHM in order to predict the spectral response to unobserved cells.

Generalized variations of the Pierson-Moskowitz spectrum and the JONSWAP spectrum are proposed in Equations 2.5 and 2.6, respectively, as potential fitting functions for the observed PSD functions of the monitored structural detail

$$S^{+}_{PM_{gen}}(\omega) = \frac{A}{\omega^5} e^{-B\omega^{-4}} \tag{2.5}$$

$$S^{+}_{JONSWAP_{gen}}(\omega) = \frac{C}{\omega^5} \exp\left(-\frac{5}{4} D^4 \omega^{-4}\right) E^{\exp\left(-\frac{(\omega-D)^2}{2D^2\sigma^2}\right)} \tag{2.6}$$

where *A* and *B* are fitting coefficients for the generalized Pierson-Moskowitz function and *C*, *D*, and *E* are fitting coefficients for the generalized JONSWAP function. The SHM data include the low and high frequency content of the structural response that are essential to fatigue life predictions. Thus, the proposed fitting functions are expanded to consider the low frequency and high frequency response components. The complete fitting functions for the observed single-sided PSD functions of the monitored structural detail take the form

$$S^{+}_{PM_{GEN}}(\omega) = \frac{A_{LF}}{\omega^5} e^{-B_{LF}\omega^{-4}} + \frac{A_{HF}}{\omega^5} e^{-B_{HF}\omega^{-4}} \tag{2.7}$$

$$S^{+}_{JONSWAP_{GEN}}(\omega) = \frac{C_{LF}}{\omega^5}\exp\left(-\frac{5}{4}{D_{LF}}^4\omega^{-4}\right){E_{LF}}^{\exp\left(-\frac{(\omega-D_{LF})^2}{2{D_{LF}}^2\sigma^2}\right)} + \frac{C_{HF}}{\omega^5}\exp\left(-\frac{5}{4}{D_{HF}}^4\omega^{-4}\right){E_{HF}}^{\exp\left(-\frac{(\omega-D_{HF})^2}{2{D_{HF}}^2\sigma^2}\right)} \tag{2.8}$$

where A_{LF} and B_{LF} are fitting coefficients for the low frequency content and A_{HF} and B_{HF} are fitting coefficients for the high frequency content of the complete generalized Pierson-Moskowitz function, $S^{+}_{PM_{GEN}}$; and C_{LF}, D_{LF}, and E_{LF} are the fitting coefficients for the low frequency content and C_{HF}, D_{HF}, and E_{HF} are fitting coefficients for the high frequency content of the complete generalized JONSWAP function, $S^{+}_{JONSWAP_{GEN}}$.

2.4. DEVELOPMENT OF THEORETICAL PREDICTION SURFACE

Missing data is a significant problem in SHM. Instrument failure, power interruptions, and erroneous measurements create gaps in recorded data (Posenato et al. 2010). Additionally, discrete monitoring practices inherently omit samples of data. The

application of data mining techniques, such as neural networks, have been applied to missing data problems in SHM (Chang et al. 2003). Neural networks map given input parameters to response characteristics based on training information (Liu and Nayak 2012). Since the performance and accuracy of neural networks lies within the range of the training data, it is not widely applicable as an extrapolation method (Lohninger 1999). Linear prediction surfaces have been employed in Zhu (2014) and Mondoro et al. (2016) to relate structural response to wave height, ship speed, and heading angle. The linear prediction surface, Ψ^{lin}, is defined as

$$\Psi^{lin} = p_1 H_s + p_2 V + p_3 \cos(\beta) \tag{2.9}$$

where H_s is the wave height, V is the ship speed, and β is the heading angle. The linear surface is useful for the ease of implementation. Additionally, it requires only a minimal amount of prediction model parameters to be estimated which limits the variations that arise based on availability of data. However, the linear surfaces lack a theoretical foundation. The following subsections present the development of the theoretically-based nonlinear prediction surfaces. The discussion is framed around the HSV-2 Swift but is readily applicable to other naval vessels.

2.4.1. Operational conditions and theoretical response

The theoretical relationship between the operational condition (i.e., wave height, ship speed, and heading angle) and ship response (i.e., vertical bending moment) is developed by investigating the response spectrum. For naval vessels, response spectrum can be decomposed into the wave spectrum and a transfer function which quantifies the

structural response to a unit sinusoid at each frequency. The response spectrum for vertical bending moment S_{VBM} is defined as

$$S_{VBM}(\omega) = [\Phi_m]^2 S_\xi(\omega) \tag{2.10}$$

where Φ_m is the transfer function for vertical bending moment and S_ξ is the wave spectrum. There are many available forms for the wave spectrum. This formulation uses the Pierson-Moskowitz wave spectrum in Eq.2.2. It is assumed that the general relationship between the wave frequency and wave height is $\Omega = 0.14g/U_{19.5}$ and $U_{19.5} = (H_s/0.021)^{0.5}$ (Pierson Jr and Moskowitz 1963; Komen et al. 1984)

The transfer function for the vertical bending moment is derived using linear strip theory for a box shaped vessel (Jensen and Mansour 2002)

$$\Phi_m = \kappa \frac{1-kT}{(k_e L)^2}\left[1-\cos\left(\frac{k_e L}{2}\right)-\frac{k_e L}{4}\sin\left(\frac{k_e L}{2}\right)\right] F_v F_c \sqrt[3]{|k\cos\beta|} \tag{2.11}$$

$$F_v = 1+3F_n{}^2 \tag{2.12}$$

$$F_c = (1-\vartheta)^2 + 0.6\left(1-F_n\sqrt{kL}\cos\beta\right)(2-\vartheta) \tag{2.13}$$

$$F_n = \frac{V}{\sqrt{g_o L}} \tag{2.14}$$

$$k_e = |k\cos\beta| \tag{2.15}$$

$$\kappa = \exp(-k_e T) \tag{2.16}$$

where k is the wave number, which for deep water waves, $k \approx \omega^2/g$, T is draught of the ship, L is length of the ship, g_o is a general characteristic of the external field, and ϑ is a function of the block coefficient C_b (Jensen et al. 2004).

The response spectrum for vertical bending moment is thus related to the significant wave height H_s through the wave spectrum, and, to β and V through the theoretical transfer function for vertical bending moment. By estimating the most probable extreme value for the response as (Hughes 1983)

$$Q_p = \sqrt{2m_0 \ln\left(\frac{1800T}{\pi}\sqrt{\frac{m_2}{m_0}}\right)} \tag{2.17}$$

m_0 and m_2 are the 0th and 2nd spectral moments, where the n^{th} spectral moment, m_n, of the PSD function is

$$m_n = \int_0^\infty \omega^n S_R^{+}(\omega) d\omega \tag{2.18}$$

where S_R^{+} is the single sided response spectrum.

The most probable vertical bending moment, M_p, can be related to H_s, V, and β. Figure 2.1 illustrates the procedure for developing the relationship between ship speed and the most probable vertical bending moment for the HSV-2 Swift using information from Brady et al. (2004). The ship speed is varied and Φ_m^2 is calculated based on Eq. 2.11 (Figure 2.1a). It is important to note that H_s, V, and β are assumed to be uncoupled in regards to M_p. Therefore, only a single parameter of {H_s, V, and β} is varied at a time. Figure 2.1b shows the wave spectrum. Since S_{PM} is not a function of V, all lines depicting the variation of S_{PM} with V lie on top of each other. The response spectrum S_{VBM} is generated for each value of V using Equation 2.10 and is shown in Figure 2.1c. S_{VBM} is then used in Eqs.2.17 and 2.18 to find the most probable vertical bending moment. The variation of M_p and V is depicted in Figure 2.1d. the vertical bending moment at each ship

speed is compared to the vertical bending moment at ship speed of 5 knots, M_{p5}. The same procedure is applied for H_s and β but figures are omitted for brevity.

2.4.2. Development of Functional Forms

A closed-form function to describe theoretical relationship between the operational condition (i.e., H_s, V, and β) and the response (i.e., M_p) is not readily available. As noted in Section 2.4.1, H_s, V, and β are assumed to be uncoupled in regards to M_p; therefore, M_p (H_s, V, β) can be decoupled into M_p (H_s), M_p (V), and M_p (β). The theoretical variations of bending moment with wave height, ship speed, and cosine of the heading angle are shown in Figure 2.2 a, b, and c respectively. Four functional forms were developed for M_p (H_s), M_p (V), and M_p (β) and are listed in Table 2.1. Polynomial functions were used to describe M_p (H_s) and M_p (V), while a two-term sinusoid, a summation of cosines and linear term, and a 4th and 6th order polynomials (similar to the 4th and 6th order Taylor series expansion for cosine) were used for M_p (β). The goodness of fit is evaluated in terms of the root mean square error (RMSE) for each of the function for M_p (H_s), M_p (V), and M_p (β) and listed in Table 2.1. In Figure 2.2 b the functions B_2, B_3, and B_4 lie on top of each other and fit the data points with a RMSE of less than 1.0E-4.

Based on the performance of the proposed functions for $M_P(H_s)$, $M_p(V)$, and $M_P(\beta)$, as presented in Table 2.1, two nonlinear prediction surfaces are proposed. The first includes 2nd order polynomial functions for $M_P(H_s)$ and $M_p(V)$ (i.e. A_2 and B_2) and the summation of cosines and linear term for $M_P(\beta)$ (i.e. C_2). These functions were chosen in order to minimize the number of coefficients, p_i, while also having a low RMSE. The first nonlinear prediction surface takes the form

$$\Psi^{nonlin} = p_1 H_s{}^2 + p_2 H_s + p_3 + p_4 V^2 + p_5 V + p_6 \cos(\cos(\beta)) - p_7 \cos(p_8 \cos(\beta)) + p_9 \cos(\beta) \quad (2.19)$$

The second proposed nonlinear prediction surface restricts itself to the use of polynomial functions for H_s, V, and $\cos(\beta)$. The 2nd order polynomial functions A_2 and B_2 are used as the contributions for $M_p(H_s)$ and $M_p(V)$, respectively, and the 4th order polynomial (i.e. C_3) is used to account for $M_p(\beta)$. The polynomial based nonlinear prediction surface takes the form

$$\Psi^{nonlin-poly} = p_1 H_s{}^2 + p_2 H_s + p_3 + p_4 V^2 + p_5 V + p_6 \cos(\beta)^4 + p_7 \cos(\beta)^3 + p_8 \cos(\beta)^2 + p_9 \cos(\beta) \quad (2.20)$$

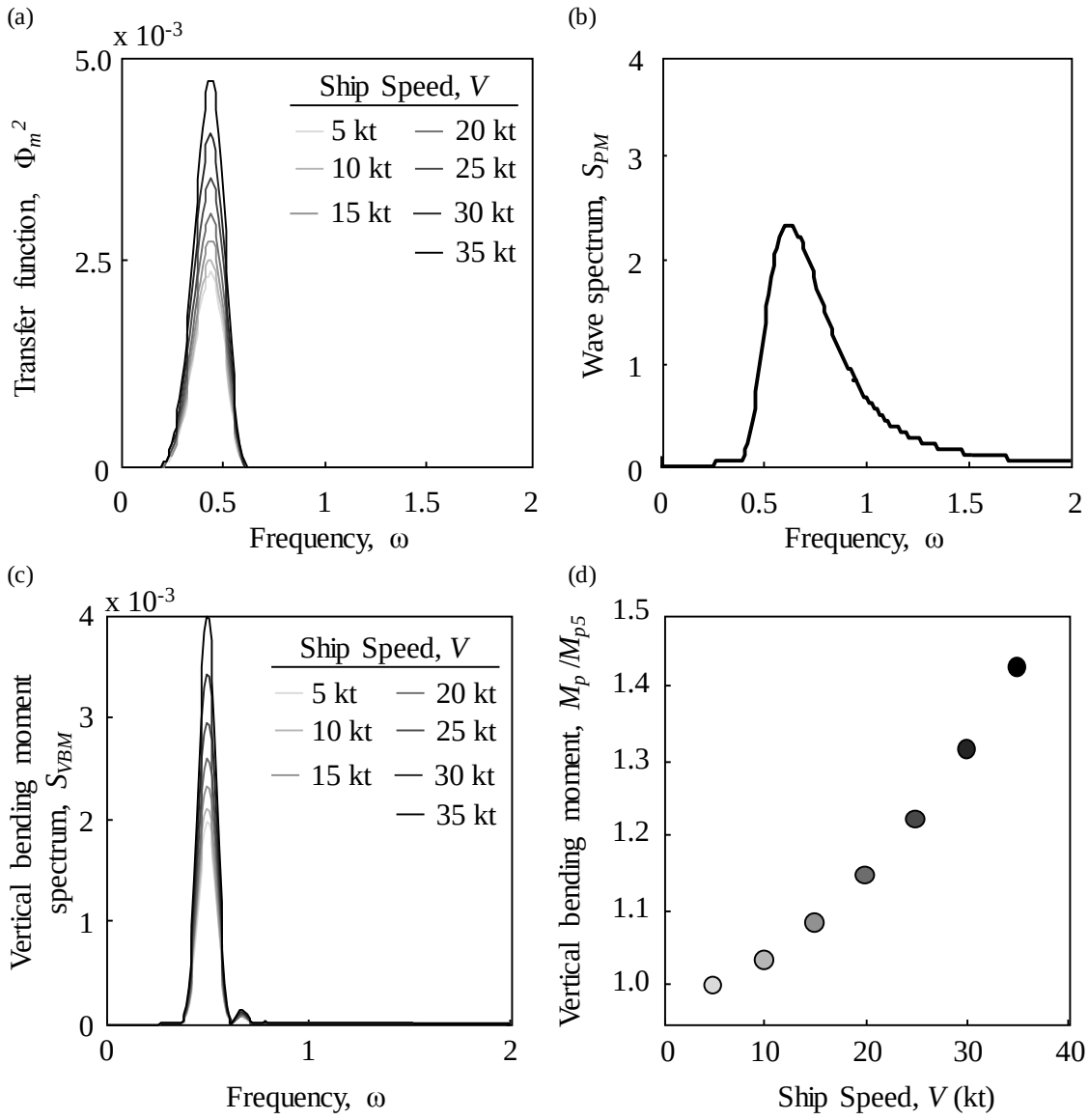

Figure 2.1. The variations in the (a) transfer function Φ_m^2, (b) wave spectrum S_{PM}, (c) response spectrum S_{VBM}, and (d) moment M_p/M_{p5} to changes in the speed of the ship.

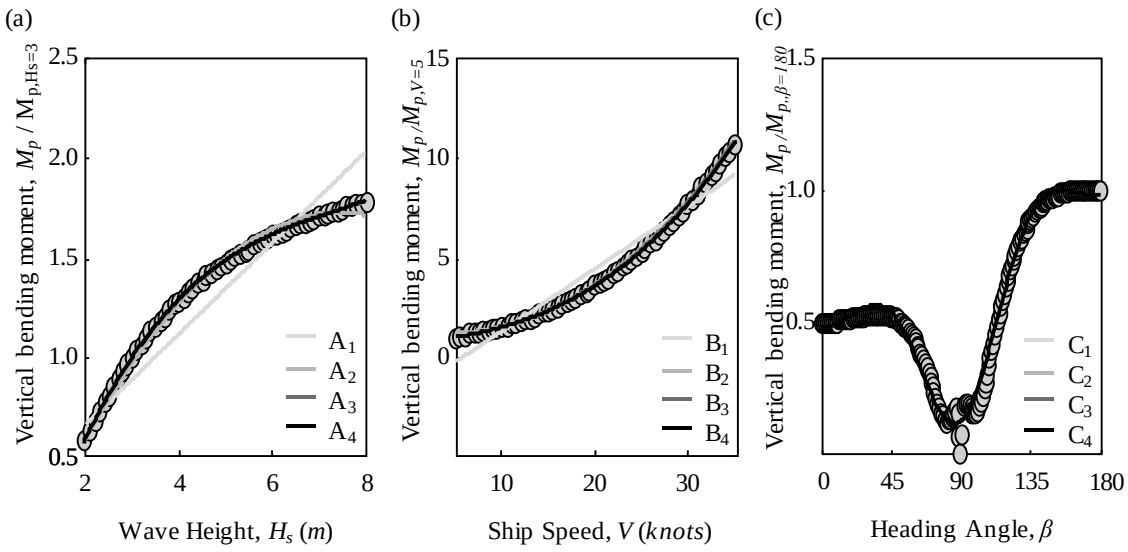

Figure 2.2. Theoretical variations of bending moment with (a) wave height, (b) ship speed, and (c) heading angle (the theoretical values are shown as black circles and proposed functional forms are fit to each and shown as solid lines)

Table 2.1. Proposed forms for M_p (H_s), M_p (V), and M_p (β) and the Root Mean Square Error.

Run	Wave Height (m)	Speed (knots)	Heading Angle	Coefficient of determination, R^2			
				Low Frequency		High Frequency	
				Fitted PSD - PM_{GEN}	Fitted PSD - $JONSWAP_{GEN}$	Fitted PSD - PM_{GEN}	Fitted PSD - $JONSWAP_{GEN}$
185	3.3	15	180	0.942	0.945	0.873	0.907
100	3.0	33	135	0.667	0.827	0.822	0.831
127	1.5	35	225	0.907	0.930	0.568	0.670
120	1.9	20	270	0.825	0.932	0.541	0.764
129	1.3	35	315	0.562	0.673	0.506	0.786
189	2.7	15	0	0.892	0.971	0.860	0.893

2.5. FATIGUE LIFE ASSESSMENT

Fatigue has been identified as one of the major thrust area of research for high-speed, high-performance naval vessels (Sielski et al. 2013). Fatigue damage on ships is a direct result of the constantly fluctuating sea waves and the associated loading cycles. Fatigue causes gradual accumulation of damage due to repeated load variations. Damage indices are useful in quantifying the state of fatigue damage of a ship as a function in time. However, if a more detailed representation of the fatigue damage state is required, fracture mechanics models may be used. Fracture mechanics models define the development of fatigue cracks in three stages: (1) crack initiation, (2) linear crack growth, and (3) the nonlinear crack growth region. This research focuses on the damage indices and their formulation in both the frequency and time domains.

The codified procedures widely implement the stress-life (S-N) approach for fatigue assessment (DNV 2010; Eurocode 9 2009). Stress-life curves relate stress ranges to the number of cycles to failure for a given structural detail. Fatigue damage indices have been introduced to quantify damage state of a given structural detail as a function of the amount of cycles spent under a particular loading history. Miner's linear damage accumulation index is an example of these indices which quantifies the state of damage for the structural detail and is expressed as

$$D = \sum_{i=1}^{n_{ss}} \frac{n_i}{N_i} \tag{2.21}$$

where n_{ss} is the number of stress range bins in a stress histogram, n_i is the number of stress cycles in i^{th} bin with stress range S_i, and N_i is the number of cycles to failure under S_i. For a linear S-N curve, the number of cycles to failure is calculated as

$$N = \frac{A}{S^m} \tag{2.22}$$

where A is the fatigue coefficient for the structural detail and m is the slope of the S-N line in logarithmic scale. There is, however, no widely accepted value at which the structural detail is known to have failed.

In the time domain, the stress range histogram is found through applying cycle counting methods to the SHM data; the damage accumulation index is found directly through Eq. 2.21. For the frequency domain, significant research has been developed to estimate the damage accumulation index from the PSD function (Benasciutti and Tovo 2007). For stationary, Gaussian, narrow-banded processes where the stress ranges follow a Rayleigh distribution, the stress range histogram can be expressed as (Bendat 1964)

$$N(S) = \sqrt{\frac{m_4}{m_2}} T \left(\frac{S}{4m_0} \exp\left(-\frac{S^2}{gm_0} \right) \right) \tag{2.23}$$

where N is the number of cycles of stress range S in T seconds.

The solution found through the narrow-band approximation is extremely conservative as it is assumed that each peak has a corresponding trough with similar magnitude. In reality, the process is a wide-band or bi-modal process with high frequency waves super-imposed on low frequency waves; both contributing significantly to the fatigue damage. (Aalberts and Nieuwenhuijs 2006; Mao et al. 2010)

An approach to estimate the stress range histogram for wide-band Gaussian processes through extensive computational analyses was introduced by Dirlik (1985). The range mean histogram for a broad-band process is (Dirlik 1985)

$$N(S) = E[P] \cdot T \cdot p(S) \tag{2.24}$$

where

$$p(S) = \frac{\frac{D_1}{Q}\exp\left(-\frac{Z}{Q}\right) + \frac{D_2 Z}{R^2}\exp\left(-\frac{Z^2}{2R^2}\right) + D_3 Z \exp\left(-\frac{Z^2}{2}\right)}{2\sqrt{m_0}} \tag{2.25}$$

and

$$D_1 = \frac{2\left(x_m - \gamma^2\right)}{1+\gamma^2} \qquad D_2 = \frac{1-\gamma-D_1+D_1^{\,2}}{1-R} \qquad D_3 = 1 - D_1 - D_2$$

$$Q = \frac{1.25\left(\gamma - D_3 - D_2 R\right)}{D_1} \qquad R = \frac{\gamma - x_m - D_1^{\,2}}{1-\gamma-D_1-D_1^{\,2}} \qquad Z = \frac{S}{2\sqrt{m_0}} \tag{2.26}$$

$$\gamma = \frac{m_2}{\sqrt{m_0 m_4}} \qquad x_m = \frac{m_1}{m_0}\sqrt{\frac{m_2}{m_4}} \qquad E[P] = \sqrt{\frac{m_4}{m_2}}$$

The resulting stress range histogram is shown to be comparable to the histogram developed through the cycle counting method (Wirsching and Shehata 1977). This research integrates the three methods for estimating the stress range histograms discussed in this section: cycle-counting methods, Bendat's narrow-band approximations, and Dirlik's broad-band approximation. For a further estimation of the long term fatigue cumulative damage factor, the observed and predicted data can be coupled with the appropriate wave scatter diagram for the anticipated operational location.

2.6. GENERATION OF RANDOM PROCESSES

Analyzing SHM data through the PSD function and predicting it in unobserved cells directly enables spectral based fatigue analysis in all cells that may be encountered in future operations. However, it also indirectly enables time domain methods; sample random processes can be generated from the PSD function and act as synthetic data for that cell. Time-history responses for unobserved cells are then readily available to be used in cycling counting methods.

The elevation of the sea surface is typically considered Gaussian (Butler et al. 2009). However, for larger waves, the shape of the wave deviates from a simple sinusoid and becomes cnoidal or otherwise Non-Gaussian (Osborne 2010). Even though waves of higher severity may be nonlinear, a linear wave assumption is often used in predicting extreme response and is included is this research (Ochi 1978; Kim 2008). This work assumes linear waves; an assumption that was reinforced during the data processing stages when the SHM data was found to be Gaussian.

For low intensity operating conditions (i.e., low speeds and low wave heights) the distribution of the recorded strains, stresses, and other observed response of the ship is also Gaussian (Naess and Moan 2012). However, due to nonlinearities in material properties, fluid-structure interaction, or extreme seas, the response may become non-Gaussian (Jensen and Dogliani 1996). An initial investigation into the distribution of the SHM data is required before simulating the random process.

The spectral representation method is highly efficient and easily implemented for generating a realization of a Gaussian random process (Shinozuka and Deodatis 1991).

For a stationary, ergodic, Gaussian random process $x(t)$, a realization of the random process is generated as a summation of sinusoids (Shinozuka and Deodatis 1991) as follows:

$$x(t) = \sqrt{2}\sum_{n=0}^{P-1}\sqrt{S_{xx}\Delta\omega}\cos(\omega_n t + \Phi_n) \tag{2.27}$$

where S_{xx} is the single sided spectral density function, ω_n is $n\,\Delta\omega$, $\Delta\omega$ is ω_u/P, ω_u is the cutoff frequency, Φ_n is uniform random from 0 to 1. Since Φ_n are independently generated and P approaches ∞, the generated sample is Gaussian through the central limit theorem. Reformulated to capitalize on the computational efficiency of the Fast Fourier Transform, Eq.2. 27 can be rewritten as

$$x(p\Delta t) = \mathrm{Re}\left\{\sum_{n=0}^{M-1} B_n \exp\left(i(n\Delta\omega)(p\Delta t)\right)\right\} \tag{2.28}$$

where Re indicates the real part, $M \geq 2P$, p = 0,1,2…M-1, $\Delta t \leq 2\pi / 2\omega_u$, and

$$B_n = \sqrt{2S_{xx}\Delta\omega}\exp(i\Phi_n) \tag{2.29}$$

While this work restricts its fatigue assessment to methods based on damage indices, crack growth models provide alternative means of assessment. The proposed methodology for developing stress range histograms in unobserved cells can be directly integrated into linear crack growth models which are dependent on the stress range distributions. For nonlinear crack growth models, the strain time-histories of the loadings are necessary (Hodapp et al. 2015). The methodology proposed for predicting the PSD and generating a random process for unobserved cells applies to strain observations as

well. Thus, in future work, the proposed methodology can be used to generate the synthetic strain histories needed to facilitate nonlinear crack growth predictions in the unobserved cells.

2.7. SUMMARY OF APPROACH

The procedure for estimating unobserved structural responses based on available structural health monitoring and using this information in the fatigue damage assessment is summarized in Figure 2.3. First, the SHM data is recorded along with the corresponding operational conditions. The data is then processed and fit with a generalized form. This generalized form enables to full PSD to be characterized with only 4 or 6 parameters. These parameters are then used as the training data to develop the prediction surface. Once the prediction surface is estimated, it can be used to determine the response in unobserved cells: the prediction surface for each parameter is developed and each parameter is estimated for the operational conditions for the unobserved cell. Therefore, the full power spectrum can be determined based on the 4 or 6 parameters. The fatigue damage may then be estimated for the structure through time-domain methods or spectral methods.

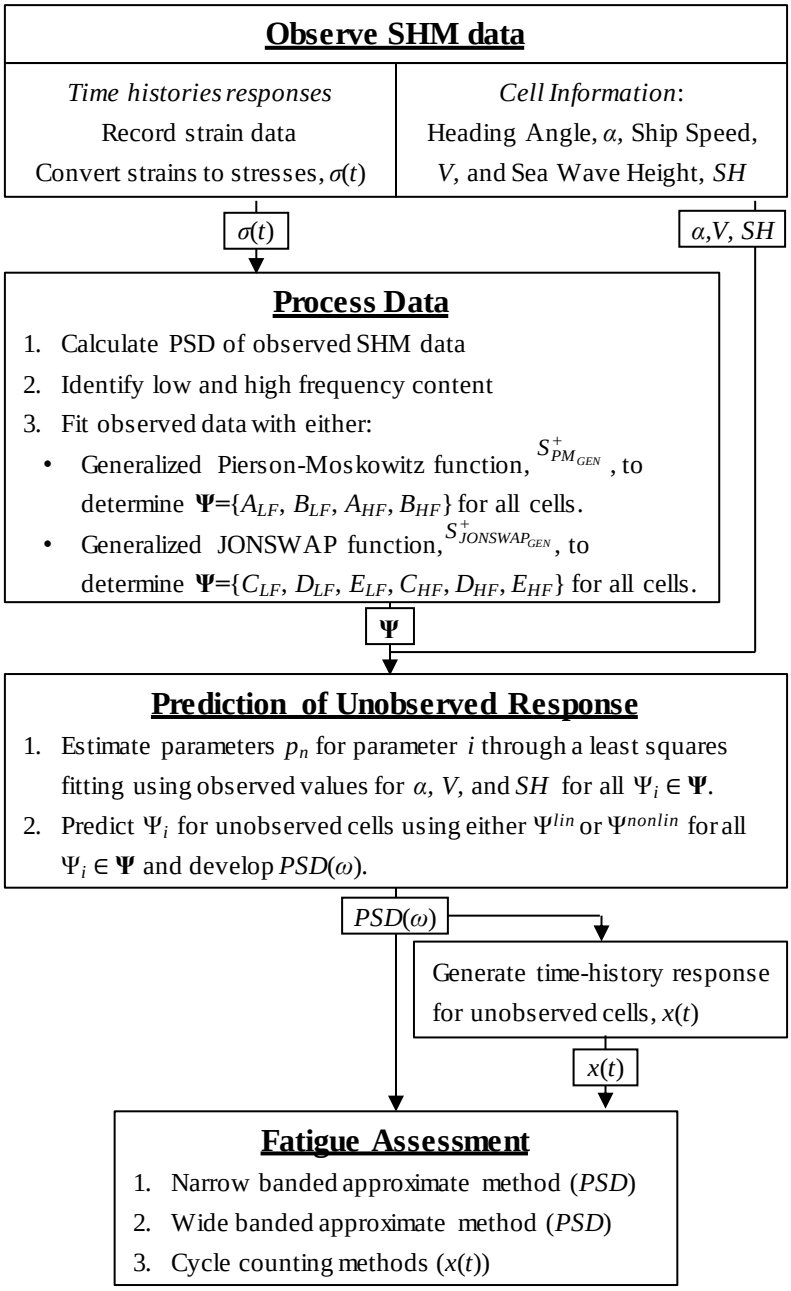

Figure 2.3. Logical scheme for the prediction of the structural response of a naval vessel based on available SHM data.

2.8. APPLICATION

The proposed methodology is applied to the to the SHM data from the HSV-2 Swift. The HSV-2 Swift is a 98 meter long aluminum vessel contracted by the U.S. Navy, designed by Revolution Design in Tasmania, Australia, and built by Incat Tasmania (Brady et al. 2004). The ship is equipped with a ride control system to stabilize motion at high speeds by deploying a T-foil. The HSV-2 Swift performed seakeeping trials and recorded SHM data and visual observations.

The HSV-2 Swift was instrumented by strain gauges and sensors that were connected to the shipboard systems. The shipboard systems, including the GPS and gyro systems, provided the track, course, and speed of the ship during operation. The sensor network was designed and implemented to capture the (a) primary load, (b) stress concentration, (c) secondary loads, and (d) ramp, crane, vehicle deck, helicopter deck, and gun mount responses. The primary load response sensors included 16 strain gauges located at optimal locations derived from finite element analysis models (Brady et al. 2004). The observed data were recorded and compared with predetermined limits and design loads. The stress concentration responses were determined through the conversion of strain gauge data collected from the T2 sensor group. The T2 sensors include 18 strain gauges installed at high-stress areas indicated in the FEA analysis results with the goal of providing stress data at fatigue critical details. The data collected from the T2-4 sensor during the HSV2-Swift trials when the T-foil was in a retracted state is used as the example of SHM data. The T2-4 sensor is located on frame 26 along the keel and is shown in Figure 2.4. The data were collected at a sampling rate of 100 Hz.

The HSV-2 Swift performed sea keeping trials in both calm and rough waters by moving at varying speeds and directions. The objective of the sea keeping trials was to observe the structural response for potential operating conditions. The vessel was operated at sustained speeds ranging from 2 to 35 knots in an octagonal pattern and recorded data for heading angles of 0°, 45°, 60°, 135°, 180°, 225°, 270°, 315°, and 360°. Data from the octagonal trials were stored with respect to their run number. Each run corresponds to a single heading angle, a single wave height, and a single speed (i.e., each run is a single cell). The data from each available run is used as the SHM data for observed cells. The 57 of the runs tested during the HSV-2 Swift seakeeping trials which reported no technical difficulties and had the t-foil retracted are included as the data set.

The strain gauge data are converted to stress data for each run (Brady et al. 2004), then windowed and averaged to determine the mean PSD of the cell. Typical runs lasted for around 30 minutes but varied based on changes in wave height. Figure 2.5 a depicts a five minute portion of the stress time history for Run 185 which is associated with a heading angle of 180° (head seas), wave height of 3.3m, and ship speed of 15 knots. The PSD function for each separate window of the time history of Run 185 are shown in Figure 2.5b, along with the mean PSD. Similarly, the mean PSD function was evaluated for all other runs and are summarized in Figure 2.6.

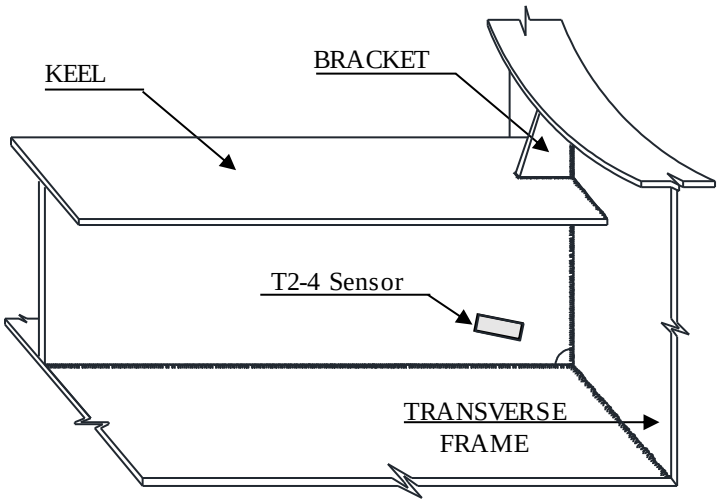

Figure 2.4. Structural detail for T2-4 sensor at the keel-to-frame connection on the HSV2-Swift.

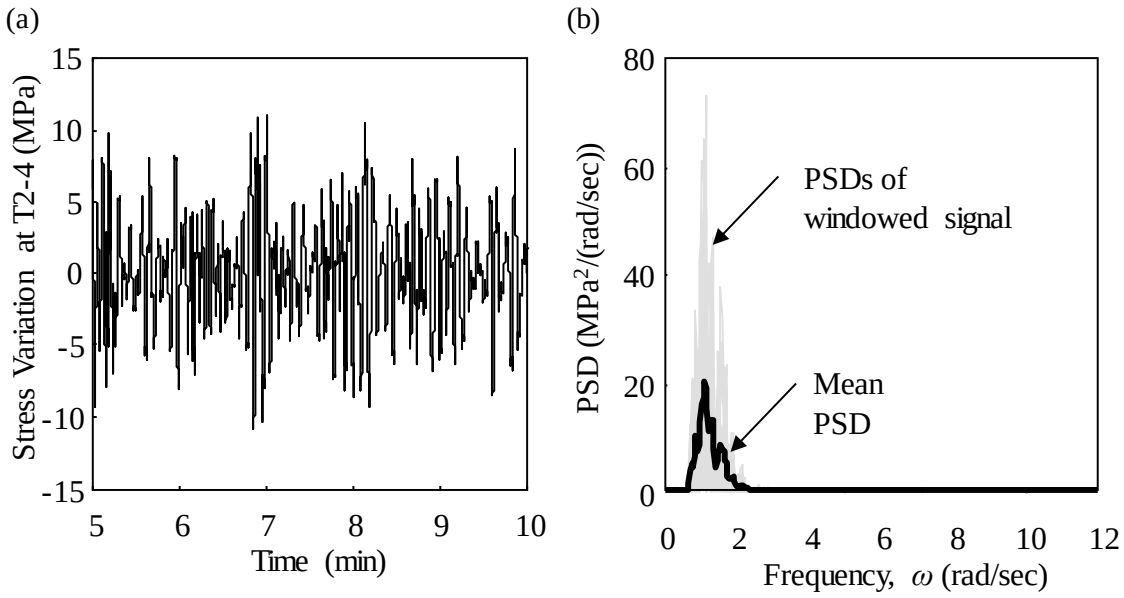

Figure 2.5. Stress time history and PSD function for T2-4 sensor during Run 185.

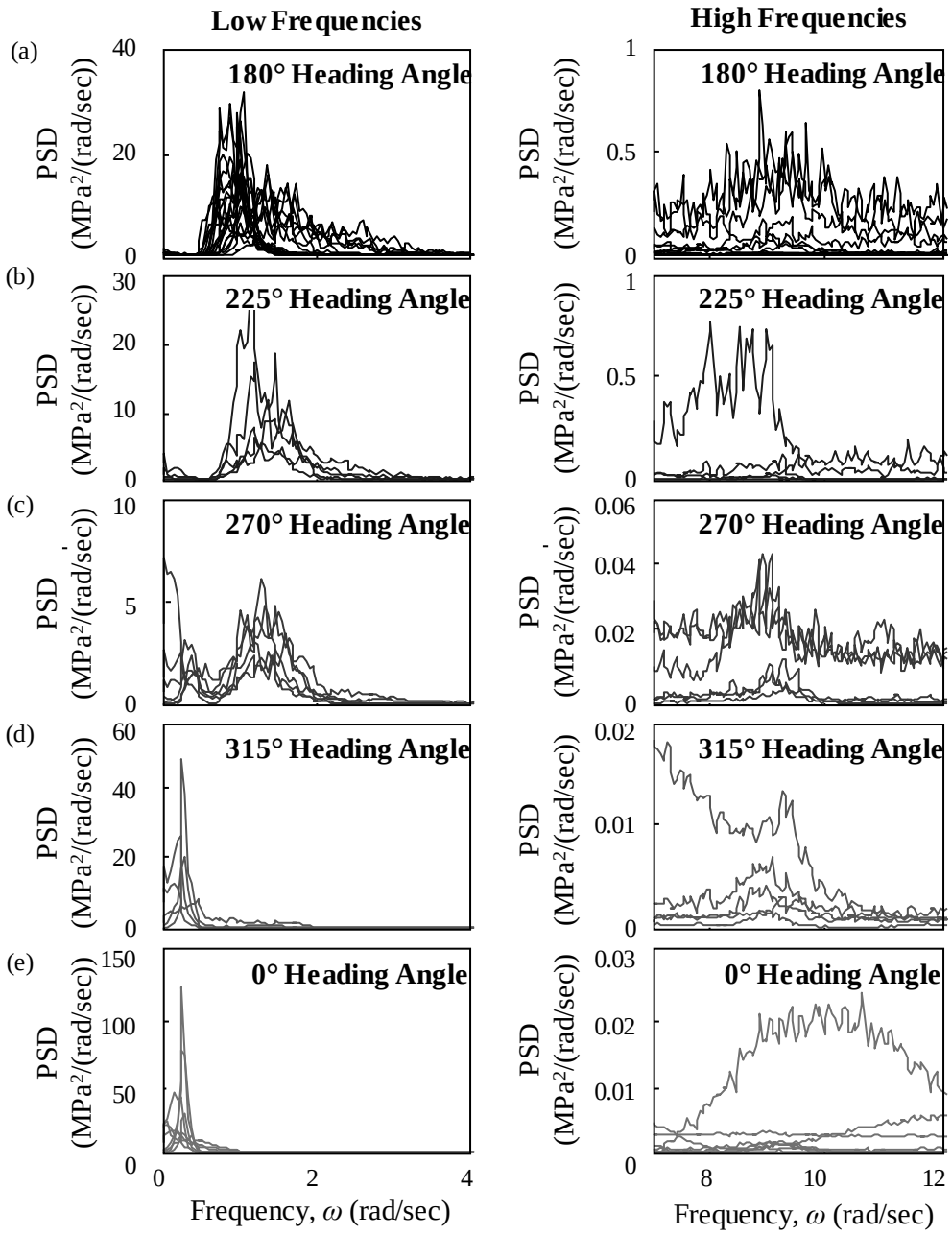

Figure 2.6. The mean PSD for the T2-4 sensor for all available runs summarized by heading angle.

2.9. RESULTS

2.9.1. Data Processing

The proposed fitting functions defined in Equations 2.7 and 2.8 are then fit to the mean PSD through the least squares fitting algorithm available in MATLAB (MathWorks 2013) for all runs. The goodness of fit for select runs is presented in Table 2.2. The select runs represent a range of operational conditions covering head seas, as well as oblique heading angles, beam seas, and following seas. The PSD of the windows, the mean PSD, the fitted generalized Pierson-Moskowitz function, and the fitted generalized JONSWAP function are shown in Figure 2.7 for Runs 185 and 100. The low frequency response and the high frequency response clearly delineated. The estimated values for the fitted generalized Pierson-Moskowitz function and the fitted generalized JONSWAP function are provided for Runs 185 and 100 in Table 2.3 as examples of the parameters used in developing the prediction surface.

The fitted generalized JONSWAP function outperforms the fitted generalized Pierson-Moskowitz function as indicated in Table 2.2 with regards to the coefficient of determination (R^2) value for both the low and high frequency components. The fitted generalized JONSWAP function takes the form of the JONSWAP spectrum, which was developed for seas with fetch limitations, non-fully developed seas, and wave-wave interactions. This spectrum is applicable to the SHM data used in this research, as evident through the trials in which some runs were denoted as confused and others had recorded swell and wave directions with different periods and heights. Additionally, the peak enhancement factor allows multiple peaks in the response spectrum to be captured as

seen in the Figure 2.7 b. Thus, the generalized JONSWAP function can include the high energy content for a broader range of frequencies.

The proposed fitting functions more accurately fit the response in the head-sea case than the other heading angles, as shown in Table 2.2. This can be attributed to the expected form of the linear transfer function for this specific ship. RAOs are ship specific functions. The variability of RAOs with heading angle and wave period differ from vessel to vessel due to the ship length, structural design, and ride characteristics, among others (Hughes 1983; Chan et al. 2002, Salvesen et al. 1970).

Table 2.2. Comparison of results for select runs with different heading angles, wave heights, and speeds.

Run	Wave Height (m)	Speed (knots)	Heading Angle	Coefficient of determination, R^2			
				Low Frequency		High Frequency	
				Fitted PSD - PM_{GEN}	Fitted PSD - $JONSWAP_{GEN}$	Fitted PSD - PM_{GEN}	Fitted PSD - $JONSWAP_{GEN}$
185	3.3	15	180	0.942	0.945	0.873	0.907
100	3.0	33	135	0.667	0.827	0.822	0.831
127	1.5	35	225	0.907	0.930	0.568	0.670
120	1.9	20	270	0.825	0.932	0.541	0.764
129	1.3	35	315	0.562	0.673	0.506	0.786
189	2.7	15	0	0.892	0.971	0.860	0.893

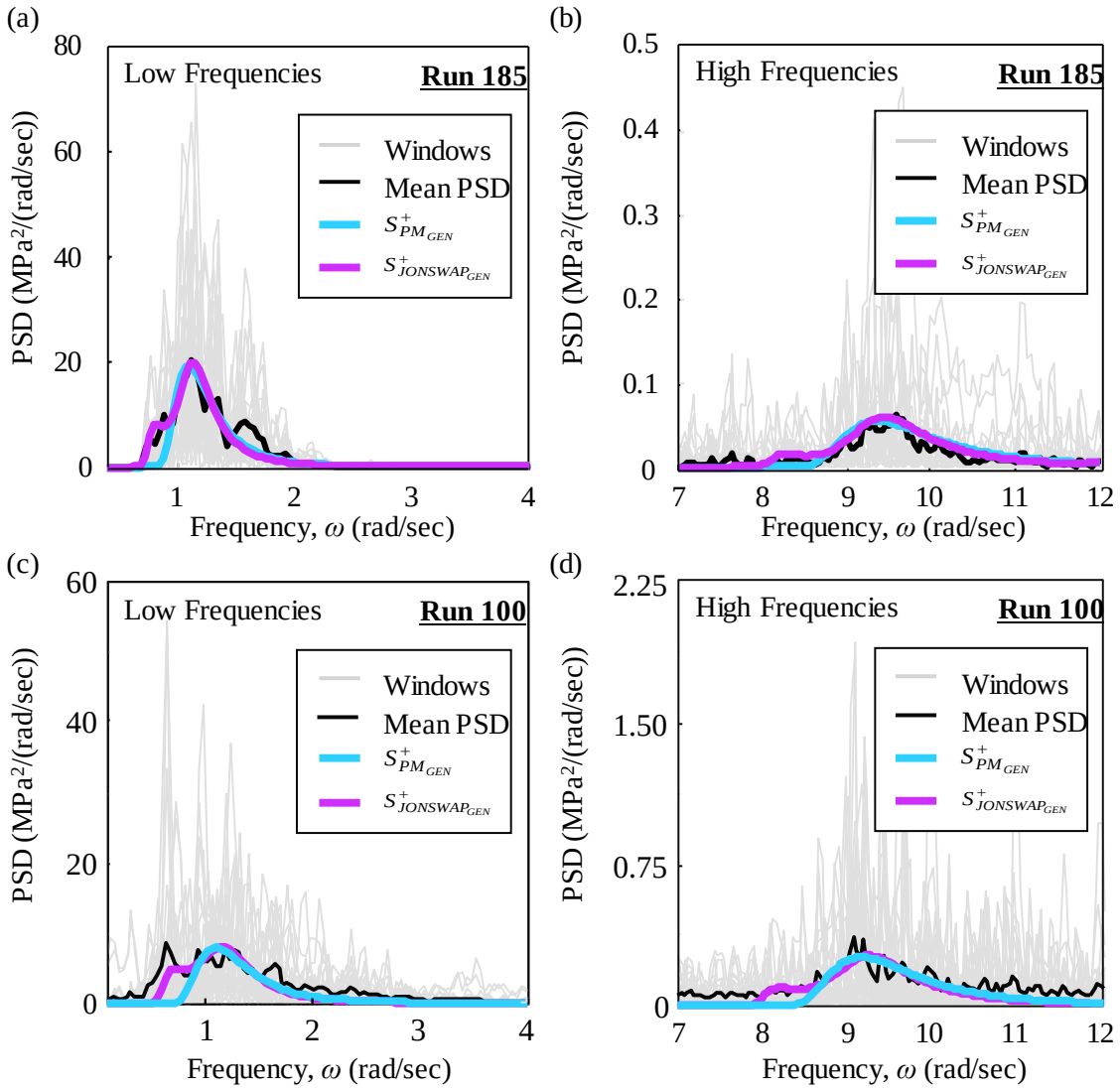

Figure 2.7. The fitted generalized Pierson–Moskowitz function and the fitted generalized JONSWAP function for the T2-4 sensor during Run 185 and Run 100. The PSD of each window is shown in light grey, the mean PSD is shown in black, the fitted generalized Pierson-Moskowitz function, and the fitted generalized JONSWAP function are labeled.

Table 2.3. Fitting Parameters for the generalized Pierson-Moskovitz and generalized JONSWAP functions for Run 185 and 100.

PM_{GEN}			$JONSWAP_{GEN}$		
Parameter	**Run 185**	**Run 100**	**Parameter**	**Run 185**	**Run 100**
A_{LF}	9.632	8.002	C_{LF}	6.939	19.10
B_{LF}	0.677	0.747	D_{LF}	0.455	0.748
A_{HF}	13.56	39.82	E_{LF}	0.074	0.321
B_{HF}	2.363	2.416	C_{HF}	8.983	29.58
			D_{HF}	1.515	1.629
			E_{HF}	0.041	0.068

2.9.2. Prediction Surface

In the data processing stage, the parameters defining the response in each cell are determined. If the generalized Pierson-Moskowitz function is used to characterize response, the parameters {A_{LF}, B_{LF}, A_{HF}, B_{HF}} are determined, or, if the generalized JONSWAP function is used, the parameters {C_{LF}, D_{LF}, E_{LF}, C_{HF}, D_{HF}, and E_{HF}} are determined for each cell in the available SHM data. It is these parameters that are used as inputs to the least squares fitting algorithm in order to determine the prediction surface parameters P_i for the linear or nonlinear prediction surfaces. A prediction of each response parameter in the sets {A_{LF}, B_{LF}, A_{HF}, B_{HF}} or {C_{LF}, D_{LF}, E_{LF}, C_{HF}, D_{HF}, and E_{HF}} must be developed in order to predict the response in unobserved cells. The following is a discussion on the performance of the linear and nonlinear prediction surfaces and how they capture the trends in the data. Discussion on how well they predict unobserved

responses and the subsequent impact on fatigue damage estimates is reserved for the Section 2.9.3.

The performance of the nonlinear surfaces (developed in Section 2.4) is first investigated with respect to their ability to capture the variation in the observed data. That is, for all parameters in sets $\{A_{LF}, B_{LF}, A_{HF}, B_{HF}\}$ and $\{C_{LF}, D_{LF}, E_{LF}, C_{HF}, D_{HF}$, and $E_{HF}\}$ for Ψ^{lin}, Ψ^{nonlin}, and $\Psi^{nonlin\text{-}poly}$, prediction parameters P_i are determined through the least squares fitting algorithm available in MATLAB (MathWorks 2013) and the mean square error (MSE) is calculated. This process is shown in Figure 2.8 for CLF. The data points for CLF are plotted as a function of wave height and heading angle for a constant ship speed in Figure 2.8a and as a function of ship speed and wave height for a constant heading angle in Figure 2.8b. Figure 2.8 a and b also show the fitted surfaces for Ψ^{lin}, Ψ^{nonlin}, and $\Psi^{nonlin\text{-}poly}$. The surfaces for Ψ^{nonlin} and $\Psi^{nonlin\text{-}poly}$ lie on top of each other in Figure 2.8 a and b and have comparable MSE, as listed in Table 2.4. The results for the MSE for Ψ^{lin}, Ψ^{nonlin}, and $\Psi^{nonlin\text{-}poly}$ for all parameters are listed in Table 2.4.

The theoretically-based nonlinear prediction surfaces typically outperform the linear surface for all low frequency parameters. The high frequency parameters show minimal or no improvement when compared to the linear surface. This can be attributed to the fact that the surfaces were developed based on wave bending moment, which is governed by the low frequencies. Slam impacts typically govern the high frequency response and would thus be better predicted by alternative nonlinear relationships.

The variability in the performance of the prediction surfaces to changes in the training data (i.e. the available data set) is investigated. In order to achieve this, 10

training sets were established around the original set of available sea keeping data. Training set 1 includes all of the data from the sea trials. Training sets 2 through 5 were developed by randomly selecting 70% of the data from the sea keeping trials. Training sets 6 through 10 were developed by randomly selecting 50% of the data from the sea keeping trials. The performance of the prediction surface to different training data sets is tracked in Table 2.5, which details the MSE for the linear and nonlinear surfaces for the parameter $C_{LF.}$

Ψ^{nonlin} and $\Psi^{nonlin\text{-}poly}$ typically perform comparably regardless of training set data. That suggests that the proposed methodology can be robustly applied. However, in training set 6 with 50% available data, local fluctuations in the prediction surface occur when Ψ^{nonlin} was used. This is shown in Figure 2.9. While the MSE for Ψ^{nonlin} and $\Psi^{nonlin\text{-}poly}$ for training set 6 are similar, $\Psi^{nonlin\text{-}poly}$ fits the overall trend while avoiding the local fluctuations shown in Figure 2.9a. While such fluctuations in the surface Ψ^{nonlin} do not have a substantial impact on this specific case, they may have large impact on other case studies. Thus, the $\Psi^{nonlin\text{-}poly}$ prediction surface is more robust and is suggested as the preferred method.

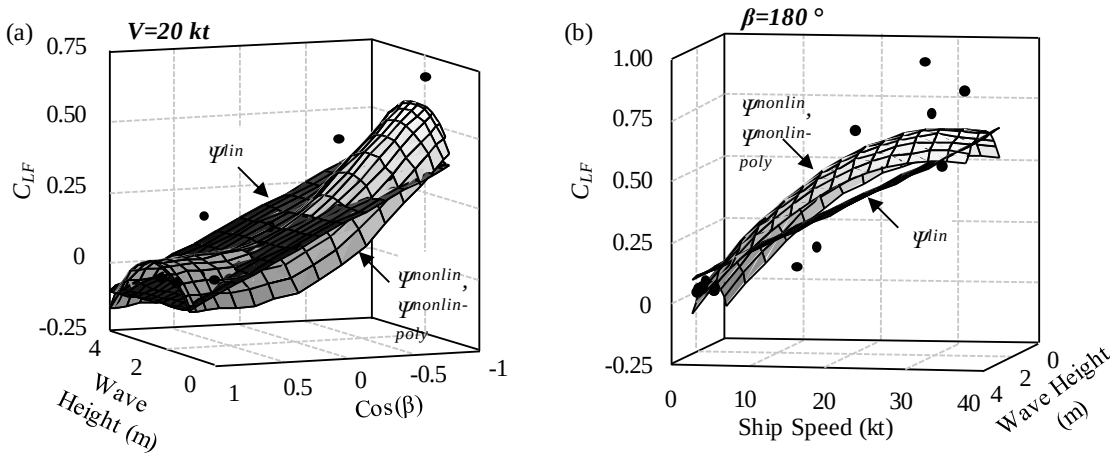

Figure 2.8. Available data points for the response parameter C_{LF} (shown as black points) and the fitted surfaces for Ψ^{lin}, Ψ^{nonlin}, and $\Psi^{nonlin\text{-}poly}$ where (a) shows the variation of C_{LF} with wave height and heading angle for a ship speed of 20 kts and (b) shows the variation of C_{LF} with ship speed and wave height for a heading angle of 180°

Table 2.4. Evaluation of proposed surfaces with respect to observed data

Parameter	Mean Square Error			Parameter	Mean Square Error		
	Ψ^{lin}	Ψ^{nonlin}	$\Psi^{nonlin\text{-}poly}$		Ψ^{lin}	Ψ^{nonlin}	$\Psi^{nonlin\text{-}poyl}$
A_{LF}	0.022	0.022	0.02	C_{LF}	0.034	0.028	0.028
B_{LF}	0.034	0.022	0.017	D_{LF}	0.022	0.012	0.012
A_{HF}	0.103	0.099	0.099	E_{LF}	0.008	0.008	0.008
B_{HF}	0.083	0.087	0.086	C_{HF}	0.175	0.163	0.161
				D_{HF}	0.048	0.046	0.046
				E_{HF}	0.005	0.005	0.004

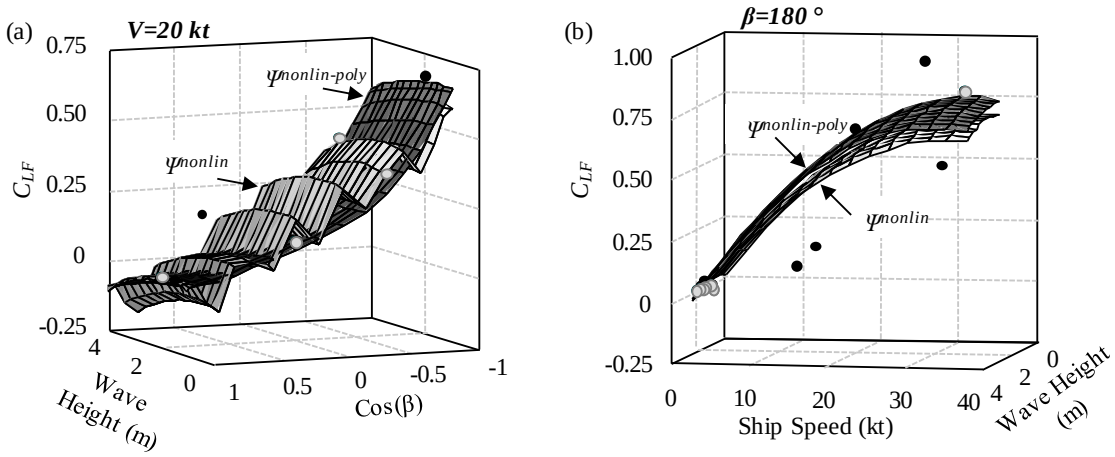

Figure 2.9. Available data points for the response parameter C_{LF} (shown as black points), missing data points (shown in light grey), and the fitted surfaces for Ψ^{lin}, Ψ^{nonlin}, and $\Psi^{nonlin\text{-}poly}$ for available data set 6; (a) shows the variation of C_{LF} with wave height and heading angle for a ship speed of 20 kts and (b) shows the variation of C_{LF} with ship speed and wave height for a heading angle of 180°.

Table 2.5. MSE for predicting Parameter C_{LF} as a function of missing data

Training Set	Percent of Total Available Data	Mean Square Error		
		Ψ^{lin}	Ψ^{nonlin}	$\Psi^{nonlin\text{-}poly}$
1	100	0.034	0.028	0.028
2	70	0.034	0.029	0.029
3	70	0.035	0.031	0.031
4	70	0.034	0.030	0.031
5	70	0.035	0.029	0.029
6	50	0.035	0.030	0.034
7	50	0.036	0.032	0.032
8	50	0.034	0.029	0.029
9	50	0.034	0.030	0.031
10	50	0.039	0.033	0.039

2.9.3. Estimation of unobserved responses

In order to demonstrate the applicability and accuracy of the prediction methodology presented, the following steps are taken: (1) a particular cell is chosen as a test point and the SHM data pertaining to that cell is removed from the training data set used to develop the prediction surfaces. In this way, the predicted value using the developed surface can be compared to the observed SHM value. (2) The SHM training set is used to develop the prediction surfaces and estimate parameters (either $\{A_{LF}, B_{LF}, A_{HF}, B_{HF}\}$ or $\{C_{LF}, D_{LF}, E_{LF}, C_{HF}, D_{HF}$, and $E_{HF}\}$) for the test point and predict the PSD for the cell. (3) A statistical analysis of the available SHM data is performed to determine if the observed responses are stationary, ergodic, Gaussian random processes. This ensures that the generation of the time-history of the test point is compatible with the expected random process for the cell. (4) The stress range histograms and fatigue damage indices are developed for the test point. The predicted values are then compared to the actual observed data.

Furthermore, to demonstrate the robustness of the methodology, two test points were chosen as representative cells for head sea conditions and oblique heading angles. These include data from Runs 185 and 100. Multiple training sets were explored in order to identify the sensitivity of the methodology to the available SHM data. Training set A includes all of the data from the sea trials. Training set B was developed by randomly selecting 70% of the data from the sea keeping trials. Training set C was developed by randomly selecting 50% of the data from the sea keeping trials.

2.9.3.1. And the PSD

Figure 2.10 demonstrates how the available data in the training set is used to develop the prediction surface and estimate the parameters A_{LF}, B_{LF}, C_{LF}, D_{LF}, E_{LF} for the test point. The change in the parameters are shown with respect to wave height and vessel speed for a 180° heading angle. This 3 dimensional surface is only a slice of the prediction surface that relates the parameter to wave height, ship speed, and heading angles (a 4 dimensional surface). The available data in training set A are shown in Figure 2.10 (a) - (e) as solid dots, the linear prediction surface is indicated, and the predicted values for the parameters of the test point are indicated with a star. In this figure, the test point is the cell equivalent to Run 185. (Similar figures for the high frequency parameters, nonlinear surfaces, other training sets, and other test point are omitted, but the methodology remains the same for all of those cases.)

The estimated value for each of the parameters of the test point are then used to develop the full PSD for that test point. The resulting PSDs are shown in Figure 2.11 a and b for Training Set A, Figure 2.11 c and d for Training Set B, and Figure 2.11 e and f for Training Set C for the test point equivalent to Run 185. While the PSDs shown in this figure were developed with the parameters found using the linear prediction surface, the same methodology applies to the parameters found using the non-linear surfaces.

For all training sets and for both test points, the PSDs predicted from the generalized JONSWAP function and the generalized Pierson-Moskowitz function are compared to the observed data for the test point and the mean square error is evaluated and listed in Table 2.6. The generalized JONSWAP function more accurately predicts the lower and

overall PSD; however, the generalized Pierson-Moskowitz function has a lower mean square error in the high frequencies. Accordingly, if the high frequency response (i.e., whipping response) is of interest, then the generalized Pierson-Moskowitz function would provide better prediction of the behavior. Similar trends are seen for the test point equivalent to Run 100 shown in Figure 2.12 and detailed in Table 2.6.

Table 2.6. Performance of predicted PSD functions as compared to the observed mean PSD for the equivalent test point.

Test Point	**Case**	**Mean Square Error**					
		Predicted PSD - PM_{GEN}			**Predicted PSD - $JONSWAP_{GEN}$**		
		Low Frequencies	**High Frequencies**	**All Frequencies**	**Low Frequencies**	**High Frequencies**	**All Frequencies**
Run 185	A	0.000551	2.14E-07	0.000267	0.000571	3.40E-07	0.000276
	B	0.000979	1.92E-07	0.000474	0.000551	2.06E-07	0.000267
	C	0.000914	2.36E-07	0.000442	0.000690	2.66E-07	0.000334
Run 100	A	0.006527	9.18E-06	0.003164	0.004921	9.17E-06	0.002386
	B	0.007188	9.15E-06	0.003483	0.005244	9.16E-06	0.002543
	C	0.003986	9.29E-06	0.001934	0.003909	9.34E-06	0.001897

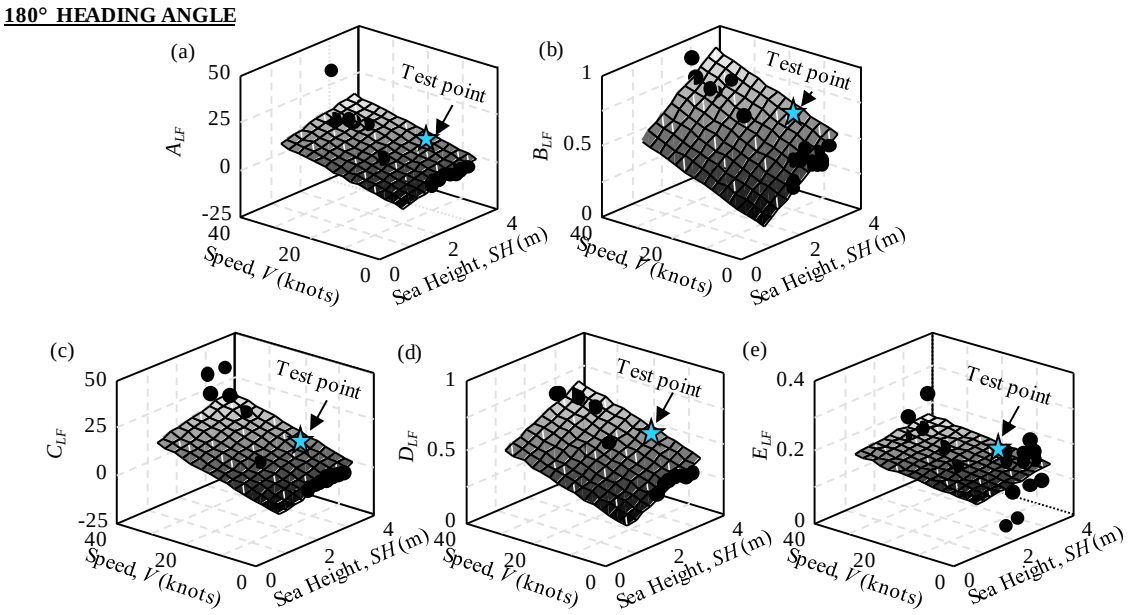

Figure 2.10. Linear extrapolation functions based on the available data (shown as black points) and the estimated value for the test point for the low frequency generalized Pierson–Moskowitz function (a) A_{LF} and (b) $B_{LF,}$ and the low frequency generalized JONSWAP function (c) C_{LF}, (d) $D_{LF,}$ and (e) E_{LF} for the test point equivalent to Run 185.

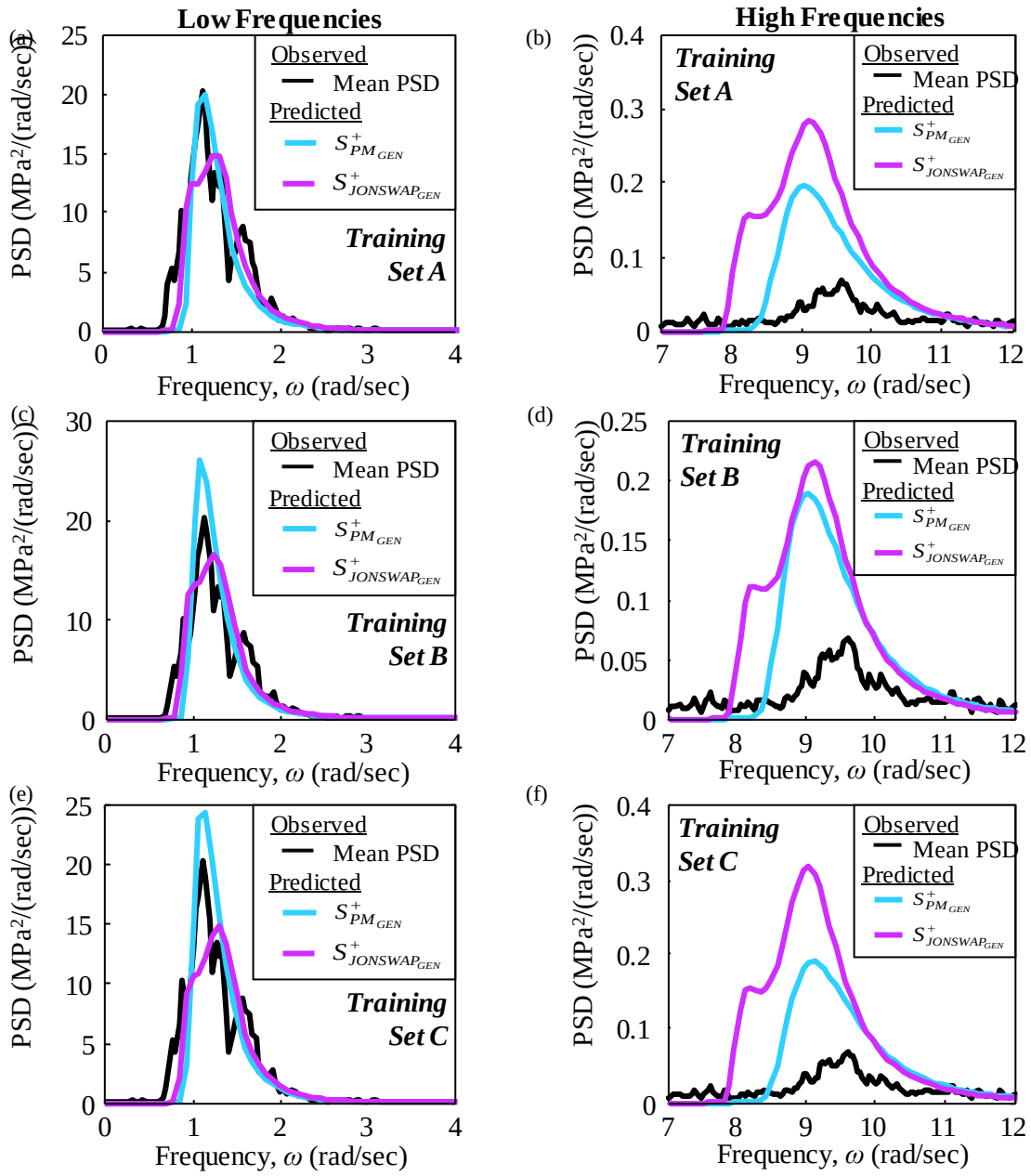

Figure 2.11. Extrapolated power spectral density functions for (a) training set A, (b) training set B, and (c) training set C and the observed PSD for the test point equivalent to Run 185 including both the low frequency and high frequency components.

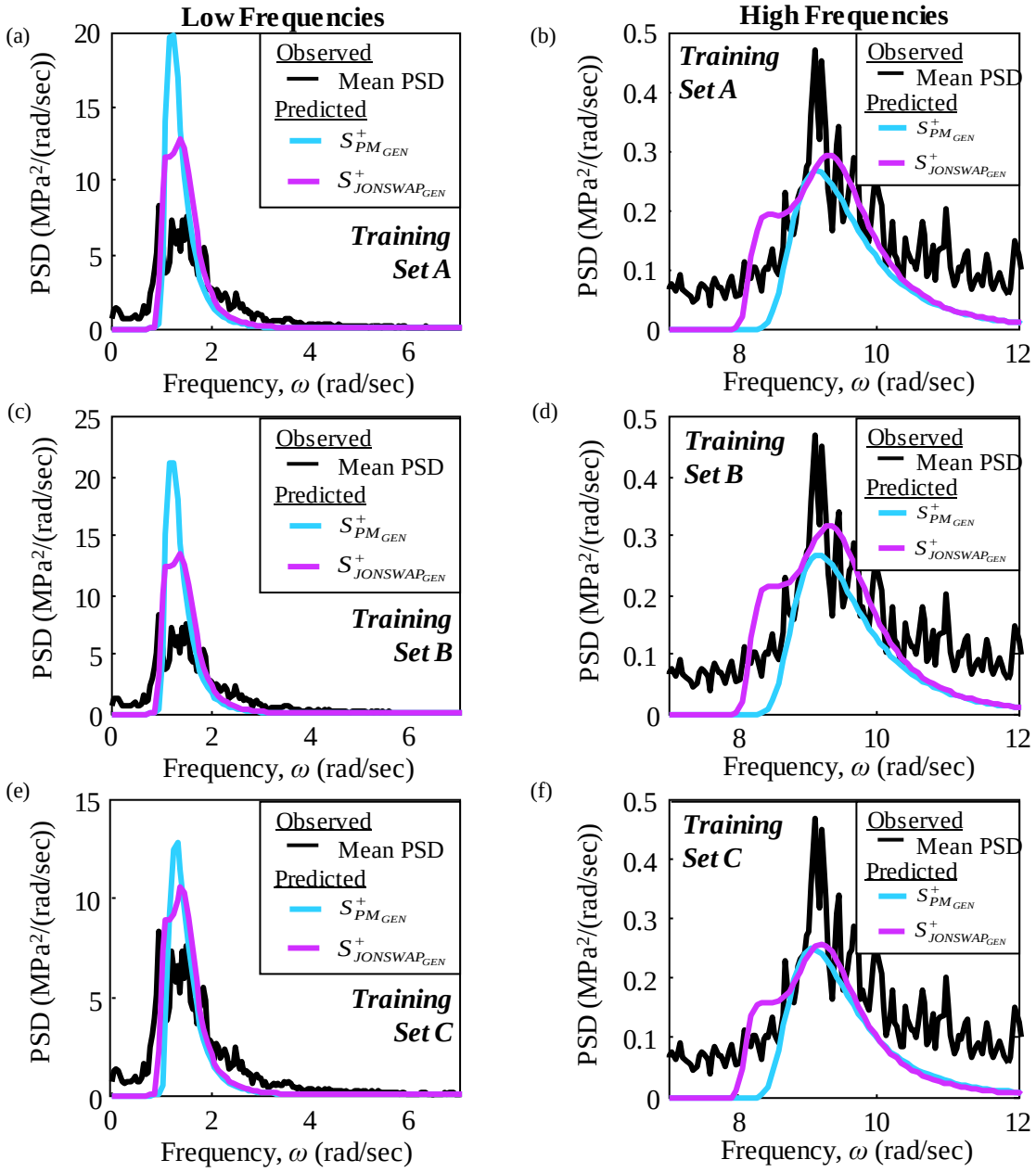

Figure 2.12. Extrapolated power spectral density functions for (a) training set A, (b) training set B, and (c) training set C and the observed PSD for the test point equivalent to Run 100 including both the low frequency and high frequency components.

2.9.3.2. And the generation of synthetic time histories

In order to enable time-domain fatigue damage estimates, the time-history of the structural responses is necessary. As previously noted, a statistical analysis of the available SHM data is needed to determine if the observed responses are stationary, ergodic, Gaussian random processes and ensure the generation of synthetic time-history data that is compatible with the expected random process for the cell.

A distribution fitting process is applied to the SHM data in the training set to determine the best fit for the stress distribution. Goodness of fit is judged for the normal, lognormal, and Weibull distribution using the Kolmogorov-Smirnov test (Ang and Tang 2007). The statistical analysis of the stress observed at the T2-4 sensor during Runs 185 and 160 are shown in the probability plots in Figure 2.13 for the (a) Normal, (b) Lognormal, and (c) Weibull distributions. The analysis shows that the normal distribution is the best fit for the data and that the methodology for generating instances of the random process detailed in Section 2.6 can be applied. Examples of the synthetic time-history data generated for the T2-4 stress response for the test point are shown for Training Sets A, B, and C in Figure 2.14 a, b, and c, respectively, for the test point equivalent to Run 185.

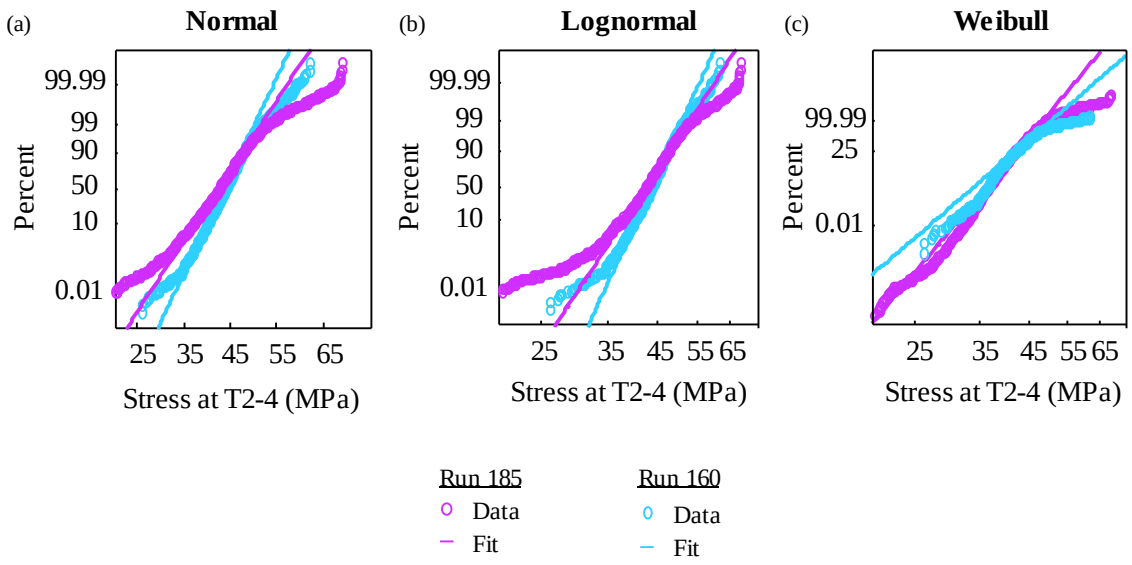

Figure 2.13. Fitting results for the stress distribution observed at the T2-4 sensor during Runs 185 and 160 for the (a) Normal, (b) Lognormal, and (c) Weibull distributions.

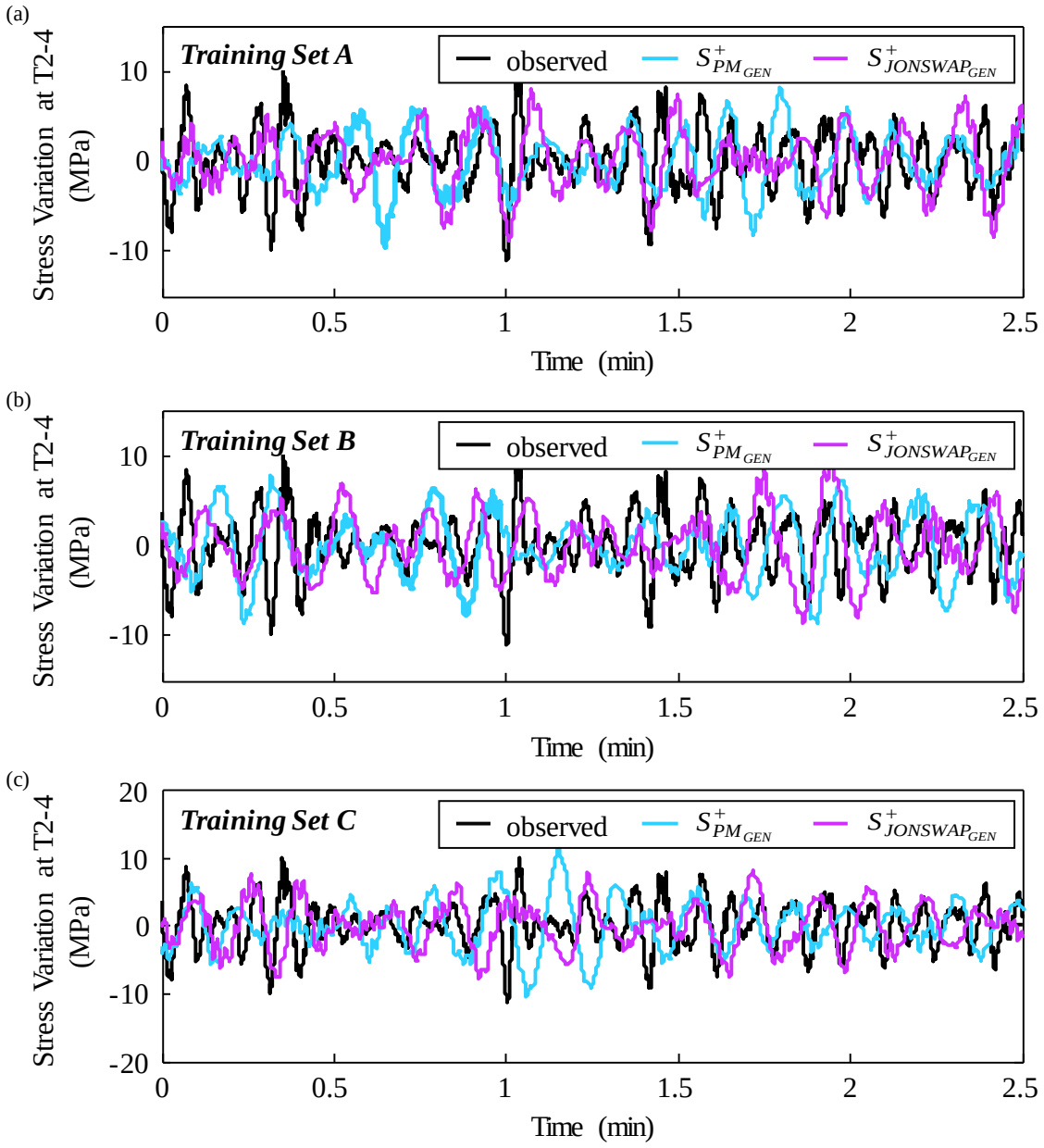

Figure 2.14. Generated random processes based on the extrapolated PSD for (a) Training Set A, (b) Training Set B, and (c) Training Set C that are the synthetic SHM data for the test point equivalent to Run 185.

2.9.3.3. And the stress range distribution

The developed PSDs and synthetic time history data are then used to estimate the stress range histograms and fatigue damage indices for the test points. The stress range histogram for the test point may be generated by applying the rain-flow counting method (Wirsching and Shehata 1997) to the synthetic time-history data for the T2-4 stress response. Spectral based methods for estimating the stress range histogram for narrow band signals (Eq. 2.23) and wide band processes (Eq.2.24) may also be used.

The resulting probability density functions (PDFs) for stress range are shown for Training Sets A, B, and C in Figure 2.15 for the test point equivalent to Run 185. The results pertaining to both the generalized Pierson-Moskowitz and the generalized JONSWAP forms are included. Additionally, the actual stress range histogram from the observed SHM data for the test point is shown for comparison. The results are further summarized in Table 2.7. The results are also shown for the test point equivalent to Run 100 in Figure 2.16 and summarized in Table 2.8.

For Training Sets A, B, and C, the mean and standard deviation of the stress range is most accurately predicted through the cycle counting method in the time domain for the synthetic data generated from the predicted PSD with the generalized Pierson-Moskowitz fitting function. For the test point equivalent to Run 185, the mean stress ranges is predicted to within 7% error for all training sets when using the cycle-counting methods as applied to the synthetic data generated from the predicted Pierson-Moskowitz PSD; the standard deviation is predicted within 8% error for training sets. The better performance of the predicted Pierson-Moskowitz PSD can partially be attributed to the contribution of the high frequency component of the response to the stress range and subsequent fatigue

damage. Similarly, the stress range parameters are most accurately predicted through the cycle counting method applied to the synthetic data generated from the predicted PSD with the generalized Pierson-Moskowitz fitting function for the test point equivalent to Run 100.

The theoretically developed nonlinear prediction outperforms the linear surface in estimating the structural response of the unobserved cell. This is shown in the comparison of the scale and shape parameters that define the stress range distribution predicted for both test points. For the test point equivalent to run 100, the nonlinear prediction surface offers a 23% increase in the accuracy for the scale parameter estimates. The gains for the head seas are not as significant as those for the oblique heading angle instances, however there is still an increase in accuracy for the head sea case (test point equivalent to run 185). Figure 2.17 and Table 2.9 detail the performance of the linear and nonlinear surfaces in predicting the stress range.

Table 2.7. Observed and Predicted Stress range parameters for the test point equivalent to Run 185

Data Source	**Method**	**Stress Range (MPa)**					
		Case A		**Case B**		**Case C**	
		Mean	**Standard Deviation**	**Mean**	**Standard Deviation**	**Mean**	**Standard Deviation**
Observed Data	Cycle Counting	1.020	0.593	1.020	0.593	1.020	0.593
Predicted PSD - $JONSWAP_{GEN}$	Cycle Counting	1.276	0.717	0.889	0.483	1.613	1.048
	Broad Banded	0.648	0.448	0.538	0.359	0.910	0.689
	Narrow Banded	7.239	3.778	6.964	3.640	6.598	3.447
Predicted PSD - PM_{GEN}	Cycle Counting	0.945	0.558	1.069	0.627	1.034	0.641
	Broad Banded	0.545	0.365	0.648	0.607	0.614	0.393
	Narrow Banded	6.329	3.309	6.391	3.337	5.805	3.034

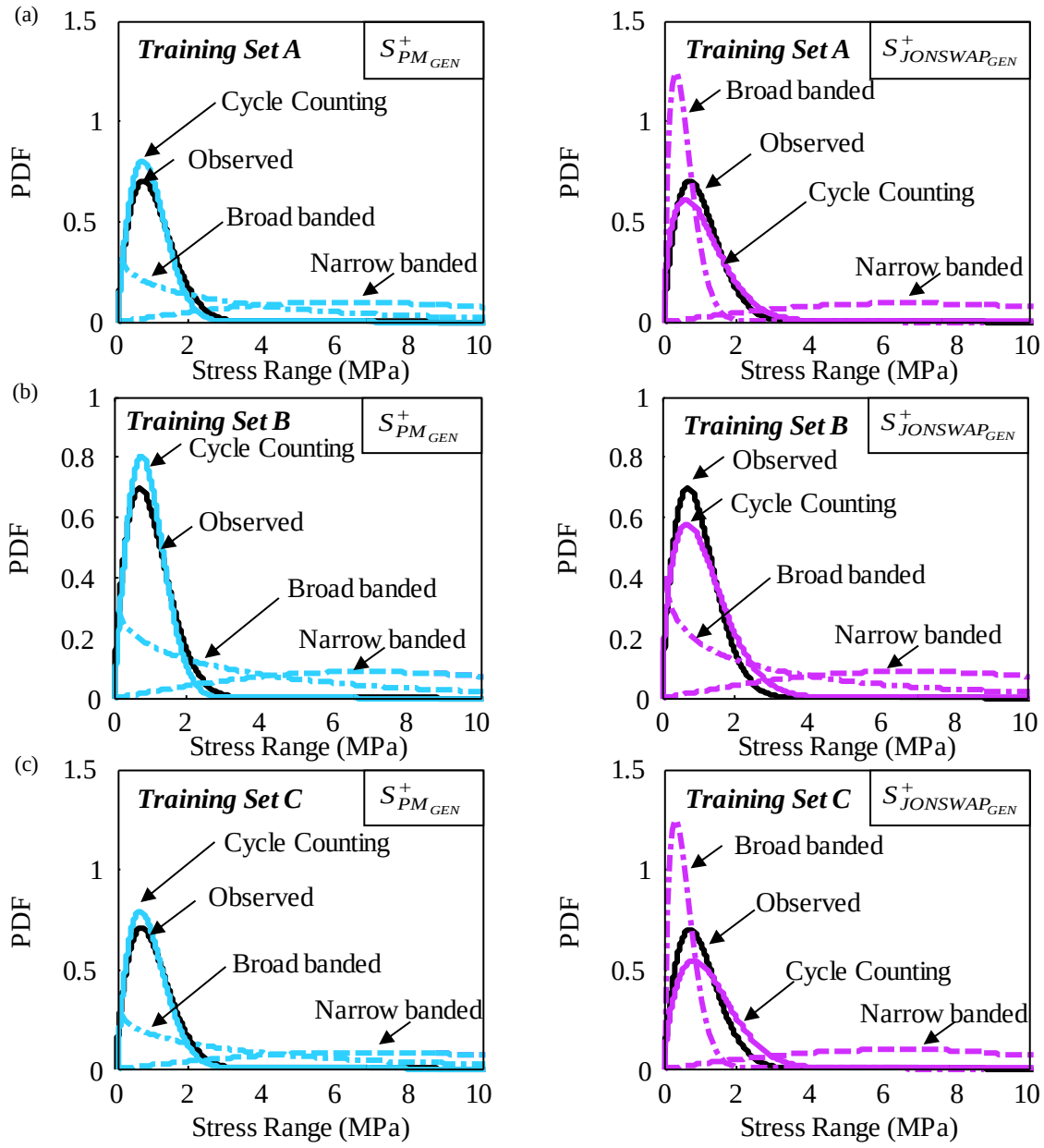

Figure 2.15. Stress range PDFs for (a) Training Set A, (b) Training Set B, and (c) Training Set C estimated using cycling counting methods, the narrow band approximation, and the wide band approximation for the test point equivalent to Run 185.

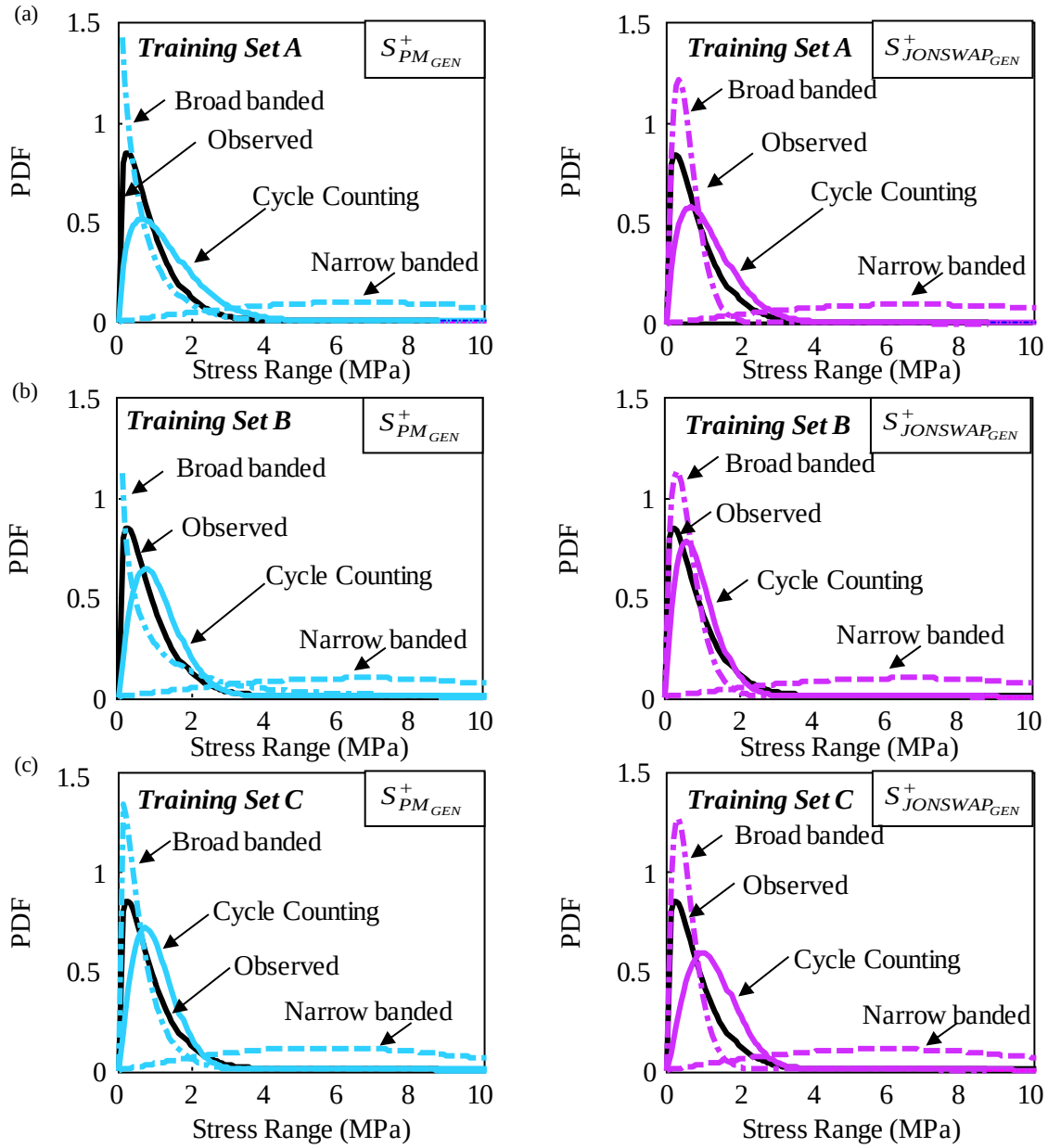

Figure 2.16. Stress range PDFs for (a) Training Set A, (b) Training Set B, and (c) Training Set C estimated using cycling counting methods, the narrow band approximation, and the wide band approximation for the test point equivalent to Run 100.

Table 2.8. Observed and Predicted Stress range parameters for the test point equivalent to Run 100

Data Source	Method	Stress Range (MPa)					
		Case A		Case B		Case C	
		Mean	Standard Deviation	Mean	Standard Deviation	Mean	Standard Deviation
Observed Data	Cycle Counting	0.123	0.104	0.123	0.104	0.123	0.104
Predicted PSD - $JONSWAP_{GEN}$	Cycle Counting	0.242	0.152	0.128	0.08	0.182	0.099
	Broad Banded	0.079	0.055	0.086	0.061	0.077	0.0544
	Narrow Banded	1.200	0.625	1.226	0.638	1.088	0.568
Predicted PSD - PM_{GEN}	Cycle Counting	0.160	0.087	0.155	0.094	0.144	0.0835
	Broad Banded	0.104	0.115	0.219	0.303	0.085	0.078
	Narrow Banded	1.186	0.618	1.226	0.639	1.013	0.529

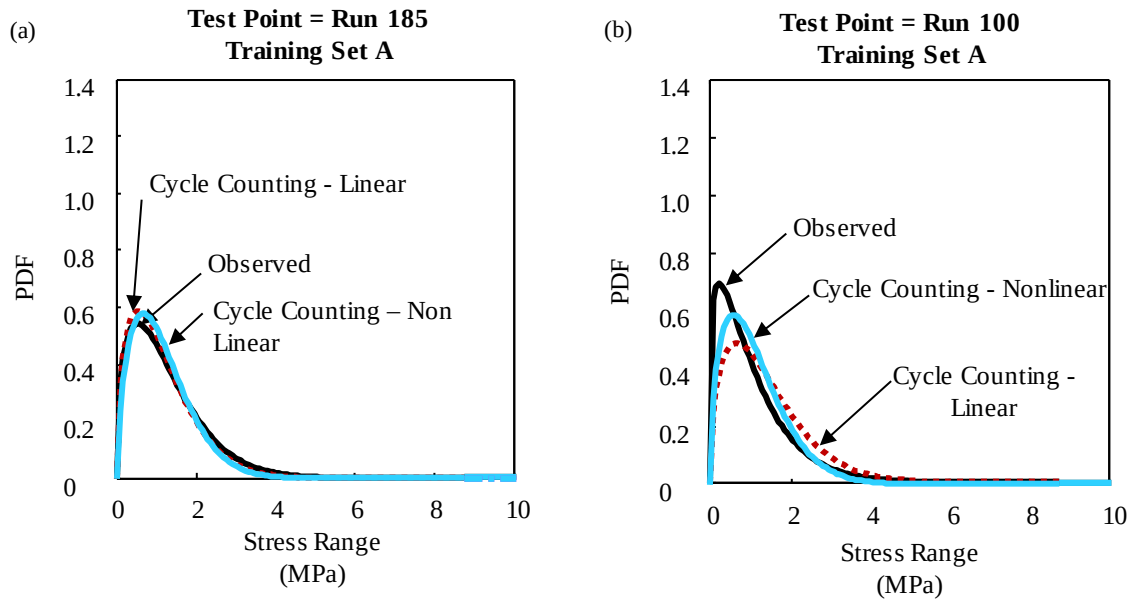

Figure 2.17. Stress range PDFs for (a) Run 185 and (b) Run 100 estimated using cycling counting methods applied to the synthetic data predicted with linear prediction surface, the nonlinear prediction surface, and the observed data.

Table 2.9. Percent difference in the estimated stress range parameters for test points equivalent to Run 185 and 100.

Test Point	Response Surface	Percent Difference	
		Scale Parameter, λ	Shape parameter, κ
Run 185	Nonlinear	6.60%	14.00%
	Linear	7.70%	4.61%
Run 100	Nonlinear	13.60%	25.90%
	Linear	37.20%	22.80%

2.9.3.4. And fatigue damage

Fatigue damage accumulation indices are calculated by assuming an operational rate of 2/3 (i.e., it is assumed that the ship is active for a total time of 2/3 of a year) and Equations 2.21 and 2.22. Given the location of the T2-4 sensor on the aluminum HSV2-Swift, the mean of the logarithm of fatigue coefficient, *A* for the structural detail is 11.47 and the slope of the S-N line in logarithm scale, *m*, is 3.37 (Collette and Incecik 2006; Tveiten 1999). Table 2.10 lists the annual damage index predicted for the test point using the synthetic data generated from the predicted PSD with the generalized Pierson-Moskowitz fitting function for training sets A, B, and C. Values for the annual damage index estimated from the observed SHM data for the test point are also included. The accuracy of the approach is dependent on the available data as shown in Table 2.10 for training sets A, B and C for both for the test point equivalent to Run 185 and Run 160. The damage index predicted for the test point for training sets A is the most accurate, due to the larger set of available SHM data. The larger set of available data has a reduced dependency on a small number of individual runs which may have experienced technical

malfunctions. Furthermore, the fatigue damage estimates based on the nonlinear surface outperform those developed from the linear surface, as shown in Table 2.11.

Table 2.10. Prediction of damage index for the test points based on the linear prediction surface for the 3 training sets. The stress ranges estimated from cycle counting methods applied to the synthetic data for the PM_{GEN} PSD.

Test Point	Case	Annual Damage Index (observed data)	Annual Damage Index (predicted data*)	Percent Difference
Run 185	A	0.0121	0.0116	4.12
	B	0.0121	0.0131	8.13
	C	0.0121	0.0141	16.3
Run 160	A	0.019	0.0146	23.3
	B	0.019	0.0177	6.52
	C	0.019	0.0091	52.3

Table 2.11. Prediction of damage index for the test points based on the linear and nonlinear prediction surfaces. The stress ranges estimated from cycle counting methods applied to the synthetic data for the PM_{GEN} PSD.

Test point	Response Surface	Fatigue Damage Index	Percent Difference from Observed
Run 185	Observed	0.0121	-
	Nonlinear	0.0116	4.1%
	Linear	0.0129	6.8%
Run 100	Observed	0.019	-
	Nonlinear	0.0173	8.8%
	Linear	0.0242	27.1%

2.10. CONCLUSIONS

This chapter, based on research reported in Mondoro et al. (2016b; 2017d), develops the methodology to predict the structural response of ship hulls based on available SHM data. In general, SHM data populates only a portion of the potential operating conditions for the vessel, but includes essential information on the as-built condition of the structure and the actual loads acting on the structure. However, in order to assess the long term hull performance, structural response in all cells must be known. This chapter details the proposed methodology for quantifying the low and high frequency content of an observed structural response under known operational conditions. The methodology is validated against SHM data from sea keeping trials of the HSV2 Swift. Furthermore, this research established a theoretically-based, non-linear prediction surface that can be used to estimate unobserved structural responses based on observed SHM data. The proposed methodology for integrating available SHM data into fatigue damage estimates is applied to data from sea keeping trials of the HSV2 Swift. The following conclusions are drawn:

- The proposed method can predict the structural response in an unobserved cell. This allows essential information regarding the as-built condition and the actual loads acting on the structure, normally captured in the SHM data, to be integrated into the fatigue life prediction.
- The PSD functions of ship SHM data can be fitted with the generalized JONSWAP function and the generalized Pierson-Moskowitz function proposed. The aforementioned functions fit the observed SHM data but are most applicable to the responses observed for a 180° heading angle for the HSV-2 Swift. While

this may vary from ship to ship, the consideration of both the low frequency and high frequency when predicting the PSD in unobserved cells is shown to be critical to estimating the fatigue damage.

- The two theoretically-based nonlinear prediction surfaces outperform linear surfaces in estimating low frequency response characteristics. For high frequency characteristics, the nonlinear and linear surfaces are comparable in their performance with linear surfaces occasionally outperforming the nonlinear ones. The polynomial nonlinear surface is preferred as it is shown to be more robust.
- By predicting the PSD functions for unobserved cells, both time domain and spectral based methods can be employed to estimate the fatigue damage accumulation. The proposed method distinguishes between the low and high frequency content of the signal and predicts the PSD in unobserved cells accordingly. The accuracy of the predicted values, however, vary with the availability of data. The results from the illustrative example indicate that the proposed approach can predict, for head sea condition and speed 15 knots, the mean and standard deviation of the stress range within 7% and 8% error, respectively, using the data generated from the fitted Pierson-Moskowitz PSD.
- With the observed SHM data for the stress response found to be Gaussian, synthetic data for unobserved cells is generated by simulating an instance of the random process from the predicted PSD. For the discussed application, stress time histories were used as the SHM data. If, however, strain time histories were used,

the synthetic strain data could further be used in nonlinear fatigue crack growth analysis.

The work presented in this chapter represents significant advancements in the field of uncertainty quantification, however future research is still needed in this field. Further advancements to the nonlinear predictions surfaces may include the development of separate functional forms for the high frequency parameters. The nonlinear forms developed here are based on the theoretical relationships of wave bending moments, which are govern low frequency responses. The high frequency response, however, are typically governed by impact and slam loads. Additionally, the accuracy of the recorded SHM data is not included in the proposed methodology, but remains a pressing problem for ship managers.

CHAPTER 3

RISK-BASED COST-BENEFIT ANALYSIS FOR THE RETROFIT OF BRIDGES EXPOSED TO EXTREME HYDROLOGIC EVENTS

3.1. OVERVIEW

This chapter focuses on the performance assessment and management of bridges vulnerable extreme hydrologic events. Bridges exposed to flooding, hurricanes, tsunamis, and other extreme hydrologic events have been observed to fail due to deck dislodgement, pier failure, or foundation failure. However, the risk assessment and retrofit methodologies for these bridges have typically only been developed around a single failure mode. The research included in this chapter addresses this gap by integrating the three observed failure modes for bridges vulnerable to extreme hydraulic events into a comprehensive risk assessment framework. Through the use of an event tree, the methodology accounts for the different consequences of failure associated with the different failure modes. Bridge management strategies are investigated to determine the effectiveness of the retrofit actions with respect to their benefit (i.e. reduction in risk) and costs. An illustrative example for riverine bridges under various exposure scenarios is presented. The risk assessment and benefit-cost analysis elucidate the need to incorporate all pertinent failure modes of the structure by highlighting the competing nature of different failure modes. The illustrative example also shows that the effective management of structures is site-specific, and, that the intensity of the hazard at the bridge location affects which management strategy is preferred. The sensitivity to

exposure level indicates that the optimal management of the structure should incorporate considerations for potential future changes in the intensity and frequency of the hazard.

3.2. INTRODUCTION

Managing bridges vulnerable to extreme natural hazards is driven by the need to preserve the functionality of the transportation network and mitigate the economic, environmental, and social impacts of bridge failures. Bridge failures such as the Schoharie Creek Bridge in New York due to flooding (LeBeau and Wadia-Fascetti 2007), the US-90 Biloxi-Ocean Springs Bridge due to Hurricane Katrina (Padgett et al. 2008), and the Utatsu Bridge during the tsunami following the 2011 Tohoku-Oki Earthquake (Akiyama et al. 2013) are a few examples where extreme hydrologic events have caused bridge failures. These failures do not imply that bridges are not designed considering hydraulic loads. Bridges are designed with respect to scour (Arneson et al. 2012; Zevenbergen et al. 2012; Shan et al. 2012; AASHTO 2012), hydraulic forces on bridge piers due to water pressure and debris (Zevenbergen et al. 2012; AASHTO 2012, Parola et al. 2000), and uplift and transverse forces on the bridge deck (Kerenyi et al. 2009; AASHTO 2008). However, floods, hurricanes, and tsunamis are low-probability high-consequence events that require the shift towards risk-based design and management methods.

Risk-based planning for the optimal retrofit of bridges vulnerable to extreme hydrologic hazards is complicated by the presence of multiple failure components and their interdependencies. For flooding events, scour, and the resulting foundation failure, is the predominant failure mode (Melville and Coleman 2000; Wardhana and Hadipriono 2003; Wang et al. 2012; Anderson et al. 2017). However, in extreme cases, piers and

decks may also fail as a result of the debris impact or extreme water pressures (LeBeau and Wadia-Fascetti 2007; Melville and Coleman 2000; Wardhana and Hadipriono 2003; Wang et al. 2012; Anderson et al. 2017; Lebbe et al. 2014; Schmocker and Hager 2011). Coastal bridges vulnerable to hurricanes and coastal storms may fail due to wave and surge loading; typical structural damage includes deck unseating due to inadequate connections to the substructure. However, scour, debris impacts, and extreme hydraulic pressures may cause failures of the foundations and piers during these events as well (Padgett et al. 2008; Okeil and Cai 2008; Robertson et al. 2007; Douglass et al. 2004). The immense hydraulic loads stemming from tsunamis have completely washed away bridge decks, damaged bridge piers, and undermined pier foundations and abutments causing failure (Akiyama et al. 2013; Kawashima et al. 2012; Ghobarah et al. 2006; Seville and Metcalfe 2005). Thus, it has been observed that bridges may be rendered unpassable by failures in their foundations, piers, and/or deck due to extreme hydrologic hazards.

However, when it comes to risk assessment and management of bridges, there is a noticeable gap between observed failure modes and those included in risk assessment methodologies. For instance, the risk assessment of bridges exposed to flooding typically includes only scour (Lagasse et al. 2013; Stein et al. 1999; Yanmaz and Apaydin 2011; Johnson and Niezgoda 2004). Alternatively, some researchers have addressed the failure of decks during floods with respect to debris impact and flow blockage to assess bridge performance (Schmocker and Hager 2011; Lyn et al. 2007). However, their optimal risk management strategies have typically been developed irrespective of considerations for

debris impact on pier and deck failures; they have only included scour and the resulting foundation failure (Stein et al. 1999; Yanmaz and Apaydin 2011). By doing so, the adverse effects that debris may have on the vulnerability to foundation failure (i.e. scour depths exacerbated by flow around debris) are systematically disregarded (Parola et al. 2000). Current methodologies for assessing the life-cycle risk of bridges vulnerable to hurricanes include deck unseating and pier failure (Kameshwar and Padgett 2014; Ataei and Padgett 2013a), and risk management strategies have focused on deck dislodgement (Mondoro et al. 2017c). It is important to note that foundation performance has been omitted from both risk assessment and management procedures in that research. For the tsunami hazard, risk assessment frameworks include bridge deck and pier failures but omit scour and the performance of the foundation (Akiyama et al. 2013; Yim 2005; Lau et al. 2011). Therefore, it can be seen that the development of optimal management strategies for bridges vulnerable to extreme hydrologic events has failed to capture the complete nature of bridge failures (i.e. the failure of the deck, piers, and/or foundations).

A management strategy includes all of the retrofits that are applied to the bridge during its service life. Retrofits are improvements made to a bridge to reduce its likelihood of failure. Deck retrofits may include the application of restrainers and shear keys with the objective of increasing the capacity to resist deck unseating failures. Piers may be retrofitted with steel jackets in order to increase their strength. Riprap may be added as a retrofit to foundations in order to limit scour. However, bridge retrofit options may have adverse effects on the overall performance of the bridge due to the interdependencies of failure modes. For example, restrainers or shears keys, which may

reduce the probability of deck dislodgement, transfer the hydraulic loads to the column and foundation and may increase the probability of failure of those components. Furthermore, by limiting displacement of the deck, submerged flow contraction scour depths may substantially decrease foundation capacity and increase the probability of failure of the foundation. The interdependencies of bridge failure modes and retrofit options have been included in seismic retrofit management. Padgett et al. (2010) included the demand increase on the piers due retrofitting the bridge with structural restraints between the deck; by increasing the capacity to resist deck failure, the demand on the pier was affected.

Due to the multiple, dependent failure modes of bridges vulnerable to extreme hydrologic events, and the recognized importance of including all modes when developing optimal management plans to avoid any adverse effects of retrofit, it is essential to develop a systematic method for evaluating risk and assessing the benefit of retrofit actions. Risk accounts for the probability of failure and the social, economic, and environmental consequences of the failure. Risk metrics have been used to prioritize management strategies and aid in the decision-making process (Stein et al. 1999; Kameshwar and Padgett 2014; Mondoro et al. 2017c; Zhu and Frangopol 2013). Multi-objective formulations have been developed around minimizing life-cycle costs, including initial costs and management costs, and minimizing life-cycle risk (Mondoro et al. 2017c; Dong et al. 2014a; Liu and Frangopol 2006). While these formulations provide insight regarding the tradeoff of life-cycle risk and life-cycle costs, the benefit-cost ratio is an alternative metric which provides a single value to express cost with respect to risk.

The benefit-cost ratio *BCR* normalizes the benefit (i.e. the reduction in life-cycle risk) to the life-cycle cost. This ratio not only provides a way to prioritize management strategies but also helps in identifying which ones are profitable (i.e. have a benefit higher than the cost, *BCR* >1). Benefit-cost ratios have been used to prioritize seismic retrofit options and the repair of aging infrastructures (Padgett et al. 2010; Walbridge et al. 2012; Dong et al. 2015; Thoft-Christensen 2012).

This research examines the importance of including all essential failure modes when assessing the risk and evaluating the cost-effectiveness of management strategies for bridges vulnerable to extreme hydrologic events. Deck, pier, and foundation failure are all included as the failure modes in this research since they best reflect the observed failure modes for bridges exposed to floods, hurricanes, and tsunamis. The methodology proposed for risk assessment systematically accounts for the different failure modes, as well as their respective consequences. An illustrative example is presented for a riverine bridge vulnerable to flooding. However, the methodology can be applied to other hydrologic events. The illustrative example evaluates the effectiveness of management strategies in terms of their benefit-cost ratios. Multiple exposure scenarios are included to highlight the importance of site-specific variations in hazard on the cost-effectiveness of retrofit.

3.3. MULTIPLE FAILURE MODES UNDER HYDRAULIC LOADS

Bridges may be rendered unpassable by failures in their foundations, piers, and/or deck. Hydraulic pressures on the deck may dislodge the deck from the pier causing deck failure. Hydraulic loads on the bridge piers, in combination with axial, shear, and bending

transferred from the deck, may cause pier failure. Scour due to stream flow may undermine the foundation and the demand on the foundation due to hydraulic loads may cause foundation failure. Bridge failure is defined as the event where the bridge deck, pier, and/or foundation fails, since all events result in the bridge being taken out of service. The hydraulic loads and failure modes are summarized in Figure 3.1.

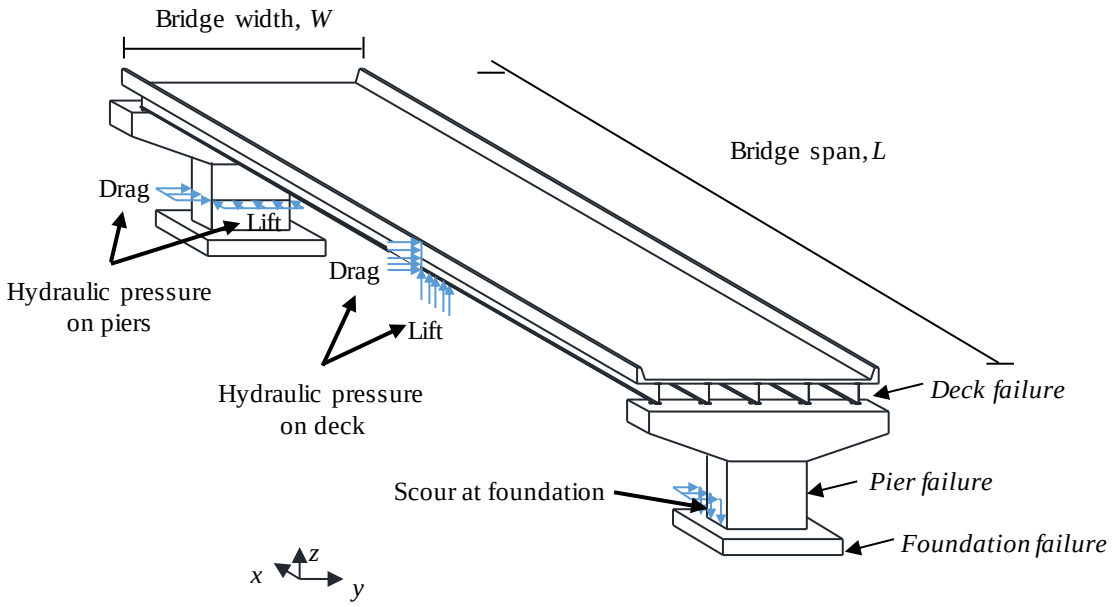

Figure 3.1. Hydraulic pressures on the bridge deck and pier and scour at the foundation of bridges over water may cause deck failure, pier failure, and/or foundation failure rendering the bridge impassable.

3.3.1. Deck Failure

When bridge decks are submerged, or partially submerged, the flowing water imparts hydraulic loads on the deck including drag $F_{D,deck,}$, lift $F_{L,deck}$, and overturning moment $M_{CG,deck}$. The drag force is in the transverse direction of the bridge deck, shown in Figure 3.2 as the + *y* direction. The uplift force on the deck is in the opposite direction of gravity, shown as the + *z* direction in Figure 3.2. The methodology for estimating the hydraulic forces on the bridge deck is found in Kerenyi et. al (2009) and summarized below.

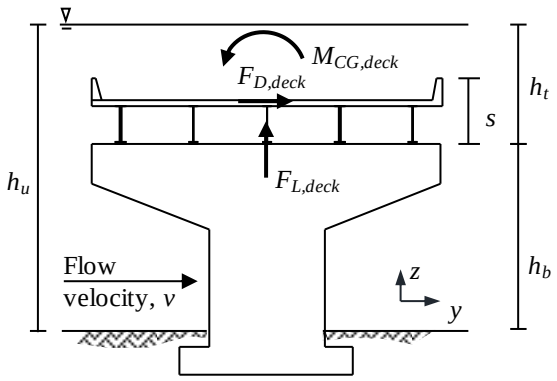

Figure 3.2. Hydraulic drag, lift, and overturning moment when the bridge deck is submerged.

The drag force on the deck is defined as

$$F_{D,deck} = \frac{1}{2} C_{D,deck} \rho v^2 (Ls) \qquad \text{if } h^* \geq 1 \tag{3.1}$$

$$F_{D,deck} = \frac{1}{2} C_{D,deck} \rho v^2 \left[L(h_u - h_b) \right] \qquad \text{if } h^* < 1 \tag{3.2}$$

where h^* is the inundation ratio

$$h^* = \frac{h_u - h_b}{s} \tag{3.3}$$

$C_{D,deck}$ is the coefficient of drag on the deck, ρ is the density of water, v is the flow velocity, L is the span length of the bridge, s is the deck thickness, h_u is the height of the water, and h_b is the height of the low chord of the bridge deck. The hydrodynamic lift force $HF_{L,deck}$ is

$$HF_{L,deck} = \frac{1}{2} C_{L,deck} \rho v^2 (LW) \tag{3.4}$$

where $C_{L,deck}$ is the coefficient for lift on the deck, W is the width of the bridge deck. The total lift force on the deck is the summation of the hydrodynamic lift force and the buoyancy force $BF_{L,deck}$ (2009)

$$F_{L,deck} = HF_{L,deck} + BF_{L,deck} \tag{3.5}$$

The overturning moment on bridge deck is

$$M_{CG,deck} = \frac{1}{2} C_{M,deck} \rho v^2 (LW^2) \tag{3.6}$$

where $C_{M,deck}$ is the coefficient for the flow induced overturning deck moment.

Deck failure is considered to occur when the deck is dislodged from the pier. This can occur when there is transverse failure or uplift failure. Transverse failure is defined as the event where the drag force exceeds the transverse resistance between the deck and the piers and the uplift force does not exceed the uplift capacity of the bridge. For bridges with no additional transverse restraint (e.g. no shear keys, steel restrainers, anchor bolts, among others), the transverse capacity of the bridge deck is the friction force μSW where μ is the coefficient of friction and SW is the self-weight of the deck (AASHTO 2008). The transverse failure event can then be defined as

$$E_{transverse} = \left(F_{D,deck} > \mu\left(SW - F_{L,deck}\right)\right) \cap \left(F_{L,deck} \leq SW\right) \tag{3.7}$$

Uplift failure is defined as the event where the uplift forces exceed the uplift capacity of the bridge and there is a non-zero drag force. In the case of a bridge with no additional vertical restraint (e.g. no steel restrainers, anchor bolts, among others), the uplift capacity of the bridge is equal to the self-weight of the deck, and the uplift failure event can be defined as

$$E_{uplift} = \left(F_{L,deck} > SW\right) \cap \left(F_{D,deck} > 0\right) \tag{3.8}$$

Therefore, when there is no additional restraint added to the structure, probability of deck failure is defined as

$$P_{f,deck} = P\left[\left(E_{transverse}\right) \cup \left(E_{uplift}\right)\right] \tag{3.9}$$

When retrofit measures are applied to the structure, the additional transverse and vertical capacities are included in the above equation accordingly. This varies extensively based on the retrofit option. For the retrofit options included in the illustrative example, this process is detailed in the application section of this chapter.

3.3.2. Pier Failure

The flow velocity varies with the height of the water but, in design procedures, it is often approximated as constant over the entire water depth. This research follows this conservative design assumption when estimating the forces acting on the submerged structural components of a bridge. The direction of flow may approach the pier at an angle to the longitudinal axis of the pier resulting in both drag and lift pressures on the

pier. The moment demand at the base of the pier is due only to the hydraulic loads acting on the pier, when $h_u < h_b$, is

$$M_{x,pier} = \frac{1}{2} p_{D,pier} h_u^{\ 2} \tag{3.10}$$

$$M_{y,pier} = \frac{1}{2} p_{L,pier} h_u^{\ 2} \tag{3.11}$$

where $M_{x,pier}$ is the moment about x-axis on pier and $M_{y,pier}$ is the moment about y-axis on pier, and where the drag and lift pressures are, respectively,

$$p_{D,pier} = \left(C_{D,pier} \frac{\gamma_w}{2g} v^2 \right) a_{pier} \tag{3.12}$$

$$p_{L,pier} = \left(C_{L,pier} \frac{\gamma_w}{2g} v^2 \right) l_{pier} \tag{3.13}$$

and $C_{D,pier}$ and $C_{L,pier}$ are the coefficients of drag and lift on the pier (AASHTO 2012), γ_w is the specific weight of water, l_{pier} is the length of the pier, and a_{pier} is the width of the pier. When $h_u > h_b$, i.e. the deck is submerged or partially submerged, the moment demand must be modified to reflect additional hydraulic loads on the deck, if the deck has not failed. The base of the pier is also subjected to the axial load due to the self-weight of the bridge deck, girders, and pier. Since the failure during extreme hydrologic events is being evaluated, it is assumed that there is no traffic on the bridge and any live-load contributions are omitted.

The probability of failure of the pier is evaluated by checking that the combined axial-bending limit state is not violated

$$P_{f,pier} = P\left[\left(\left(\frac{M_{x,pier}}{M_{nx,pier}}\right)^{\alpha} + \left(\frac{M_{y,pier}}{M_{ny,pier}}\right)^{\alpha}\right) > 1\right] \tag{3.14}$$

where $M_{nx,pier}$ is the moment capacity about x-axis of pier, $M_{ny,pier}$ is the moment capacity about y-axis of pier, and α is a constant dependent on the ratio between applied axial load and axial load capacity (Bresler 1960). Alternatively, the load interaction surface can be developed for the reinforced concrete section and checked against the applied loads (AASHTO 2012).

3.3.3. Foundation Failure

The depth of sediment removed from the stream bed due to flowing water is referred to as the total scour depth at a bridge. Streambed degradation, local scour, and contraction scour contributes to the total scour depth. Degradation is a long-term lowering of the stream bed due to sediment transport. Local scour is the removal of material around the piers and abutments due to the local flow obstructions. Contraction scour is the removal of material across the stream width due to a constriction in flow.

Local scour is typically estimated through the use of the Hydraulic Engineering Circular HEC-18 pier scour equation for scour due to an exposed pier stem in flow $y_{s,pier}$ (Arneson et al. 2012)

$$y_{s,pier} = 2.0K_1K_2K_3\left(\frac{a_{pier}}{h_u}\right)^{0.65} Fr^{0.43}h_u \tag{3.15}$$

where K_1 is the correction factor for pier nose shape, K_2 is the correction factor for angle of attack of flow, K_3 is the correction factor for bed condition, and Fr is the Froude number

$$Fr = \frac{v}{\sqrt{gh_u}} \tag{3.16}$$

where g is the gravitational constant. For complex pile foundations the local scour depth is estimated through superposition of scour components, where the components include scour due to the pier $y_{s,pier}$, pile cap $y_{s,pc}$, and pile group $y_{s,pg}$ The components are estimated individually as defined in Arneson et al. (2012) and then summed together. The total local scour is then defined as

$$y_{s,local} = y_{s,pier} + y_{s,pc} + y_{s,pg} \tag{3.17}$$

and is shown in Figure 3.3a.

Contraction scour is the removal of material across the stream width due to a constriction in flow. A narrowing of the channel width at the bridge is typically the constriction that is considered. However, submerged flow is also an instance of flow constriction where flowing water is forced under the bridge deck inducing scour, as shown in Figure 3.3b. Submerged flow contraction scour $y_{s,SFCS}$ is defined as

$$y_{s,SFCS} = \left(\frac{V_{ue}h_{ue}}{K_u D_{50}^{1/3}}\right)^{6/7} + \left[0.2\left(\frac{h_b h_t}{h_u{}^2}\right)^{0.2}\left(1-\frac{h_w}{h_t}\right)^{-0.1} - 1\right]h_b \tag{3.18}$$

where V_{ue} is the effective average approach velocity directed under the bridge, h_{ue} is the effective approach flow depth directed under the bridge, K_u is a constant equal to 11.17 ft^2/s, D_{50} is the median grain size, h_t is the flow depth above the bottom of the bridge superstructure, h_w is the height of the weir flow overtopping the bridge (Shan et al. 2012). The total scour depth used to evaluate the capacity of the pier is

$$y_s = y_{s,SFCS} + y_{s,local} \tag{3.19}$$

when submerged flow contraction scour and local scour are the main sources of sediment removal.

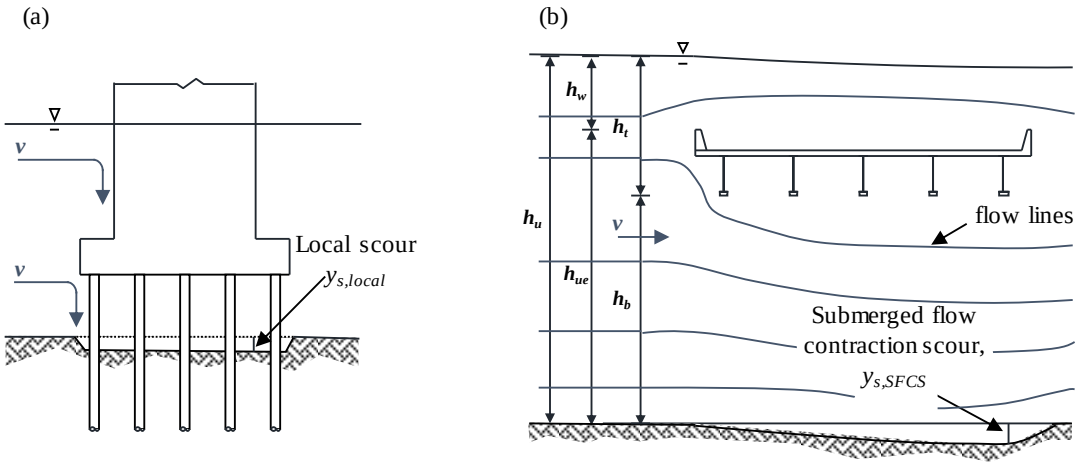

Figure 3.3. Contributions to the total scour depth include (a) local scour due to local obstructions in flow and (b) contraction scour due to submerged flow conditions.

The above scour equations are the conservative, deterministic scour approximations used in design. As such, this is used as the scour estimation method for this research. Alternatively, researchers have investigated probabilistic scour methodologies, but a comprehensive, probabilistic method is not readily available for submerged flow contraction scour estimates or local scour estimates for complex pile groups.

The probability of failure can be estimated for the foundation considering the axial capacity, lateral capacity, and structural capacity as

$$P_{f,found} = P\left[\left(P_{pg} > R_{pg,c}\right) \cup \left(V_{pg} > R_{pg,l}\right) \cup \left(\frac{P_p}{P_{n,p}} + \frac{8}{9}\left(\frac{M_{x,p}}{M_{nx,p}} + \frac{M_{y,p}}{M_{ny,p}}\right) > 1\right)\right] \tag{3.20}$$

where P_{pg} is the axial load on pile group, V_{pg} is the lateral load on pile group, $R_{pg,c}$ is the resistance of pile group to axial compressive loads, $R_{pg,l}$ is the resistance of pile group to lateral loads, P_p is the axial load on pile in pile group, $P_{n,p}$ is the nominal axial capacity of pile in pile group, $M_{x,p}$ is the moment about x-axis on pile in pile group, $M_{y,p}$ is the moment about y-axis on pile in pile group, $M_{nx,p}$ is the moment capacity about x-axis of pile in pile group, and $M_{ny,p}$ is the moment capacity about y-axis of pile in pile group (AASHTO 2012).

3.3.4. Bridge Failure

The bridge may fail through deck, pier, and/or foundation failure modes; if either the deck, pier, or foundation fails, the bridge is considered to fail since it is rendered impassable. The event tree in Figure 3.4 shows the mutually-exclusive collectively exhaustive set of events considered in this work for failure for a bridge exposed to hydraulic loads. Each branch represents a mutually-exclusive event that together form a collectively exhaustive set of possible outcomes. The probability of bridge failure can be written as

$$P_{f,bridge} = \sum_{i=1}^{7} P_{B,i} \tag{3.21}$$

where $P_{B,i}$ is the probability of branch i. It may also be useful to track the probability of failure associated with deck failure, pier failure, and foundation failure separately in order to understand the interdependencies between failure modes and the importance of accounting for all when making management decisions. The probability of deck failure $P_{f,deck}$ can be expressed as the summation of the probability of branches 1, 2, 3 and 4. The

probability of pier failure $P_{f,pier}$ can be expressed as the summation of the probability of branches 1, 2, 5 and 6. The probability of foundation failure $P_{f,found}$ can be expressed as the summation of the probability of branches 1, 3, 5 and 7.

$$P_{f,deck} = P_{B,1} + P_{B,2} + P_{B,3} + P_{B,4} \tag{3.22}$$

$$P_{f,pier} = P_{B,1} + P_{B,2} + P_{B,5} + P_{B,6} \tag{3.23}$$

$$P_{f,found} = P_{B,1} + P_{B,3} + P_{B,5} + P_{B,7} \tag{3.24}$$

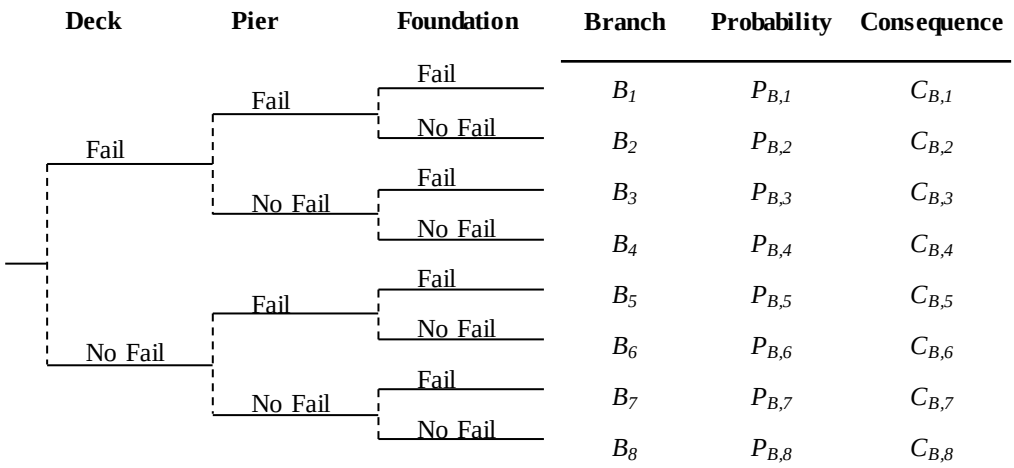

Branch	Probability	Consequence
B_1	$P_{B,1}$	$C_{B,1}$
B_2	$P_{B,2}$	$C_{B,2}$
B_3	$P_{B,3}$	$C_{B,3}$
B_4	$P_{B,4}$	$C_{B,4}$
B_5	$P_{B,5}$	$C_{B,5}$
B_6	$P_{B,6}$	$C_{B,6}$
B_7	$P_{B,7}$	$C_{B,7}$
B_8	$P_{B,8}$	$C_{B,8}$

Figure 3.4. Event tree for bridge response to hydraulic loads composed of mutually exclusive, collectively exhaustive events, with the probability of occurrence and consequence associated with each branch i denoted at $P_{B,i}$ and $C_{B,i}$.

3.4. RISK

Risk is a useful metric to assess the performance of a structure exposed to natural hazards since it accounts for the social, economic, and environmental consequences of failure during extreme events as well as the likelihood of the failure event. Risk is defined as

$$R = \kappa P_f \tag{3.25}$$

where P_f is the probability of failure and κ is the total, monetarized consequences associated with failure. This includes considerations for direct and indirect economic, social, and environmental costs

$$\kappa = \kappa_{reb} + \kappa_d + \kappa_{tl} + \kappa_{rem} \tag{3.26}$$

where κ_{reb} is the rebuilding cost, κ_d is the costs associated with the detour, κ_{tl} is the time loss consequence, and κ_{rem} is the removal costs

$$\kappa_d = C_v L_d T_d ADT \tag{3.27}$$

$$\kappa_{tl} = \left[C_{tva} O_{car} \left(1 - \frac{T_{trk}}{100} \right) + C_{tvtk} O_{trk} \frac{T_{trk}}{100} \right] \frac{L_d T_d ADT}{V} \tag{3.28}$$

$$\kappa_{rem} = C_{rem} WL \tag{3.29}$$

where C_v is the average running cost for vehicles, L_d is the length of the detour, T_d is the duration of the detour, ADT is the average daily traffic, C_{tva} is the value of time per adult, O_{car} is the average car occupancy, O_{trk} is the average truck occupancy, T_{trk} is the average daily truck traffic, C_{tvtk} is the time value of the truck, C_{rem} is the cost of removal per square area, and V is the average detour speed (Stein et al. 1999).

The formulation of risk as defined in Equation 3.25 is useful in instances where the consequence of failure κ takes a single value regardless of failure mode. However, a bridge failure may have different consequences based on which failure mode occurs. That is, if only the deck fails, then it may be possible to replace only the deck (i.e. low rebuilding costs) and do so quickly (i.e. in a short period of time with low detour and time-loss costs), resulting in smaller consequences then if the foundation failed and the entire bridge had to be replaced. Therefore, it is more appropriate to calculate the risk in accordance with the failure mode of the structure. This can be accomplished using the event tree in Figure 3.4 where individual consequences can be assigned to each branch in accordance with their appropriate rebuilding costs, detour cost, time loss consequences, and removal costs. The total risk associated with the bridge can then be written as

$$R_{bridge} = \sum_{i=1}^{8} P_{B,i} C_{B,i} \tag{3.30}$$

where $C_{B,i}$ is the consequence associated with branch i.

For comparison, it may also be useful to track the risk associated with deck failure, pier failure, and foundation failure separately in order to understand the interdependencies among failure modes and the importance of accounting for all when making management decisions. The risk only due to deck failure R_{deck} can be expressed as the summation of the risks associated with branches 1, 2, 3 and 4 (shown in Figure 3.4). The risk only due to pier failure R_{pier} can be expressed as the summation of the risks associated with branches 1, 2, 5 and 6. The risk only due to foundation failure R_{found} can be expressed as the summation of the risks associated with of branches 1, 3, 5 and 7

$$R_{deck} = C_{B,1}P_{B,1} + C_{B,2}P_{B,2} + C_{B,3}P_{B,3} + C_{B,4}P_{B,4} \tag{3.31}$$

$$R_{pier} = C_{B,1}P_{B,1} + C_{B,2}P_{B,2} + C_{B,5}P_{B,5} + C_{B,6}P_{B,6} \tag{3.32}$$

$$R_{found} = C_{B,1}P_{B,1} + C_{B,3}P_{B,3} + C_{B,5}P_{B,5} + C_{B,7}P_{B,7} \tag{3.33}$$

3.5. BENEFIT-COST ANALYSIS FOR MANAGEMENT STRATEGIES

The benefit-cost analysis, also referred to as cost-benefit analysis, is a systematic method used to evaluate the performance of alternative options. Benefits, typically expressed as a monetary value, are normalized with respect to the costs of an option in order to prioritize strategies. For a given management strategy, benefit is herein defined as the reduction in life-cycle risk attained by retrofitting the structure and is expressed as

$$Benefit_{MS_i} = R_{bridge,MS_0} - R_{bridge,MS_i} \tag{3.34}$$

where $R_{bridge,MSi}$ is the benefit associated with management strategy i, $R_{bridge,MSo}$ is the life-cycle risk associated with the bridge without retrofit, and $R_{bridge,MSi}$ is the life-cycle risk associated with the management strategy i, MS_i. The benefit-cost ratio BCR for the given management strategy is the ratio between the benefit and the life-cycle costs

$$BCR_{MS_i} = \frac{Benefit_{MS_i}}{C_{MS_i}} \tag{3.35}$$

where C_{MSi} is life-cycle costs associated with the management strategy. Management strategies with higher BCR_{MSi} have larger benefits per monetary unit and should be prioritized. Furthermore, management strategies with a BCR_{MSi} greater than one indicate that the return on the investment is larger than the cost, are denoted as profitable, and

should be implemented. While the benefit in this case is a reduction in risk, profitable is still the terminology that is used to describe management strategies. Similar to risk and probability of failure, it may also be useful to track the *BCR* associated with deck failure, pier failure, and foundation failure separately in order to understand the importance of considering all relevant failure modes when evaluating the cost-effectiveness of a management strategy. Therefore, the *BCR* can be defined for the deck only failure mode by using the risk associated with deck failure when evaluating the benefit. By incorporating that benefit into Equation 3.34 the *BCR* for the deck only failure mode can be defined as

$$BCR_{deck,MS_i} = \frac{R_{deck,MS_0} - R_{deck,MS_i}}{C_{MS_i}} \tag{3.36}$$

Likewise the *BCR* for pier only and foundation only failures can be defined as

$$BCR_{pier,MS_i} = \frac{R_{pier,MS_0} - R_{pier,MS_i}}{C_{MS_i}} \tag{3.37}$$

$$BCR_{found,MS_i} = \frac{R_{found,MS_0} - R_{found,MS_i}}{C_{MS_i}} \tag{3.38}$$

3.6. APPLICATION

An illustrative example is presented for a riverine bridge vulnerable to flooding. The bridge has a span length of 36 m, deck width of 14.3 m, and deck thickness (i.e. the height of the girders, deck, and parapet) of 2.6 m, and pier geometry shown in Figure 3.5. The dead load from the superstructure transferred to the pier is 9900 kN. The pier stem has seventy-six 32.2 mm diameter steel bars equally spaced around its perimeter with a

50 mm cover. The pile cap is supported with HP12x74 piles driven 12 m deep bearing on 48 MPa rock with soil along the length with a skin friction of 80 kPa; the soil line extends 0.61 m above to base of the pile cap.

The riverine bridge is vulnerable to flooding, characterized by flow velocity and height of the water (i.e. the stage height). Observations from gauging stations aid management strategy in the estimation of stream flow characteristics to determine the probability distribution of discharge for a river. Annual stream discharge is typically modeled with a log-Pearson type III distribution and the mean, variance, and skew are estimated based on gauge data (FDOT 2011). This research investigates the effect of exposure on the effectiveness of management strategies by including three exposure cases, A, B, and C, with stream flow discharges as shown in Figure 3.6. The stage height is then estimated with Manning's equation

$$Q = \frac{c}{n} A \left(\frac{A}{P} \right)^{2/3} S^{1/2} \tag{3.39}$$

where Q is the discharge, c is 1.00, n is Manning roughness coefficient, A is the cross-sectional area of flow, P is the wetted perimeter, and S is the channel bed slope (Lagasse et al. 2013). When the profile of the streambed is known, the above equation can be used to determine the flow height given the discharge. The stream flow velocity v is then

$$v = \frac{Q}{A} \tag{3.40}$$

For the illustrative example, the stream is assumed to be an isosceles trapezoid with the banks of the river at a 60deg angle, a bottom width of 36 m, and a slope of 0.00001 m/m. Thus, for this example problem, Equation 3.40 can be used to estimate A and stage

height h_u. In order to account for the underlying epistemic and aleatory uncertainties in stream flow estimation and the stream profile, a model uncertainty factor k_v is introduced (Lagasse et al. 2013). k_v is assumed to be a normally distributed random variable with a mean of 1.0 and a coefficient of variation of 0.15 and modifies Equation 3.40 as

$$v = k_v \frac{Q}{A} \tag{3.41}$$

In this way, flow height and flow velocity are the random variables used to define the hazard.

The management strategies evaluated in the illustrative example include retrofits for bridge deck failure, pier failure, and foundation failure. Steel restrainers and reinforced concrete shear keys are included as deck retrofit options. The steel restrainers limit deck displacement in the transverse (y) and uplift (z) direction; it is assumed that there is no deck displacement in the longitudinal (x) direction. The yield capacity of the steel restrainer is $f_y A_s$, where f_y is the yield strength of the steel and A_s is the area of the steel. In the illustrative example, restrainers with A_s of 143 mm^2 and f_y of 1210 MPa are included. The shear keys restrain transverse displacement based on the shear capacity if the bridge as not been lifted above the height of the key. A quasi-static approach is used to estimate a failure surface for the shear key with respect to flow height and velocity by checking if the hydraulic forces have caused the deck to dislodge. The shear keys included as alternative retrofit measures are 0.25 m tall and are applied to the piers or supports at either end of the bridge span. Retrofit for the pier column could include steel reinforcement to reduce its probability of failure. Riprap is a common retrofit option that armors the stream bed against the removal of material and reduces the potential for

foundation failure. The riprap, however, may also fail if the stream conditions displace the riprap material. The design velocity of the riprap included in the illustrative example is 2.75 m/s.

The consequences associated with failure are the summation of the rebuilding cost of the structure, detour costs, the time-loss costs, and the removal costs. If the bridge foundation and/or piers fail, the entire bridge must be replaced. However, if only the deck fails, only the deck has to be replaced. In this way, the consequences for foundation and/or pier failure are different from the consequences of deck-only failure. The deck-only consequences, including the cost of rebuilding the deck, the removal of the deck, and the detour and time-loss costs associated with a detour duration of 180 days, can be estimated using the information presented in Table 3.1. Likewise, the consequences for pier or foundation failures include the cost of rebuilding the entire structure, the removal costs, and the detour and time-loss costs calculated with a detour duration of 365 days. Only the deck is considered in the removal costs due to the fact that old piers may be left in place to act as flow altering structures or sacrificial piers. This assumption implies that there is no excessive displacement in the piers or foundations; however if these structural components need to be removed as well, the removal costs can be adjusted accordingly.

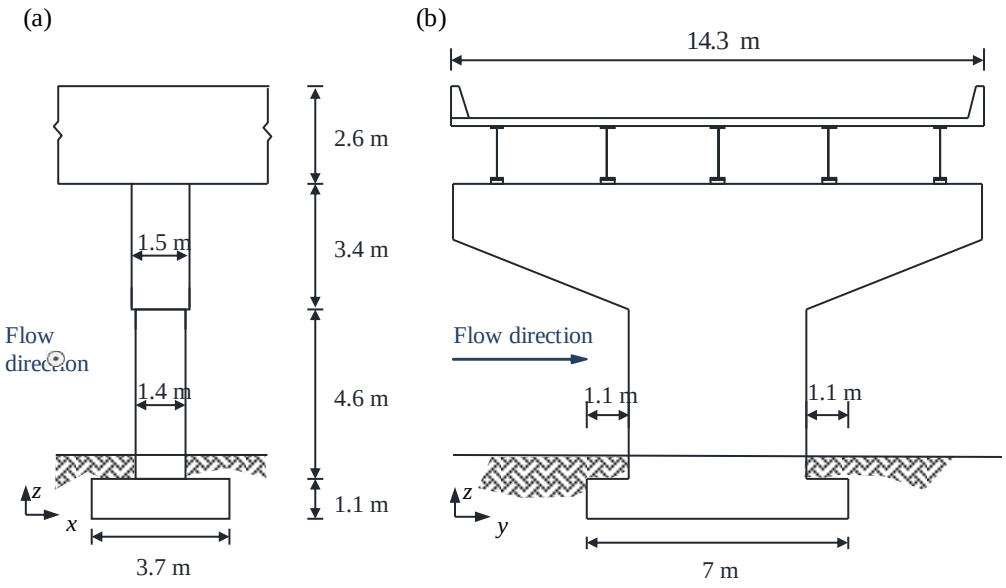

Figure 3.5. Bridge geometry for illustrative example (excluding the foundation piles) in the (a) *x*-*z* plane and (b) the *y*-*z* plane.

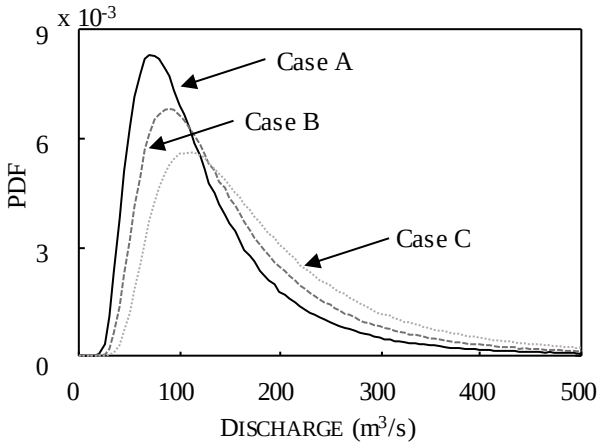

Figure 3.6. Stream discharge for exposure Cases A, B, and C where the discharge follows the Log-Pearson Type III distribution.

Table 3.1. Variables for consequence evaluation

Description	Notation	Value	Reference
Cost of rebuilding the deck (USD)	κ_{reb}	1,880,000	*
Cost of rebuilding entire bridge (USD)	κ_{reb}	2,439,109	*
Removal costs (USD)	κ_{rem}	61,130	(FDOT 2011)
Average running cost for vehicles ($/km)	C_v	0.375	American Automobile Association (2014)
Length of the detour (km)	L_d	8	example
Average daily traffic	ADT	4000	example
Average occupancy of trucks	O_{trk}	1	example
Average vehicle occupancy	O_{car}	1.67	Mallela and Sadasivam (2011)
Average detour speed (km/h)	V	56	example
Value of the truck ($/hr)	C_{tvtk}	20.75	Mallela and Sadasivam (2011)
Value of time per adult ($/hr)	C_{tva}	24.19	Santos et al. (2011)
Average daily truck traffic	T_{trk}	10	example

* estimated with respect to illustrative example and WSDOT (2016), FDOT (2017), and Bradshaw and Baxter (2006)

3.7. RESULTS

The benefit-cost analysis for individual management strategies is evaluated for the example bridge under the river flows expected for the three exposure cases. The management strategies investigated include applying (1) riprap around the pier, (2) 4 restrainers, one at each at the exterior girders of either end of the span, (3) shear keys, (4) riprap and 4 restrainers, and (5) riprap and shear keys. Management strategies are herein denoted as MS_i for i from 1 to 5 for their respective strategy and MS_o is the initial, unmaintained structure. The costs for each management strategy are estimated based on retrofit costs listed in Padgett et al (2010) and Pearson et al (2006) and are listed in Table 3.2.

Table 3.2. Description and costs of management strategies

Management Strategy	Description	Cost (*USD*)
MS_o	Nothing	0
MS_1	Riprap	50000
MS_2	Restrainers	5640
MS_3	Shear keys	5250
MS_4	Riprap and Restrainers	55640
MS_5	Riprap and Shear Keys	55250

The probability and risk of bridge failure is determined for all management strategies for all three exposure cases with Monte Carlo sampling using 10^7 samples and the methodology detailed above (specifically, Equations 3.21 and 3.30). The probability of failure and risk associated with the individual failure modes are also calculated (Equations 3.22-3.24 and 3.31-3.33). The probability of failure and risk for all management strategies under Case A are shown in Table 3.3. For Case A, the initial bridge has a probability of failure of 0.00378. The probability of the deck failing (i.e. 0.00366) is the highest of all failure modes investigated. The foundation has a probability of failure of 1.22E-4 and the pier failure probability was found to be negligible. Furthermore, the pier was found to have negligible effects on the performance of the structure in any of the management scenarios as detailed in Table 3.3 for Case A.

Table 3.3. Probability of failure and risk for initial structure and management strategies

Strategy	Probability of Failure				Risk (*USD*)			
	Deck $P_{f,deck}$	Pier $P_{f,pier}$	Foundation $P_{f,,found}$	Bridge $P_{f,bridge}$	Deck R_{deck}	Pier R_{pier}	Foundation R_{found}	Bridge R_{bridge}
MS_o	0.00366	<1.0E-07	0.000122	0.00378	29510	0	1820	31330
MS_1	0.00366	<1.0E-07	<1.0E-07	0.00366	29510	0	0	29510
MS_2	2.24E-05	<1.0E-07	0.00214	0.00216	180	0	31960	32140
MS_3	<1.0E-07	<1.0E-07	0.00216	0.00216	0	0	32290	32290
MS_4	2.24E-05	<1.0E-07	<1.0E-07	2.24E-05	180	0	0	180
MS_5	<1.0E-07	<1.0E-07	<1.0E-07	<1.0E-07	0	0	0	0

The probability of deck failure, foundation failure, and overall bridge failure is summarized for all management strategies for Case A in Figure 3.7a; pier failure is omitted from Figure 3.7a due to its negligible contributions. Figure 3.7a shows that all management strategies result in a reduction of the probability of bridge failure when compared to the performance of the initial structure. Management strategy 1, applying only riprap, increases the capacity to resist scour and decreases the potential for foundation failure. This results in a reduction in the overall probability of failure of the bridge of 3.2%. This limited reduction is as expected since there is only a small contribution to the failure of the bridge stemming from foundation failure. MS_2, attaching the deck to the pier with steel restrainers, results in a larger reduction in the probability of failure of the bridge (i.e the $P_{f,bridge}$ for the initial structure is reduced by 42% using MS_2). This larger reduction is intuitive since deck failure is the prominent cause for failure of the initial structure. However, it is important to note that the reduction in the probability of failure of the bridge is not equivalent to the reduction in the probability of failure of the deck. This is due to the adverse effects of deck retrofit on foundation performance. By retrofitting the deck, dislodgement becomes less likely, but

the demand on the foundation increases, submerged flow contraction scour intensifies scour depths, and foundation failure becomes more likely. MS_4 and MS_5 include multiple retrofit measures and result in the largest reductions in the probability of bridge failure. Since the multiple retrofit measures include accommodations to prevent deck and foundation failure, the adverse effects of retrofitting for deck dislodgement are mitigated by the addition of riprap.

While every management strategy leads to a decrease in the probability of failure of the structure, there is not a unilateral decrease in risk level when the management strategies are applied. Figure 3.7b shows that there is an increase in life-cycle risk for MS_2 and MS_3 where the R_{bridge} for MS_2 and MS_3 exceeds the line marking the risk level for MS_o. This can be attributed to the higher consequences associated with foundation failure and the adverse effects of deck retrofit on foundation performance. Alternatively, management strategies that reinforce the foundation or address the adverse effects of deck retrofit through the incorporation of multiple retrofit measures, i.e. MS_1, MS_4, or MS_5, result in reductions in risk.

The benefit-cost ratio provides further insight into the effectiveness of the management strategies since it normalizes the benefits, i.e. reductions in risk, by the costs the management strategy. The *BCRs* for each management strategy for Case A is listed in Table 3.4 and shown in Figure 3.8. The *BCRs* are provided with respect to deck failure, foundation failure, and bridge failure. From these results, it becomes clear that it is essential to include all relevant failure modes when assessing the benefits of retrofitting a structure. If, for instance, only the deck failure mode was considered and the *BCR* was

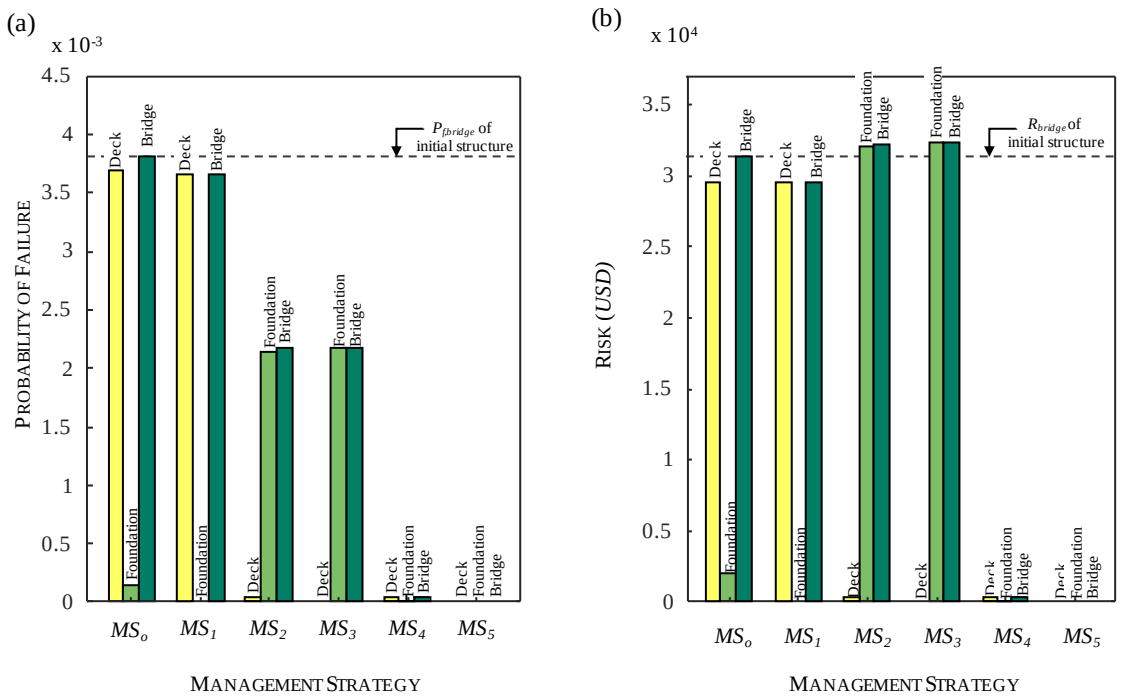

Figure 3.7. The probability of failure (a) and the risk (b) associated with the initial structure MS_o and the five management strategies.

assessed with respect to R_{deck}, management strategies MS_2 and MS_3 would have $BCR > 1$, as shown in Figure 3.8 and Table 3.4. MS_3 would be optimal because it has the larger *BCR*. However, when risk is assessed using all relevant failure modes, i.e. R_{bridge}, MS_2 and MS_3 have *BCRs* have a negative benefit, the smallest *BCRs*, and, are not desirable. Instead, the management strategies that incorporate multiple retrofit measures, i.e. MS_4, or MS_5, yield a reduction in risk, have a positive *BCR*, and are more favorable. The *BCR* for MS_5 is larger than MS_4 and is the preferred management strategy for Case A when using the *BCR* as the decision criteria. However, it is important to note that while MS_5 is optimal, it does not have a positive return on investment and is not strictly profitable.

Exposure Cases A, B, and C represent situations where the flood hazard range from less severe (Case A) to more severe (Case C). The probability of failure of the bridge, the risk, benefit, and benefit-cost ratios were evaluated in the same procedure detailed above. The results are summarized in Table 3.5 and Figure 3.9. The risk associated with the initial structure increases significantly with exposure cases: there is a 135% increase in risk for MS_o in Case B from Case A where there is only a 2.4% increase in mean stream discharge. Likewise for Case C, which is a 4.8% difference (increase) in mean stream discharge from Case A, there is a 410% difference (increase) in risk for the initial structure MS_o. All management strategies, MS_1 to MS_5, show similar changes in risk associated with the increased exposure to flooding in Cases B and C. The increase in life-cycle risks for MS_2 and MS_3, attributed to the adverse effects of deck retrofit on foundation performance in Case A, are also apparent in Cases B and C. The higher exposure cases (B and C) amplify these effects resulting in even lower BCRs for those cases. Alternatively, the *BCR*s for MS_4 and MS_5 in the higher exposure cases (B and C) become larger and the management strategies are profitable as seen in Table 3.5 and Figure 3.9. This change in *BCR* for the different management strategies from favorable but not profitable to favorable and profitable demonstrates that it is essential to consider site-specific exposure cases when developing optimal management strategies. It also highlights the importance of considering potential future natural or anthropogenic variations that may change the exposure of the bridge to hydraulic loads. Future changes in the hazard may change the optimal management of the bridge and whether or not the optimal strategy is profitable.

Table 3.4. Benefit-Cost Ratio for structure considering only deck risk, only foundation risk, or risk due to all failure modes.

Strategy	Benefit-Cost Ratio		
	Deck, BCR_{deck}	Foundation, BCR_{found}	Bridge, BCR
MS_1	0.00	0.04	0.04
MS_2	5.20	-5.34	-0.14
MS_3	5.62	-5.80	-0.18
MS_4	0.53	0.03	0.56
MS_5	0.53	0.03	0.57

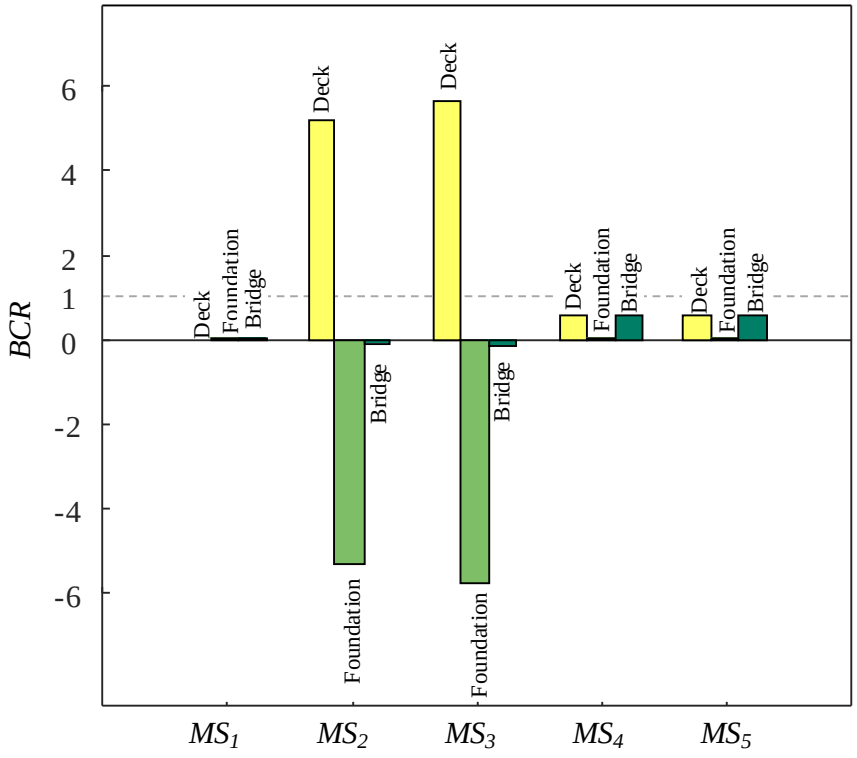

Figure 3.8. The benefit-cost ratio for the deck, foundation, and bridge risk for all management strategies.

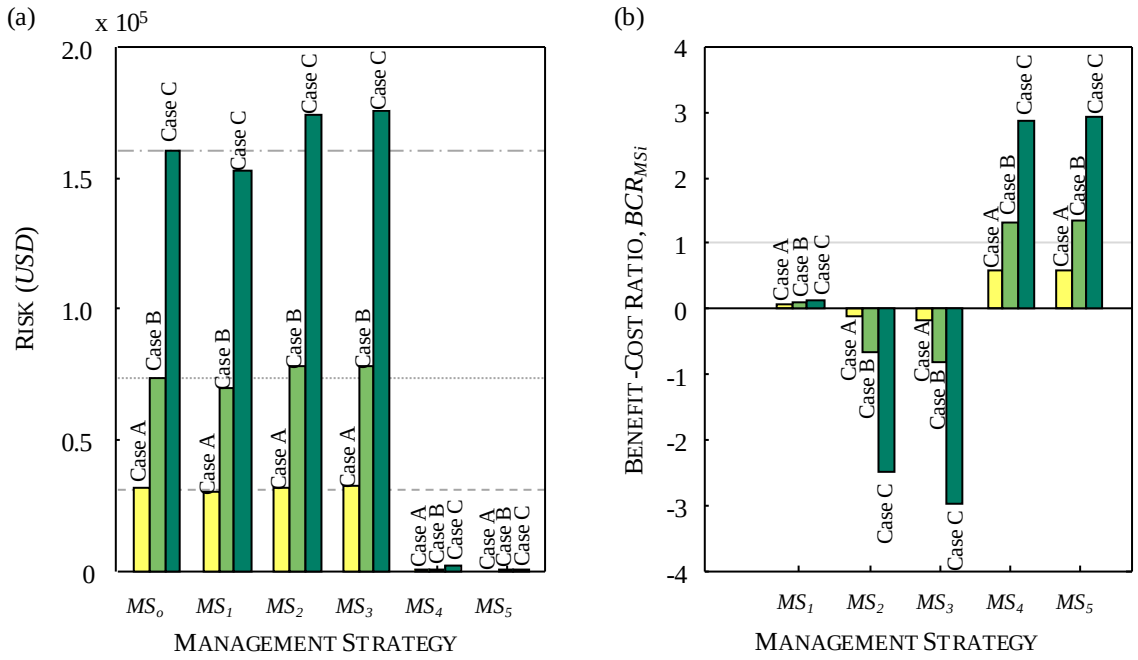

Figure 3.9. The (a) risk and (b) cost-benefit ratio for each management scenario under exposure Case A, B, and C.

Table 3.5. Risk and benefit-cost ratio for all management strategies for exposure Cases A, B, and C.

Strategy	**Risk (*USD*)**			**Benefit-Cost Ratio**		
	Case A	Case B	Case C	Case A	Case B	Case C
MS_o	31330	73700	160160	n/a	n/a	n/a
MS_1	29510	70170	153400	0.04	0.07	0.14
MS_2	32140	77420	174220	-0.14	-0.66	-2.49
MS_3	32290	77960	175900	-0.18	-0.81	-3.00
MS_4	180	640	2010	0.56	1.31	2.84
MS_5	0	10	40	0.57	1.33	2.90

3.8. CONCLUSIONS

This research, based on Mondoro and Frangopol (2017), demonstrates that it is essential to include all relevant failure modes when assessing the effectiveness of management strategies aimed at reducing life-cycle risk. A detailed methodology is presented for assessing the vulnerability of bridges to failure during extreme hydrologic events through damage to either the deck, pier, and/or foundation and the associated risk. The developed methodology allows for a clear understanding of the adverse effects of bridge retrofit actions on the overall performance of the structure level in terms of probability of failure, risk, and benefit-cost ratio. It also reveals the importance of accounting for the site-specific variations in the hazard. The proposed methodology was applied to an illustrative example in order to assess the effectiveness of five management strategies for three different exposure cases in terms of life-cycle risk and benefit-cost ratio. Preferred retrofit strategies were then identified. The following conclusions are drawn:

- All of the bridge retrofit options included in this study lead to a reduction in the total probability of failure. However, retrofitting for deck failure lead to an increase in probability of scour failure though there was a reduction in the probability of deck failure and the total probability of failure.
- Not all of the bridge retrofit options included in this study lead to a reduction in risk. This is due to the difference in economic and social consequences associated with failure of the deck and the failure of the foundation.

- The inclusion of all pertinent failures modes is essential for identifying preferred risk management strategies. If only deck failure modes are considered in the risk assessment of management strategies then only retrofitting the deck has a high benefit-cost ratio and indicates that the retrofits should be performed since there would be a positive return on investment. But, if all failure modes were considered, such actions increase risk and have negative benefit-cost ratios.

- Site specific variations in the hazard are critical to for identifying preferred risk management strategies. The benefit-cost ratios are sensitive to the exposure of the bridge to flood hazards. In areas where the exposure of the bridge is higher (e.g. Cases B and C), retrofitting the bridge with measures aimed at reducing both deck and foundation failure are profitable cost-effective at reducing risk. However, in Case A, it may be economically prudent to do nothing.

The reported results also highlight a need to account for potential shifts in exposure that may be occur over the service life of the structure when assessing risk, benefit-cost ratios, and optimal management strategies. This may be of particular interest in regions where natural and anthropogenic climate changes affect the frequency and intensity of hydrologic events. While the illustrative example is presented with respect to flooding, the applicability of the methodology can be extended to other extreme hydrologic events such as hurricanes and tsunamis.

CHAPTER 4

RISK-BASED APPROACH FOR THE OPTIMAL MANAGEMENT OF BRIDGES EXPOSED TO HURRICANES

4.1. OVERVIEW

This chapter focuses on the performance assessment and management of coastal bridges vulnerable to hurricanes and corrosion damage. Currently, bridge management strategies in coastal regions are designed to mitigate the effects of corrosion on bridge performance. However, recent large scale hurricanes, and their associated damage to bridges, have demonstrated the need to consider hurricanes when making bridge management decisions. The proposed approach considers the uncertainties associated with hazards, the consequences of failure under traffic loads, and the consequences of failure under hurricanes. This work develops a risk-based management framework that includes both repair actions to address deteriorating performance under traffic loads and retrofit actions to minimize the potential for failure during hurricanes. The optimal management strategies are achieved by formulating and solving a bi-objective optimization problem. The objectives include (1) minimizing the life-cycle costs accrued from repair and retrofit actions and (2) minimizing the maximum risk over the life-cycle of the bridge. The proposed risk-based approach is applied to a steel girder bridge located in a hurricane-prone region.

4.2. INTRODUCTION

Coastal bridges are subjected to corrosive marine environments and are exposed to multiple hazards throughout their life-cycle. While initially designed to withstand expected traffic and environmental loads, the capacity of bridges decay over time due to various aging phenomena such as corrosion (Zhu and Frangopol 2013). As of 2013, the American Society of Civil Engineers (ASCE) identified one in nine of the bridges in the United States as being structurally deficient. The Federal Highway Administration (FHWA) estimated a required investment of $76 billion to address the needs of these bridges and eliminate their deficiencies (ASCE 2013). This required investment and limited available resources highlight the need to develop efficient management strategies. However, in order to be useful in reestablishing a properly functioning infrastructure in the United States, optimal management strategies must consider the pertinent hazards.

Bridges along the Eastern and Gulf Coasts of the United States are subjected to multiple extreme natural hazards over their life-cycle; of which, hurricanes are among the most costly. Hurricane Katrina caused an estimated $105.8 billion in total damages, whereas Hurricanes Andrew and Floyd caused $45.6 and $9.2 billion, respectively (Blake et al. 2011). A significant part of the financial losses is attributed to the cost of repair and replacement of infrastructure damaged by wind and surge induced loads. While increased wind speeds are a major source of damage when evaluating the failure of buildings, the associated storm surge is the significant factor in the failure of bridges (Ataei and Padgett 2013b). During Hurricane Ivan in 2004, 56 spans of the I-10 Escambia Bay Bridge were unseated and 66 spans were left misaligned (Meng and Jin 2007). Furthermore, Hurricane

Katrina damaged multiple bridges in Mississippi, Alabama, and Louisiana including the failure of multiple spans of the I-90 Biloxi-Ocean Springs Bridge.

The effect of hurricanes the performance of bridges and infrastructure has been the focus of current, and past, research. Lwin et al. (2014) discussed the damage to bridges sustained during Hurricane Katrina including damage attributed to wind loads, storm surge, water-borne debris impact, and scour. The main source of damage on bridges is the surge and wave induced loading on the bridge (Lwin et al. 2014). Simply supported spans with typical bearing joints are the most susceptible to damage during hurricanes due to the lack of vertical and horizontal connections to prevent the superstructure from lifting off of the supports and displacing horizontally. When the positive vertical (aka upwards) and horizontal displacements surpass the supports, the bridge becomes unsupported and deck unseating occurs. Deck unseating is identified as the most prominent failure mode for simply supported bridges during a hurricane (Chen et al. 2009; Kulicki 2010) and has been included in the probabilistic assessment of the performance of individual bridges, and of regions with multiple susceptible bridges (Ataei and Padgett 2013b; Kameshwar and Padgett 2014). Although approaches for probabilistic performance assessment were developed in these studies, the management for bridges susceptible to hurricane damage was not addressed, nor were considerations for corrosion damage.

The increased attention to hurricane related failures and the lack of guidance in the AASHTO Bridge Design Specifications (AASHTO 2012) for the design of bridges with respect to coastal storm waves precipitated the development of *Guide Specifications for Bridges Vulnerable to Coastal Storms* (AASHTO 2008). These specifications provide a

guidance for designing and assessing bridges subjected to coastal storms and the hydrostatic and hydrodynamic loads on the structure. Despite the existence of guidelines, the consideration of such loads in the management of existing bridges is still lacking. The deteriorated states of bridges across the nation and bridge failures during hurricanes underscore the need to include retrofit options to address and prevent hurricane failures in bridge management plans. Accordingly, this research develops an approach for the optimization of bridge management strategies to include the timing and type of both repair and retrofit actions performed throughout the life of the bridge. The optimization routine considers the hurricane loads, and the impact of corrosive marine environment and daily traffic loads.

Studies have been performed to establish optimal management strategies for bridges based on condition ratings (Saydam et al. 2013), reliability indices (Estes and Frangopol 1999), and, more recently, risk levels (Li et al. 2012; Zhu and Frangopol 2013). While all of these metrics are useful, risk combines the probability of hazard occurrence, the probability of failure due to this hazard, and the consequences of this event. The incorporation of consequences allows risk, as a performance metric, to include the economic, environmental, and social costs of failure, and to act as a normalizing quantity when performing multi-hazard analysis; the disparate probability of occurrences of traffic loads and hurricane loads is offset by the disparate consequences of failure. While environmental costs associated with bridge failure due to traffic loads and hurricane loads may be similar, the economic costs of failure may increase substantially when rebuilding a bridge in a post-natural disaster state (FEMA 1997). Accordingly, the objective of this

research is to develop a risk-based approach to identify the optimum maintenance schedules for deteriorating bridges in hurricane-prone regions and to investigate the importance of post-disaster economic conditions on the optimal repair and retrofit strategies of coastal bridges. The proposed approach simultaneously minimizes the maximum life-cycle risk and the total life-cycle cost of repair and retrofit actions performed during the service life of the bridge. The approach is applied to a steel girder bridge located in a hurricane-prone region.

4.3. MAXIMUM LIFE-CYCLE RISK

This research focuses on minimizing the maximum risk over the life-cycle of a structure. In general, the risk arising from a single hazard is expressed as (Ellingwood and Kinali 2009)

$$R_i = \kappa_i P\left[F|H_i\right]P\left[H_i\right] \tag{4.1}$$

where κ_i is the monetary consequence associated with failure, $P[F|Hi]$ is the probability of failure given the occurrence of the i^{th} hazard, and $P[H_i]$ is the probability of occurrence of the ith hazard. For N independent hazards, the total risk R is the summation of the individual risks R_i (Ellingwood and Kinali 2009)

$$R = \sum_{i=1}^{N} R_i \tag{4.2}$$

In the case of traffic and hurricane hazards, independence is assumed due to the cessation of traffic during hurricanes. The maximum risk associated with a given repair and retrofit plan is the maximum value of the total risk level over the life-cycle of the

structure. Due to corrosion deterioration affecting bridges in coastal regions, the resistance of bridge members (e.g., girders and the deck) to traffic loads will decrease as time progresses. Since the corrosion penetration depth is increasing between repair and retrofit actions, the probability of failure and risk are also increasing. Therefore, the maximum value of the risk occurs either immediately preceding repair or retrofit actions or at the end of the service life. Figure 4.1 is a qualitative depiction of the change in risk levels as a function of time in which the maximum total risk occurs (a) before a repair action or (b) at the end of the required life.

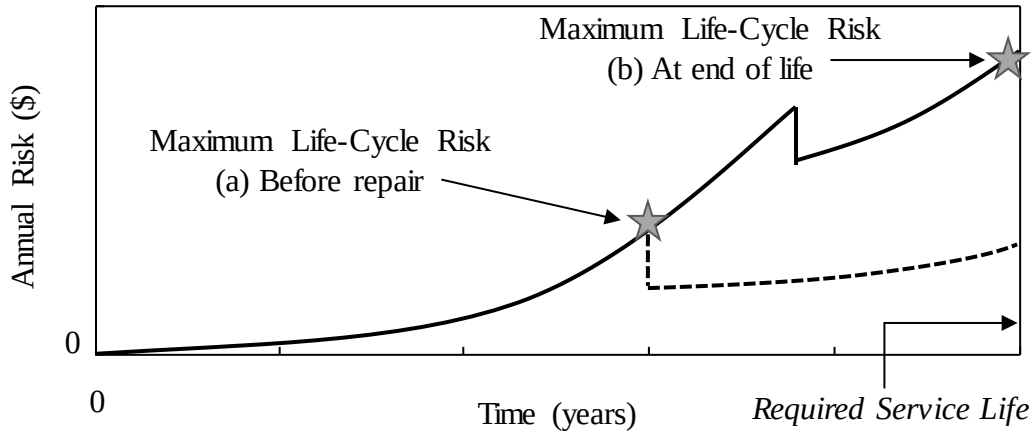

Figure 4.1. Life-cycle risk as a function of time wherein the maximum risk occurs (a) before a repair action and (b) at the end of the required life.

4.4. HURRICANES: QUANTIFYING THE HAZARD

Low clearance bridges in coastal regions are susceptible to damage during coastal storms and hurricanes. The storm surge and waves accompanying the high wind speeds and atmospheric pressure generate hydrodynamic and hydrostatic loadings on the bridge.

Bridge deck unseating may occur during hurricanes when the storm surge, wind, and pressure induced waves generate vertical and lateral forces sufficient to dislodge the superstructure from the substructure. This was found to be the prominent failure mode for low clearance simply supported bridges during hurricanes (Chen et al. 2009; Kulicki 2010; Ataei and Padgett 2013b). The hydrodynamic and hydrostatic loads acting on the bridge during a hurricane are the result of the storm surge height, wind speed, local geography and bathymetry, and bridge superstructure geometry (AASHTO 2008). Therefore, it is necessary to define the distribution of surge heights and wind speeds to obtain the hurricane risk at a given bridge location.

Annual storm surge heights and wind speeds can be represented through their joint distributions (Phan et al. 2007), marginal distributions and correlation, or through a relationship between the two fields coupled with the marginal distribution of one (Irish et al. 2008). The method presented in Phan et al. (2007) details the generation of the probabilistic information for the joint wind speed and storm surge events. It involves (1) the generation of a stochastic set of hurricanes, (2) the hydrodynamic analysis of the physical region, and (3) the statistical analysis of the outputs. Phan et al. (2007) and Pei et al. (2013) generate the stochastic hurricane set using the Florida Public Hurricane Loss Model (FPHLM) to define track, translational speed, maximum wind speed, radius to maximum wind speed, and pressure differential. The hydrodynamic simulation can be implemented through available simulation models, including Sea, Lake, and Overland Surges from Hurricanes (SLOSH) in order to estimate the surge height for the given geographic region (Wiggert and Jarvinen 1995). SLOSH is developed by the National

Weather Service and has an accuracy of ±20 %. A statistical analysis is then performed to determine the joint annual probability of exceedance for the surge heights and wind speeds. In doing the statistical analysis, it is assumed that the maximum wind speed and maximum storm surge for a given storm occur at the same point in time. Though the maximum wind speed typically does not occur at the same time as the maximum storm surge, this conservative assumption is included in the procedure developed by Phan et al. (2007).

Alternatively, Irish et al. (2008) proposed a methodology to use storm data based on past, current, and idealized storms to run numerical simulations for surge height. In this analysis, the slope of the continental shelf was assumed to be constant over the region and the simulations were performed for various slope magnitudes. A polynomial curve fit to the data was used to define the relationship between storm characteristics and surge height for a given continental shelf slope. The method was implemented in Bjarnadottir et al. (2014) as the surge model when assessing the vulnerability of residential structures.

The Saffir-Simpson scale generated by the National Oceanic and Atmospheric Administration categorizes hurricanes by the maximum wind speed, central pressure, and storm surge heights (Herbert and Taylor 1975). However, numerous incidents where the wind speed and pressure of the storm did not match expected surge heights have led to the removal of surge heights from the scale in 2010. This incongruous classification is highlighted by the fact that the storm surge during Hurricane Katrina, a Category 3 at landfall, was significantly larger than that produced by Hurricane Camille, a Category 5 at landfall (Irish et al. 2008). The National Hurricane Center (NHC 2015) has generated

storm surge maps by splicing together results from individual SLOSH basins showing the Maximum of Maximums (MOMs) surge height (Wiggert and Jarvinen 1995). The results provide the worst case scenario surge height for each location.

This work relates the MOMs surge height for a given hurricane category with the maximum wind speed associated with that category. Multiple fit models were investigated for the surge-wind speed relationship and minimal disparities were found between surge predictions based on linear and nonlinear models; a linear fit model was chosen for its ease of implementation. With this relationship defined, only a single annual distribution, for example, the annual wind distribution, is required to formulate the probability of hazard occurrence.

It is generally accepted that a Weibull distribution can be used to define the annual wind speed distribution and that design storms are quantified by their return period, T (Peterka and Shahid 1998). Using the log transform that defines the Weibull cumulative distribution function, $F_V(v)$, which takes the form

$$\ln\left[-\ln\left[1-F_V(v)\right]\right] = \alpha \ln(v) - \alpha \ln(\mu) \tag{4.3}$$

where μ is the scale parameter, α is the shape parameter, the probability of non-exceedance for a given return period of a storm, defined as

$$F_V(v) = P\left[V \le v\right] = 1 - \frac{1}{T} \tag{4.4}$$

and the given wind speed data taken from wind speed maps for return period storms, the Weibull parameters can be estimated. While the parameters can be estimated based on two different return period storms, in the case where data for more than two return

periods are used, linear regression estimates the parameters for best fit. As an example, consider wind and surge data for Red Bank, NJ. The expected peak gust wind speeds associated with return periods of 50, 100 and 500 years, are 177, 193 and 241 km/hr, respectively (Vickery et al. 2000), and the respective surge heights for hurricane categories 1, 2, 3, and 4, are negligible, up to 0.9 m, between 0.9m and 1.8 m, and between 1.8 m and 2.7 m, respectively (National Hurricane Center Storm Surge Unit 2014). Figure 4.2 depicts the annual wind speed distributions and surge heights for this location.

4.5. HURRICANES: RETROFIT OPTIONS

During hurricanes and coastal storms, the storm surge and associated waves generate upward vertical and horizontal forces for which, low clearance bridges may have not been designed to carry. Typically, the girders of simply supported bridges are not restrained from moving upward by the bearings under this type of loading; if they are, the bearings tend to have inadequate strength to resist uplift (Robertson et al. 2007). In 2008, AASHTO provided guidelines for the design of new bridges in order to reduce the water induced loading on new bridges (AASHTO 2008), which in turn will prevent future failures in properly designed bridges. Design suggestions include elevating the bridge, limiting the structural depth of the superstructure, and the use of grated surfaces, among others. For existing bridges, retrofit options have been discussed with the same overall goal of mitigating the wave forces on the structure by (1) limiting entrapped air between spans and reducing buoyancy forces, and (2) providing restraints to limit the vertical and horizontal displacement of the superstructure with respect to its support.

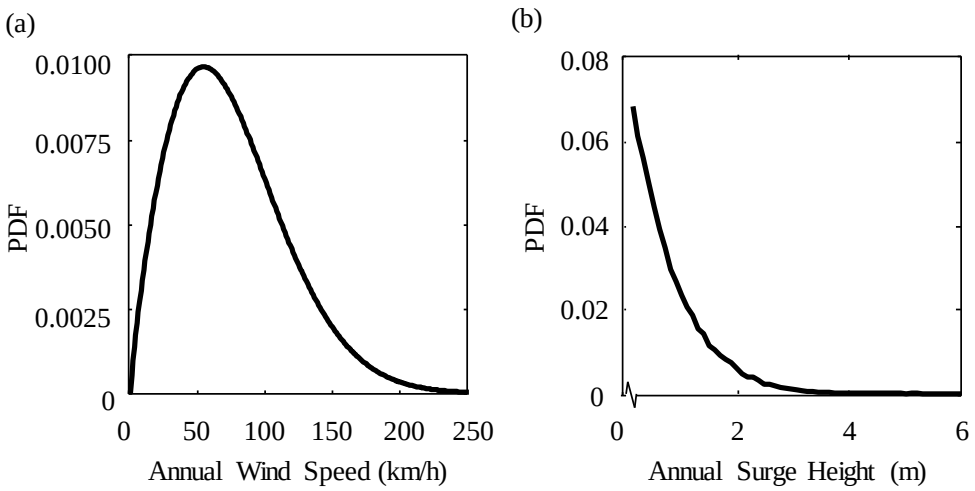

Figure 4.2. Annual wind speed and surge height distributions for Red Bank, New Jersey.

Limiting the entrapped air in between spans has the potential to limit the buoyancy force on the superstructure. This can be done by coring holes in the concrete deck to create vents, shown in Figure 4.3a, which allow air to flow from below the deck to above as the water level rises during a storm (Sawyer 2008). Coring holes, however, must be done with precision so as not to sever any deck reinforcement bars. If reinforcing bars in the deck are severed or damaged, the capacity to resist applied loads is adversely affected. Alternatively, the cell can be vented through the end diaphragms rather than the deck.

Alternatively, the potential for failure can be reduced through establishing a connection between the sub and superstructure through the use of steel angle restraints, shear blocks, steel tie-downs, and restrainers. Steel angle restraints provide both lateral and vertical connections between the girders and the bridge supports when placed on either side of the girder. The angle restraints provide additional capacity to resist uplift and horizontal loads but may fail due to bolt pullout, shearing of the bolts, or spalling of

the concrete in substructure (Robertson et al. 2007). Concrete vertical shear blocks provide a passive connection between the sub and superstructure by allowing for a higher tolerance of vertical uplift without the potential for horizontal displacement. The angled concrete shear blocks provide a more active connection, limiting both horizontal and vertical movements (Figure 4.3b). The survival of the CSX Biloxi-Ocean Springs railroad bridge during Hurricane Katrina is partially attributed to the presence of 38 cm high concrete shear blocks limiting the horizontal displacement of the deck (U.S. Department of Commerce, 2006). Steel retrofit options include restrainers and vertical tie-downs (Figure 4.3c, d). This work considers the addition of vertical tie-downs as the retrofit option in the illustrative example; however the methodology can be extended to incorporate other retrofit options.

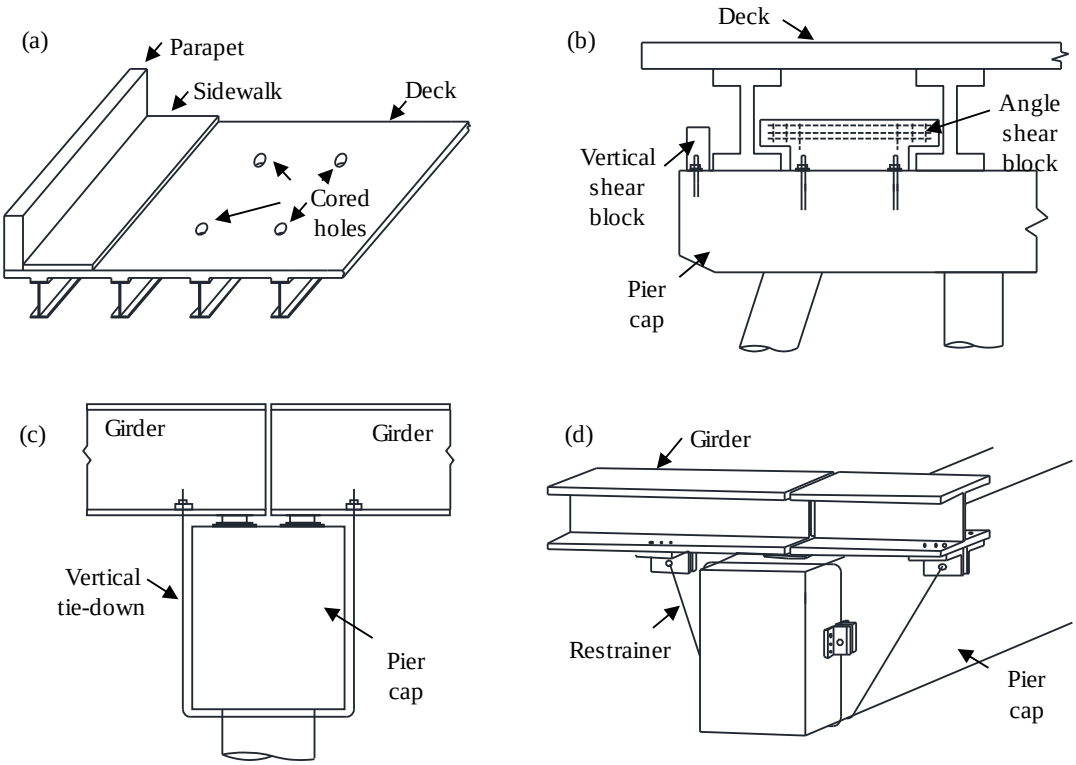

Figure 4.3. Retrofit options for bridges vulnerable to hurricane loads including (a) cored holes in deck, (b) concrete shear keys, (c) vertical tie downs and (d) steel restrainers.

4.6. HAZARD ANALYSIS

Hazard analysis is the first step in assessing risk. It incorporates the uncertain nature of the event by estimating the probability of occurrence of a single hazard $P[H_i]$. This research considers two predominant hazards in coastal regions: hurricanes and traffic. For bridges erected for daily vehicle traffic and pedestrian use, the probability of traffic load occurrence is considered to be equal to one. It is assumed that traffic loads cease during the occurrence of a hurricane; however, due to the brevity of the hurricane on a per annum basis, the reduction to bridge usage by traffic is negligible. Therefore, the probability of occurrence of the hurricane hazard is quantified by the annual distribution of wind speed and surge height.

4.7. VULNERABILITY ANALYSIS

Vulnerability analysis is the second step in assessing the risk coincidental with a given hazard. This involves evaluating the probability of failure given that the hazard has occurred. In general, limit states which relate the capacity of a structure C to resist the demand D can be formulated. For hazards where only a single failure mode is considered, as is the case for hurricane loads, failure probability of the structure is defined as the probability that the demand exceeds capacity

$$P_f = P\left[\left(C - D\right) < 0\right] \tag{4.5}$$

However, there may be multiple failure mechanisms under a given hazard. In this case, the system can be modeled as a series, parallel, or series-parallel combinations of failure modes. Accordingly, for a series system consisting of L parallel sub-systems,

where each parallel sub-system k has N_k components, the overall system failure probability is

$$P_f = P\left[\bigcup_{k=1}^{L}\bigcap_{m=1}^{N_k}\{g_{km}(\mathrm{X}) \le 0\}\right] \tag{4.6}$$

where $g_{km}(\boldsymbol{X})$ denotes the performance function of the m^{th} component in the k^{th} parallel system and $\mathbf{X}$ is the vector of random variables. The vulnerability assessment for a structure under hazards due to traffic loads and hurricanes, and the effect of corrosion are detailed next.

4.7.1. Hurricanes

This research addresses the primary failure mode of deck unseating for low clearance simple span bridges during hurricanes. Deck unseating is predominately caused by the vertical uplift forces that unseat the deck from the supports and horizontal forces that dislodge the deck from the pier. These loads can be estimated through (1) advanced computational modeling or (2) approximate methods based on experimental results.

Detailed hydrodynamic modeling using Computational Fluid Dynamic (CFD) software can be performed on a 3D structure to analyze wave structure interaction. Jin and Meng (2011) outlined the procedure for 3D CFD modeling but categorized the method as computationally expensive and proposed an alternative 2D method. For the probabilistic analysis of a bridge throughout its life-cycle, even the 2D method becomes computationally infeasible, especially if simulation techniques are used to obtain the failure probability.

Approximate methods for estimating the wave and surge forces on bridges have been developed based on the adaptation of the methodology used to approximate forces acting on jetties and other coastal structures (McConnell et al. 2004) while accounting for the bridge interference with surface wave propagations (Douglas et al. 2006). In an effort to adequately design and retrofit bridges, the FHWA authorized an investigation into the effects of coastal storms on bridges. In 2008, the American Association of State Highway and Transportation Officials (AASHTO) developed guidelines to establish a basis for estimating the forces on a bridge during a hurricane (AASHTO 2008). This research uses the AASHTO model. The following is a review of adopted method to estimate the forces acting on a bridge.

The vertical uplift forces generated during a storm include the maximum quasi-static vertical force and the associated vertical slamming force. The total vertical uplift force is the summation of these two components as the vertical slamming force often occurs at the time of maximum upward vertical quasi-static force (AASHTO 2008). Maximum quasi-static vertical force refers to the buoyancy force that is imparted on the structure once any portion is submerged. According to this model, the maximum quasi-static vertical force is

$$F_{v-\max} = \gamma_w \overline{W} \beta \left(-1.3 \frac{H_{\max}}{d_s} + 1.8 \right) \left(1.35 + 0.35 * \tanh(1.2 T_p - 8.5) \right) \left(b_0 + b_1 x + \frac{b_2}{y} + b_3 x^2 + \frac{b_4}{y^2} + \frac{b_5 x}{y} + b_6 x^3 \right) (TAF) \quad (4.7)$$

where γ_w is the unit weight of water, $\overline{W}$ β, x, and y are parameters related to the wetted width of the bridge deck defined in AASHTO (2008), H_{max} is the maximum probable

wave height, d_s is the water depth at or near the bridge, T_p is the period of the wave with the greatest energy exhibited, *TAF* is entrapped air coefficient, and b_0, b_1, ..., b_6 are coefficients based on bridge type. The associated vertical slamming force occurs when the wave exerts an impact load on the structure. According to AASHTO (2008), the vertical slamming force is

$$F_S = A\gamma_w H_{\max}{}^2 \left(\frac{H_{\max}}{\lambda} \right)^B \tag{4.8}$$

where *A* is the projected area subjected to the current storm water level, *B* is a coefficient related to the wave crest height and distance from the storm water level to the bottom of the girder, and

$$\lambda = \frac{gT_p{}^2}{2\pi} \sqrt{\tanh\left(\frac{4\pi^2 d_s}{T_p{}^2 g} \right)} \tag{4.9}$$

where *g* is the gravitational constant.

Wave period and maximum wave height are essential in finding the demand on a bridge deck and they differ based on geographical location. The significant wave height and wave period are computed in terms of wind stress factor, average water depth, and fetch length and are expressed, respectively, as

$$H_S = 0.283 \tanh\left[0.53 \left(\frac{gd}{U*_t} \right)^{3/4} \right] \tanh\left[\frac{0.00565 \left(\frac{gF}{U*_t} \right)^{1/2}}{\tanh\left[0.53 \left(\frac{gd}{U*_t} \right)^{3/4} \right]} \right] \frac{U*_t{}^2}{g} \tag{4.10}$$

$$T_p = 7.54 \tanh\left[0.833\left(\frac{gd}{U*_t}\right)^{3/8}\right] \tanh\left[\frac{0.0379\left(\frac{gF}{U*_t}\right)^{1/8}}{\tanh\left[0.833\left(\frac{gd}{U*_t}\right)^{3/8}\right]}\right]\frac{U*_t}{g} \quad (4.11)$$

where F is the fetch length, d is the average depth over the fetch, and $U*_t$ is the wind stress factor. H_{max} is taken a $1.80H_s$ (AASHTO 2008). Thus, the demand on the bridge is the direct summation of the maximum quasi-static vertical force and vertical slamming force. The weight of the structure, F_w, and the maximum restraint forces of the steel tie-downs, F_{res}, provide the capacity to withstand uplift. Since the AASHTO forces are defined as a force per unit length of the bridge, the weight of the structure and capacity of the restrainers are also generated as such. F_w is defined by the weight per unit length of the structure and F_{res} is the yield strength of the tie-downs which is normalized by the length of the span. The performance function for the deck unseating failure mode is

$$g_{hurr} = \left(F_w + F_{res}\right) - \left(F_{v-\max} + F_s\right) \quad (4.12)$$

As corrosion deteriorates the steel within the structure, the capacity of the bridge to withstand hurricane loads decreases; therefore, the probability of failure increases.

4.7.2. Traffic Loads

The AASHTO bridge design specifications outline the design methodology and criteria for estimating the loads acting on different bridge components. The initial design is developed to provide enough capacity to withstand these loads. As the resistances of the structural components deteriorates with time, the capacity of the bridge reduces. The bridge may then collapse as a result of different failure modes including: bending in the

deck, shear in the girders, and bending in the girders. These failure modes provide the limit states for a component-based reliability analysis, and may then be incorporated into the system-based reliability analysis of the structure. This research considers a combination of failure modes of the superstructure covering failure of the deck and/or girders, in a system-based reliability model. Flexural failure of the deck is defined by the limit state equation

$$g_{deck} = M_{c,deck} - M_{d,deck} = 0 \tag{4.13}$$

where $M_{c,deck}$ is the bending moment capacity of the deck and $M_{d,deck}$ is the moment demand on the deck as determined by the equivalent strip method (AASHTO 2012). Both flexural and shear failure modes are considered for the failure of the girders and are defined, respectively, by the following limit states

$$g_{girder,f} = M_{c,girder} - M_{d,girder} = 0 \tag{4.14}$$

$$g_{girder,v} = V_{c,girder} - V_{d,girder} = 0 \tag{4.15}$$

where $M_{c,girder}$ and $V_{c,girder}$ are the capacity of the composite girder in flexure and shear, respectively, and $M_{d,girder}$ and $V_{d,girder}$ are the respective flexural and shear demands determined based on the design truck and the location within the system as outlined in AASHTO (2012).

4.7.3. Corrosion

Corrosion affects the structural components within a bridge and reduces its capacity to resist both traffic and hurricane induced loads. The steel reinforcement in the concrete slab degrades as chloride ions penetrate through the concrete cover to the steel-concrete

interface. The diffusion of the chloride ions may cause pitting or uniform corrosion. In this research, corrosion is assumed to uniformly reduce the area of steel reinforcement in the slab as a function of time. After the initiation of corrosion the residual area of steel reinforcement $A_r(t)$ at time t is (Stewart and Rosowsky 1998)

$$A_r(t) = n\frac{\pi}{4}\left[d_i - 2(0.0116 i_{corr})(t - T_i)\right]^2 \tag{4.16}$$

where n is the number of reinforcement bars, d_i is the initial diameter of reinforcement, and i_{corr} (normally expressed as μA/mm) is the corrosion rate based on cover and water-cement ratio, and the T_i is the corrosion initiation time which is defined as the time for chloride concentration to reach a critical level and can be expressed as (Vu and Stewart 2000)

$$T_i = \frac{1}{D}\left(\frac{x}{2erf^{-1}\left(1 - \frac{C_{cr}}{C_o}\right)}\right)^2 \tag{4.17}$$

where D is the diffusion coefficient, C_{cr} is the critical concentration of chlorides at which corrosion begins, and C_o is the surface chloride content.

For exposed steel, the corrosion wastage is assumed to follow the model proposed by (Albrecht and Naeemi 1984) where the average penetration depth of the corrosion is defined as

$$C(t) = At^b \tag{4.18}$$

in which A and b are regression parameters obtained based on the environmental conditions. For girders, the corrosion occurs along the web height and bottom flanges at

the supports, while at mid-span, corrosion only affects the lower quarter of the web height and top of the bottom flanges (Estes and Frangopol 1999). The steel tie-downs are assumed to be uncoated and the corrosion penetrates around the wire.

4.8. CONSEQUENCE EVALUATION

Consequence evaluation is the last component to risk analysis and is the essential step in quantifying the impact that a structural failure has on the community which it serves. This impact include economic, social, and environmental components. The economic losses can be defined as the cost to the replace the structure, as well as the cost of damages to surrounding property caused by the structural failure. For failure due to traffic loads, the economic consequences incorporated in this research include the rebuilding cost of the structure, κ_{reb}, the detour consequence, κ_{det}, the time loss consequence, κ_{tl}, and the removal costs, κ_{rem}. The latter three consequences are defined respectively as (Stein et al. 1999)

$$\kappa_{\det} = C_{veh} L_{\det} T_{\det} A_{dt} \tag{4.19}$$

$$\kappa_{tl} = \left[C_{tva} O_{car} \left(1 - \frac{T_{trk}}{100} \right) + C_{tvtk} \frac{T_{trk}}{100} \right] \frac{L_{\det} T_{\det} A_{DT}}{V} \tag{4.20}$$

$$\kappa_{rem} = C_{rem} WL \tag{4.21}$$

where C_{veh} is the average running cost for vehicles, C_{reb} is the rebuilding cost per square foot, W is the bridge width, L is the length of the bridge, C_{tva} is the value of time per adult, O_{car} is the average vehicle occupancy, T_{trk} is the percentage of average daily truck

traffic to total average daily traffic, C_{tvtk} is the time value of the truck, V is the average detour speed, L_{det} is the length of the detour, T_{det} is the duration of the detour, and A_{DT} is the average daily traffic.

The social and environmental consequences are not as easy to quantify. Environmental costs in risk analysis typically include the emission of toxic gasses or waste in the surrounding environment as can happen with power plants or production facilities. However, bridge failure releases only concrete, steel, and other construction materials as debris. Thus, the environmental cost sustained is the debris removal cost C_{rem}. Social consequences can include, but are not limited to, the casualties associated with bridge failure. This social consequence κ_{sl} is associated with the number of casualties sustained in the event of a bridge failure and takes the form (Stein et al. 1999)

$$\kappa_{sl} = \left(\frac{L}{D_s} + 1\right)\left[O_{car}\left(1 - \frac{T_{trk}}{100}\right) + O_{trk}\frac{T_{trk}}{100}\right] ICAF \tag{4.22}$$

where D_s is the safe following distance, O_{trk} is the average occupancy of trucks, and $ICAF$ is the implied cost of averting a fatality for bridge engineering. The total consequence of failure for the traffic hazard, is thus defined as

$$\kappa_{traffic} = \kappa_{reb} + \kappa_{\det} + \kappa_{tl} + \kappa_{sl} + \kappa_{rem} \tag{4.23}$$

In the case of hurricanes, the loss of life due to bridge failure is negligible as it is assumed that no traffic crosses the bridge during the storm. However FEMA identified that there are increased costs associated with rebuilding a bridge in a post-disaster region. This due to the rush schedule put in place to limit the impact of the bridge failure on the regional economy and facilitate a more rapid recovery (FEMA 1997). Additionally, in the

aftermath of a natural disaster, construction resources become scarce driving up the cost. The consequence of failure during a hurricane event is thus written as

$$\kappa_{hurricane} = S\kappa_{traffic} \tag{4.24}$$

where S is the scale factor adjusting for the post-disaster economic status, as well as the reduced social consequences due to limited traffic during a hurricane.

4.9. RISK MITIGATION AND OPTIMAL REPAIR AND RETROFIT STRATEGIES

Risk mitigation can be achieved by repairing and retrofitting a bridge throughout its life to reduce the probability of failure associated to certain hazards. The number of repair actions may be highly variable over the life-cycle of a structure if both preventative and essential actions are considered, and have been included as a design variable in past bridge management frameworks (Miyamoto et al. 2000, Okasha and Frangopol 2010). However, the large variability in number of maintenance actions is typically due to the consideration of preventative actions such as re-painting (Kong and Frangopol 2003, Thoft-Christensen 2009). For essential repairs, typically fewer actions are included in optimal management plans (Okasha and Frangopol 2010). Since this research considers only essential maintenance actions, such as replacing the deck or girders, the proposed optimization problems considers a maximum of two repair actions to be applied based on the required service life of the structure. Each repair or retrofit action has an associated cost and the optimal management plans must consider the available budget while mitigating risk. This poses two conflicting objectives: (a) minimizing the maximum life-

cycle risk, and (b) minimizing life-cycle costs. A bi-objective optimization problem is therefore proposed to determine the optimal repair and retrofit times and types in order to minimize both the maximum life-cycle risk, R_{life}, and the total life-cycle costs, C_{life}. The optimization problem is formulated a

$$\textit{Minimize}: R_{life} \tag{4.25}$$

$$\textit{Minimize}: C_{life} \tag{4.26}$$

$$\textit{given}: \boldsymbol{B_C}, \boldsymbol{B_L}, \boldsymbol{C} \text{ and } t_{req} \tag{4.27}$$

$$\textit{find}: t_{r1}, m_{r1}, t_{r2}, m_{r2}, t_{ret}, m_{ret} \tag{4.28}$$

$$\textit{such that} \quad t_{r1} < t_{r2}, \tag{4.29}$$

where t_{r1} is the time of first repair action m_{r1}, t_{r2} is the time of second repair action m_{r2}, t_{ret} is the time of retrofit action m_{ret}, m_{r1}, m_{r2}, and m_{ret} are identifiers of the selected optimum repair/retrofit type. R_{life} is defined as the maximum life-cycle risk value and is qualitatively shown in Figure 4.1 for two potential management strategies, $\boldsymbol{B_C}$ is the set of data on the bridge characteristics, $\boldsymbol{B_L}$ is the set of data specific to the bridge location, **C** is the set of data for cost, and t_{req} is the required service life. Bridge geometry data include span lengths, deck width, deck and girder dimensions, structural properties, and connections between sub- and superstructure when applicable; bridge location data include the wind speeds and surge heights data and statistical descriptors for the corrosive environment. The data set for cost, **C**, includes the cost of the q^{th} repair type, $\boldsymbol{C(q)}$ and retrofit type j, $\boldsymbol{C(j)}$. The life-cycle cost of repair and retrofit actions, C_{life}, is accumulated throughout the service life based on the cost of each individual action. Considering two repair actions and one retrofit throughout the service life, this cost can be expressed as

$$C_{life} = C(m_{r1}) + C(m_{r2}) + C(m_{ret}) \tag{4.30}$$

Each repair and retrofit action is performed at a discrete point in time. In order to make an accurate summation of the costs, the future costs should be discounted to the present value

$$PV = \frac{C}{(1+r)^n} \tag{4.31}$$

where r is the real interest rate, n is the number of compounding periods, and C is the cost of the repair or retrofit action in the future. Thus, Equation 28 can be rewritten as

$$C_{life} = \frac{C(m_{r1})}{(1+r)^{t_{r1}}} + \frac{C(m_{r2})}{(1+r)^{t_{r2}}} + \frac{C(m_{ret})}{(1+r)^{t_{ret}}} \tag{4.32}$$

The real interest rate is a description of the expected rate of interest after adjusting for inflation (Fisher 1930)

$$r = \frac{1+i}{1+p} - 1 \tag{4.33}$$

where i is the nominal interest rate and p is the expected inflation rate. The real interest rate indicates the growth rate in the purchasing power of a dollar. Variations in economic factors may lead to cases where the real interest rate is positive (the interest rate is larger than the inflation rate), negative (the inflation rate is larger than the interest rate), and zero (rates are equal). Therefore, the real interest rate and time of each repair/retrofit action effects the life-cycle cost; the net effect on the Pareto optimal solution will be investigated for representative cases of the economic conditions.

4.10. ILLUSTRATIVE EXAMPLE

The proposed life-cycle risk mitigation approach is illustrated on the S-17 West Front Street Bridge in New Jersey. The bridge is a 146 m steel girder with 6 equal spans (24.4 m each); girder dimensions are shown in Figure 4.4. The S-17 Bridge is 14.3 m wide with a 21.6 cm thick deck with a thin overlay on top. There are two travel lanes with 1.2 m shoulders and 1.8 m wide sidewalks and 1.4 m tall parapets on either side of the bridge as shown in Figure 4.5a. The system failure considered in this research is associated with the series-parallel model which assumes that failure will occur with the failure of the deck and/or the failure of any two adjacent girders as shown in Figure 4.5b. The bridge carries an average daily traffic load of 17,000 cars per day. The S-17 Bridge is over the Swimming River which has an average depth of 1.2 m across a fetch length of 76.2 m. The bridge is designed as a continuous span bridge over the 5 piers but is modeled as a simply supported bridge for this study. The initial distribution for the capacity of the bridge to withstand uplift forces, (F_w+F_{res}), and the uplift forces, $(F_{v\text{-}max}+F_s)$, is shown in Figure 4.6.

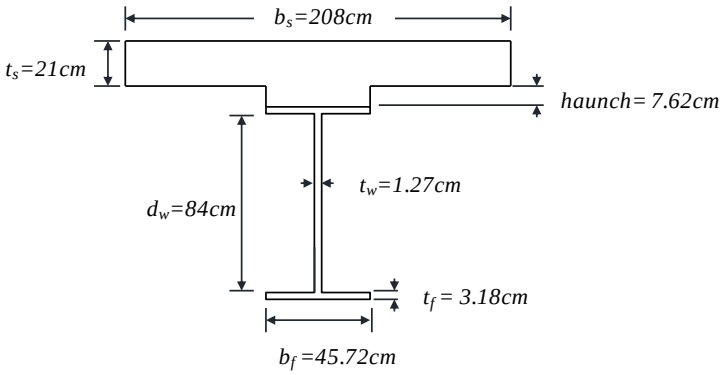

Figure 4.4. Composite girder section of S-17 Bridge. All dimensions are in cm.

(a) Transverse section

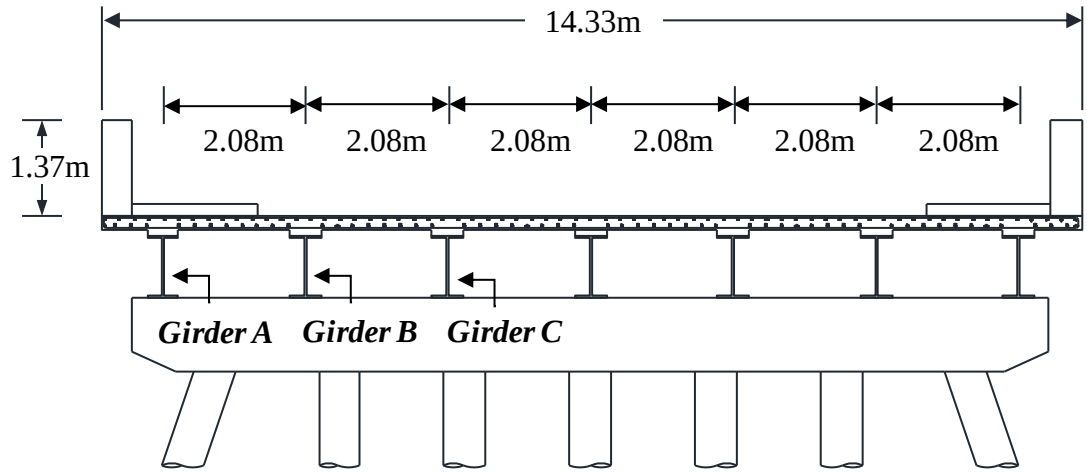

(b) System model

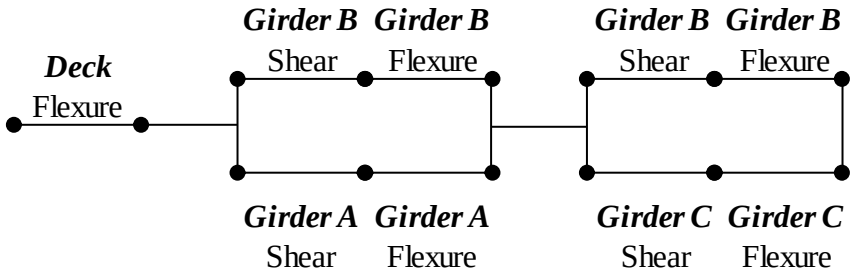

Figure 4.5. Transverse section of S-17 Bridge and system model. All dimensions are in m.

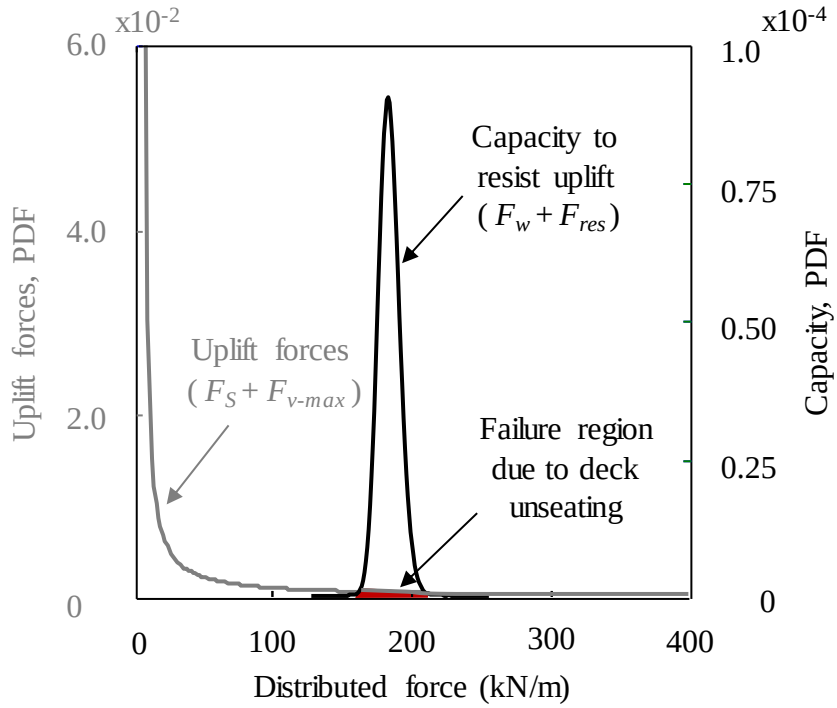

Figure 4.6. Distribution of the demand on the S-17 Bridge superstructure due to vertical loads imposed by hurricanes and the distribution of capacity to withstand the loads.

Repair options include replacing the deck, the exterior girders, the deck and exterior girders, and entire superstructure. The costs of repairs and replacement of the girders and deck are estimated from similar repairs and replacements in the S-31 Bridge located in the same region of the analyzed bridge (North Jersey Transportation Planning Authority, 2011) and are summarized in Table 4.1. The costs of repairs were estimated as follows: For the S-31 Bridge, repairs were made to the concrete deck including the removal of deteriorated concrete, work on existing steel rebar and new rebar, and the pouring of new concrete. Repairs were also made to the steel elements of the S-31 Bridge including repairs to steel angles and buckled stringers, and steel plate repairs for steel girders. The

costs of the repairs were normalized for the length of the repair, which, in the case of the S-31 Bridge, was the span length. The costs per unit length were then scaled by the span length of the S-17 Bridge. The hurricane retrofit costs per tie-down were estimated from Shirole and Malik (1993); and retrofit actions include adding 2, 4, 6 or 8 tie-downs of 1 inch diameter steel wire. The total cost of a retrofit action includes installation and access costs in addition to the total cost of the tie downs. The inputs for consequence analysis are listed in Table 4.2. All values are listed in 2012 US Dollars (USD). For values which are not initially provided in 2012 USD, the consumer price index was used to convert the monetary value (Lewis and Grogan 2013) to 2012 US dollars. The corrosion parameters used to estimate the deterioration of steel components over time as listed in Table 4.3.

Table 4.1. Cost of Repair and Retrofit Options

Option	Cost (USD)
Replace deck	443,550
Replace exterior girders	415,050
Replace deck and exterior girders	754,850
Replace superstructure	1,283,200
Cost per tie-down	3,900
Installation and access costs for retrofit action	105,000

Table 4.2. Input variables for consequence evaluation

Description	Notation	Value	Reference
Rebuilding cost($)	K_{reb}	1,283,220	North Jersey Transportation Planning Authority (2011)
Average running cost for vehicles ($/mile)	C_{veh}	0.60	American Automobile Association (2014)
Length of the detour (miles)	L_{det}	1.90	Estimated
Duration of the detour (days)	T_{det}	133	North Jersey Transportation Planning Authority (2011)
Average daily traffic	A_{DT}	17,000	North Jersey Transportation Planning Authority (2011)
Average daily truck traffic	t_{trk}	10	estimated
Value of the truck ($/hr)	c_{trk}	20.75	Mallela and Sadasivam (2011)
Value of time per adult ($/hr)	c_{tva}	24.19	Santos et al. (2009)
Average vehicle occupancy	o_{car}	1.67	Santos et al. (2009)
Average detour speed (mph)	V	35	Estimated
Safe following distance (ft)	DS	166	New Jersey Motor Vehicle Commission (2014)
Average occupancy of trucks	o_{trk}	1	Estimated
Implied cost of averting a fatality for bridge engineering ($)	$ICAF$	3,328,000	Rackwitz (2002) and Lewis and Grogan (2013)
Removal cost ($/m^2)	C_{rem}	35	Florida Department of Transportation (2011)

Table 4.3. Statistics for Corrosion Parameters

Description (units)	Notation	Distribution
Corrosion parameter (in/yr)*	A	L(70.6,0.66)
Corrosion parameter*	b	L(0.789,0.49)
Initial chloride concentration (kg/m^3)**	C_o	L(3.5,0.5)
Diffusion coefficient (m^2/yr) **	D	L(0.000123,0.75)
Critical chloride concentration (kg/m^3)**	C_{cr}	U(0.6,1.2)
Initiation Time (yr) ***	T_i	L(15.8,0.7)

Note: L(μ,δ) denotes a lognormal distribution with mean = μ and Cov= δ
U(a,b) denotes a uniform distribution with min = a and max =b
*Albrecht and Naeemi (1984)
** Stewart and Rosowsky (1998)
*** fitted

The proposed optimization framework is applied considering a required service life of 50 years with 3 representative real interest rates denoting the cases where (1) the inflation rate is larger than the nominal interest rate, r = - 0.01, (2) the rates are equal, r = 0.00, and (3) the inflation rate is smaller than the nominal interest rate, r = 0.01. The problem is solved by using the Global Optimization Toolbox provided in version 3.2.5 of MATLAB (Mathworks 2014). The Pareto optimal set of solutions are depicted in Figure 4.7 and highlight the conflicting objectives of minimizing life-cycle risk and minimizing cost. The relatively flat portion of the Pareto front associated with low cost-high risk solutions indicates that significant improvements in risk can be achieved through minimal increases in costs. Solution A1, A2, and A3, detailed in Table 4.4, represent, respectively, optimal repair strategies for high cost-low risk, intermediate cost-risk, and low-cost high-risk management plans. The risk levels associated with the three solutions are shown as a function of time in Figure 4.8. Solution A3 involves repairing the exterior girders at year

46 at a life-cycle cost of $415,064 and achieves a maximum life-cycle risk of $166,132. Solution A2 consists of a single repair action (i.e., repairing the deck) at year 32 but also involves retrofitting the bridge with 6 tie-downs at year 22. Solution A2 provides a 69% reduction in risk as compared to A3 for a corresponding 34% increase in cost. Thus, by applying repairs and retrofit, substantial gains can be made in minimizing life-cycle maximum risk for a minimal increase in life-cycle costs.

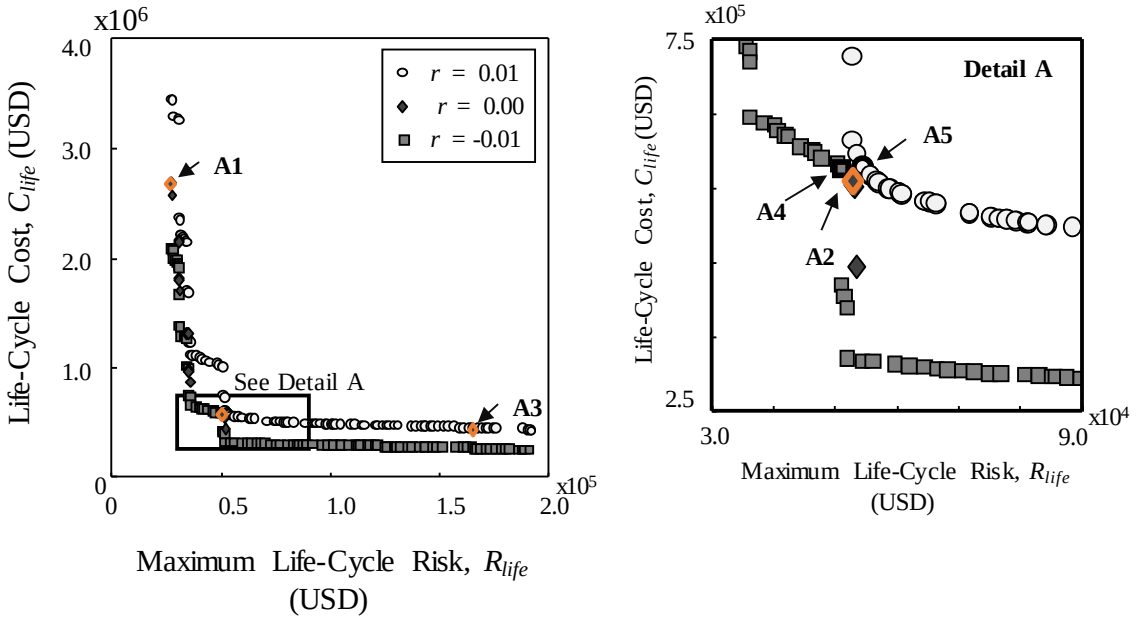

Figure 4.7. Pareto-optimal solution set for the bridge management scheduling for a required service life of 50 years.

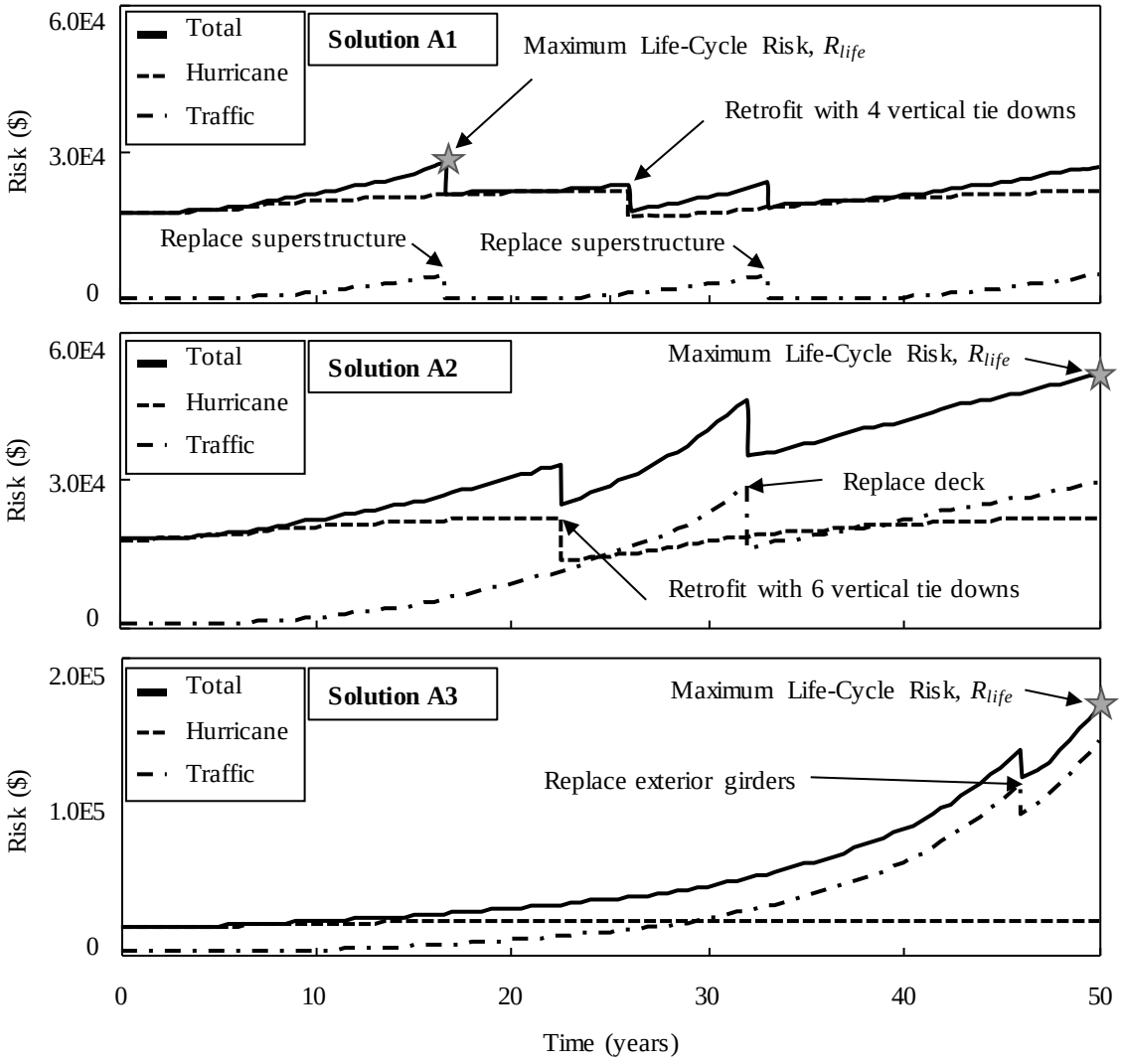

Figure 4.8. Risk as a function of time for representative solutions A1, A2, and A3 from Pareto-optimal set for 50 year required service life.

Table 4.4. Representative solutions for optimal management repair strategies

Solution	Repair 1		Repair 2		Retrofit		Maximum Life-Cycle Risk, R_{life} (USD)	Cycle Risk Cost $C_{life,}$ (USD)
	time, t_{r1}	type, m_{r1}	time, t_{r2}	type, m_{r2}	time, t_{ret}	type, m_{ret}		
A1	16.67	4	33.34	4	26	2	27,437	2,679,276
A2	32.01	1	-	-	22.73	3	51,198	560,291
A3	46.47	2	-	-	-	-	166,132	415,064
A4	31.72	1	48.87	2	-	-	50,936	576,457
A5	26.35	1	62.55	2	-	-	53,613	576,521
B1	30.54	1	41.99	2	-	-	46,635	598,459
B2	37.49	1	66.87	1	60.23	1	70,372	590,227
B3	42.22	1	-	-			98,852	290,180
B4	42.25	1	-	-	45.71	1	99,059	358,873
C1	9.73	2	24.28	1	-	-	48,828	1,022,025
C2	23.75	3	31.53	1	22.69	3	49,246	1,709,417

Note: m_{rq} = 1 : replace deck
m_{rq} = 2 : replace exterior girders
m_{rq} = 3 : replace deck and exterior girders
m_{rq} = 4 : replace superstructure
m_{ret} = j : retrofit with 2j vertical tie downs

It should be noted that the solution of the bi-objective problem provides the decision maker with the useful insight into return on investment; which, in this case, is the decrease in R_{life} that can be achieved with an increase in cost (i.e. C_{life}). For example, the Pareto front shown in Figure 4.7 has a relatively flat section that is associated with low-cost high-risk solutions. This indicates that significant improvements in risk can be achieved through minimal increases in costs. However, the solution will not necessarily give the decision maker insight on what the maximum acceptable R_{life} is. This is dependent on the risk attitude of the decision maker. The role of the risk attitudes of decision makers and optimal management plans are discussed in depth in Sabatino et al. (2015) and Patidar (2007).

The economic conditions affect optimal management solutions as the time-value of the dollar changes based on real interest rates; as the real interest rates decrease, the buying power of the dollar increases and more repair and retrofit actions can be performed for the same amount of money. Detail A in Figure 4.7 focuses on solutions A2, A4, and A5. These are solutions taken from the Pareto fronts from the different economic cases that have the lowest risk for a life-cycle cost less than $580,000. At a high real interest rate, the optimal solution A5 involves a single replacement of the deck at year 31. As the rate decreases to 0, the optimal solution A2 includes a retrofit action, as well as a deck repair. This retrofit action decreases the maximum life-cycle risk, as shown in Figure 4.9. With a further decrease in the real interest rate, the optimal solution A4 includes two repair actions which provide a further decrease in maximum life-cycle risk. The application of both repair and retrofit options occur in optimal solutions to help minimize maximum life-cycle risk. Since the economic market is variable, an extension of the optimization problem can be proposed wherein the different economic conditions are represented in the constraints based on their likelihood in a stochastic optimization problem.

The required service life also affects the optimal management strategies. Solutions that may be optimal for a required service life of 50 years may not be optimal as the service life requirement is increased as can be seen by comparing the Pareto optimal solutions for a 50 and 80 year required service life presented in Figure 4.10.

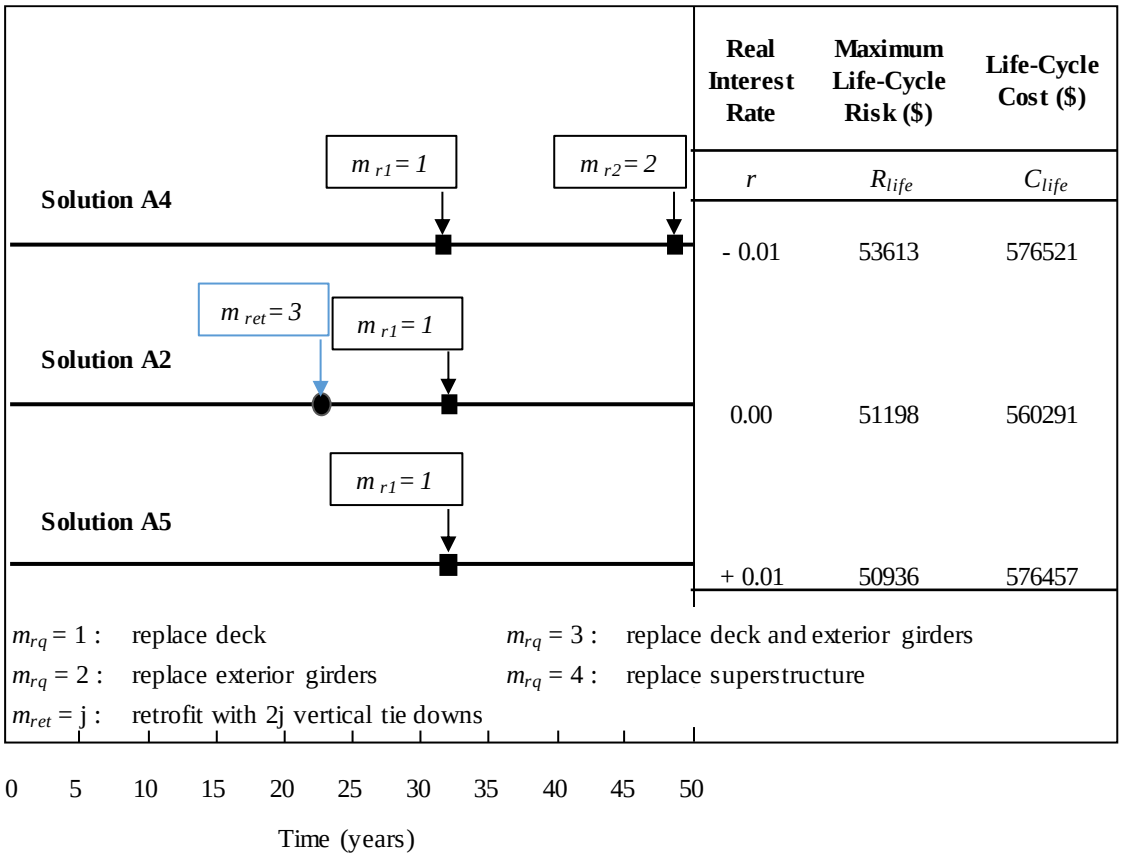

Figure 4.9. Representative solutions from Pareto-optimal set for 50 year required service life based on different real interest rates.

Representative solutions B1, B2, B3, and B4 are detailed in Table 4.4. B1 and B2 are the optimal solutions for a 50 and 80 year service life, respectively, which minimize risk for a life-cycle cost of less than $600,000. B1 involves replacing the deck at year 30 and the exterior girders at year 41 while B2 involves replacing the deck at years 37 and 66, and retrofitting the bridge with two tie-downs at year 60. Comparatively, the initial repair of the bridge is delayed and the time in-between solutions increases with the increase in the required service life. Figure 4.11a depicts risk levels as a function in time for solution B1, and the drastic increase in risk levels after the required service life (50 years) which prevents it from being optimal for the 80 year case. Figure 4.11b shows the life-cycle risk

profiles for solution B2, wherein the inclusion of retrofit actions and the modified timing of the repair actions is necessary to minimize maximum life-cycle risk for the 80 year case. Thus, the solution that is optimal for the 50 year service life (B1) is no longer optimal for the specified cost level of less than $600,000 at an extended service life of 80 years.

B3 and B4 are representative solutions taken from the 50 and 80 year cases which minimize life-cycle cost for a risk level of less than $100,000. Both solutions involve replacing the deck at year 42, but B4 also requires retrofitting the bridge with two tie-downs. In order to maintain the same risk levels for both service life cases, the optimal maintenance plans must consider and address both hazards. This is achieved with additional investments in repair and retrofit actions and it is accompanied by an increase in cost.

The scale factor adjusting for the post-disaster economic status, *S*, is included to address the increased demand for construction after a natural disaster. A parametric study on the impact of *S* on the optimal management strategies is included in this example problem. Figure 4.12 shows the Pareto optimal solution fronts *S* values of 1.2, 1.5, and 2. As shown, the general shape of the Pareto fronts are the same. Detail A in Figure 4.12 focuses on the region including typical solutions C1 and C2 where *S* is 1.2 and 2, respectively; these are optimal solutions which minimize cost for a maximum life-cycle risk value of $50,000. C1 and C2 involve two repair actions over the life-cycle, but C2 also includes the application of three vertical tie-downs at year 22. This indicates a shift in the optimal management strategies for a given desired risk level. This is achieved in

the optimization by including retrofit actions to reduce the cost of failure due to hurricanes, which will increase relative to the cost of failure under daily traffic loads as S increases.

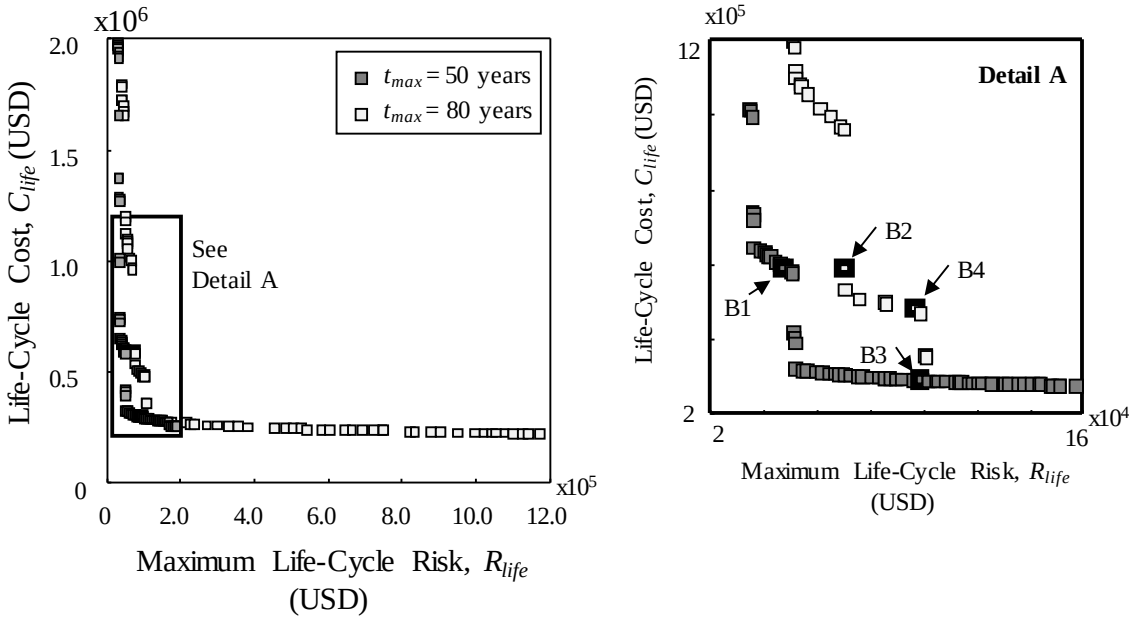

Figure 4.10. Pareto-optimal set for required service life of 50 and 80 years for a real interest rate of +0.01.

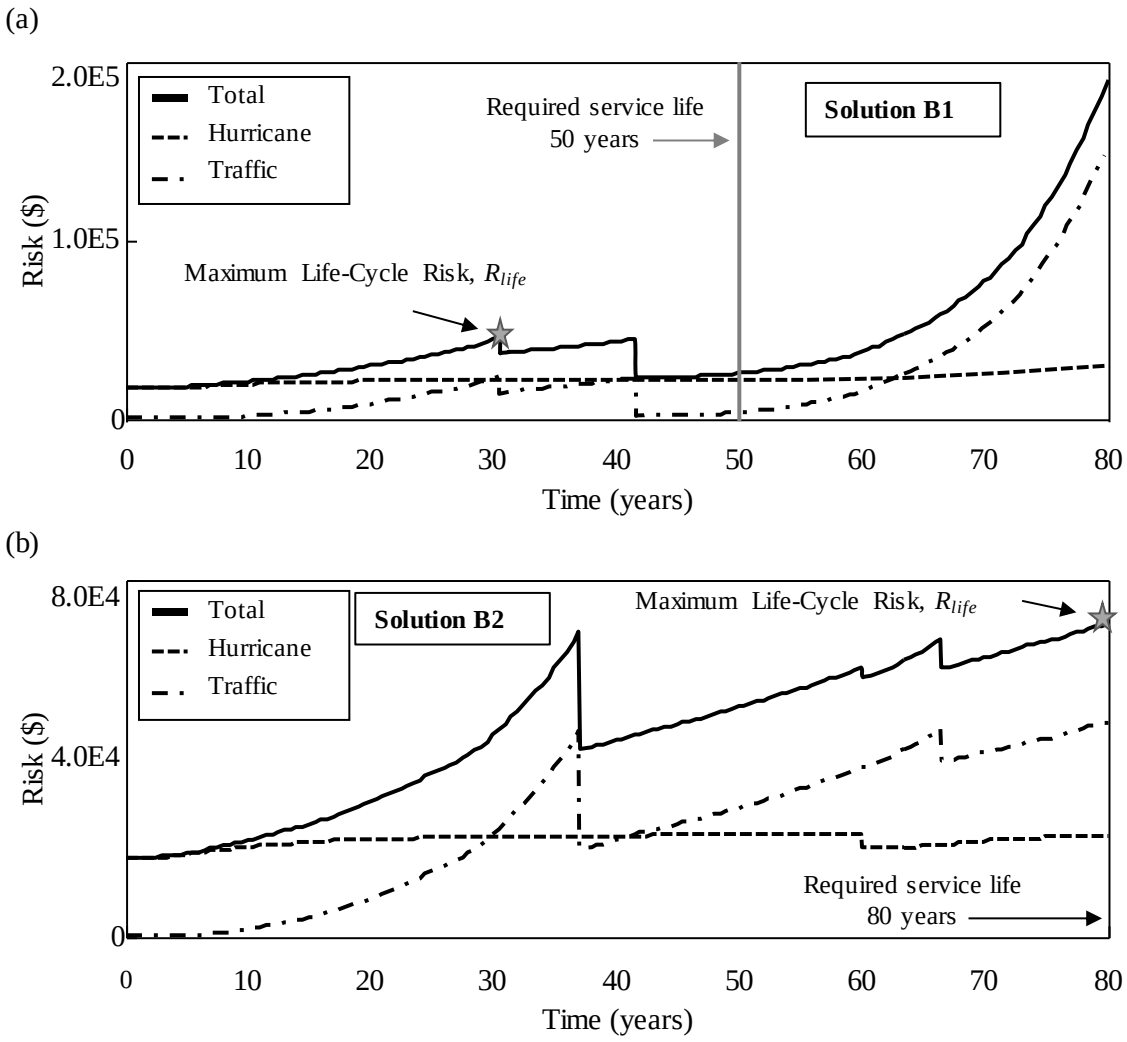

Figure 4.11. Risk as a function of time for representative solutions B1 and B2 from Pareto-optimal set in Figure 4.10.

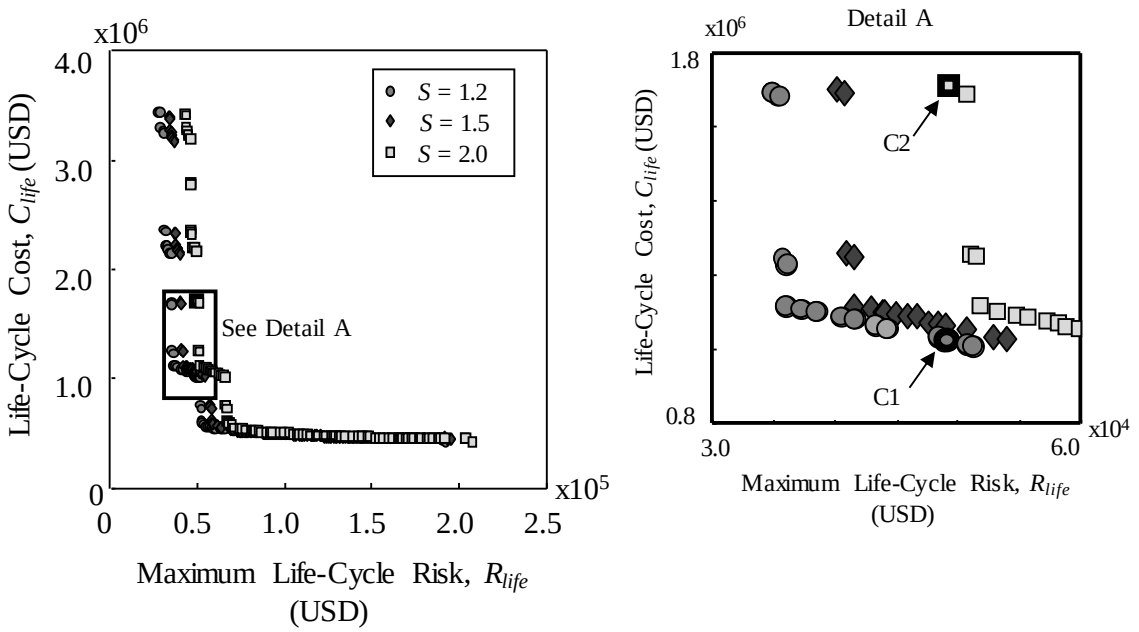

Figure 4.12 Pareto-optimal set for required service life of 50 years where the failure costs due to hurricane is varied to represent different post-disaster economic scenarios.

4.11. CONCLUSIONS

This research, based on Mondoro et al. (2017c) and discussed further in Mondoro and Frangopol (2016) and Mondoro et al. (2016a), proposes an approach to develop optimal bridge management strategies in coastal regions addressing the risk associated with the predominant natural hazard, hurricanes, the intrinsic traffic hazard, and the aggressive environment. The proposed methodology formulates the timing and type of repair and retrofit actions, in order to minimize both the life-cycle costs and the maximum life-cycle risk. The application of vertical tie-downs is the primary retrofit action investigated in this framework; however, the inclusion of additional retrofit actions, such as coring holes

in the deck, and/or shear keys can be easily integrated. Maximum life-cycle risk provides a metric of comparison that efficiently combines the likelihood of and the consequences from failure due to the everyday traffic hazard and the extreme natural hazard of hurricanes. Bi-objective optimization problems were solved in order to understand the impact of economic conditions (i.e. real interest rates), required service life, and the consequence of failure due to the hurricane hazard. The following conclusions are drawn

- The proposed optimization approach is effective in establishing optimal management strategies for bridges considering hurricanes, traffic, and deterioration mechanisms. The risk metric provides an opportune standard as it incorporates the failure and consequences of the diverse hazards.
- Minimizing life-cycle costs and minimizing the maximum life-cycle risk are conflicting objectives in which repair and retrofit actions increase the life-cycle cost but decrease the maximum life-cycle risk. Optimal management strategies associated with high-risk low-costs solutions can be drastically improved through minimal additional investments.
- The increased cost of construction materials and labor in a post-disaster region is an important consideration in the development of optimal management strategies. High relative hurricane failure consequences drive optimal management strategies to include retrofit actions in order to maintain a desired risk level.
- Economic conditions such as the real interest rate affect optimal management strategies; the timing, number, and type of repair and retrofit vary based on economic circumstance.

The vulnerability of bridges to extreme hydrologic events of hurricanes and flooding may be affected by natural and anthropogenic climate changes. The work included in this chapter assumes a stationary climate, thus omitting the potential climate changes. Chapters 5 and 6 are dedicated to identifying the impact of climate changes on the performance of bridges and methodologies for managing structures considering these impacts.

CHAPTER 5

BRIDGE ADAPTATION AND MANAGEMENT UNDER CLIMATE CHANGE UNCERTAINTIES: A REVIEW

5.1. OVERVIEW

The management of civil infrastructure, including the allocation of scarce resources, is an engineering issue that now must also consider the highly debated, highly politicized hazard of climate change. Bridges, in particular, are increasingly vulnerable to damage as a result of the sea level rise, increasingly intense precipitation, and increasingly intense hurricanes that accompany climate change. This chapter reviews the current challenges facing bridge owners and managers as a result of anthropogenic and natural climate changes. The complexities of climate change are discussed and the current state of research regarding the direct relationship to anthropogenic climate changes, as well as natural climate patterns, is presented. Potential adaptation measures are outlined for repair and retrofit measures that may help mitigate the negative impact of climate change. Methodologies for planning under uncertainty, including stochastic and robust optimization methods, are discussed with respect to bridge management under climate change.

5.2. INTRODUCTION

The increased vulnerability of civil infrastructure under uncertain anthropogenic climate changes poses a significant challenge to city planners and bridge managers. Climate

change effects exacerbate the harsh environments that corrode structures; extreme, natural events are seen to occur with greater frequency (IPCC, 2014a). This work reviews the hazard of climate change as it pertains to bridges, potential adaptation methods, and the challenges of managing structures under climate change and uncertainties.

Sea level rise (SLR), heat waves, increasingly intense precipitation, increasingly intense hurricanes, and arctic warming are the major components of climate change that affect civil infrastructure (Schwartz, 2010; Rowan et al., 2013). Since the damage to bridges resulting from extreme events may have large economic consequences (Blake et al., 2011; Pielke and Pielke, 1997; Anthes et al., 2006; Henderson-Sellers et al., 1998), this review focuses on three major aspects of climate change: SLR, increasingly intense precipitation, and increasingly intense hurricanes. While these hazards intensify over the time, structures continue to deteriorate due to corrosive environments. Climate change may also intensify the rate at which these structures deteriorate, further increasing their vulnerability (Bastidas-Arteaga et al., 2013; Bastidas-Arteaga and Stewart, 2015; Chaves et al., 2016; Stewart et al., 2011, Wang et al., 2012). Currently 11% of bridges in the United States are considered structurally deficient and require 76 billion United States Dollar (USD) to be repaired (ASCE, 2013).

Thus, transportation planners are simultaneously faced with the difficulties of addressing climate change concerns while managing aging structures. Research efforts have begun to help enable planners to identify which structures are vulnerable to significant damage due to climate change. Wright et al. (2012) indicated that the number of deficient bridges could increase to up to 25% of all bridges over water in the

continental United States by the end of the 21st century. Furthermore, Neumann et al. (2015) demonstrated that climate change has a potentially high impact on both coastal and noncoastal infrastructure sectors. Rowan et al. (2013) developed a sensitivity matrix which enumerated specific components of transportation networks (i.e. bridge, road, railroads, airports, etc) and identified critical assets and the components of the climate change hazard which present a significant threat. Vogel et al. (2011) has proposed modification factors that address the increased occurrence of flood events to be accounted for in design practices.

State Departments of Transportation (DOTs) have recognized the need to address the impact of climate change (Paulsen and Phillips, 2011; FHWA 2017; ICF International, 2016). However, the magnitude and occurrence of SLR, heat waves, increasingly intense precipitation, and increasingly intense hurricanes differ across the United States (Hunt and Watkiss, 2011; Meyer, 2008; Meyer and Weigel, 2010; Paulsen and Phillips, 2011). In coastal cities, these anthropogenic climate changes are coupled with urbanization and land use changes, making bridges increasingly vulnerable (Hunt and Watkiss, 2011). Regional variations in vulnerabilities are starting to be addressed on the state level. DOTs in multiple states have begun planning for climate change; 13 states have already including adaptation considerations in their regional planning efforts (Paulsen and Phillips, 2011). Furthermore, coastal cities such as New York, Boston, and Miami have conducted in-depth studies on the vulnerability to climate change (Rosenzweig et al., 2011; Kirshen et al., 2008; Stanton and Ackerman, 2007). These studies highlight vulnerabilities to permanent inundation, increased flood zones, and extreme damage

during hurricanes. They unanimously identify uncertainty as a significant obstacle for planning for climate change.

Uncertainty in climate change predictions comes from three main sources: model uncertainty, scenario uncertainty, and natural variability (Hawkins and Sutton, 2011; Paulsen and Phillips, 2011; Groves and Lempert, 2007). Model uncertainty is the variability generated from using different global climate models (GCMs) to determine future climates. There are more than 30 models, which vary from simple energy balances to atmosphere-ocean climate models. Their applicability and accuracy varies based on region and climate feature investigated (Flato et al., 2013). The second source of uncertainty is scenario uncertainty, or the variation in future emission scenarios due to socio-economic changes in population, land use, regulatory efforts, and the advancement of alternative energy sources (Carter et al., 2007). The Intergovernmental Panel on Climate Change (IPCC) has developed a set of 40 feasible emission scenarios. Each emission scenario is a feasible alternative for future emissions, but the likelihood of each scenario is unknown and no probability of occurrence can be assigned to scenarios (Nakicenovic and Swart, 2000). The final source of uncertainty is natural variability. Natural variability refers to the variation in climate due to natural oscillatory patterns and processes.

Managers are weary to make decisions regarding the management of structures under the aforementioned uncertainties (Paulsen and Phillips, 2011; Schwartz, 2010; Lempert and Schlesinger, 2000). However, these uncertainties are not likely to be eliminated, or substantially reduced, within the time frame available to these decision makers

(Hallegate, 2009; IPCC, 2014a). Yet, actions must be taken now to incorporate climate change into the design of new structures and the management of existing structures in order to mitigate future damage to bridges.

The objective of this work is to provide a review of challenges facing decision makers when developing design and management strategies for coastal bridges vulnerable to climate change effects. The section 5.3 provides a thorough review of the current state of research on the direct links between the aforementioned hazards and climate change. It is essential to identify the extent to which anthropogenic and natural forces are driving changes in SLR, hurricanes, and extreme precipitation in order to then develop adaptation strategies for mitigating the impact of climate change. Section 5.4 reviews adaptation measures. The means of adaptation is dependent on the stage of a structure. If the structure is still in the design phase, adaptation includes the reevaluation of flood plains, surge maps, and sea levels, and their subsequent use in the design and management of structures. However, if the structure is in service, adaptation includes applying countermeasures to the structure to prevent damage due to increased hydraulic loads associated with climate change. Within the discussion on retrofit, key failure modes are identified and countermeasures are detailed for coastal bridges. Section 5.5 provides a review of optimization techniques as it applies to the design and management of bridges under climate change and uncertainties. The final section provides a set of concluding remarks, including the challenges and difficulties of managing bridges under climate change.

5.3. THE CLIMATE CHANGE HAZARD

Sea level rise, increasingly intense precipitation, and increasingly intense hurricanes pose a significant threat to the performance of coastal bridges. The current state of research regarding the link between anthropogenic changes and these hazards is detailed herein. Since the management of public infrastructure is a social and political concern as much as it is an engineering issue, it is essential to understand the delineation and interaction of anthropogenic climate changes and natural climate patterns, and the role they play in developing management strategies.

5.3.1. Sea Level Rise

The IPCC noted an unequivocal warming of the climate that has caused oceanic temperatures to increase and ice and snow formations to melt (IPCC, 2014a). As a result, the global average sea level has risen due to an increased volume from (1) the thermal expansion of water from higher sea surface temperatures (SSTs) and (2) the added mass from retreating glaciers (Nicholls and Cazenave, 2010; Church and White, 2006; Jevrejeva et al., 2009). Over the past 150 years, 75% in the global average SLR is directly attributed to anthropogenic climate changes (Jevrejeva et al., 2009).

Changes in sea level are spatially variable and affected by both SLR and local subduction (Nicholls and Cazenave, 2010; NOAA, 2016). Table 5.1 summarizes notable sea level changes that have been observed over the past decades, and in some cases, centuries, for various locations in the Northeast, Gulf Coast, and West Coast regions of the United States (NOAA, 2016). The rates listed are the SLR per year at each specific site corresponding to a linear sea level rise over the observational period. The spatial

variability in the observed annual sea level rise demonstrates one of the difficulties in establishing consistent action plans for all geographic locations: specific climatic patterns must be accounted for each site as they differ by location (FHWA 2017; IPCC, 2014b; ICF International, 2016). It is important to note that flooding still poses a significant threat to infrastructure regardless of whether the sea level changes are due to sea level rise or land subsidence (Burkett et al. 2002; Dalton and Mote, 2013).

Similar to the observed trend, climate change predictions for SLR indicate similar spatial variability patterns for the United States. However, there is uncertainty in the GCMs, emission scenarios, and natural climate patterns that result in range of predicted SLR rather than a deterministic set. For example, the predicted SLR by 2080 for New York City is expected to be between 30.0 and 95.8 cm by 2080 (Gornitz et al., 2002) and between 11.7 to 142.7 cm for Portland, Oregon (Dalton and Mote, 2013). The most significant source of uncertainty for short-term SLR predictions is the behavior of ice sheets: it is unknown if ice sheets will continue to recede at the current rate, collapse, or partially collapse (Nicholls and Cazenave, 2010). Furthermore, variability in local subduction of land due to seismic activity, underground mining, or natural compaction adds to the uncertainty in climate change predictions for SLR (Dalton and Mote, 2013; Burkett et al., 2002).

Table 5.1. Observed sea level rise in the contiguous United States (adapted from NOAA 2016)

Region	City	Observational Period		Mean Annual Sea Level Trends (mm/yr)	95% confidence interval (mm/yr)
		Start	Final		
North East	Portland, ME	1912	2015	1.87	± 0.15
North East	Boston, MA	1921	2015	2.79	± 0.16
North East	Providence, RI	1938	2015	2.22	± 0.25
North East	The Battery, NY	1856	2015	2.84	± 0.09
North East	Atlantic City, NJ	1911	2015	4.07	± 0.16
North East	Philadelphia, PA	1900	2015	2.93	± 0.19
North East	Washington, DC	1924	2015	3.22	± 0.29
Gulf Coast	Miami Beach, FL	1931	1981	2.39	± 0.43
Gulf Coast	St. Petersburg, FL	1947	2015	2.66	± 0.25
Gulf Coast	Dauphin Island, AL	1966	2015	3.3	± 0.61
Gulf Coast	Grand Isle, LA	1947	2015	9.05	± 0.46
Gulf Coast	Corpus Christi, TX	1983	2015	3.8	± 0.17
West Coast	Los Angeles, CA	1923	2015	0.95	± 0.24
West Coast	San Francisco, CA	1897	2015	1.94	± 0.19
West Coast	South Beach, OR	1967	2015	1.55	± 0.76
West Coast	Neah Bay, WA	1934	2015	-1.73	± 0.31
West Coast	Seattle, WA	1899	2015	2.01	± 0.15

5.3.2. Hurricanes

The relationship between hurricanes and climate change is a complex issue intensified by political debate and societal implications. The current state of research on climate change and hurricanes suggests that the recent increase in intensity can be attributed to natural climate patterns, anthropogenic climate changes, or the confluence of both. The following discussion will use the term tropical cyclone as it is the broadest term used to define rapidly rotating storm systems with a low-pressure center and high precipitation rates (WMO, 2005). It is only in the North and South Atlantic and the Northeast Pacific where

tropical cyclones with 1-minute sustained wind speeds larger than 119 km/h are identified as hurricanes (WMO, 2005).

Tropical cyclones may form when the following environmental factors are present: sea surface temperatures exceeding 26°C, high humidity, low vertical wind shear, atmospheric instability, sufficient Coriolis force, and a preexisting low level focus or disturbance (Gray, 1968). Climate change researchers have based their theoretical arguments for the direct causality of increasingly intense hurricanes by anthropogenic climate changes on the environmental factor of warmer SSTs. The argument is as follows: tropical cyclones gain energy from warm seas (Emanuel, 1987); it has been shown that SSTs have increased due to the emissions of greenhouse gases (IPCC, 2014a); thus, anthropogenic climate changes may increase the intensity of hurricanes (Emanuel, 1987; Mitchell et al., 2006; Anthes, 2006; Knutson and Tuleya, 2004).

Researchers have used statistical analysis of past temporal trends to support the notion that anthropogenic climate changes have increased the intensity of tropical cyclones. Webster et al. (2005) demonstrated that global maximum wind speed and the total number of Categories 4 and 5 hurricanes increase in time throughout all basins. Elsner (2006) showed that hurricane activity, in the Atlantic basin increases in time along with SST. However, other researchers have indicated that it is unclear if there is a clear correlation between anthropogenic climate change and the intensity of tropical cyclones (Knutson et al., 2010; Seneviratne et al., 2012). Furthermore, recent increases in observational technologies and systems may be skewing the observations of tropical

cyclones and the resulting statistical inferences (Knutson et al., 2010; Vecchi and Knutson, 2008; Goldenberg et al., 2001; Shao et al 2016).

The statistical analysis of tropical cyclone activity is obscured by the presence of the natural oscillatory patterns (Knight et al., 2006; Alexander et al., 2014). Climate researchers have identified oscillatory patterns such as the Atlantic Multidecadal Oscillation (AMO), El Niño–Southern Oscillation (ENSO), and North Atlantic Oscillation (NAO) as key driving factors for the cyclogenesis, path, and the recent intensification of tropical cyclones in the Atlantic. This includes not only an increase in the intensity (Herbert et al., 1996; Mann et al., 2009; Gray, 1984) but also changes increase in the number of hurricanes that make landfall (Hurrel et al., 2003; Elsner et al., 2000; Herbert et al., 1996; Landsea et al., 1999; Bove et al., 1998). In order to capture the various factors influencing tropical cyclones, predictions are typically made on a large-scale coarse mesh. The results are then downscaled to refined meshes for local areas in order to assess the change in tropical cyclones due to climate change (Knutson et al. 2010; IPCC 2014a). The confidence in the downscaled results for hurricane predictions remains low contributing to high levels of uncertainty (Knutson et al., 2010, IPCC 2014b).

5.3.3. Precipitation

The IPCC noted an unequivocal increase in average temperature (IPCC, 2014a). Since warmer sea surface and atmospheric temperatures increase evaporation rates and water carrying capacity of the atmosphere, increased intensity of precipitation is a theoretically viable consequence of anthropogenic climate changes (Trenberth, 2011; Schwartz, 2010;

Rowan et al., 2013). Initial studies identified that extreme precipitation events have increased with increases in temperature (Easterling et al., 2000; Condon et al., 2015; Hawkins and Sutton, 2011). The severity and recurrence of extreme flooding events have also been linked to anthropogenic climate changes (Vogel et al., 2011; Rootzén and Katz, 2013; Condon et al., 2015).

It is difficult to isolate increases in flooding that are associated with anthropogenic climate changes from those that may be attributed to natural climate variability (Small et al., 2006), the urbanization of a region (Vogel et al., 2011; Merz et al., 2012) or local regional variations (Douglas et al., 2000). However, significant research has identified that flooding events in the United States are nonstationary (Vogel et al., 2011; Rootzén and Katz, 2013; Condon et al., 2015). Predictions for future flooding events parallel the statistical trends and predict increasingly intense events. Predicted shifts in the return period of flooding events have been estimated by GCMs for regions across the United States (Kirshen et al., 2008; Rosenzweig et al., 2011). For example, the return period for 100-year flood in New Jersey may be shifted to 2-10 years by 2100 (Kirshen et al., 2008).

Individual GCMs use different climate indicators and threshold values to identify if, and when, extreme precipitation events occur. Typical indicators include atmospheric moisture, mean sea level pressure, and vorticity; each yielding a different precipitation prediction (Wilby and Wigley, 2000). This results in a high variability in the prediction of extreme precipitation events based on which GCM is used. The uncertainty of the predicted extreme precipitation is compounded by the need to downscale the outputs from the GCM course grid to the refined mesh where local precipitation events are

evaluated (Chen et al., 2011). Hawkins and Sutton (2011) analyzed the contributions to uncertainty in the prediction of global mean precipitation, among other environmental metrics. The results indicated that the predominant source of uncertainty in precipitation prediction for all time horizons is model uncertainty. The contributions of model uncertainty, scenario uncertainty, and natural climate variability to the variance in the predicted global mean precipitation are shown in Figure 5.1. Hawkins and Sutton (2011) demonstrated that, among scenario uncertainty and natural climate variability, natural climate variability contributions dominate for short time horizons (e.g. less than 30 years). However, contributions from scenario uncertainty surpass those of natural climate variability over long time horizons, providing up to 25% of the uncertainty for time horizons around 90 years as shown in Figure 5.1.

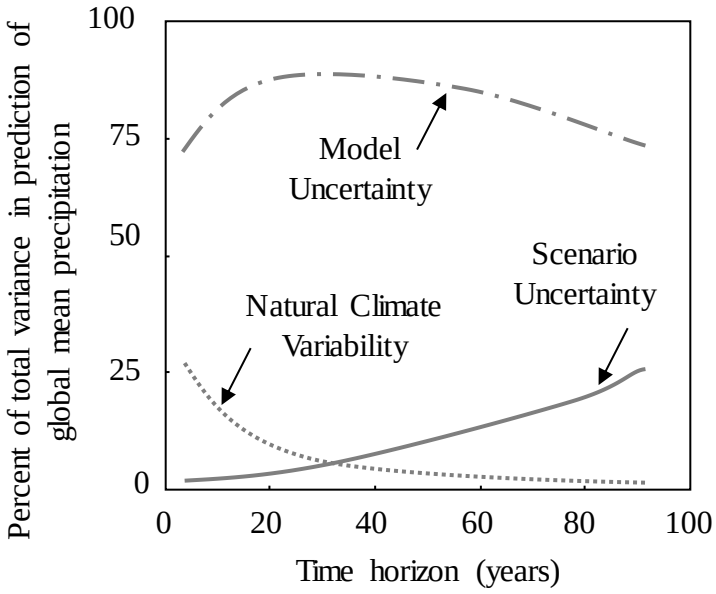

Figure 5.1. The contributions of model uncertainty, scenario uncertainty, and natural climate variability to the variance in predicted global mean precipitation (adapted from Hawkins and Sutton (2011)).

5.4. ADAPTATION

The impacts of climate change may be mitigated through an adjustment in a system, an adaptation effort (IPCC, 2014a). Adaptation efforts can be made during two distinct phases: the design phase and the in-service phase. The former requires an adjustment in the design process; flood plains, surges, and sea levels must be reassessed in order to account for nonstationary climate trends and incorporated into design and management procedures. When the structure is in service, adaptation includes the application of repair or retrofit measures to prevent damage. The following sections outline adaptation efforts that may be made in the design phase of a new structure or applied to existing structures. Adaptation in the design phase is discussed with respect to the particular hazard, while in-service adaptation is discussed with respect to the failures modes that may be exacerbated by climate change effects. This was done to enable a more complete discussion of potential retrofit measures that may mitigate damage. These failure modes, however, can be tracked back to their particular hazard. In order to provide a clear summary, Table 5.2 details the connection between the natural hazard effected by climate change, design phase adaptation, and in-service adaptation.

5.4.1. Adaptation in the Design Phase

Design procedures are currently developed around the statistical analysis of past events. The design loads and exposure categories are assumed to be the same in the future; that events will occur with the same magnitude for a given recurrence interval. A

Table 5.2. Climate change hazards, failure modes, and adaptation methods for coastal bridges

Hazard	Design Phase Adaptation	Potential Failure Modes	In-Service Adaptation
Sea Level Rise	▪ *Rezone low lying regions for future development*	Permanent Inundation	▪ *Elevate or Abandon*
		Coastal Erosion	▪ *Seawalls, groins, etc*
Hurricanes	▪ *Include hydraulic considerations in design and assessment procedures* ▪ *Update surge maps with respect to SLR*	Deck Unseating	▪ *Elevate critical infrastructure* ▪ *Insert holes* ▪ *Tie-down, restrainers, anchorage bars, etc* ▪ *Concrete shear tabs, etc*
		Substructure Failure	▪ *Surface coatings, pile wraps, pile jackets, pile jackets with reinforcement, etc*
		Wind Damage	▪ *Cladding: toe nails, hurricane straps, adhesives , or epoxy-bonded wood blocks, etc* ▪ *Fatigue: detail specific*
		Scour	▪ *Riprap, partially grouted riprap, concrete block systems, gabion mattresses and grout-filled mattresses, etc* ▪ *Upstream walls and obstructions, collars, etc*
Intense Precipitation (Flooding)	▪ *Update magnitudes for design period storms to account for non-stationarity* ▪ *Update flood plains with respect to SLR*	Scour	▪ *Riprap, partially grouted riprap, concrete block systems, gabion mattresses and grout-filled mattresses, etc* ▪ *Upstream walls and obstructions, collars, etc*
		Substructure Failure	▪ *Surface coatings, pile wraps, pile jackets, pile jackets with reinforcement, etc*
		Deck Unseating	▪ *Elevate critical infrastructure* ▪ *Insert holes* ▪ *Tie-down, restrainers, anchorage bars, etc,* ▪ *Concrete shear tabs, etc*

reassessment of design loads and exposure categories for SLR, hurricanes, and precipitation is essential to the adaptation process. The following sections outline the potential vulnerabilities of bridges and current and potential efforts that can be made in the design phase to mitigate the effects of climate change.

5.4.1.1. Sea Level Rise

Gradual changes in sea level may not appear to be imminent threats to the performance of bridges, but Wu et al. (2009) showed that 2,600 km^2 in the Mid- and Upper Atlantic Regions of the United States may be permanently submerged by 2100. SLR may result in low clearance structures being permanently submerged. Roadways in coastal zones may be permanently inundated rendering coastal bridges useless. Adaptation in the design phase include reevaluating building codes and zoning provisions to prevent further new development in vulnerable regions. In this way, investments in infrastructure have a beneficial return on investment even under climate change impacts. Maine, Massachusetts, Rhode Island, and South Carolina have been implemented restrictions on new development to include considerations for changes in the sea level (McLean et al., 2001). Additionally, SLR amplifies the vulnerability of regions to flooding and damage during intense precipitation and hurricane events (Mann et al., 2009; Rosenzweig et al., 2011; Burkett et al., 2002). Therefore, adaptation measures for SLR including adjusting floods maps and surge maps to account for SLR and changes in the coastal profile.

5.4.1.2. Hurricanes

The direct link between an increase in the intensity of tropical cyclones and anthropogenic climate changes is highly debated. However, researchers unanimously

agree on the devastating impact of tropical cyclones that make landfall; the societal and economic losses can be devastating to a region (Blake et al., 2011; Pielke and Pielke, 1997; Anthes et al., 2006; Henderson-Sellers et al., 1998). The tenuous relationship between climate change and hurricanes does not mean that adaptation measures for the hazard can be omitted. Previously, the increases in the vulnerability to damage due to hurricanes have only been incorporated after a major natural disaster. For instance, changes in the Federal Emergency Management Agency (FEMA) flood maps were implemented after major flooding events and hurricanes (FEMA, 2015), and, new specifications were developed for structures vulnerable to coastal storms after Hurricanes Ivan and Rita severely damaged structures (AASHTO, 2008). Adaptation measures in the design phase should consider the potential for SLR to increase flood zones and exacerbate damage during hurricane events.

5.4.1.3. Precipitation

Intense precipitation, coupled with urbanization and land-use changes, increases the exposure of bridges to severe flooding scenarios. Adaptation in the design phase must integrate the increased potential for damage under the extreme hydraulic loads into design and management procedures. Currently, Vogel et al. (2011) proposed a flood modification factor to address changes in the intensity of precipitation. Their methodology included a factor to quantify changes in the magnitude of design period storms and/or the recurrence interval of intense floods as a result of anthropogenic changes. This would provide engineers with a systematic method to account for anthropogenic climate changes in the design and management of structures. Additionally,

Rootzén and Katz (2013) proposed that the time horizon, or required service life, be included in estimating the impact of climate change on structures. The design life level integrates the probability of exceeding an extreme level with the expected time horizon, and does not include considerations of climate changes beyond the required service life of the structure.

The aforementioned methods for adaptation to intense precipitation and floods do not consider the cause of the intense precipitation or floods. However, these events may be caused by tropical cyclones, convective storms, or winter storms; each stemming from their own unique climatological patterns). For example, the probability distribution function (PDF) of the annual flood magnitude for a specific location in the current climate can be broken down into its contributions from the inciting storms including tropical cyclones, convective storms, and winter storms (Merz 2014). If tropical cyclones are deemed nonstationary in an area, then the number of floods and their magnitudes due to tropical cyclones in that area may increase, causing a shift in the total distribution of annual floods. The potential future climate would then be categorized with a new pdf for annual flood magnitudes as shown qualitatively in Figure 5.2, curve (b). Nonstationary trends in convective and winter storms, stemming from the emission of greenhouse gases, cause shifts in the convective and winter storm contributions to the total distribution of annual floods respectively; the net effect of which is shown in Figure 5.2, curve (c). However, it may prove that all three storm types (tropical cyclones, convective storm, and winter storm) are nonstationary due to anthropogenic changes and generate an alternative shift in the annual flood magnitude distribution for future climates, shown as

curve (d) in Figure 5.2. Thus, the stationarity, or non-stationarity, of the individual storm types must be considered when assessing the impact of anthropogenic climate change and the reassessment of floods. Since tropical cyclones are one of the major hazards in the climate change set, but also impact the flooding, one of the other major hazards in the set, it is necessary to include the joint probability of occurrence of the events when developing adaptation plans for climate change. This joint occurrence is not accounted for in the methodologies established by Rootzén and Katz (2013) or Vogel et al. (2011).

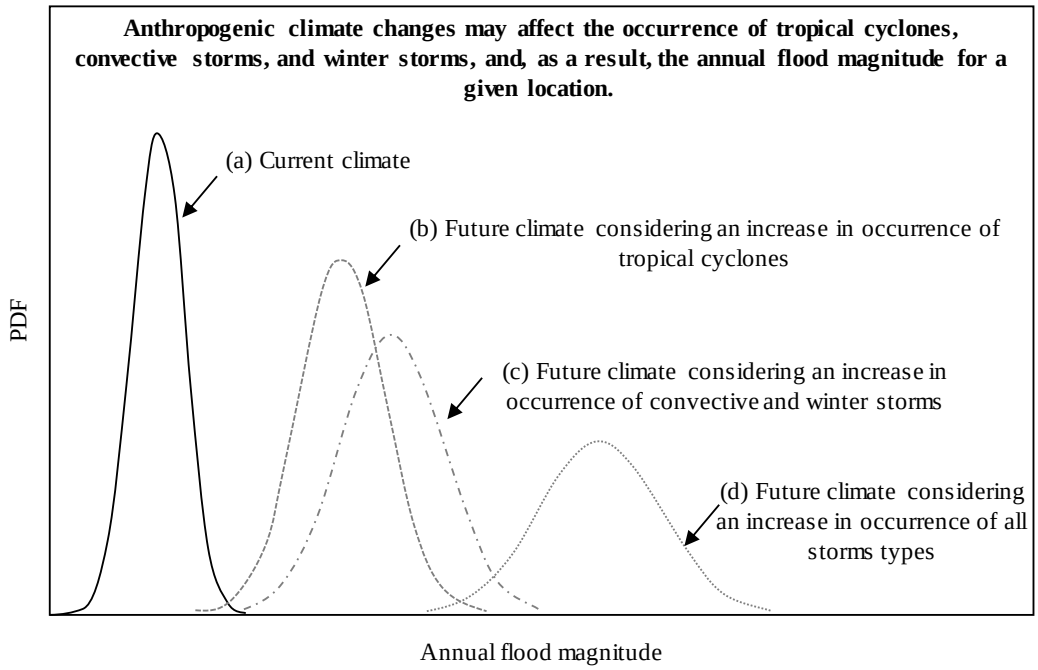

Figure 5.2. Qualitative depiction of the shifts in annual flood magnitude distributions that may occur as the result of climate change. The current climate for a site has floods that are caused by tropical cyclones, convective storms, and winter storms. Anthropogenic climate changes may increase the occurrence tropical cyclones, convective and winter storms, or all storm types and cause a shift in the annual flood distribution for the site as shown in curves b, c, and d, respectively.

5.4.2. Adaptation of In-Service Structures

Retrofit measures may be applied to existing structures to help reduce damage and prevent failure over their expected life. These measures are specific to the failure modes which they are trying to prevent. The following section discusses key failure modes that may become increasingly important to consider because of climate change effects. The following failure modes and their associated retrofit actions are outlined: deck unseating, substructure failure, coastal erosion, wind damage, and scour.

The failure modes were chosen due to their direct relationship to the climate change effects on SLR, increasingly intense precipitation, and increasingly intense hurricanes. Sea level rise may permanently inundate structures and amplifies coastal erosion damaging natural or manmade barriers causing an increase in the vulnerability of bridges to hurricane damage. Since the main solutions to permanent inundation are elevation, which may be prohibitively expensive, and abandonment, only coastal erosion is detailed. Hurricanes may cause deck unseating, substructure failure, wind damage, and scour. Flooding may precipitate scour damage, substructure failure, or deck unseating. The following sections detail the specific failures modes and retrofit options can be used as in-service adaptation measures. These are summarized in Table 5.2 in conjunction with the hazards and the design phase adaptation efforts.

5.4.2.1. Deck unseating

Low clearance bridges may be extensively damaged by the extreme hydraulic forces accompanying the tropical cyclone surge or extreme flooding events (Chen et al., 2009; Kulicki, 2010; Ataei and Padgett 2013b). The bridge decks of simply supported bridges

may become misaligned or dislodged from their supports due to extreme uplift and transverse hydraulic forces. Retrofit measures for bridges that are vulnerable to deck unseating can be divided into two categories: (a) measures aimed at reducing hydraulic forces on a superstructure, and (b) measures that increase the capacity of a bridge to resist hydraulic loads.

The simplest way to reduce hydraulic forces is to elevate critical infrastructure. In this way the bridge is well above the limit of the potential storm surge inundation and wave height. Elevation, however, may be economically or socially infeasible (Rosenzweig et al., 2011; AASHTO, 2008). Alternatively, inserting holes in the superstructure to allow entrapped air to flow out from beneath the superstructure helps reduce the buoyancy force acting on the structure during the event (Sawyer, 2008; AASHTO, 2008). Caution must be taken when coring vent holes in the bridge in order to avoid any significant reductions in the capacity (Sawyer, 2008; AASHTO, 2008).

Tie-down, restrainers, and anchorage bars, among others, may be added to bridges to provide a connection between the sub- and superstructure. These increase the capacity to resist upward and transverse movement during surge events (Okeil and Cai, 2008; Ataei and Padgett 2013b). Alternatively, connecting adjacent spans may increase the capacity to resist unseating. Since waves have finite crest lengths and multiple adjacent spans are not typically loaded simultaneously, developing continuity increases the weight of the structure that resists uplift without increasing the demand loads (AASHTO, 2008). Concrete shear tabs increase the capacity to resist transverse hydraulic forces. These are typical seismic retrofit options that are used to prevent dislodgement during earthquakes

but effectively reduce transverse displacement during surge events as well (Robertson et al., 2007). It should be noted that the performance of such a measure is limited by physical height of the shear tab; once the vertical displacement of the superstructure exceeds the height of the tab, the transverse restraint is no longer viable (Kawashima et al. 2012).

5.4.2.2. Substructure Failure

Substructure failure is discussed with regards to the structural capacity of the piers and bents and is separated from scour damage, which is discussed subsequently. Substructure capacity may become a concern when the connection between the superstructure and substructure is sufficient to prevent unseating during extreme hydraulic events. The transverse hydraulic loads acting on the superstructure are transferred to the piers increasing the shear and moment demand already on the substructure from direct hydraulic loads. The shear and flexural capacity of the substructure may be exceeded and failure may ensue. The continued exposure to chlorides corrodes structural components further enhancing the potential for substructure failure. Repairs may be made to corroded substructures to restore the initial shear and flexural capacity to the pier. Retrofits in the form of surface coatings and pile wraps can be applied to steel, concrete, and timber piles to prevent damage. However, if the current piles are significantly damaged either due to corrosion or spalling, pile jackets, pile jackets with reinforcement, or their complete replacement may be necessary to prevent failure (Brown et al., 2010).

5.4.2.3. Coastal Erosion

Natural and manmade barriers help protect inland regions from damage due to hurricanes and storm surges. Structural retrofit measures, such as seawalls and groins, are designed to decrease the erosion of these natural and manmade barriers. Their placement helps maintain the integrity of the barrier and, in some cases, absorb energy from the surge (Rosenzweig et al., 2011; USACE, 1996).

Sea walls may be placed parallel to the shore to limit erosion landward. Sea walls with heights extending beyond the height of the natural barrier may enhance the performance. The exposed sea walls may also absorb and dissipate energy from the surge and reduce the magnitude of hydraulic loads inland (Bridges et al., 2013). The sea wall, however, may induce higher erosion rates for the beach directly in front of it (USACE, 1996). Groins may be placed parallel to the shore to limit longshore erosion within a given region. However, this may have negative implications elsewhere along the shoreline leaving other areas more vulnerable to erosion and storm damage (USACE, 1996). For further review of coastal erosion countermeasures, issues, and implications, the reader is directed to the USACE report for on coastal risk reduction (Bridges et al., 2013).

5.4.2.4. Wind Damage

Extreme winds during hurricanes have the largest impact on movable bridges and long-span bridges. These bridges rely on the performance of the mechanical and electrical systems in order to accommodate both daily traffic loads on the bridge and marine traffic in the channel. Extreme winds rip the cladding systems (i.e. the siding and roofing) away

from the structure and expose the mechanical systems to water damage (Padgett, 2008; Reed et al., 1997; Rosowsky and Cheng, 1999; Stewart, 2016). The inundation of the mechanical systems renders the bridge immovable, and forces the operators to either (a) leave the bridge in the current location to allow traffic to pass or (b) force the bridge open to allow for traffic in the channel to pass. The forced movement of the structure may cause further damage to the mechanical or structural systems (Padgett, 2008).

Retrofit measures for wind damage would thus include the strengthening of the connection between the building envelope and the main structural system. Reinforcing the connections between the individual roof shingles, roof sheathing, and roof structure to the main structural system is essential to establishing a vertical load path. The roof structure can be retrofitted with additional toe nails, hurricane straps, or epoxy-bonded wood blocks (Reed et al., 1997). The connection between the roof sheathing and the roof structure can be enhanced through the application of additional nails or mechanicals fasteners. However, the quality of the installation can impact the overall effectiveness of the retrofit (Huang et al., 2009; Reed et al., 1997). FEMA (2010) advised that wrong nail sizes, over driven nails, and placement of the nails are common problems that must be avoided. Roof tiles are initially attached through mechanical fasteners or adhesives. The adhesives have the potential to unseal over time and lose capacity. Though the mechanisms of unsealing are not well established, their effects on the performance of cladding system during hurricanes have been observed (Dixon et al., 2014). Retrofit measures to mitigate failure of the individual roof tile include the application of nails or metal fasteners (FEMA, 2010).

Extreme wind loads pose a significant threat to long span bridges. High stress-ranges may be sustained during extreme winds inducing crack formations in critical locations, and propagating the growth of existing cracks. While the duration of this event is relatively small compared to the life-cycle of the structure, the damage sustained during the extreme event contributes significantly to the fatigue damage, along with the damage from daily cyclical loading (Li et al., 2002; Zhang et al., 2014). In order to prevent failure due to fatigue, retrofit actions should be applied (Bennett et al., 2014; Fisher, 1990; Khalil et al., 1998; Dexter and Ocel, 2013; Hassan and Bowman, 1996). A detailed collection of fatigue inspection and repair actions is provided in Dexter and Ocel (2013) and the manual for bridge evaluation (AASHTO, 2012).

5.4.2.5. Scour

As a result of extreme precipitation events or tropical cyclones, bridge piers and abutments are vulnerable to damage during periods of high river flows. Scour holes undermine the capacity and stability of the substructure when soil is transported away from the piers and abutments by swiftly flowing rivers. Scour damage may be reduced through armoring measures or flow alerting measures. For an extensive description of scour prevention methods, the reader is directed to Arneson et al. (2012), Agrawal et al. (2007), Barkdoll et al. (2007), Brown et al. (2010), and Lagasse et al. (2007). The following is a brief review of potential measures to avoid scour damage to bridges.

Armoring measures alter the surface of the channel bed and embankments to resist the transportation of sediment away from the area (Agrawal et al., 2007). Riprap is the most common measure used by DOTs to mitigate scour damage during flooding

(Barkdoll et al., 2007; Lagasse et al., 2007). This is an armoring measure which involves layering down rock on the river bed to prevent erosion of the soil. The rock may also be partially grouted to enhance performance (Heibaum and Trentmann, 2010). Additional measures for preventing soil erosion and scour include concrete block systems, gabion mattresses and grout-filled mattresses (Lagasse et al., 2007).

Alternatively, flow modifications divert the flow of water around the supports in order to avoid scour at the supports. Walls and obstructions may be placed on the upstream side of piers in order to alter flow paths; however, such alterations may have significant impacts further downstream (Barkdoll et al., 2007). Collars may be applied to bridge piers in order to reduce the magnitude of scour damage. The collars change the downward vertical flow of water along the pier and reduce the magnitude of vortices that induce local erosion (Heidarpour et al., 2010). The effectiveness of collars varies with size and placement along the column (Zarrati et al., 2006; Heidapour et al., 2010). Additionally, sacrificial piers may be added to the bridge in order to enhance the overall performance of the load bearing pier group (Melville and Hadfield, 1999).

In addition to the aforementioned retrofit measures, scour monitoring devices may be also be installed to provide an indication on the current performance of a bridge (Legasse et al., 2007; Prendergast and Gavin, 2014). Such devices may provide more reliable and comprehensive information than visual inspections or standing bar measurements from a boat (Fukui and Otuka, 2002). This information is useful after extreme events to see if the bridge is safe, and when deciding if any of the preceding adaptation measures are necessary.

5.5. MANAGEMENT UNDER UNCERTAINTY

Bridge managers are continuously presented with the challenge of allocating scarce resources for the maintenance and repair of a large stock of vulnerable structures. Deterministic optimization techniques provide a systematic methodology for identifying optimal management plans when information about future conditions is known and singular. This is not the case in the climate change problem where uncertainties, both quantifiable and unknown, prohibit the use of deterministic optimization techniques and hinder the formation of a clear adaptation plan (Paulsen and Phillips, 2011; Hallegate, 2009; Niang-Diop et al., 2004; Lempert and Schlesinger, 2000). DOTs have started to recognize the importance of including climate change considerations in their adaptation efforts; 32 states have taken steps to reduce emission, and 10 have called for the development of a comprehensive adaptation plan (FHWA 2012; Cruce, 2009). Additionally, 19 state DOTs and Metropolitan Planning Organizations (MPOs) have completed pilot programs to assess their vulnerability and the challenges of integrating climate change into decision making (ICF International, 2016). Despite the call for developing comprehensive adaptation plans, risk managers and planners are uncomfortable with the high variability in climate change predictions, the inability to assign a likelihood to different climate scenarios, and the lack of confidence in downscaled climate predictions (Paulsen and Phillips, 2011; ICF International, 2016; FHWA 2017). Schwartz (2010) stated that such uncertainties cannot be the cause for inaction; but rather, should be accounted for in regular planning processes in order to develop a more robust and resilient infrastructure.

Since optimal management plans must be developed under uncertainty, the first component of the problem is to quantify and reduce uncertainty when possible. To address the former, statistical modeling and Monte Carlo sampling can be used to account for the aleatory uncertainty associated with natural climate variability. Scenario uncertainty is not quantifiable, as noted by the IPCC (Nakicenovic and Swart, 2000). Improving solution methodologies and refining computational models can help reduce the model uncertainty (Hallegate, 2009; Hawkins and Sutton, 2011). Improvements are limited, however, by the region and climate feature investigated (Flato et al., 2013).

When optimal management plans must be developed under uncertainty, the second component of the problem is to identify the relevant hazards over the life cycle of the structure. Corrosion (Mori and Ellingwood, 1994), scour (Stein et al., 1999; Johnson and Niezgoda, 2004), tropical cyclones (Mondoro et al., 2017c), and earthquakes (Dong et al., 2014a) have been included as relevant hazards for life-cycle optimization problems. Optimal management frameworks were developed for the structures exposed to these hazards. Researchers have investigated the importance of considering the complete transportation network when optimizing the repair and management of structures (Augusti et al., 1998; Liu and Frangopol, 2006; Bocchini and Frangopol, 2011; Dong et al. 2015; Lounis and Vanier, 1998). However, in each of these cases, the future life-cycle loads were considered to be the same as the past.

The third component is to identify systematic methodologies to solve the problem. The significant challenge to optimizing under climate change is the existence of uncertain, future scenarios. It is important to note that these future scenarios no longer

refer to only future emission scenarios. Instead, a single future scenario is defined by the model used, the given emission scenario, and the given natural environment. If models range from $i=1,2,...N$, emission scenarios range from $j=1,2,...J$, and samples for natural variability range from $k=1,2,...K$, future scenarios FS_{ijk} are in the set $\{FS_{111}, FS_{112}, ... ,FS_{11N}, ...,FS_{ijk},... FS_{NMK}\}$. A structure evaluated under each future scenario would have an associated probability of failure. Figure 5.3 is a qualitative representation of the potential range of future scenarios that bridge managers must consider. The different future scenarios may entail large increases in the potential for failure due to SLR, hurricanes, and flooding. However, there may also be scenarios where the change in the potential for failure over time is negligible.

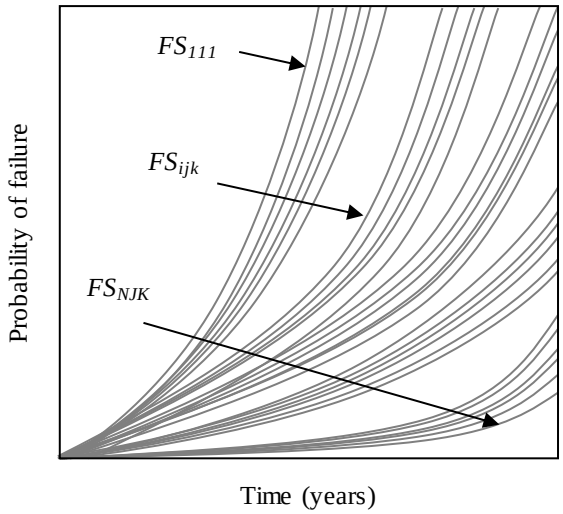

Figure 5.3. Time dependent probability of failure of a structure under potential future scenarios FS_{ijk}. The future scenarios may be developed by using models ranging from $i = 1,2,...N$, emission scenarios ranging from $j = 1,2,...J$, and samples for natural variability ranging from $k = 1,2,...K$. This generates the set of future scenarios $\{FS_{111}, FS_{112}, ... ,FS_{11N}, ...,FS_{ijk},... FS_{NMK}\}$.

Decision makers in the fields of finance, inventory and logistics, humanitarian aid, among others, have to manage assets under future social and economic climates that are also highly variable (Gabrel et al., 2014; Snyder, 2006). The fields of stochastic optimization and robust optimizations have been developed to aid in the decision making process under scenario uncertainty. Typically, objective metrics such as robustness, flexibility, risk, or utility are optimized with respect to future scenario for a given time horizon (Niang-Diop et al., 2004; Gabrel et al., 2014; Groves and Lempert, 2007, FHWA 2017). Similar to single scenario optimization frameworks, the design variables include the timings and types of repairs and retrofits.

Stochastic optimization is defined as the optimization of an objective function in the presence of uncertainties. Typically, the uncertainties are thought of as continuously distributed random variables with a known distribution; though sometimes they may be bounded and approximated with a discrete representation. In the case of climate change, the occurrence of a scenario is uncertain, as are the parameters within each scenario as shown in Figure 5.4. This figure considers 3 scenarios, each with a probability of occurrence P_i which may be known or unknown; typically they are unknown for climate change emission scenarios (Nakicenovic and Swart, 2000). Within each scenario, the occurrences of hazards (e.g. wind speed, surge height, precipitation, and corrosion) are uncertain and can be treated as random variables with known distributions. Generally, stochastic optimization techniques are developed to solve the optimization problem when information about both sets of uncertainties is known.

In order to develop a well-defined stochastic optimization formulation for management plans, the probability of occurrence of each potential future scenario is needed. For the example shown in Figure 5.4, this is the set $\{P_1, P_2, P_3\}$. This information is not readily available because (a) all IPCC emission scenarios are all valid but have no assigned probability of occurrence (Nakicenovic and Swart, 2000; IPCC, 2014a), and (b) there is no clearly defined method to indicate which GCM is more likely to predict correct future climates (Flato et al., 2013). Hallegate (2009) indicated that such a formulation is not viable due to the lack of information regarding the probability of future scenarios.

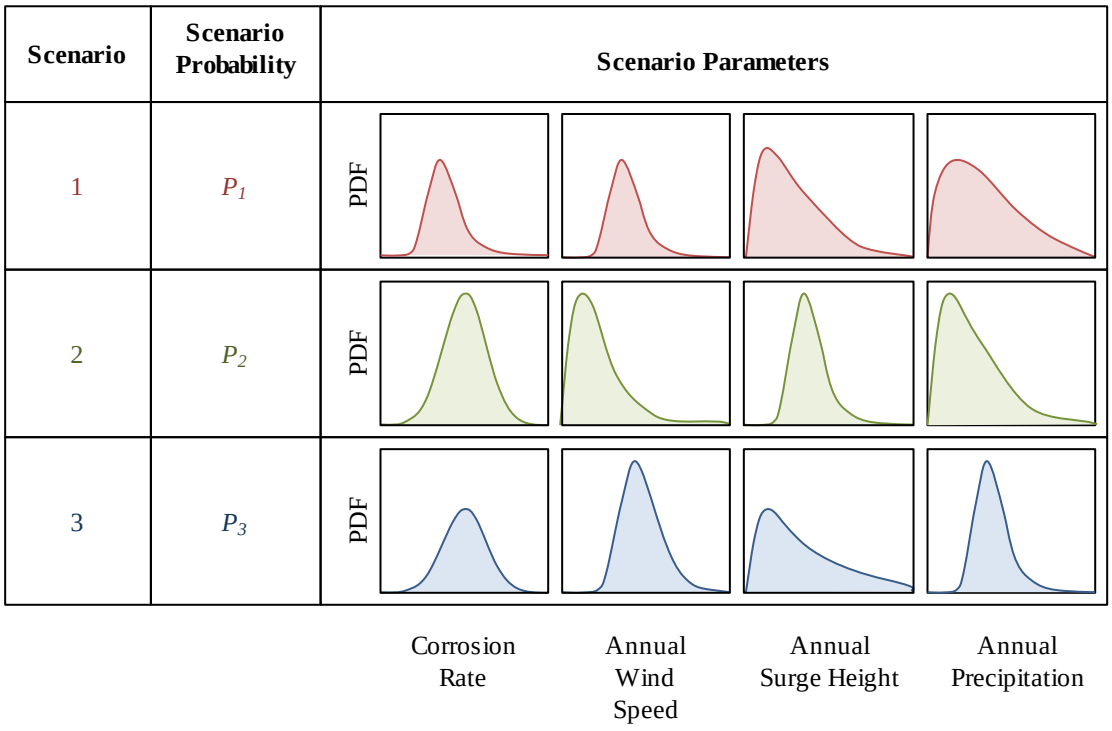

Figure 5.4. In order to develop stochastic optimization formulation for a case with 3 future scenarios, information is required regarding (1) the likelihood of each future scenario P_i and (2) the probability distribution of corrosion rate parameters, annual wind speeds, annual surge heights, and annual precipitation.

Robust optimization refers to optimizing a certain measure of robustness in order to yield a solution that is feasible for any realization of the uncertainties (Bertsimas et al., 2011). Robust options may be developed against a wide range of future scenarios and do not require a full probabilistic description of future scenarios. For the example shown in Figure 5.4, this means that information on the set $\{P_1, P_2, P_3\}$ is not required. Therefore, robust optimization formulations may directly be applied to the climate change adaptation problem to find no regret or low regret options. No regret options, or worst-case scenario options, are solutions that are feasible in all scenarios and optimized for the worst. Regret is defined and the difference between the expected performance function of an option under the uncertain set of scenarios and its performance under perfect information. No-regret options tend to be over conservative, but may be justified for engineering applications where failures have large consequences (Gabrel et al., 2014). Low regret options help provide a logical basis for decisions made by a group, whose willingness to choose high risk plans may differ drastically (Lempert and Schlesinger, 2000).

The development of practical methodologies has been explored by pilot programs throughout the United States (ICF International, 2016; FHWA, 2012). State DOTs and MPOs evaluated the impact of climate change on the vulnerability of their infrastructure. Adaptation measures were evaluated and ranked based on their effectiveness, cost-benefits, flexibility of design, and implementation barriers (ICF International 2016, FHWA 2017). Professional experience and stakeholder input were relied on to select the desired adaptation strategy. A number of challenges were encountered in the vulnerability

assessment and decision making processes that included (a) a lack of knowledge on how to account for different scenarios, (b) uncertainties in the climate models and outcomes, (c) the uncertainties in downscaling results, and (d) how to identify the optimal solution, among others.

Currently, robust decision making has been identified as a useful tool to help circumvent some of these challenges to aid in the decision-making process. It has been applied to cases in water and infrastructure management to account for the lack of information regarding the probability of occurrence of different climate change scenarios (Groves et al. 2008, Lempert and Collins 2007, Stewart et al. 2014). Alternatively, Hall et al. (2012) considered info-gap method for identifying optimal decisions; highlighting the need to expand the robust decision making (RDM) tools to best aid in determining optimal adaptation strategies. Both RDM and Info-gap methods account for uncertain future scenarios and provide decision support by evaluating how well the strategies perform over the range of scenarios. Info-gap explicitly considers the potential gains and losses from future condition, while RDM does not. However, RDM is more useful to decision makers since it characterizes the scenario uncertainty in a way that elucidates the tradeoffs among the management strategies (Hall et al. 2012). Alternatively, robust prioritization has also been integrated into decision support for transportation infrastructure adaptation (Espinet et al. 2017). The methodology requires the development of a payoff table for each potential adaptation strategy in each potential future scenario. The payoff table is then used to estimate the Regret associated with each potential adaptation strategy and determine its robustness. Further research into the

application of stochastic and robust optimization techniques as they directly apply to infrastructure management under climate change effects may directly aid decision makers manage structures under large uncertainties and risk.

5.6. CONCLUSIONS

This chapter, based on Mondoro et al. (2017a), provides a review of the issues of sea level rise, increasingly intense hurricanes, and increasingly intense precipitation, the potential impacts on bridges, associated adaptation measures, and available methods for optimizing under uncertainties. Civil infrastructure management is an increasingly complex engineering problem. Bridges are exposed to multiple hazards over their life-cycle. While they are initially designed to withstand design period storms, corrosive environment reduces their structural capacity. Climate changes have intensified the occurrence of intense precipitation and hurricanes; the impacts of which are further amplified as a result of SLR. While SLR is directly attributed to anthropogenic climate changes, the increased intensity of tropical cyclones and the correlation anthropogenic climate changes is highly debated. Regardless, researchers unanimously agree that there is a need to adapt to the changing climate in order to prevent and/or mitigate future damage to structures.

The adaptation of the built environment can be accomplished by integrating the expected changes in the hazards into the design procedures and vulnerability assessments. Reevaluating the exposure to flooding and surge loads to account for the increased occurrence of tropical cyclones and extreme precipitation is essential to finding the expected loads on the structure over its life-cycle. Developing regulations that limit

development in low-lying regions that are vulnerable to permanent inundation over the expected life of the structure reduces wasteful spending. Adaptation must go further and include the retrofit of existing structures. Retrofit measures for deck unseating, scour, coastal erosion and others, can increase the capacity of existing bridges to resist damage during their expected life.

CHAPTER 6

METRICS AND MODELS FOR OPTIMAL ADAPTATION OF BRIDGES VULNERABLE TO CLIMATE CHANGES

6.1. OVERVIEW

In order to adapt civil infrastructure to changing climate conditions, quantifiable and deep uncertainties must be integrated into the decision-making process. The quantifiable uncertainties, i.e. variability for which a likelihood can be defined, are typically integrated into the management process by considering the reliability or risk level of a structure. The deep uncertainties, i.e. the variability for which a likelihood cannot be defined, are beginning to be integrated in the decision making process as a few robust decision making procedures have been proposed. When decision are made, the governing mentality is to maximize expected utility. However, the deep uncertainty associated with the multiple feasible future climate scenarios also provokes a "wait and see" mentality for some decision makers, causing the flexibility of a strategy to be valued. Additionally, in the face deep uncertainty, there is also a desire to not choose a suboptimal solution. This chapter proposes the Gain-Loss Ratio and Regret as metrics to support decision making under the deep uncertainty of climate change. Additionally, robust and stochastic models for determining optimal bridge adaptation are proposed; the advantages and disadvantages of each are highlighted as they pertain to the management of a typical riverine bridge.

6.2. INTRODUCTION

The vulnerability of civil structures and infrastructure systems to climate driven hazards, such a floods and hurricanes, dictates that climate changes be integrated into the development of optimal bridge management strategies. However, the uncertainties of climate change increase the difficulty facing decision makers when it comes to determining optimal adaptation strategies (Hallegate 2009; Hunt and Watkiss 2011; Mondoro et al. 2017a). The challenges lie in the efficient integration of both quantifiable and deep uncertainties.

Quantifiable uncertainties are those for which a probability of occurrence is well defined; whereas deep uncertainty refers to instances where probabilities cannot be agreed upon (Hallegatte et al. 2012; Espinet et al. 2017). Examples of quantifiable uncertainties may include those associated with the physical properties of a structural system, the natural variability of wind, precipitation, and flooding, and the variability in structural deterioration processes. The presence of these uncertainties typically precipitate the use of vulnerability assessment methodologies to evaluate the effectiveness of adaptation strategy. The probability of failure, reliability, or risk have been integrated in optimization routines in order to determine optimal strategies (Stewart et al. 2001; Padgett et al. 2010; Adey et al. 2003; Mondoro et al. 2017c; Dong et al. 2014b).

Deep uncertainties, those for which probabilities are not available or cannot be agreed upon, may include future economic and/or climate scenarios. In the climate adaptation engineering, deep uncertainties stem from both the Representative Concentration Pathways (RCPs) used to define greenhouse gas trajectories and the

Global Climate Models (GCMs) to predict future climate scenarios. Since no RCP is more or less likely (IPCC 2014a) and there is no consensus on which GCM is the most applicable (Flato et al. 2013), there is no probability that can be objectively assigned to the occurrence of future climate scenarios.

The deep uncertainties of climate change pose two unique problems. First, the scenario uncertainty drives a desire for flexibility, as well as efficiency, in an adaptation strategy. Second, decision makers must aggregate the future climate scenarios into one, or, otherwise account for all potential scenarios in the decision-making process.

Typically, the efficiency of an adaptation strategy is quantified by the benefit, Benefit-Cost ratio (BCR) or Net Present Value (NPV). All of which have been integrated into the development of management strategies for (Padgett et al. 2010; van der Pol et al. 2015). The benefit of an adaption strategy is the reductions in risk achieved by that strategy. BCR and NPV consider both the benefit for society, and the economic efficiency of the action. However, some decision makers may also prefer to consider the option value in a strategy (i.e. the value of the flexibility of the strategy). This is related to the timing of adaptation: postponing adaptation may allow the decision maker to observe climate conditions and wait for improved climate information to become available. This then allows the flexibility of adapting at a more favorable time or not adapting. While the desire for flexibility in adaptation strategies has been identified and discussed qualitatively (Hallegatte et al. 2012; Lin et al. 2004; Lindquist and Wendt 2012), there is no systematic methodology for assessing the flexibility of an adaptation strategy as it pertains to the management of structural assets.

When the decision maker has identified the metric with which to evaluate an adaptation strategy, they must still determine how they are going to aggregate the performance across all scenarios. Robust optimization models have been developed to find optimal strategies against potential scenarios without requiring the probabilities of occurrence of scenarios to be known. Non-probabilistic robust optimization models, such as maximin or maximax models, consider the performance of the adaptation strategy against all scenarios without assigning a probability of occurrence to them (Giuliani and Castelletti 2016). Maximin formulations typically optimize over the worst-case scenario, while maximax formulations typically optimize over the best possible scenario. By choosing the formulation of the problem, the decision makers are predisposing themselves to a particular preference: maximin formulations assume a pessimistic outlook on future scenarios and maximax, an optimistic one. Alternatively, a robustness index can be used to assess the variability of the performance of a strategy across all potential scenarios (Espinet et al. 2017); thus, aggregating the response across all scenarios and enabling the use of a maximization optimization formulation. When optimizing using the robustness index, the decision makers are not giving preference to any one scenario, but consider how well the strategy performs across all scenarios. It implicitly assigns the same probability of occurrence to all scenarios. Thus, this last model falls into the category of a probabilistic robust optimization model, i.e. a stochastic optimization model.

This chapter proposes three metrics that may be used to evaluate the performance of an adaptation strategy including the Gain-Loss Ratio (GLR) and Regret associated with

the BCR. These metrics provide a basis to systematically evaluate the feasibility of flexibility. Furthermore, this chapter outlines the optimization models that can be used to support decisions under deep uncertainty. Single and bi-objective optimization formulations are proposed. The methodology is applied to two illustrative examples; both include a typical bridge over a river vulnerable to climate changes. The climate change trends in the two examples are modeled after expected trends in the Mississippi and Columbia Rivers in the United States in order to identify the effect of spatial variation of the climate change hazard.

6.3. CLIMATE CHANGE

Natural and anthropogenic factors have forced an overall change in the climate. Sea level rise, increasingly intense precipitation, and increasingly intense hurricanes are among the major components of climate change that affect riverine bridges (Mondoro et al. 2017a; Lindquist and Wendt 2012). Heat waves, arctic warming, and increased temperature and humidity may also affect the life-cycle performance of civil infrastructure (Mondoro et al. 2017a; Schwartz 2010; Wang et al. 2012). Together, all of these aspects define the climate change hazard and may have adverse effects on the performance of civil infrastructure (IPCC 2014a, Schwartz 2010). This chapter will focus on the changes in flooding that accompany the climate change hazard. Alternative aspects of the climate change hazard may also be included, but since hydraulic events (including scour, debris impact, debris accumulation, among others) are the predominant source of damage to bridges (Wardhana and Hadipriono 2003), river discharge and flooding are the main hazards considered herein. It is important to note, however, that the framework and

concepts presented in herein for the development of optimal adaptation strategies for riverine bridges can be applied to other aspects of climate change for other civil infrastructure systems.

The change in flooding is typically described by a change in the return period of a discharge of a specific magnitude; typically, this is the discharge associated with the 100-year flood (Milly et al. 2002; Vogel et al. 2011; Hirabayashi 2013). The 100-year flood discharge under the current climate, denoted herein as Q_{100}, is associated with a probability of exceedance of 0.01, as shown in Figure 6.1. A statistical analysis of outputs from GCMs at the end of a period of time provides the probability of exceedance of the Q_{100} discharge for a future climate. The climate change is then reported as a change in the recurrence interval of the 100-year flood; in Figure 6.1 the future recurrence period is denoted as *T'*.

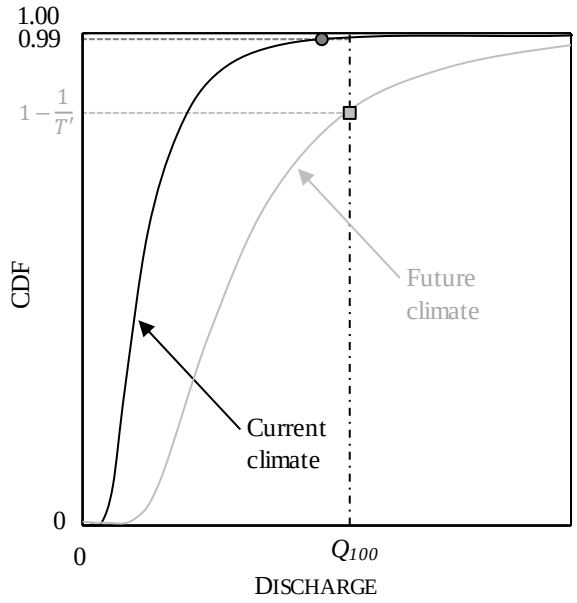

Figure 6.1. The cumulative distribution of discharge for a current and future climate.

The predicted climate change effect on flooding varies based on which RCP is evaluated in with which GCM. As a result, a set of future recurrence intervals exists for a specific location rather than a single value. Since no likelihoods can be assigned to the different RCPs (IPCC 2014a) and no agreement (at this time) can be made on which GCM is most accurate (Flato et al. 2013), no likelihood can be assigned to the set of future recurrence intervals; the scenario uncertainty and model uncertainty are both sources of deep uncertainty. A climate change scenario, as shown in Figure 6.2 is thus defined by an RCP and a GCM (sources of deep uncertainties) and includes the natural variability physical materials and natural processes (sources of quantifiable uncertainties). Currently there are four RCPS (RCP 8.5, RCP 6, RCP 4.5, and RCP 2.6). Figure 6.2 is shown generically for *N* RCPs since the number RCPs in the IPCC Assessment reports have varied. It is also important to note that RCPs replace the emission scenarios used in previous reports (IPCC 2014a).

It is important to remember that the deep uncertainties are only one layer of uncertainties when trying to adapt to climate change. Within each climate change scenario, there is still the natural variability of the extreme events that must be accounted for. This natural variability is addressed as a quantifiable uncertainty. The layer of deep uncertainties and the layer of quantifiable uncertainties are illustrated in Figure 6.3 with respect to flooding. The discrete branches of the figure illustrate the deep uncertainty associated with not being able to assign a probability of occurrence to the climate change scenarios. The distribution of discharge illustrates the quantifiable uncertainty that stems from the natural variability of the extreme event.

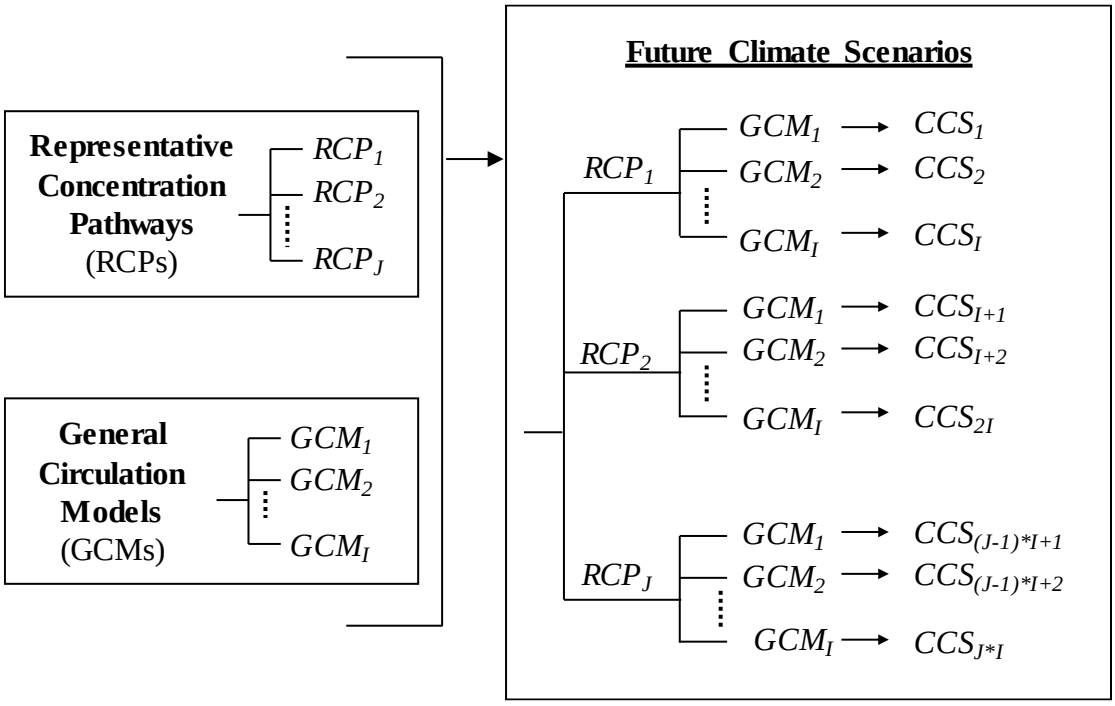

Figure 6.2. The deep uncertainties of future climate scenarios include the deep uncertainties stemming from the set of RCPs that define future projections and the GCMs used to evaluate them.

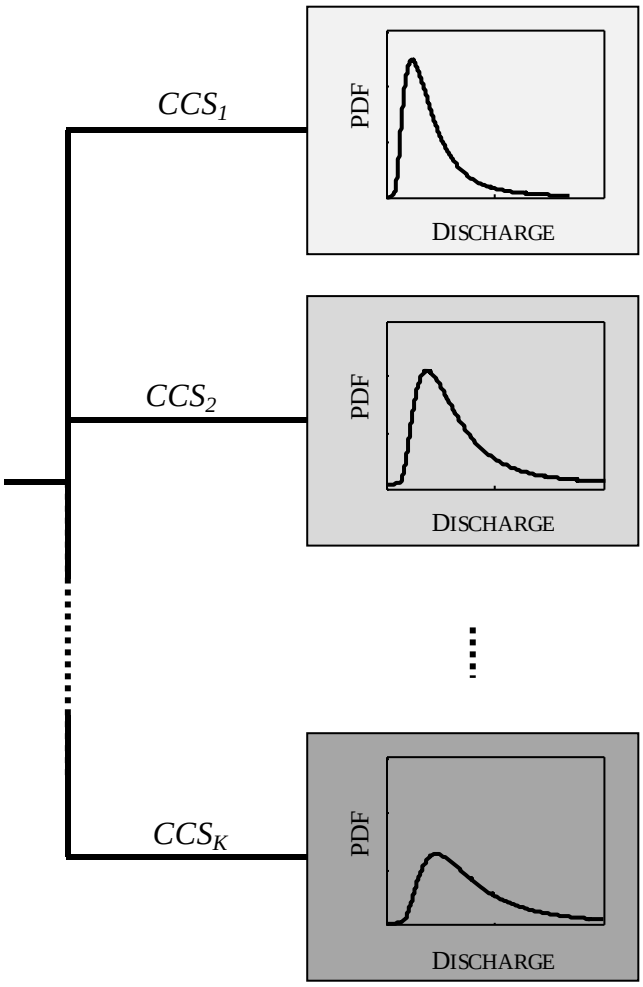

Figure 6.3. Qualitative illustration of the quantifiable uncertainties associated with flooding (shown as the distribution of discharge) and the deep uncertainties associated with climate change scenarios (shown with the discrete lines and denoted as climate change scenario *k*, CCS_k) that must be included in managing bridges vulnerable to climate change.

Hirabayashi et al. (2013) provided insight into the changes into the spatial variation of global flooding. The outputs from 11 GCMs for RCP 8.5 were used to obtain a change in the return period of the 100-year flood for various rivers across the world. The minimum, 25th percentile, median, 75th percentile, and maximum return periods from the 11 outputs were reported for rivers across all continents. Two rivers in the United States were reported: the Mississippi and the Columbia. The expected climate trends in these rivers are detailed in Figure 6.4.

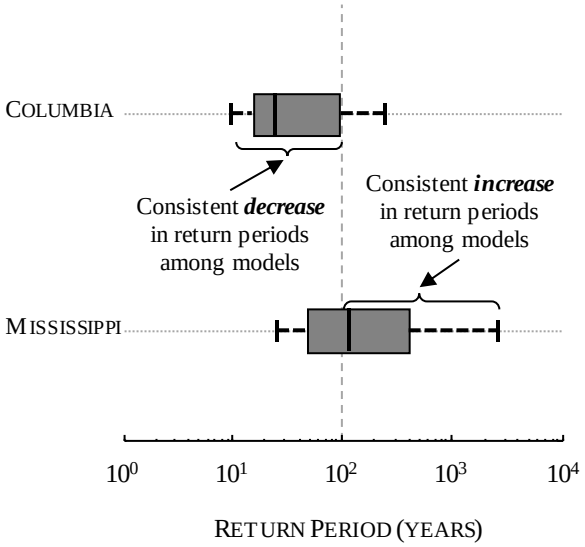

Figure 6.4. Box and whisker plots for the projected return periods of the 100-year flood for the Columbia and Mississippi river at the end of the 21st century (adopted from Hirabayashi et al. (2017)). The interquartile range (25th-75th percentile) is indicated by the height of the grey box, the solid line within each box indicates the median, and the dashed lines represent the maximum and minimum return periods.

The predicted shifts in the return periods for these two rivers highlight two main points: (1) the variation in GCMs is significant and may be contradictory. For the Columbia River, 8 out of 11 models determined that the return period would decrease, leaving 3 models suggesting that the return period would increase (Hirabayashi 2013). For the Mississippi River, 7 out of 11 models determined that the return period would increase, leaving 4 models suggesting that the return period would decrease. (2) It is essential to consider the spatial effects of climate change when developing adaptation plans for structures: while flooding in Columbia River is consistently projected to increase in severity, the severity of flooding for the Mississippi river is consistently projected to decrease.

6.4. EVALUATING ADAPTATION STRATEGIES FOR OPTIMALITY

An adaptation strategy is a plan to mitigate the adverse impacts of climate change. In previous chapters and other research not specifically pertaining to climate change, this is referred to as a management strategy. Adaptation strategies include the type of adaptation action, a_a, and the time the adaptation action is applied to the structure t_a. Strategies are optimized with respect to a planning horizon, $T_{ph,}$ since it is essential to define the length of time into the future that must be accounted for. In the life-cycle analysis of structures, this may also be referred to as the expected life of the structure, service life, or expected remaining life.

In order to determine an optimal adaptation strategy, decision makers must first choose a performance metric with which to evaluate the life-cycle implications of a strategy. Typically, the metric is utility, benefit, or benefit cost ratio, etc. Modern

Economic Theory then states that the optimal solution maximizes the metric. In the case of climate change adaptation, there may also be a desire to wait for more accurate information regarding future scenarios. Additionally, there may also be a desire to not be wrong a different metric is needed. In section 5.6, the Gain-Loss Ratio is developed to systematically investigate the feasibility of waiting for more accurate information. The Regret metric is developed to systematically investigate the desire not to be wrong. In section 5.7, optimization frameworks are presented to identify optimal adaptation strategies. They are based around the metrics proposed in section 5.6 but also consider that decision makers can consider multiple metrics when evaluating a strategy; single and bi-objective formulations are presented.

6.5. STRUCTURAL PERFORMANCE AND TIME-VARIANT RISK

In order to evaluate the effectiveness of an adaptation strategy, the time-variant risk profile must be estimated. The performance of a structure may decrease over time as individual components corrode and the capacity of the structure deteriorates, or, as the intensity of natural hazards increase the demand on the structure. Though, in some regions, changes in climate may also decrease the demand on the structure. In either likelihood, the time-variant performance of a structure must be assessed in order to determine what adaptation actions should be taken. The probability of failure of a structure is defined as

$$P_f(t) = P[S(t) - D(t)] \tag{6.1}$$

where $S(t)$ is the time-variant capacity of the structure and $D(t)$ is the time variant demand. By defining performance probabilistically, the quantifiable uncertainties are integrated into the assessment methodology.

Risk incorporates the impact that a structural failure has on the community it serves. The consequences of failure, $\kappa(t)$, modify the structural performance to formulate the risk

$$R_m(t) = P_{f,m}(t)\kappa(t) \tag{6.2}$$

where $R_m(t)$ is the time-variant risk associated with adaptation strategy m, $P_{f,m}(t)$ is the time-variant probability of failure for adaptation strategy m. The adaptation strategy is composed of a specific adaptation action a_a and adaptation time t_a. A qualitative representation of the time-variant profile of annual risk for an adaptation strategy m, where an adaptation action is applied at time t_a is shown in Figure 6.5a. The increase in annual risk over time may be attributed to climate change-related increases to the hazard, structural deterioration, or a combination of both. The sharp decrease in annual risk at t_a is due to the increase in structural capacity provided by the adaptation action. The average annual risk μ_{Rm}, or the mean value of the annual risk over the planning horizon of the management strategy m, is

$$\mu_{Rm} = \frac{1}{T_{ph}} \sum_{t=1}^{T_{ph}} R_m(t) \tag{6.3}$$

and provides a single metric to quantify the life-cycle risk associated with the adaptation strategy. In life cycle performance assessment, the maximum annual risk, i.e. the largest annual risk over the required planning horizon, or cumulative risk, i.e. the summation of risk over the planning horizon, has also been used to evaluate management strategies

(Mondoro et al. 2017c; Zhu and Frangopol 2016). However, average annual risk is considered since it has a unique value for all potential strategies that may increase or decrease due to climate changes or the effectiveness of adaptation actions.

6.6. DECISION SUPPORT FOR CLIMATE CHANGE ADAPTATION: METRICS

6.6.1. Benefit-Cost Ratio

Due to the vast amount of bridges needing maintenance and repair (ASCE 2017) and the limited availability of financial resources, the economic effectiveness of an adaptation strategy is often included in the decision-making process. The benefit of an adaptations strategy comes at a cost to the managers; which, for publicly funded projects, becomes a burden on the taxpayers. Therefore, benefit-cost analysis is used to systematically determine options that are economically efficient, as well as beneficial.

The benefit-cost analysis, also referred to as cost-benefit analysis, is a systematic method used to evaluate the performance of alternative options. The benefit-cost ratio *BCR* normalizes the benefit (i.e. the reduction in life-cycle risk) to the life-cycle cost. This ratio not only provides a way to prioritize management strategies but also helps in identifying which ones are profitable (i.e. have a benefit higher than the cost, $BCR > 1$).

The benefit of an adaptation strategy is the improvement achieved by the adaptation action applied at the associated time. Benefit is, herein, defined as the reduction in average annual risk an adaptation strategy provides when compared to the average annual risk of the unmaintained structure

$$B_m = \mu_{R0} - \mu_{Rm} \tag{6.4}$$

where μ_{R0} is the average annual risk of the unmaintained structure, and B_m is the benefit associated with adaptation strategy *m*. Thus, in order to calculate the benefit for a strategy, a life-cycle risk assessment must be performed for both the unmaintained structure in order to determine $R_0(t)$ and for the structure considering adaptation strategy *m* in order to define $R_m(t)$ as shown in Figure 6.5b. It is important to note that benefit derived from an adaptation strategy is dependent on the future climate scenario. Thus, adaptation strategy *m* will have a different benefit for each climate scenario *k* and is denoted as B_{mk}.

The benefit cost ratio *BCR* for an adaptation strategy *m* is defined as

$$BCR_m = \frac{B_m}{C_m} \tag{6.5}$$

where C_m is the present value of the cost of the adaptation action. It is assumed that the cost of each maintenance action is constant over the planning horizon: the cost of implementing adaptation strategy *m* at the time that the adaptation action is applied is denoted as $C_m^{'}$. The cost is converted to constant value in order to compare the BCRs of strategies where actions are performed at different times. In this analysis, the present value is used as the basis of comparison, and the cost associated with an adaptation strategy must be discounted to the present value

$$C_m = \frac{C_m^{'}}{(1+r)^{t_a}} \tag{6.6}$$

where t_a is the year that the retrofit action is applied in adaptation strategy m, and r is the discount rate. Likewise, the present value of consequences are used when evaluating risk in Equation 6.2, and is thus implicit in the benefit formulation. Profitable strategies will have a return on investment that is larger than the investment cost (i.e. BCR > 1). Strategies with larger BCRs are preferred as they have a larger benefit per dollar invested. Similar to benefit, the benefit-cost ratio for an adaptation strategy is dependent on the future climate scenario that is included. Thus, each adaptation strategy m will have a benefit-cost ratio for each climate scenario k, BCR_{mk}.

6.6.2. Gain-Loss Ratio

While the main goal of adaptation engineering is to ensure that existing and new infrastructure are protected from the long-term effects of climate change (IPCC 2014a), another goal may be to keep the consequences of being wrong about the future climate as low as possible (Hallegate 2009; FHWA 2017; Lin et al. 2004). This promotes the desire for a flexible strategy (i.e. one that postpones adaptation in to allow the decision maker to observe market conditions and wait until a more favorable time to act or to observe climate information and abandon (or otherwise revise) the strategy). For example, in an urban planning problem the consequences of underestimating future flooding may mean that early investments in development are made and then lost due permanent inundation or extreme flooding. The decision to develop early is an inflexible strategy, that may seem viable since there is the prospect of short term profit, but is infeasible due to long-term losses. Alternatively, not developing an area is a flexible strategy. The decision makers wait for further climate information to become available before acting, and may

develop or not develop based on the updated information. However, it comes at the cost of missing the early gains that could be realized if a favorable climate change were to occur.

The concept of flexible options can be extended to structural management: an adaptation strategy that defers application of retrofit actions until further information is available may be defined as flexible since it allows the decision maker to "wait and see" what to do once more information becomes available. This allows the decision maker the opportunity to not spend money on retrofits if it turns out that the impact of climate change is favorable. However, if climate change is unfavorable, the delay in action comes at the cost of losing out on potential reductions in risk. The following formulations for gains, losses, and GLR are presented as a systematic methodology for assessing the impact of delaying adaptation.

Gain is herein defined as the present value of interest earned by delaying investment. It considers the timing of the application of retrofit. It is defined as the difference between the present value of the cost of the retrofit option included in adaptation strategy *m* if it were applied at time t_0 (i.e. $C_m^{'}$) and the present value of the cost of the retrofit option included in adaptation strategy *m* applied at the time specified in adaptation strategy *m* (i.e. C_m),

$$G_m = C_m^{'} - C_m \tag{6.7}$$

The additional time before the application of adaptation measures also may lead to advancements in technology that reduce the uncertainty associated with future scenario prediction and/or observational information can be used to update estimates. However, in

order to provide a systematic methodology for quantifying the value of delaying the action, the value of these advancements and information are omitted. Instead, only the financial gains made by delaying are included.

Conceptually, the costs and gains adaptation strategy *m* are shown in Figure 6.5c. C_m' is the dollar amount paid at the time of application t_a. The present value of this cost, C_m, is assessed with Equation 6.6. The gain, as shown in Figure 6.5c, for this strategy is difference between the present value of the cost of the adaptation action included in the adaptation strategy if it were applied at $t_a = 0$, and the present value of the action as applied at t_a for the adaptation strategy. This gain, however, comes with an opportunity loss. By foregoing early action, the maximum reduction in average annual risk would not be able to be achieved. Thus, the loss associated with delay is defined as

$$L_m = \mu_{Rm}' - \mu_{Rm} \tag{6.8}$$

Loss, like gains, considers only timing of the application of retrofit, and therefore compares the average annual risk of the retrofit option included in adaptation strategy *m* applied at the time specified for adaptation strategy *m* (i.e. μ_{Rm}) and the average annual risk of that same option if it were applied at time t_0 (i.e. μ_{Rm}'). This is shown conceptually in Figure 6.5.

Comparable to the economic efficiency, it is important to assess the flexibility in terms of both the benefit (i.e. gain, *G*) to cost (loss, *L*). Therefore, the Gain-Loss Ratio for adaptation strategy *m*, GLR_m, is defined as

$$GLR_m = \frac{G_m}{L_m} \tag{6.9}$$

In this way, a strategy with high gains accrued by delaying adaptation and low potential losses would have a high GLR. Strategies with low gains but large losses would have a low GLR. The options with the highest GLR are preferred. It is important to note that GLR is not a direct value of flexibility, but, instead, a metric that systematically assesses the effect of delaying adaptation. The Gain-Loss Ratio for an adaptation strategy *m* will vary for each climate scenario *k*, and will be denoted as GLR_{mk}.

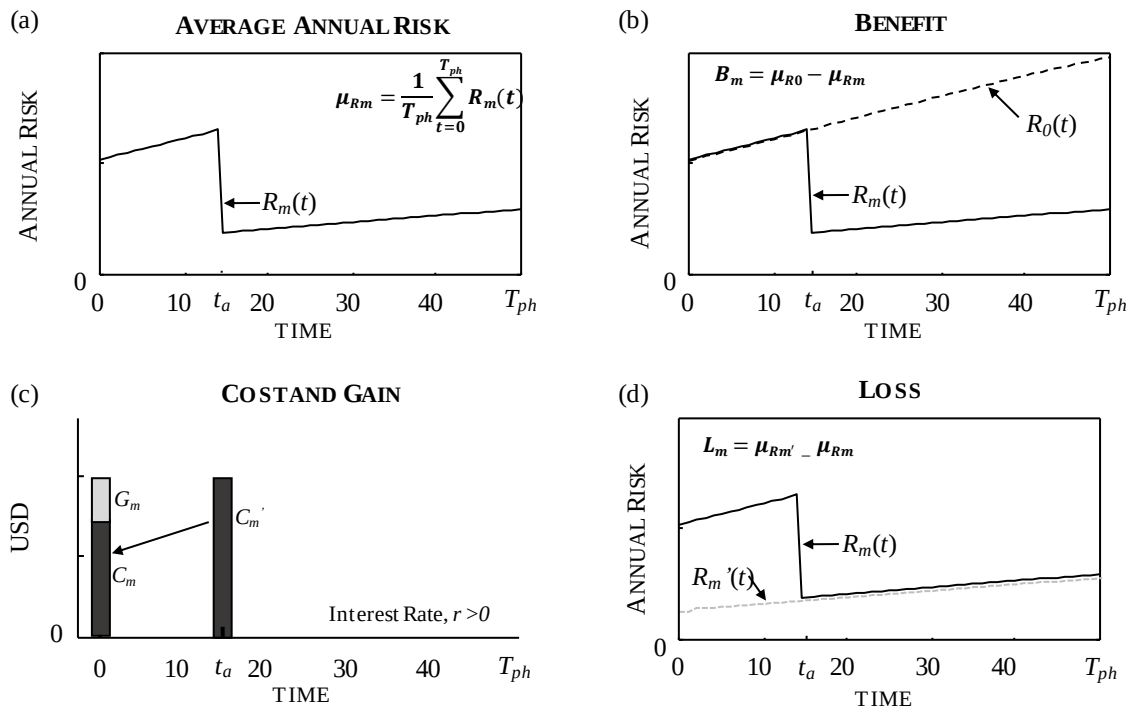

Figure 6.5. Conceptual depiction of the time-variant risk profiles and cost information needed to determine the (a) average annual risk, (b) benefit, (c) cost and gain, and (d) loss for adaptation strategy *m*.

6.6.3. Regret

The presence of multiple future scenarios, each providing a feasible alternative but none of which whose likelihood can be assigned, provokes decision makers to ask the questions: "what if?": "what if I wait?", "what if a worse scenario occurs?", "what if I plan for the worst case and the best case occurs?", "what if I plan for the best case and the worst case occurs?". It is in instances like this, where maximum expected utility fails to capture the complexity of human decisions (Landman 1993).

Regret was integrated into the decision making process in order to account for the paradoxes surrounding decision making under uncertainty (Bell 1982); the paradoxes being that decision makers would chose strategies that would not maximize utility. Although, an alternative rational for why the maximum utility choice is not taken is that the strategy cannot be fully quantified with a single metric and thus not fully described with utility; instead both utility and regret are needed (Landman 1993).

Typically, Regret is discussed in terms of the economic regret associated with not choosing the best alternative, similar to the concept of opportunity loss (Su and Tung 2012). However, Regret may also include psychological regret, i.e. the desire for the decision makers not to perform poorly for their boss, their peers, and their community. In this research, the metric Regret is defined as the economic regret associated with a strategy

$$Rgt_m = \max_{\Phi}\left(payoff_m\right) - payoff_m \tag{6.10}$$

where Rgt_m is the Regret for adaptation strategy m, and Φ is the set of potential adaptation strategies $\{1, 2, \ldots, M\}$. The payoff is evaluated in terms of BCR, and Equation 6.10 can be rewritten as

$$Rgt_m = \max_{\Phi}\left(BCR_m\right) - BCR_m \tag{6.11}$$

The Regret associated with an adaptation strategy m is determined by (1) enumerating all potential adaptation strategies Φ, (2) evaluating the payoff of each strategy, and (3) evaluating Equation 6.11 for Regret, Rgt_m. Figure 6.6 outlines this process. For each adaptation strategy, the BCR is evaluated, the maximum benefit cost ratio is determined from the set $B = \{BCR_1, BCR_2, \ldots, BCR_M\}$, outlined in a light gray box in Figure 6.6. The Regret is the evaluated for each strategy by comparing the strategy with the best performer.

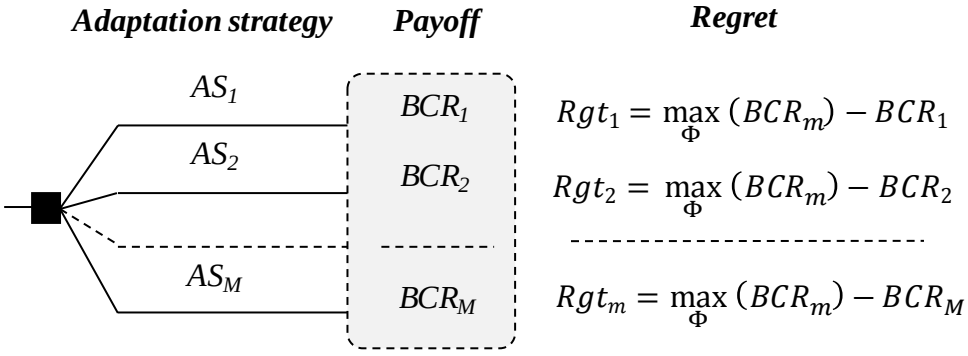

Figure 6.6. The payoff and Regret associated with potential adaptation strategies m =1, 2, …, M when the benefit-cost ratio is the payoff assessed.

Since Regret compares the performance of an adaptation strategy to the performance of all other potential strategies for a single future scenario, the analysis must be repeated for all potential future scenarios. This is process is outlined in Figure 6.7. First, the benefit-cost ratio is assessed for all adaptation strategies and all future scenarios. Then, Regret is evaluated as

$$Rgt_{mk} = \max_{\Phi}\left(BCR_{mk}\right) - BCR_{mk} \tag{6.12}$$

where k is the future scenario k =1, 2, …, K. The maximum BCR for each scenario is chosen from the set $B_k = \{BCR_{1k}, BCR_{2k}, \ldots, BCR_{Mk}\}$. B_1 is outlined in a light gray boxes in Figure 6.7 for future climate scenario 1, $B_1 = \{BCR_{11}, BCR_{21}, \ldots, BCR_{M1}\}$.. Each adaptation strategy then has a set of Regrets associated with it. . Outlined with dark gray boxes in Figure 6.7 are the Regrets associated with the adaptation strategy under each future scenario, the entries of which have no assigned probability due to the deep uncertainties associated with future climate and economic scenarios.

It is important to note that the systematic calculation of Regret requires a full enumeration of feasible adaptation strategies and the performance assessment of each. This may prove to be computationally infeasible if the potential set of adaptation strategies is too large or a computationally-intensive model is required to assess performance.

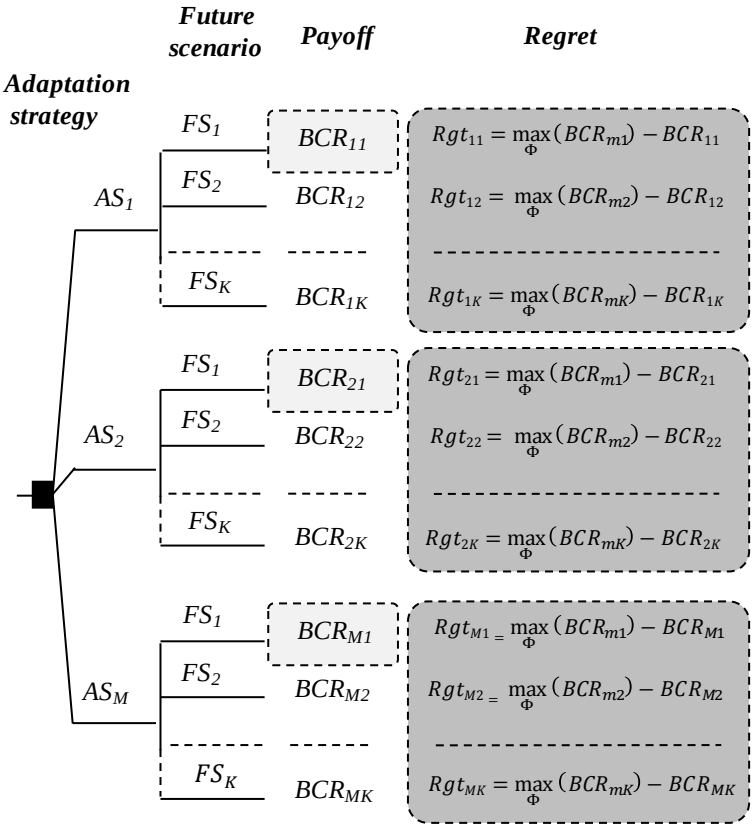

Figure 6.7. The payoff and Regret associated with potential adaptation strategies m = 1, 2, …, M for all future scenarios k = 1, 2, …, K stemming from potential climate and economic scenarios

6.7. DECISION SUPPORT FOR CLIMATE CHANGE ADAPTATION: FRAMEWORKS

The performance of an adaptation strategy is assessed for multiple climate change scenarios, and unless there is a systematic methodology for aggregating the performance across the set of scenarios, the search for an optimal strategy cannot proceed. Robust optimization models and decision-making tools have been developed in order to integrate the uncertainties associated with climate change into adaptation planning (Hallegatte et al. 2012; Espinet et al. 2017; Giuliani and Castelletti 2016; Hall et al. 2012; Lempert and Schlesinger 2000). There are two predominant formulations associated with the non-probabilistic, robust optimization models: maximin and maximax.

Maximin formulations inherently plan for the worst possible outcome while trying to maximize payoff. They are typically associated with a 'risk-averse' attitude and take the form

$$m^* = \max_{\Phi}\left(\min_{\Psi} Payoff_{mk} \right) \tag{6.13}$$

where m^* is the optimal adaptation strategy composed of the optimal adaptation action of a_a^* and its time of application t_a^*, Φ is the set of potential adaptation strategies $m = 1, 2, \ldots, M$, and Ψ is the set of climate scenarios $k = 1, 2, \ldots, K$. For the adaptation of civil infrastructure, $Payoff_{mk}$ can refer to the BCR_{mk} or GLR_{mk} of an adaptation strategy.

Maximax formulations involve maximizing the maximum payoff, inherently assuming an optimistic view on future scenarios, and are typically associated with a 'risk-taking' attitude. The maximax formulation takes the form

$$m^* = \max_{\Phi}\left(\max_{\Psi} Payoff_{mk}\right) \tag{6.14}$$

By formulating the adaptation problem in either a maximax or maximin approach, an optimal strategy can be systematically determined without knowing (or subjectively assigning) the probability of the future scenarios. However, there may be significant difficulties in integrating such formulations into the decision-making process if there are divergent risk-taking perspectives within a group of decision makers.

As an alternative, a robustness index has previously been proposed as

$$RI_m = \sqrt{\frac{1}{K}\sum_{k=1}^{K} Payoff_{mk}^2} \tag{6.15}$$

where RI_m is the robustness index for payoff for adaptation strategy m (Espinet et al. 2017). The robustness indices for the BCR and GLR can be written as

$$RI_m^{BCR} = \sqrt{\frac{1}{K}\sum_{k=1}^{K} BCR_{mk}^2} \tag{6.16}$$

$$RI_m^{GLR} = \sqrt{\frac{1}{K}\sum_{k=1}^{K} GLR_{mk}^2} \tag{6.17}$$

respectively. The robustness index can then be integrated into an optimization formulation to maximize robustness

$$m^* = \max_{\Phi}\left(RI_m\right) \tag{6.18}$$

in order to identify an adaptation strategy that performs well across all scenarios. While this methodology does not explicitly assign a probability to each scenario, the contribution of each scenario is equally weighted. Thus, it implicitly assigns an equal

probability to the occurrence all scenarios. Based on Equation 6.15, the robustness index is always non-negative and therefore does not differentiate between positive and negative values of the payoff metrics. This may prove to be a significant impediment to the use of RI as metric if future climate and/or economic scenarios yield negative payoff values.

6.7.1. Benefit-Cost Ratio and Gain-Loss Ratio

6.7.1.1. Maximize Minimums: A Pessimistic Approach

The pessimistic formulation accounts for the worst-case scenario when making decisions. The non-probabilistic minimax model for the bi-objective problem does not assign any likelihood to climate scenarios and takes the form

$$\text{Objective: } \max_{\Phi}\left(\min_{\Psi} BCR_{mk}\right) \quad \text{and} \quad \max_{\Phi}\left(\min_{\Psi} GLR_{mk}\right) \tag{6.19}$$

$$\text{Find: } m^{*} \tag{6.20}$$

$$\text{Given: } \Phi, \mathbb{C}, S_A, \Psi, S_B \tag{6.21}$$

where m^{*} includes the adaptation action a^{*} and the time of adaptation t_a^{*}, Φ is the set of potential adaptation strategies, $\mathbb{C}$ is the set of costs for the potential adaptation actions in Φ, S_A is the structural design information for all potential adaptation actions, Ψ is the set of climate scenarios, and S_B is the structural design information for the bridge.

6.7.1.2. Minimize Maximums: An Optimistic Approach

The optimistic formulation assumes that the best of all possible scenarios will occur and that the optimal strategy should be developed around that. The bi-objective formulation of the optimistic approach takes the form:

$$\text{Objective: } \max_{\Phi}\left(\max_{\Psi} BCR_{mk}\right) \quad \text{and} \quad \max_{\Phi}\left(\max_{\Psi} GLR_{mk}\right) \tag{6.22}$$

Find: m^* (6.23)

Given: Φ, $\mathbb{C}$, S_A, Ψ, S_B (6.24)

In the single objective formulation, the maximax model relies on the assumption that the best possible scenario will occur. When extended to the bi-objective formulation with conflicting objectives, this assumption may be invalid since the best scenario for one metric may not be the best scenario for the other. Thus, the objective function values associated with the optimal solution found for this formulation may be an over estimate of what is actually feasible. This concept is future discussed in the illustrative example.

6.7.1.3. Maximize Robustness Indices: A Stochastic Approach

The final bi-objective formulation relies on an implicit assignment of probability to the occurrence of each climate change scenario included in the assessment. It is formulated as follows in order to find a strategy the performs well under most scenarios

Objective: $\max_{\Phi}\left(RI_m^{BCR}\right)$ and $\max_{\Phi}\left(RI_m^{GLR}\right)$ (6.25)

Find: m^* (6.26)

Given: Φ, $\mathbb{C}$, S_A, Ψ, S_B (6.27)

6.7.2. Regret and Benefit-Cost Ratio

6.7.2.1. Maximize Minimums: BCR

The benefit-cost ratio is a direct assessment of how a given adaptation strategy performs. Since the larger BCR is preferred, the pessimistic formulation of the adaptation problem is a maximin model. The optimization problem for bridge adaptation is formulated as

$$\text{Objective: } \max_{\Phi}\left(\min_{\Psi} BCR_{mn}\right) \tag{6.28}$$

$$\text{Find: } m^{*} \tag{6.29}$$

$$\text{Given: } \Phi,\ \mathbb{C},\ S_A,\ \Psi,\ S_B \tag{6.30}$$

By maximizing the minimum BCR for a given adaptation strategy, the decision maker assumes that the worst-case scenario will be realized and is choosing to plan for it.

6.7.2.2. Minimize Maximums: Regret

Regret quantifies the desire of decision makers to avoid the sense of loss associated with having made the wrong decision. Since, a lower Regret value is preferred, the pessimistic formulation of the adaptation problem is a minimax model. The optimization problem for bridge adaptation is formulated as

$$\text{Objective: } \min_{\Phi}\left(\max_{\Psi} Rgt_{mk}\right) \tag{6.31}$$

$$\text{Find: } m^{*} \tag{6.32}$$

$$\text{Given: } \Phi,\ \mathbb{C},\ S_A,\ \Psi,\ S_B \tag{6.33}$$

By minimizing the maximum Regret for a given adaptation strategy, the decision maker assumes that the worst-case scenario will be realized and is choosing to plan for it. It is important to note that the worst-case scenario for Regret may not be the same as the worst-case scenario for BCR.

6.7.2.3. Bi-objective Formulation: Maximize Minimum BCR and Minimize Maximum Regret

While modern economic decision theory suggests that an individual will choose the strategy that provides the largest payoff (in this case BCR), the presence of multiple feasible future scenarios instills the emotion of loss associated with having made a wrong decision and promotes the desire to minimize Regret. Thus, a single objective optimization formulation using only one of the two metrics (BCR and Regret), fails to capture the complexities in the decision. Bell (1982) and Loomes and Sugden (1982) propose the use of a weighting factor and optimizing over a combined, single objective of expected utility. The maximum payoff and Regret were integrated into a single metric through the use of utility factors; the choice of these factors weights the decision maker's attitude towards one or the other. In order to avoid requiring the definition of a weighting factor, and imposing such predispositions into the formulation of the optimization problem, this paper proposes the use of a multi-objective formulation from which a Pareto set of optimal solutions may be found. The set represents solutions where one objective cannot be improved without negatively impacting the performance of the other. Once the set is determined, the decision maker, or group of decision makers, may then choose their preference after having preformed a diligent and unbiased search for information.

The following is the bi-objective formulation for the adaptation problem:

$$\text{Objective: } \max_{\Phi}\left(\min_{\Psi} BCR_{mk}\right) \text{ and } \min_{\Phi}\left(\max_{\Psi} Rgt_{mk}\right) \tag{6.34}$$

Find: m^* (6.35)

Given: Φ, $\mathbb{C}$, S_A, Ψ, S_B (6.36)

6.8. ILLUSTRATIVE EXAMPLE: BCR AND GLR

An illustrative example is herein presented for the management of a riverine bridge under the climate change hazard of flooding. An illustrative example is herein presented for the management of a riverine bridge under the climate change hazard of flooding. The illustrative example is divided into two sub-examples. The only difference between the examples is the climate change trends expected for the given river. Example A includes the riverine bridge over a river with potential climate change trends similar to those expected in the Columbia River. Example B includes the same riverine bridge over a river with potential climate change trends similar to the Mississippi river. This section details the rivers and their climate change trends for Examples A and B, the details the bridge structure, and reviews the adaptation measures that may be applied to prevent failure.

The rivers included in Example A and B both have a 100-year flood discharge assumed to be 310 m^3/sec, with the discharge distribution following a Lognormal Type 3 distribution (Kroll and Vogel 2002) with a mean of 88 m^3/sec and standard deviation of 60 ft^3/sec for the 21st Century climate. The change in discharge over time for River A, i.e. the river considered in Example A, follows that expected in the Columbia River. The climate change scenarios considered in the illustrative example address range of GCM outputs include the return periods corresponding to the minimum value, 25th percentile,

median, 75th percentile, and maximum value for RCP 8.5 as presented in Hirabayashi et al. (2013). These are denoted as Climate Change Scenarios CCS_k where k is 1, 2, 3, 4, and 5, respectively and make up the set of climate scenarios Ψ. CCS_0 is the current (20th Century) climate. Since the predominant source of uncertainty for precipitation predictions is model uncertainty (Hawkins and Sutton 2011), the inclusion of only these climate change scenarios is deemed sufficient for the illustrative examples. However, the methodology proposed herein is developed generically and can accommodate other RCPs and GCMs. The discharge distribution at the end of the 21st century for the five *CCSs* included on Example A are shown in Figure 6.8a. The change in discharge distribution for River B, i.e. the river considered in Example B, follows that expected in the Mississippi River (Hirabayashi 2013) the discharge distribution at the end of the 21st century for the five *CCSs* included are shown in Figure 6.8b.

In order to assess the average annual risk for a potential adaptation strategy, it is assumed that there is a linear increase in the discharge over the 100-year span to achieve the change in probability of occurrence of the initial climate's 100-year discharge event. It should be noted, that this assumption may vary from both that predicted with the GCM and the actual future climate. While the illustrative example assumed the linear trend, the same methodology for adaptation optimization can be applied to any available time variant climate trend.

The structural design of the riverine bridge S_B included in both illustrative examples is detailed Chapter 3, along with the methodology for assessing the probability of failure and risk of the bridge for a given climate. In summary, the probability of deck failure,

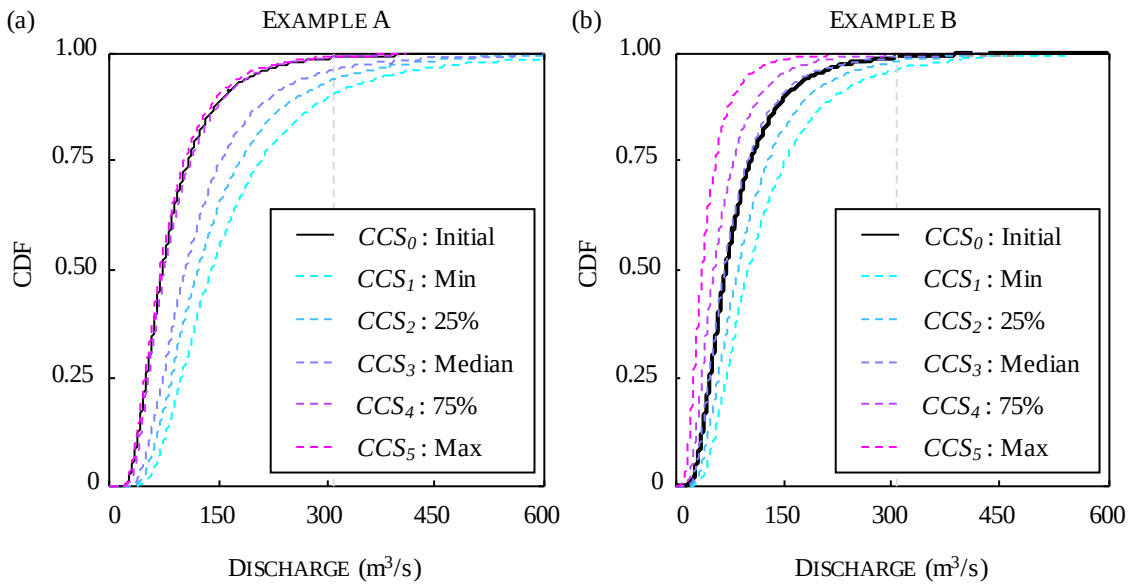

Figure 6.8. Discharge distribution for the current climate (solid black line) and the future climate (dashed lines) for the climate change scenarios included for (a) Example A, and (b) Example B.

estimated, and the total risk for the bridge is assessed. This methodology is repeated at each point in time in order to determine the time-variant risk profile of a given adaptation strategy. For Examples A and B, the time variant risk profiles for the bridge under the future climate change scenarios are shown in Figure 6.9 for a planning horizon, T_{ph}, of 60 years. The risk profiles correspond to an unmaintained structure. A discount rate of zero (i.e. $r = 0$) is assumed in order to highlight the direct impacts of future climate change scenarios. For Example A, the annual risks for CCS_1 through CCS_4 increase over time. Only CCS_5 corresponds to a decrease in annual risk that is attributed directly to anticipated changes in the climate. However, for River B, the majority of climate scenarios (i.e. CCS_3 through CCS_5) correspond to a decrease in annual risk as time progresses.

The design variables in the optimization routine include both the type and timing of adaptation: The adaptation action a_a may include the application of (1) riprap around the pier, (2) steel restrainers (3) shear keys, (4) riprap and steel restrainers, or (5) riprap and shear keys. The structural details S_A, cost $\mathbb{C}$, and methodology for assessing failure of each of these retrofit measures is detailed in Chapter 3. The time of adaptation t_a may be any integer ranging from year 1 to one year before the end of the planning horizon (i.e. $T_{ph} - 1$). The set composed of all possible combinations of adaptation actions and adaptation time form the set of potential adaptation strategies Φ. The discount rate assumed is detailed in the results sections since a single value is assumed for the optimization problems regarding BCR and GLR, while a set of discount rates is included for the optimization problems regarding Regret and BCR. A constant discount rate of 0.04 was considered.

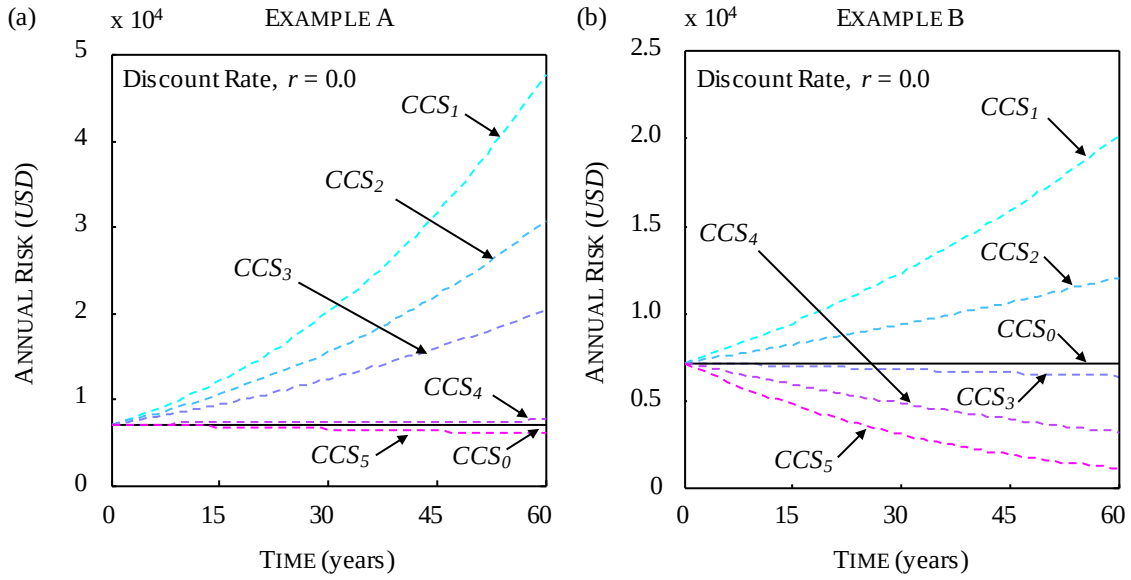

Figure 6.9. Time-variant risk profiles for the example bridge under a stationary (current) climate (solid black line) and the future climate (dashed lines) for the climate change scenarios included for (a) Example A, and (b) Example B.

6.9. RESULTS: BCR AND GLR

The optimization formulations presenting in section 6.7.1 were applied to the management of the illustrative example bridges. The pareto optimal solutions were obtained through an extensive search for both illustrative examples. The optimal adaptation strategies determined for the pessimistic formulation, optimistic formulation, and the robust formulation are shown in Figure 6.10 a, b, and c, respectively, for Example A. The top plot shows the tradeoff between the two objectives where the marker type denotes the specific adaptation action that is implemented in the Pareto optimal solution. The bottom plot is a 3-dimensional representation of the Pareto optimal solutions where the timing of the adaptation action is on the vertical axis.

In the pessimistic formulation (i.e. $\max_{\Phi}\left(\min_{\Psi} BCR_{mk}\right)$ and $\max_{\Phi}\left(\min_{\Psi} GLR_{mk}\right)$), the worst-case scenario is being planned for. In order to maximize the minimum BCR for Example A, the application of shear keys is performed at $t_a^* = 0$. Economic efficiency is maximized when the structure is adapted as soon as possible. However, there is no flexibility (i.e GLR = 0) in this solution. The maximum flexibility (i.e largest GLR) is achieved when riprap and restrainers are applied at year 1. This may appear contradictory to the desire for flexibility in an adaptation strategy. However, it stems from the maximin formulation: by maximizing the minimums, only the worst climate change scenario is being addressed. If the worst-case scenario suggests any intensification of the hazard, the pessimistic model negates any desire for flexibility. Thus, for Example A, the pessimistic formulation fundamentally negates any desire for flexibility. However, it is useful since it does not require an estimation of the probability of different climate scenarios.

The Pareto optimal solutions for the optimistic formulation (i.e. $\max_{\Phi}\left(\max_{\Psi} BCR_{mk}\right)$ and $\max_{\Phi}\left(\max_{\Psi} GLR_{mk}\right)$) are shown in Figure 6.10b. The two separate groupings include (1) adaptation strategies with 2 retrofit measures are applied, and (2) adaptation strategies with only 1 retrofit measure is applied. This is due to the manner in which gains are defined; allowing for a larger magnitude in the gains for the adaptation strategies with 2 retrofit measures. Additionally, among the separate groupings, solutions with the largest GLR are applied later in the planning horizon. The adaptation strategy with the highest Gain-Loss Ratio includes the application of riprap and shear keys at year 59. This is the year just before the planning horizon is reached, the latest t_a considered in Φ. For locations where there is at least one potential scenario where the flooding intensity may decrease, and an optimistic outlook on future scenarios considered (as is the case with the optimistic formulation) the gains that can be accrued by waiting for more information are high, and losses low. The trade-off between the GLR and BCR as seen in Figure 6.10b reinforces the concept that efficiency and flexibility are two competing metrics.

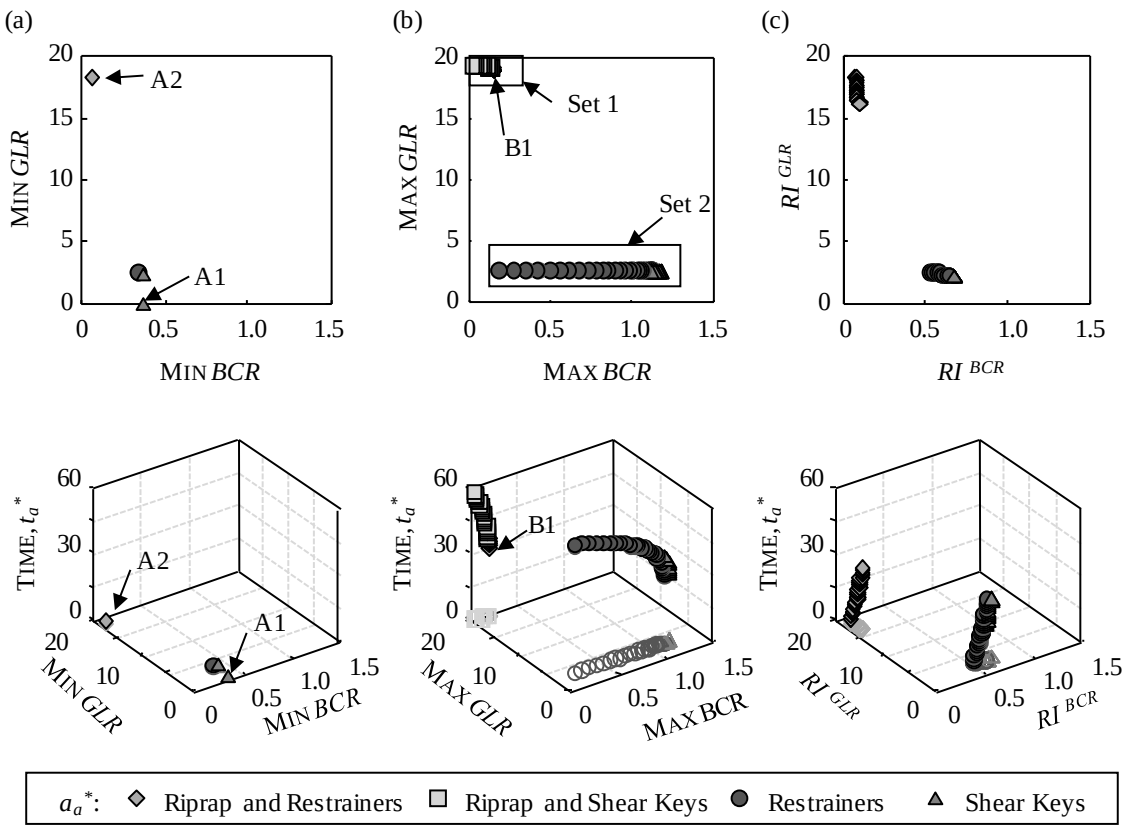

Figure 6.10. Pareto optimal solutions for the (a) pessimistic formulation, (b) optimistic formulation, and (c) robust formulation considering climate changes in River A. The top plots include the 2D presentation of the Pareto optimal solutions, and the bottom plots show the Pareto optimal solutions 3D and also include the projection onto the 2D surface.

However, the bi-objective optimistic formulation dictates the assumption that the future scenarios that are optimal for both efficiency (i.e. BCR) and flexibility (i.e. GLR) are realized. However, since these are conflicting objectives, the climate scenario that maximizes the BCR for adaptation strategy *m* is not always the same as the climate scenario that maximizes the GLR. For instance, the Pareto optimal solution B1, as indicated in Figure 6.10b, includes the application of riprap and restrainers at year 31. Figure 6.11 details the BCR and GLR of this management strategy (i.e. applying riprap

and restrainers at year 31) for climate change scenarios 1 through 5, as well as the BCR-GLR pair that is included in the optimistic, pessimistic and robust solution. It is apparent that the realization of climate change scenario CCS_5 corresponds with the maximum GLR, while the realization of CCS_1 corresponds with the maximum BCR. By maximizing the maximums of both metrics, the solution to the optimistic formulation corresponds to a point that is unrealistic under any future scenario. Conversely, by maximizing the minimum of both metrics, the optimal solution corresponds to a conservative estimate of BCR and GLR and will be outperformed under a realization of any future scenario.

The robust formulation, which maximizes the robustness index of each metric, accounts for the variability amongst the different scenarios rather than just the worst or best case. The most flexible solutions (i.e. solutions with the largest GLR) for the robust formulation also indicate that adaptation should occur early in the planning horizon for example A. This is attributed to the intensification of the hazard expected in CCS_1, CCS_2, CCS_3, and CCS_4. The low gain-loss ratios associated with delayed adaptation under these scenarios outweigh the higher GLR expected if CCS_5 is realized. Since the robustness metric considers how an adaptation strategy performs across all scenarios (Equation 6.15), the early adaptation yields the largest robustness in flexibility RI^{GLR} for Example A. Thus, the desire to delay adaptation (i.e. an inherent desire to be flexible and wait for more information before acting) is not beneficial. This conclusion, however, is site specific.

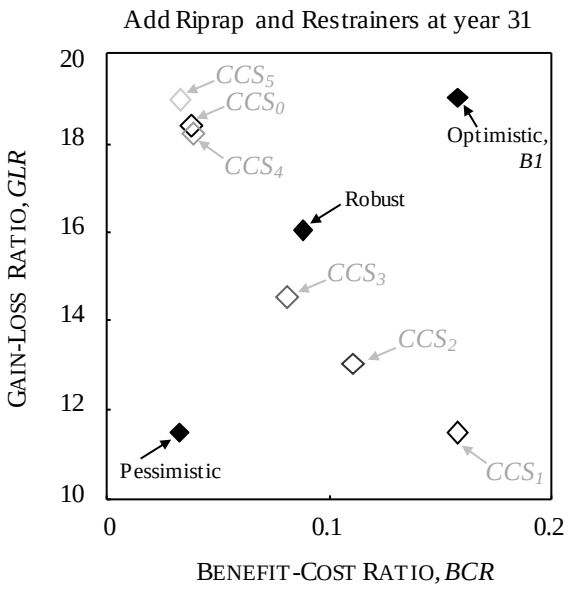

Figure 6.11. The BCR and GLR of the management strategy where riprap and restrainers are applied at year 31 for the climate change scenarios predicted for River A.

The comparison of the Pareto optimal solutions for Example A and Example B provides insight into the importance of the spatial variation of the climate change effects. In Figure 6.12 a, b, and c, the Pareto optimal solutions for the pessimistic formulation, optimistic formulation, and the robust formulation are illustrated, respectively, for Example B. Similar to Example A, the optimal solutions for Example B for the pessimistic formulation yield adaptation strategies that require immediate action (i.e. at year 0 or year 1). This, again, is due to the assumption that the worst-case scenario will be realized. The worst-case scenario for Example B also includes an intensification of the flooding hazard. The Pareto optimal solutions for the optimistic approach for Example B demonstrate the same trade-off between objectives and include options that range in application time. The options that have the highest flexibility (i.e. GLR) are applied later

in life, while the most economically efficient option is applied at year 23. The assumed interest rate, $r = 0.04$, and the relatively large decrease in the intensity of the hazard in the best-case scenario for River B leads to the most economically beneficial strategy that includes a delay in adaptation actions.

The optimal adaptation strategies found for the example bridge over River B for the robust model highlights the validity of the desire for flexible solutions. In Example B, the financial gains associated with delaying adaptation outweigh the losses that may accrue. The most flexible strategy delays the application of adaptation actions. While this solution is the most flexible, there is no benefit associated with it. Thus, the group of decision makers must decide on the preference that will be given to BCR and GLR when determining a course of action. Additionally, the optimal strategies identified for Examples A and B for the robust formulation of the climate change adaptation problem shows that the desire for flexibility may be systematically justified for a certain site. However, for other sites, the "wait and see" mentality cannot be systematically justified when valuing the potential gains and losses associated with delay.

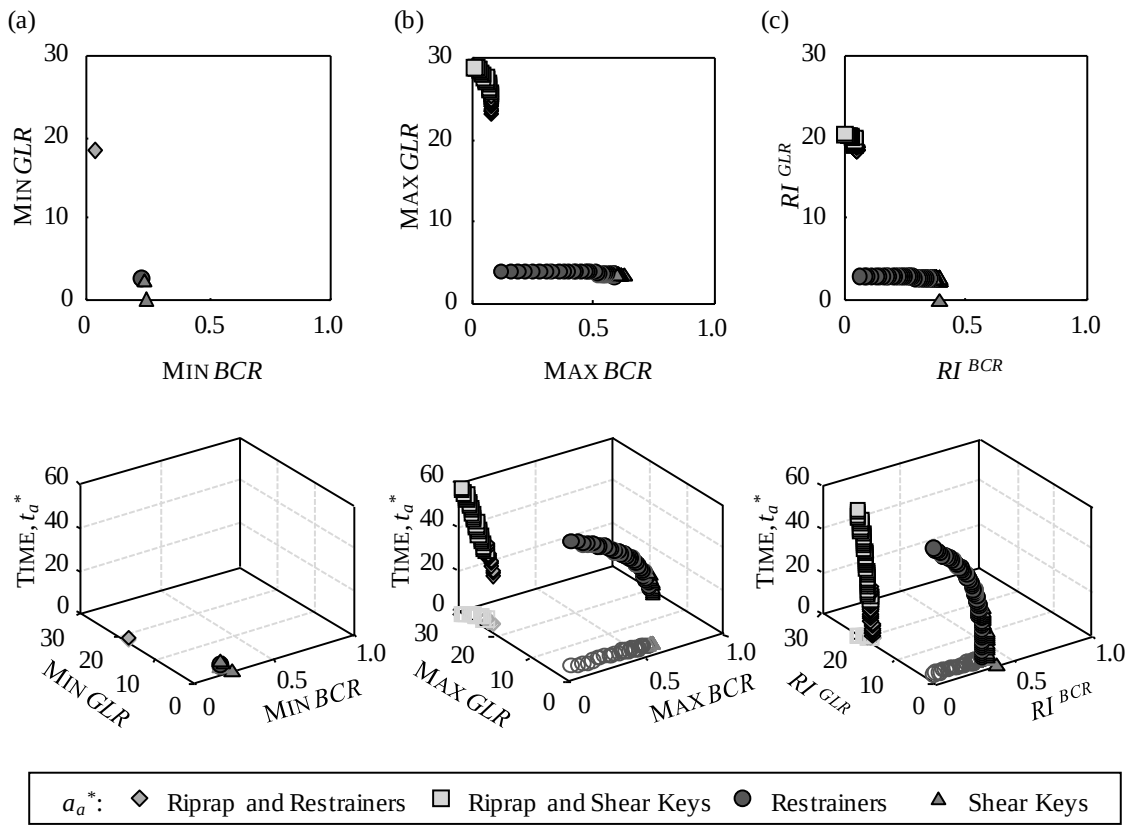

Figure 6.12. Pareto optimal solutions for the (a) pessimistic formulation, (b) optimistic formulation, and (c) robust formulation considering climate changes in River B. The top plots include the 2D presentation of the Pareto optimal solutions, and the bottom plots show the Pareto optimal solutions 3D and also include the projection onto the 2D surface.

6.10. ILLUSTRATIVE EXAMPLE: REGRET AND BCR

The illustrative example included in this section is similar to that presented in Section 6.8: The same bridge is included and the two example rivers are the same. The differences lie in the adaptation actions included in the set of potential measures Φ and the discount rate. The adaptation strategies included in the set of potential adaptation

strategies Φ consist only of the application of shear keys and riprap at an adaptation time t_a. By only having a single potential adaptation action, a_a^* is no longer a design variable in the optimization problem but a deterministic quantity (a_a = the application of shear keys and riprap). This results in the only difference among the set of potentials strategies being the time of adaptation t_a. The assumed planning horizon is 60 years and the adaptation times range from t_a = 0 to t_a =58 years, since solutions with t_a = 60 are not logical. The example included only one adaptation action in order to investigate the effect of timing rather than performance (which was assessed in Chapter 3). While the illustrative example only includes one adaption action type, the methodology presented is generic and can be expanded to include alternative adaption actions.

The optimization formulations presenting in Section 6.7.2 were applied to the management of the illustrative example bridges considering a set discount rates. A set was chosen in order to highlight how the methodology can also be applied when there are deep uncertainties associated with the future economic climate. There are disagreements on the value and variability of discount rates put forth by federal guidelines, academic research, and state of practice: (1) federal guidelines suggest a single, deterministic value set by the Office of Management and Budget (OMB), (2) Federal Highway Administration (FHWA) specifications for a probabilistic set of values developed from historical date, and (3) a deterministic value may be chosen based on professional judgement (Jawad and Ozbay, 2006).

The deterministic value does not add to the uncertainties associated with climate change adaptation; however the latter two do. If the discount rate is considered with

respect to FHWA guidelines, the specified distribution can be integrated into the risk assessment. However, if the discount rate is chosen based on professional judgement, a single value may not be agreed upon within a group of professionals. The set of discount rates that they settle on would then be another source of deep uncertainty, where each rate is a potential future economic scenario. The economic scenarios addressed in this example include a set of discount rates that range from 3 to 5% at intervals of 0.1%. This set was developed in order to cover the logical range of discount rates that practicing engineers may choose (Jawad and Ozbay 2006). The set of future scenarios Ψ included in the optimization problem thus accounts for the future scenarios FS_f dictated by environmental climate change scenarios CCS_k and economic climate scenarios ES_e as shown in Figure 6.13.

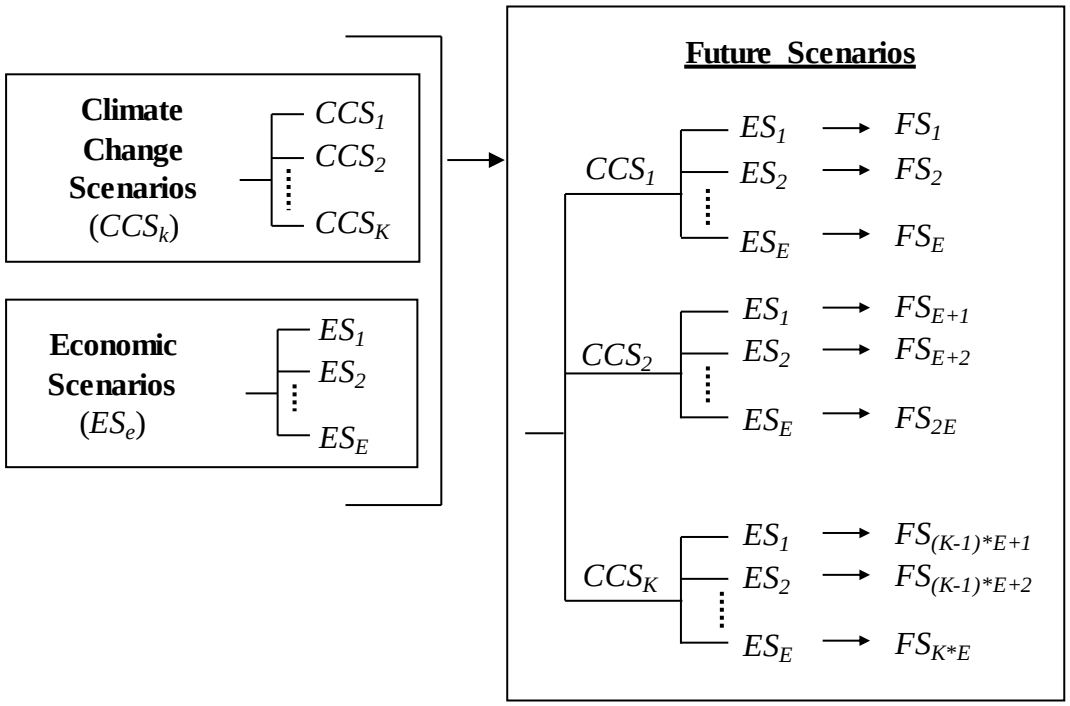

Figure 6.13. The future scenarios *FS* included in Ψ account for the environmental climate change scenarios CCS_k and economic climate scenarios ES_e

6.11. RESULTS: REGRET AND BCR

The BCR ratio and Regret is calculated for each future scenario included in the illustrative example; the box-and-whisker plot for which is shown in Figure 6.14 for example A. The minimum and maximum values are denoted with a solid black line, and the height of the grey box indicates the interquartile range (75^{th} – 25th percentile) with the thick black line within each box indicating the median value of each metric for each adaptation strategy. The timing on the adaptation action is also denoted on the top of each plot. In Figure 6.14a, the minimum BCR for each strategy is shown with a circle. The optimal solution for the pessimistic formulation for BCR includes the application of the adaptation action at the earliest possible time, $t_a = 0$, shown as the solid black dot on Figure 6.14a and denoted as A^*.

In Figure 6.14b, the maximum Regret for each strategy is shown with a circle. The optimal solution for the single objective optimization formulation of minimizing maximum Regret includes the application of the adaptation action at $t_a = 22$, shown as the solid black dot on Figure 6.14b and denoted as B^*. The divergent solutions to these optimization problems reiterate the concept that maximizing payoff and minimizing Regret may not lead to the same optimal strategy.

In order to understand why the optimal solution found by maximizing minimum BCR is not the same as that found by minimizing maximum Regret, the variation of BCRs and Regrets for the adaptation strategies with climate change scenarios can be isolated by considering a deterministic discount rate of 4%. The BCR and Regrets associated with the adaptation strategies in set Φ are detailed for the five climate change

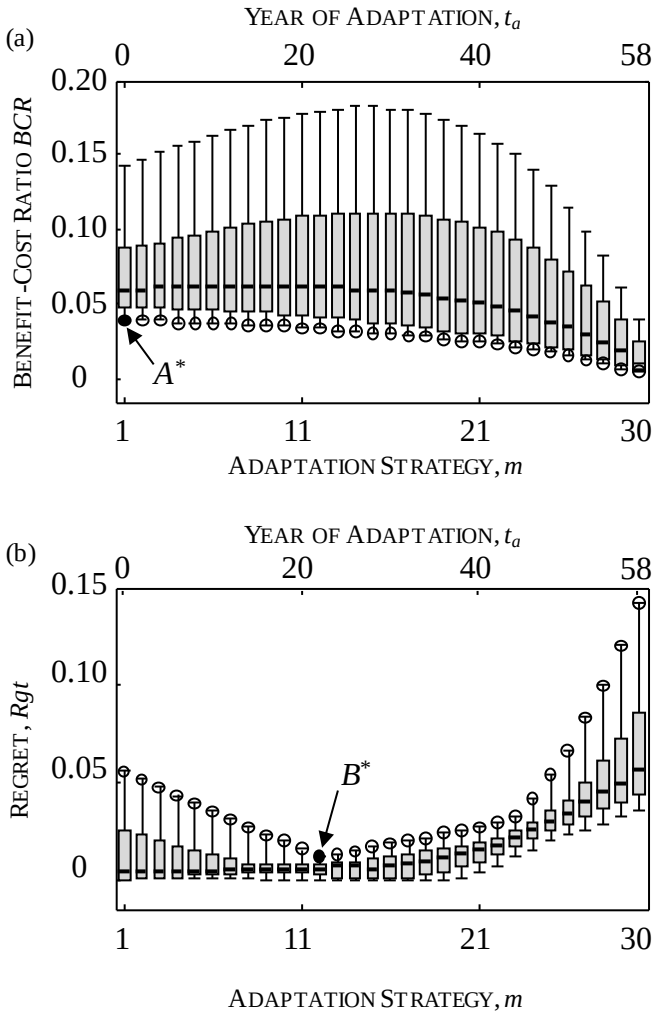

Figure 6.14. Box-and-whisker plots for the adaptation strategies with regards to (a) BCR and (b)Regret, *Rgt* considering all future (climate and economic) scenarios. The circles denote the (a) the minimum values of BCR across all potential future scenarios and (b) the maximum Regret across all potential future scenarios. In (a) the minimum values are maximized to find the optimal strategy *A**, and in (b) the maximum values are minimized to find the optimal strategy *B**. Both (a) and (b) pertain to Example A: climate change trends similar to those expected in the Columbia River

scenarios CCS_1 to CCS_5 and their individual values are super imposed over the box-and-whisker plots in Figure 6.15 for example A. Figure 6.15a shows that BCRs for CCS_2 to CCS_4 are bounded between the BCR for CCS_1 (the largest BCR) and those for CCS_5 (the smallest). Thus the worst-case scenario for the maximin BCR problem is CCS_5; in this scenario flooding is expected to decrease in intensity. A lower propensity to flood leads to lower risk levels and a low benefit associated with retrofit. The most economical time to act is at the initial time, when the adaptation efforts can mitigate current risk levels. Since the pessimistic approach plans for the worst case, this solution is optimal for maximizing minimum BCR. However, Figure 6.15b shows that maximum Regret is associated with different climate change scenarios over time (as opposed to the minimum BCR which was always associated with CCS_5). For strategies with early adaptation times (between 0 and 22 years), the maximum Regret occurs when CCS_1 is realized. That is, the failure to act at an early stage in life leads to large foregone benefits if there turns out to be an increase in the intensity of flooding (as is the case for CCS_1). Similarly, CCS_1 dominates the Regret when the adaptation time is towards the end of the planning horizon of 60 years. CCS_5, however, presents the largest regret for strategies associated with adaptation times between 22 and 44 years. This is due to the regret of inaction over time that stems from the decreased benefit associated with adaptation later in life when flooding intensity is expected to decrease. Similar trends exist across all economic scenarios, resulting in the same trends appearing in Figure 6.15 to appear in the illustrative example results shown in Figure 6.14. Based on the previous observations, the single objective optimization formulations yield different solutions due to the fact that the

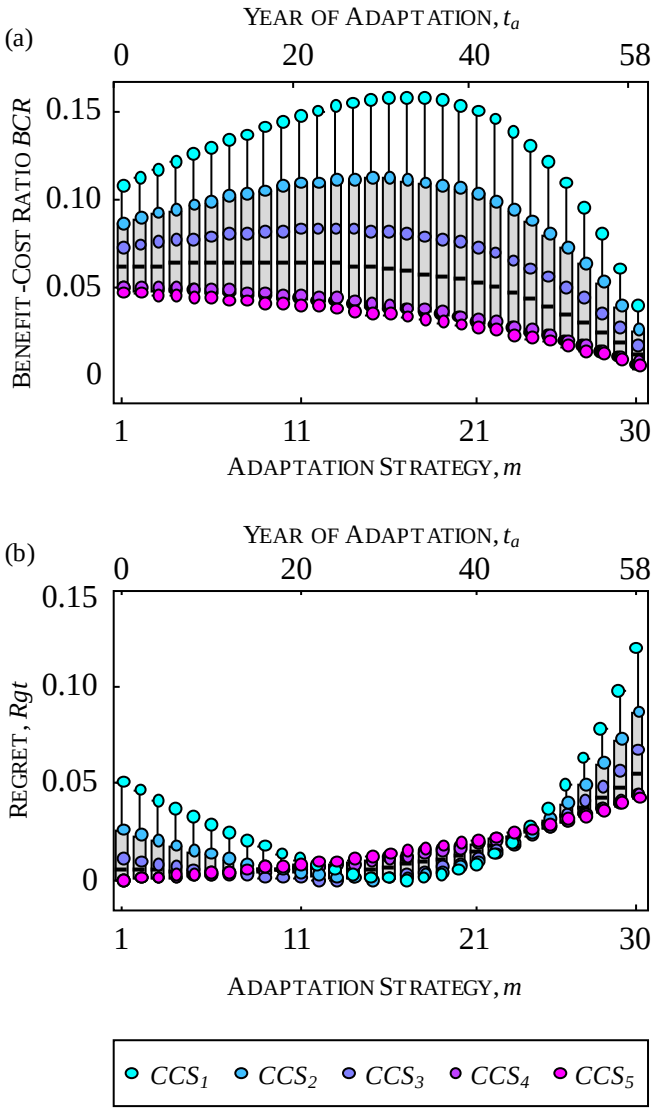

Figure 6.15. Box-and-whisker plots for the adaptation strategies with regards to (a) BCR and (b) Regret, *Rgt* considering all future climate scenarios but only one economic scenario. The circles denote the value of the metric for the noted climate scenario. Both (a) and (b) pertain to Example A: climate change trends similar to those expected in the Columbia River

"worst-case" scenario for BCR is different from the "worst-case" scenario for Regret. Therefore, the optimal solution found by maximizing minimum BCR is not the same as that found by minimizing maximum Regret.

The Pareto set of optimal solutions developed for the bi-objective optimization problem reiterates the conflicting nature of the two objectives: maximizing minimum BCR and minimizing maximum Regret for Example A. The Pareto optimal solution is presented in Figure 6.16. The trade-off between BCR and Regret in the Pareto optimal solution is as follows: the maximum Regret cannot be minimized without further decreasing the BCR. The single objective solution for the pessimistic formulation regarding BCR, appears on the Pareto front, denoted as A^* in Figure 6.16 (and Figure 6.14) involves the application of the adaptation action at the earliest possible time, $t_a = 0$. The single objective solution for the pessimistic formulation regarding Regret, appears on the Pareto front, denoted as B^* in Figure 6.16 (and Figure 6.14), involves the application of the adaptation action at year 22. The other optimal strategies in the Pareto optimal set have application times ranging between the bounds set by A^* and B*. The decision maker may use the Pareto front as the basis for which to make decisions based on their individual preferences for payoff and Regret.

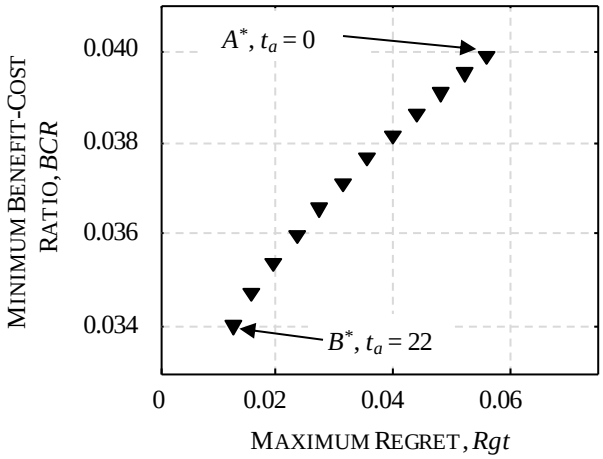

Figure 6.16. Pareto optimal set of solutions to the bi-objective optimization problem for climate change adaptation that minimizes the maximum Regret and maximizes the minimum BCR pertaining to Example A: climate change trends similar to those expected in the Columbia River.

The results for Example B are summarized in Figure 6.17 for the single objective optimization problems, and Figure 6.19 for the bi-objective optimization problem. The optimal strategy for the maximin BCR problem is the application of adaptation efforts at $t_a = 0$ denoted as C^* in Figure 6.17a and Figure 6.19; for the minimax Regret problem is the application of adaptation efforts at $t_a = 8$, denoted as D^* in Figure 6.17b and Figure 6.19. It again is shown that minimizing maximum Regret and maximizing minimum BCR are competing objectives.

In order to understand why the optimal solution found by maximizing minimum BCR is not the same as that found by minimizing maximum Regret for Example B, the variation of BCRs and Regrets climate change scenarios for a single, deterministic discount rate of 4% is investigated. The results shown in Figure 6.19 exhibit the same trends and the argument presented for Example A is applicable for Example B. Therefore, since both Example A and Example B have climate change scenarios where

the flooding is expected to intensity and at least one where the flooding is expected to become less intense, the optimal solutions for minimizing maximum Regret and maximizing minimum BCR are different.

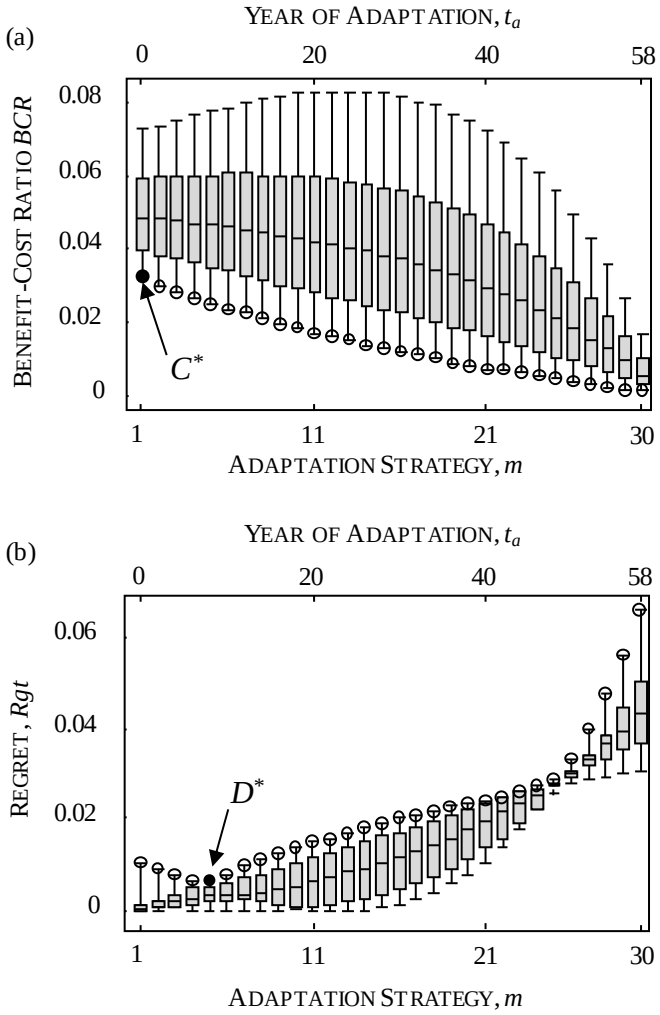

Figure 6.17. Box-and-whisker plots for the adaptation strategies with regards to (a) BCR and (b)Regret, *Rgt* considering all future (climate and economic) scenarios. The circles denote the (a) the minimum values of BCR across all potential future scenarios and (b) the maximum Regret across all potential future scenarios. In (a) the minimum values are maximized to find the optimal strategy *C**, and in (b) the maximum values are minimized to find the optimal strategy *D**. Both pertain to Example B: climate change trends similar to those expected in the Mississippi River

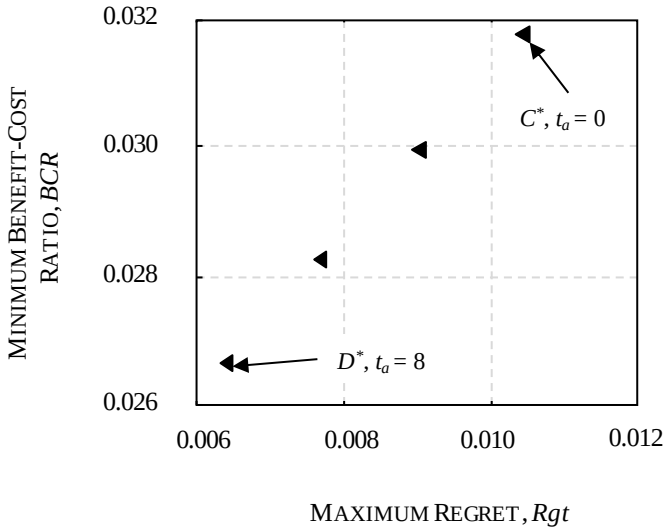

Figure 6.18. Pareto optimal set of solutions to the bi-objective optimization problem for climate change adaptation that minimizes the maximum Regret and maximizes the minimum BCR pertaining to Example B: climate change trends similar to those expected in the Mississippi River

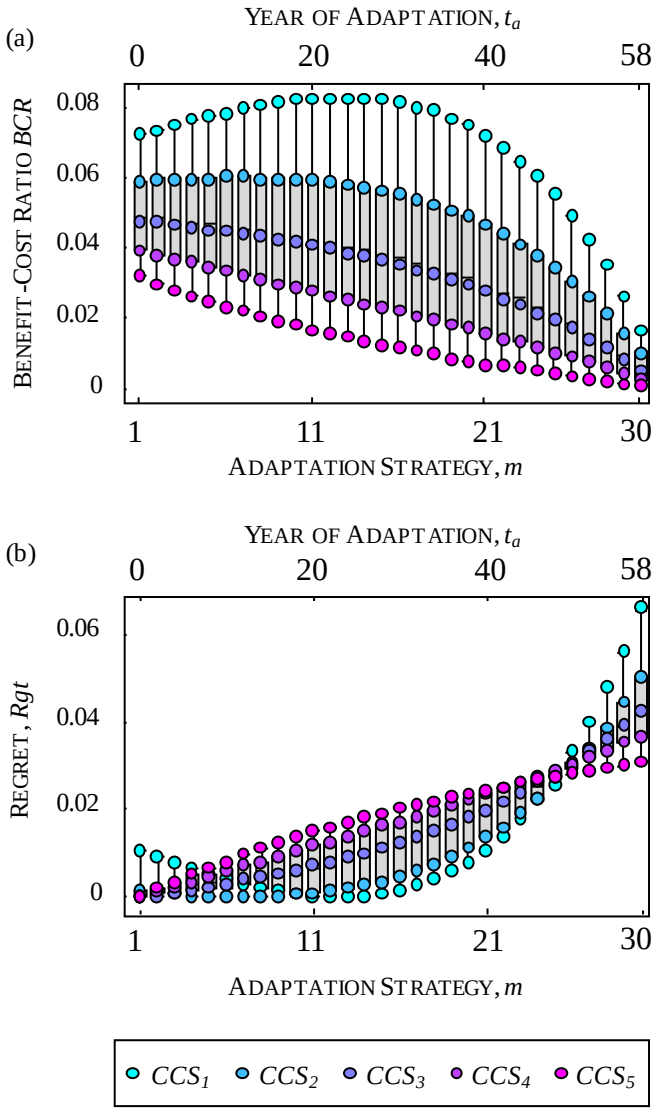

Figure 6.19. Box-and-whisker plots for the adaptation strategies with regards to (a) BCR and (b) Regret, *Rgt* considering all future climate scenarios but only one economic scenario. The circles denote the value of the metric for the noted climate scenario. Both (a) and (b) pertain to Example B: climate change trends similar to those expected in the Mississippi River

6.12. CONCLUSIONS

Robust optimization models aid in the decision-making process for adapting civil infrastructure to a changing climate. The deep uncertainties associated with future climate scenarios that stem from both the variety of GCMs that may be used to predict future climate and the different RCPs which define potential future Greenhouse Gas concentrations must be systematically integrated into the decision making process. This chapter, based on Mondoro et al. (2017b; 2017e) and Mondoro and Frangopol (2018), (1) develops two metrics for the assessment of adaptation strategies and (2) presents robust optimization formulations for identifying optimal climate change adaptation strategies. The metrics and optimization formulations are developed to aid in identifying strategies that are both flexible and beneficial. The optimization models are applied to two illustrative examples that consider a typical bridge over two rivers having comparable climate change trends to the Columbia River and Mississippi River. In the former, flooding is consistently anticipated to intensify, while in the later, flooding is consistently expected to become less intense. The following conclusions are drawn with respect to:

1. Metrics for evaluating the performance of adaptation strategies:

    - The Gain Loss Ratio provides a systematic method for quantifying gain accrued by delaying adaptation until more information is acquired with respect to future climate predictions while considering the losses associated with such delay. This support the rational decision making process and can be integrated into robust optimization frameworks.

- The tradeoff between GLR and BCR in the bi-objective optimization results highlights the competing desire for flexibility and efficiency.
- Regret quantifies the performance of an adaptation strategy in comparison to all other potential strategies. It is useful in supporting decision making under deep uncertainty since it provides a procedurally rational approach to define desire not to choose a suboptimal strategy.
- The tradeoff between Regret and BCR in the Pareto optimal solutions to the bi-objective optimization process demonstrate the conflicting nature of these objectives. The trade-offs highlight that the use of only one metric fails to capture the complexities of decision making under uncertainty.

2. Robust optimization frameworks:
   - The pessimistic formulation yields solutions that plan for the worst-case scenario. As such, there are no potential gains by delaying adaptation if the worst-case scenario includes an intensification of the hazard. This conservative formulation is useful for risk averse decision markers, but antithetical to the desire for flexibility.
   - The bi-objective optimistic formulation, is useful for decision makers who do not want to assign any probability of occurrence to climate scenarios. However, the Pareto front represents unattainable value, since the maximum values for BCR and GLR require the realization of different scenarios.

- The robustness formulation considers the dispersion in the performance of adaptation strategies over all potential scenarios. However, the formulation of the robustness index assigns an equal likelihood to all potential scenarios. It does not differentiate between positive and negative values of the payoff metrics (i.e. BCR or GLR) and thus has a significant drawback to implementation.

3. Site-specific variations in anticipated climate changes:

    - In regions where the climate change scenarios include an overall intensification of the hazard, the desire for flexibility is outweighed by the need to adapt in order to prevent significant losses.

    - In regions where there the climate change scenarios include an overall decrease in the intensity of the hazard, the desire for flexibility can lead to optimal adaptation strategies that delay adaptation until additional information is available. There is a trade-off between the objectives of economic efficiency and flexibility where low BCR must be accepted for high GLR and vice-versa.

CHAPTER 7

SUMMARY, CONCLUSIONS, AND FUTURE WORK

7.1. SUMMARY

Continuously deteriorating structures, calls for increased service lives, limited finances, the occurrence of extreme hydrologic events, changing future loading conditions, and limited available resources are only some of the issues driving research in the field of life-cycle management. The instrumentation of civil and naval structures has led to the availability of SHM data that may be used to quantify uncertainties in past and current performance. However, missing data due to discrete monitoring practices or potential changes in future operating conditions lead to challenges in future response prediction. The work detailed in Chapter 2 demonstrates how available SHM data can be used to estimate missing data and enable fatigue damage predictions. The work is developed around naval vessels and the developed framework addresses expected variations in structural performance due to ship speed, heading angle, and wave height.

Chapters 3 and 4 focuses on the performance assessment and management of bridges vulnerable to extreme hydrologic events. Chapter 3 demonstrates the pressing need to include all relevant failure modes when determining the probability of failure and risk associated with a structure and developing optimal management strategies. The adverse effects of retrofitting a structure to prevent deck failure on the scour failure may outweigh the benefits and may lead to an increase in risk, rather than a decrease. This research highlighted the economic efficiency of retrofit for multiple failure modes together (i.e.

retrofit the deck and foundation to prevent deck dislodgement and scour). Chapter 4 focused on the management of coastal bridges. Coastal bridges are exposed to corrosive marine environments and are vulnerable to damage during hurricanes. Managing these structures requires attention given to the constant deterioration process of corrosion and the discrete occurrence of hurricanes and their resulting damage. The framework developed in Chapter 4 addresses these challenges while also accounting for the differences in costs associated with post disaster economic conditions.

Chapters 5 and 6 identify and address the challenges of climate change in developing management strategies for bridges. The impact of climate change on natural hazards and the potential interactions with bridges are detailed in Chapter 5. This chapter also identifies the uncertainties associated with climate change prediction and the difficulties in developing a systematic approach to management. Chapter 6 addresses some of the challenges that stem from the deep uncertainties of climate change. Decision support metrics for evaluating a performance strategy are proposed and frameworks are presented to aid in identifying optimal strategies.

The work presented in this dissertation contributes to the development of the field life-cycle management by enhancing (1) the use of SHM data to quantify uncertainties in fatigue life predictions for naval structures, (2) performance assessment methodologies and optimal management frameworks for bridges vulnerable to floods and hurricanes, and (3) decision support metrics and methodologies for climate change adaptation.

7.2. CONCLUSIONS

A detailed set of conclusions is provided within each chapter. The following is a summary of the major conclusions of the research presented for

Uncertainty Quantification and the use of SHM (Chapter 2)

- Available SHM data can be quantified using generalized functions and a prediction surface can be used to estimate structural response in unobserved operation condition. This allows essential information regarding the as-built condition and the actual loads acting on the structure, normally captured in the SHM data, to be integrated into the fatigue life prediction while addressing the issue of missing data.
- Two generalized fitting functions for PSD functions of ship SHM data care developed: the generalized JONSWAP function and the generalized Pierson-Moskowitz function. The aforementioned functions fit the observed SHM data for the HSV-2 Swift but are most applicable to the responses observed for head seas.
- The methodology for quantifying the SHM data considers both the low frequency and high frequency when predicting the PSD in unobserved cells. This inclusion of both low frequency and high frequency content is critical for estimating the fatigue damage.
- When estimating unobserved structural responses, the theoretically-based nonlinear prediction surfaces outperform linear surfaces in estimating low frequency response characteristics. The polynomial nonlinear surface is preferred

as it is shown to be more robust. For high frequency characteristics, the nonlinear and linear surfaces are comparable in their performance with linear surfaces occasionally outperforming the nonlinear ones.

Management of Bridges under Vulnerable to Floods (Chapter 3)

- It is essential to include all relevant failure modes when assessing the effectiveness of management strategies aimed at reducing life-cycle risk. While retrofit options may decrease the probability of failure of a structure, they may increase the risk associated with the structure due to differences in economic and social consequences associated with different failure modes.

- Site specific variations in the hazard are critical to for identifying preferred risk management strategies: The benefit-cost ratios are sensitive to the exposure of the bridge to flood hazards. In areas where the exposure of the bridge is higher, retrofitting the bridge with measures aimed at reducing both deck and foundation failure are profitable cost-effective at reducing risk. However, in low exposure cases, it may be economically prudent to do nothing.

Management of Coastal Bridges (Chapter 4)

- A proposed optimization approach for establishing optimal management strategies for bridges considering hurricanes, traffic, and deterioration mechanisms is an effective tool to support the decision making process for managing coastal bridges. The risk metric incorporates both the probability of failure and consequences of the diverse hazards.

- Minimizing life-cycle costs and minimizing the maximum life-cycle risk are conflicting objectives in which repair and retrofit actions increase the life-cycle cost but decrease the maximum life-cycle risk. Optimal management strategies associated with high-risk low-costs solutions can be drastically improved through minimal additional investments for coastal bridges vulnerable to hurricanes.
- Economic conditions such as the increased cost of construction materials and labor in a post-disaster region and the discount count rate of money are important to consider. High relative hurricane failure consequences drive optimal management strategies to include retrofit actions in order to minimize risk.

Climate Change and the Management of Structures (Chapter 5 and 6)

- Changes in climate have led to sea level rise, increasingly intense hurricanes, and increasingly intense precipitation, leaving civil infrastructure more vulnerable to damage during extreme hydrologic events. The deep uncertainties associated with climate change predictions present unique challenges to bridge managers.
- Metrics for evaluating the performance of adaptation strategies have been developed to support the rational decision making process. The Gain Loss Ratio provides systematic method for quantifying gain accrued by delaying adaptation until more information is acquired regard future climate predictions while consider the losses associated with such delay. Regret quantifies the performance of an adaptation strategy in comparison to all other potential strategies. It is useful in supporting decision making under deep uncertainty since it provides a

procedurally rational approach to define desire not to choose a suboptimal strategy.

- The results from robust optimization models used to determine optimal strategies without assigning a probability of occurrence to different scenarios demonstrate the conservative nature of the pessimistic formulation and the lack of conservativeness in the optimistic formulation. Robustness indices provide a solution that considers the dispersion in the performance of adaptation strategies over all potential scenarios, but implicitly assigns an equal probability of occurrence to all scenarios.
- Site specification variations in climate changes result in different optimal strategies. In regions where the climate change scenarios include an overall intensification of the hazard, the desire for flexibility is outweighed by the need to adapt in order to prevent significant losses. However, in regions where the climate change scenarios include an overall decrease in the intensity of the hazard, the desire for flexibility can be systematically rationalized with the use of the GLR and the optimal adaptation strategy may include a delay adaptation.

7.3. FUTURE WORK

The research presented in this dissertation represents advancements in the use of SHM data to assess the performance of a structure, the life-cycle management of structures vulnerable to hurricanes and flooding, and developing optimal climate change adaptation

strategies. However, there are still challenges that remain in the field of life-cycle management and further topics of research are identified as follows.

On the life-cycle assessment and management of naval structures:

- In order to extend the operational life and support the effective management of naval structures, additional research is needed on how to use SHM data for a single detail to inform system performance updates. Currently, SHM data is only available at the gauge locations (since it is economically infeasible to instrument an entire ship). However, it is important to identify how the damage at a single detail is related to the performance of the overall performance of the vessel. Due to the aging fleet and the high costs of building new ships, the work to support system performance assessment should be prioritized as it enables the effective management of existing ships.

On the management of bridges: In order to support the effective management of coastal bridges, further work is needed to (1) address network-level management and (2) identify alternative methods for solving the robust optimization problem of bridge adaptation to climate changes. These works should be addressed in parallel in order to efficiently tackle the effective management of infrastructure vulnerable to climate changes. They are detailed as follows:

- The methodologies presented for prioritizing bridge repair and retrofit actions were developed for a single bridge. However, in coastal regions and areas vulnerable to floods, it is often the case that there are multiple vulnerable bridges that all fall under the management of a single agency. In this regard, the single

agency must allocate money to mitigate risk on a network level. Further work is needed to address the optimal management of bridge networks that are vulnerable to floods and/or hurricanes. This includes considerations for how the failure of bridges affects the typical flow of traffic through the network, access to evacuation routes, and access to hospitals, among others.

- The optimization frameworks for identifying optimal adaptation strategies presented in this research include both non-probabilistic models that plan for the worst-case scenario (i.e. a pessimistic formulation) or for the best-case scenario (i.e. an optimistic formulation) and probabilistic models that subjectively assign equal probabilities of occurrence to potential scenarios. Further work is necessary on incorporating alternative non-probabilistic models, such as Robust Decision Making (Lempert et al. 2010) or Info-Gap (Hall et al. 2012) methods, as the optimization methodologies used to develop robust strategies. Specific attention should be given to the extent to which these methods are non-probabilistic and alternative methodologies should also be explored.

REFERENCES

Aalberts, P. J. and Nieuwenhuijs, M. W. (2006). Full scale wave and whipping induced hull girder loads. In: *Proceedings of the 4th International Conference on Hydroelasticity*, Wuxi, China.

AASHTO. (2008). *AASHTO Guide specifications for bridges vulnerable to coastal storms*. American Association of State Highway and Transportation Officials, Washington, D.C.

AASHTO. (2012). *AASHTO LRFD Bridge design specifications*. American Association of State Highway and Transportation Officials, Washington, D.C.

Adey B., Hajdin R., and Brühwiler, E. (2003). Risk-based approach to the determination of optimal interventions for bridges affected by multiple hazards. *Engineering Structures*, 25(7): 903-912.

Agrawal, A. K., Khan, M. A., Yi, Z., and Aboobaker, N. (2007). *Handbook of scour countermeasures designs*. New Jersey Department of Transportation.

Akiyama, M., Frangopol, D.M., Arai, M. and Koshimura, S. (2013). Reliability of bridges under tsunami hazards: Emphasis on the 2011 Tohoku-oki earthquake. *Earthquake Spectra*, 29(1): S295-S314.

Albrecht, P. and Naeemi, A. H. (1984). *Performance of Weathering Steel in Bridges*, NCHRP Report 272, Transportation Research Board, National Research Council, Washington, D.C.

Alexander, M. A., Kilbourne, K. H., and Nye, J. A. (2014). Climate variability during warm and cold phases of the Atlantic Multidecadal Oscillation (AMO) 1871–2008. *Journal of Marine Systems*, 133, 14-26.

American Automobile Association. (2014). *Your Driving Costs*. Heathrow, FL.

Anderson, I., Rizzo, D.M., Huston, D.R. and Dewoolkar, M.M. (2017). Analysis of bridge and stream conditions of over 300 Vermont bridges damaged in Tropical Storm Irene. *Structure and Infrastructure Engineering*, 1-14.

Anthes, R. A., Corell, R. W., Holland, G., Hurrell, J. W., MacCracken, M. C., and Trenberth, K. E. (2006). Hurricanes and global warming-potential linkages and consequences. *Bulletin of the American Meteorological Society*, 87(5): 623-628.

Arneson, L. A., Zevenbergen, L. W., Lagasse, P. F., and Clopper, P. E. (2012). *Evaluating scour at bridges*. Report No. FHWA-HIF-12-003 HEC-18, Federal Highway Administration, 340 pp.

ASCE. (2013). *2013 Report card for America's infrastructure*, American Society of Civil Engineers, Reston, VA, USA.

ASCE. (2017). *ASCE's 2017 Report Card for America's Infrastructure*. American Society of Civil Engineers, Reston, VA, USA.

Ataei, N. and Padgett, J.E. (2013a). Limit state capacities for global performance assessment of bridges exposed to hurricane surge and wave. *Structural Safety*, 41: 73-81.

Ataei, N. and Padgett, J. E. (2013b). Probabilistic modeling of bridge deck unseating during hurricane events. *Journal of Bridge Engineering*, 18(4): 275-286.

Augusti, G., Ciampoli, M. and Frangopol, D.M. (1998). Optimal planning of retrofitting interventions on bridges in a highway network. *Engineering Structures*, 20(11): 933-939.

Barkdoll, B. D., Ettema, R., and Melville, B. W. (2007). *Countermeasures to protect bridge abutments from scour.* NCHRP Report 587, Transportation Research Board.

Bastidas-Arteaga, E., and Stewart, M.G. (2015). Damage risks and economic assessment of climate adaptation strategies for design of new concrete structures subject to chloride-induced corrosion. *Structural Safety*, 52: 40-53.

Bastidas-Arteaga, E., Schoefs, F., Stewart M.G., and Wang, X. (2013). Influence of global warming on durability of corroding RC structures: A probabilistic approach. *Engineering Structures*, 51: 259-266.

Bell, D.E. (1982). Regret in decision making under uncertainty. *Operations Research*, 30(5): 961-981.

Benasciutti, D., and Tovo, R. (2007). On fatigue damage assessment in bimodal random processes. *International Journal of Fatigue*, 29(2): 232-244.

Bendat, J. (1964). *Probability functions for random responses prediction for peaks, fatigue damage, and catastrophic failures*. Vol. 33. National Aeronautics and Space Administration, 1964.

Bennett, C., Matamoros, A., Barrett-Gonzalez, R. and Rolfe, S. (2014). *Enhancement of welded steel bridge girders susceptible to distortion-induced fatigue.* No. FHWA-

KS-14-03. The University of Kansas Center for Research, Inc. Lawrence, KS, USA.

Bertsimas, D., Brown, D. B., and Caramanis, C. (2011). Theory and applications of robust optimization. *SIAM Review*, 53(3): 464-501.

Bjarnadottir, S., Li, Y., and Stewart, M. G. (2014). Regional loss estimation due to hurricane wind and hurricane-induced surge considering climate variability. *Structure and Infrastructure Engineering*, 10(11): 1369-1384.

Blake, E. S., Landsea, C., and Gibney, E. J. (2011). *The deadliest, costliest, and most intense United States tropical cyclones from 1851 to 2010 (and other frequently requested hurricane facts)*. NOAA, Technical Memorandum NWS NHC-6.

Bocchini, P. and Frangopol, D.M. (2011). A probabilistic computational framework for bridge network optimal maintenance scheduling. *Reliability Engineering & System Safety*, 96(2): 332-349.

Bove, M. C., O'Brien, J. J., Eisner, J. B., Landsea, C. W., and Niu, X. (1998). Effect of El Niño on US landfalling hurricanes, revisited. *Bulletin of the American Meteorological Society*, 79(11): 2477-2482.

Bradshaw, A.S., and Baxter, C.D.P. (2006). *Design and construction of driven pile foundations– lessons learned on the Central Artery/Tunnel Project*. No. FHWA-HRT-05-159.

Brady, T., Bachman, R., Donnelly, M., and Griggs, D. (2004). *HSV-2 Swift instrumentation and technical trials plan*. Naval Surface Warfare Center, Carderock Division (NSWCCD), West Bethesda, Maryland.

Bresler, B. (1960). Design criteria for reinforced columns under axial load and biaxial bending. *Journal Proceedings;* (57)11: 481-490.

Bridges, T., Henn, R., Komlos, S., Scerno, D., Wamsley, T., and White,K. (2013). *Coastal risk reduction and resilience: using the full array of measures.* CWTS 2013-3 US Army Corps of Engineers (USACE).

Brown, T. M., Collins, T. J., Garlich, M. J., O'Leary, J. E., and Heringhaus, K. C. (2010). *Underwater bridge repair, rehabilitation, and countermeasures*. Federal Highway Administration Report NHI-10-029.

Burkett, V. R., Zilkoski, D. B., and Hart, D. A. (2002). Sea-level rise and subsidence: implications for flooding in New Orleans, Louisiana. In *US Geological Survey Subsidence Interest Group Conference: Proceedings of the Technical Meeting*, Galveston, Texas, 27-29 November 2001, pp. 63-71.

Butler, R. W., Machado, U. B., and Rychlik, I. (2009). Distribution of wave crests in a non-Gaussian sea. *Applied Ocean Research*, 31(1): 57-64.

Carter, T.R., Alfsen, K., Barrow, E., Bass, B., Dai, X., Desanker, P., Gaffin, S.R., Giorgi, F., Hulme, M., Lal, M., Mata, L.J. , Mearns, L.O., Mitchell, J.F.B., Morita, T. , Moss, R., Murdiyarso, D., Pabon-Caicedo, J.D., Palutikof, J., Parry, M.L., Rosenzweig, C. , Seguin, B., Scholes, R.J. , and Whetton, P.H. (2007). General guidelines on the use of scenario data for climate impact and adaptation. Version 2. *Prepared on behalf of the Intergovernmental Panel on Climate Change*, Task Group on Data and Scenario Support for Impact and Climate Assessment.

Chan, H.S., Atlar, M. and Incecik, A. (2002). Large-amplitude motion responses of a Ro–Ro ship to regular oblique waves in intact and damaged conditions. *Journal of Marine Science and Technology*, 7(2): 91-99.

Chang, P. C., Flatau, A., and Liu, S. (2003). Review paper: health monitoring of civil infrastructure. *Structural Health Monitoring*, 2(3): 257-267.

Chaves, I.A., Melchers, R.E., Peng, L., and Stewart, M.G. (2016), Probabilistic remaining life estimation for deteriorating steel marine infrastructure under global warming and nutrient pollution. *Ocean Engineering*, 126: 129-137.

Chen, Q., Wang, L., and Zhao, H. (2009). Hydrodynamic investigation of coastal bridge collapse during Hurricane Katrina. *Journal of Hydraulic Engineering*, 135(3): 175-186.

Chen, J., Brissette, F. P., and Leconte, R. (2011). Uncertainty of downscaling method in quantifying the impact of climate change on hydrology. *Journal of Hydrology*, 401(3): 190-202.

Church, J.A. and White, N.J., (2006). A 20th century acceleration in global sea-level rise. *Geophysical Research Letters*, 33(1).

Collette, M. and Incecik, A. (2006). An approach for reliability-based fatigue design of welded joints on aluminum high-speed vessels. *Journal of Ship Research*, 50(1): 85-98.

Condon, L. E., Gangopadhyay, S., and Pruitt, T. (2015). Climate change and non-stationary flood risk for the upper Truckee River basin. *Hydrology and Earth System Sciences*, 19(1): 159-175.

Cruce, T.L. (2009). *Adaptation planning–what US states and localities are doing*. Pew Center on Global Climate Change.

Dalton, M. M., and Mote, P. W. (2013). *Climate change in the Northwest: Implications for our landscapes, waters, and communities*. Washington, DC: Island Press.

Dexter, R. J., and Ocel, J. M. (2013). *Manual for repair and retrofit of fatigue cracks in steel bridges*. FHWA-IF-13-020, Federal Highway Administration.

Dirlik, T. (1985). Application of computers in fatigue analysis. Ph.D. thesis, University of Warwick, Coventry, England.

Dixon, C. R., Masters, F. J., Prevatt, D. O., Gurley, K. R., Brown, T. M., Peterka, J. A., and Kubena, M. E. (2014). The influence of unsealing on the wind resistance of asphalt shingles. *Journal of Wind Engineering and Industrial Aerodynamics*, 130: 30-40.

DNV. (2010). *Fatigue methodology of offshore ships*, Det Norske Veritas Classification, Høvik, Norway.

Dong, Y., Frangopol, D. M., and Saydam, D. (2014a). Pre-earthquake multi-objective probabilistic retrofit optimization of bridge networks based on sustainability. *Journal of Bridge Engineering*, 19(6): 04014018.

Dong Y., Frangopol D.M., and Saydam D. (2014b). Sustainability of highway bridge networks under seismic hazard. *Journal of Earthquake Engineering*, 18(1): 41-66.

Dong, Y., Frangopol, D.M., and Sabatino, S. (2015). Optimizing bridge network retrofit planning based on cost-benefit evaluation and multi-attribute utility associated with sustainability. *Earthquake Spectra*, 31(4): 2255-2280.

Douglas, E. M., Vogel, R. M., and Kroll, C. N. (2000). Trends in floods and low flows in the United States: impact of spatial correlation. *Journal of Hydrology*, 240(1): 90-105.

Douglas, S., Chen, Q., Olsen, J., and Edge, B. (2006). *Wave forces on bridge decks,* U.S Department of Transportation Report, Federal Highway Administration, McLean, VA, USA.

Douglass, S.L., Hughes, S., Rogers, S. and Chen, Q. (2004). *The impact of Hurricane Ivan on the coastal roads of Florida and Alabama: a preliminary report.* Rep. to Coastal Transportation Engineering Research and Education Center, Univ. of South Alabama, Mobile, AL, USA.

Easterling, D. R., Meehl, G. A., Parmesan, C., Changnon, S. A., Karl, T. R., and Mearns, L. O. (2000). Climate extremes: observations, modeling, and impacts. *Science*, 289(5487): 2068-2074.

Ellingwood, B. R. and Kinali, K. (2009). Quantifying and Communicating Uncertainty in Seismic Risk Assessment. *Structural Safety*, 31(2): 179-187.

Elsner, J. B. (2006). Evidence in support of the climate change–Atlantic hurricane hypothesis. *Geophysical Research Letters*, 33(16).

Elsner, J. B., Liu, K. B. and Kocher, B. (2000). Spatial variations in major U.S. hurricane activity: Statistics and a physical mechanism. *Journal of Climate*, 13: 2293–2305.

Emanuel, K. A. (1987). The dependence of hurricane intensity on climate. *Nature*, 326: 483–485.

Espinet X., Schweikert A., and Chinowsky, P. (2017). Robust prioritization framework for transport infrastructure adaptation investments under uncertainty of climate change. *ASCE-ASME Journal of Risk and Uncertainty in Engineering Systems, Part A: Civil Engineering,* 3(1), E4015001.

Estes, A. and Frangopol, D. (1999). Repair optimization of highway bridges using system reliability approach. *Journal of Structural Engineering*, 125(7): 766-775.

Eurocode 9 (2009). *Design of aluminum structures part 1-3, additional rules for structures susceptible to fatigue.* CEN – European Committee for Standardization, Brussels, Belgium.

FDOT Florida Department of Transportation. (2011). *Bridge costs,* Transportation Costs Report, Tallahassee, FL, USA.

FDOT. (2017). *Structures design guidelines*. Florida Department of Transportation No. 625-020-018.

FEMA. (1997). *Report on costs and benefits of natural hazard mitigation*, Federal Emergency Management Agency, Washington, D.C.

FEMA. (2010). *Home builder's guide to coastal construction*. FEMA P-499. Federal Emergency Management Agency, 184 pp.

FEMA. (2015). *Guidelines and standards for flood risk analysis and mapping*. Federal Emergency Management Agency.

Fisher, J. W. (1990) *Distortion-induced fatigue cracking in steel bridges*. No. 336. Transportation Research Board.

FHWA. (2017). The Federal Highway Adminsitration's Climate change and extreme weather vulnerability assessment framework [online]. *FHWA Publication No: FHWA-HEP-13-005 2012*; <http://www.fhwa.dot.gov/environment/climate_change/adaptation/publications_and_tools/vulnerability_assessment_framework/fhwahep13005.pdf>. Accessed June 2017.

Fisher, I. (1930). *The theory of interest*, Macmillan Co., NY.

Flato G., Marotzke J., Abiodun B., Braconnot P., Chou S.C., Collins W., Cox P., Driouech F., Emori S., Eyring V., Forest C., Gleckler P., Guilyardi E., Jakob C., Kattsov V., Reason C., and Rummukainen M. (2013). Evaluation of climate models. In: *Climate Change 2013: The Physical Science Basis*. Contribution of Working Group I to the Fifth Assessment Report of the Intergovernmental Panel on Climate Change. Cambridge University Press, Cambridge, United Kingdom and New York, NY, USA.

Fukui, J. and Otuka, M. (2002). Development of the new inspection method on scour condition around existing bridge foundations. In *Proceedings of the First International Conference on Scour of Foundations*, Texas, pp. 410-420.

Gabrel, V., Murat, C., and Thiele, A. (2014). Recent advances in robust optimization: An overview. *European Journal of Operational Research*, 235(3): 471-483.

Ghobarah, A., Saatcioglu, M. and Nistor, I. (2006). The impact of the 26 December 2004 earthquake and tsunami on structures and infrastructure. *Engineering Structures*, 28(2): 312-326.

Giuliani M., and Castelletti A. (2016). Is robustness really robust? How different definitions of robustness impact decision-making under climate change. *Climatic Change*, 135(3-4):409-424.

Goldenberg, S. B., Landsea, C. W., Mestas-Nuñez, A. M., and Gray, W. M. (2001). The recent increase in Atlantic hurricane activity: Causes and implications. *Science*, 293(5529): 474-479.

Gornitz, V., Couch, S., and Hartig, E. K. (2002). Impacts of sea level rise in the New York City metropolitan area. *Global and Planetary Change*, 32(1): 61-88.

Gray, W. M. (1968). Global view of the origin of tropical disturbances and storms. *Monthly Weather Review*, 96(10): 669-700.

Gray, W. M. (1984). Atlantic seasonal hurricane frequency. Part I: El Niño and 30 mb quasi-biennial oscillation influences. *Monthly Weather Review*, 112(9): 1649-1668.

Groves, D.G. and Lempert, R.J. (2007). A new analytic method for finding policy-relevant scenarios. *Global Environmental Change*, 17(1): 73-85.

Groves, D. G., Yates, D., and Tebaldi, C. (2008). Developing and applying uncertain global climate change projections for regional water management planning. *Water Resources Research*, 44(12).

Hall, J. W., Lempert, R. J., Keller, K., Hackbarth, A., Mijere, C., and McInerney, D. J. (2012). Robust climate policies under uncertainty: a comparison of robust decision making and info-gap methods. *Risk Analysis*, 32(10): 1657-1672.

Hallegate, S. (2009). Strategies to adapt to an uncertain climate change. *Global Environmental Change*, 19(2): 240-247.

Hallegatte S., Shah A., Brown C., Lempert R., and Gill S. (2012). Investment decision making under deep uncertainty--application to climate change. *Policy Research Working Papers WPS 6193*; World Bank, Washington, D. C.

Hassan, A. F., and Bowman, M. D. (1996). Fatigue crack repair of steel beams with tapered cover plate details. *Journal of Structural Engineering*, 122(11): 1337-1346.

Hasselmann, K., Barnett, T., Bouws, E., Carlson, H., Cartwright, D., Enke, K., Ewing, J., Gienapp, H., Hasselmann, D., and Kruseman, P. (1973). *Measurements of wind-wave growth and swell decay during the Joint North Sea Wave Project (JONSWAP*), Deutches Hydrographisches Institut.

Hawkins E. and Sutton, R. (2011). The potential to narrow uncertainty in projections of regional precipitation change. *Climate Dynamics*, 37(1-2): 407-418.

Heibaum, M. and Trentmann, J. (2010). Partial grouted riprap for enhanced scour resistance. *Scour and Erosion*, 210, 1.

Heidarpour, M., Afzalimehr, H., and Izadinia, E. (2010). Reduction of local scour around bridge pier groups using collars. *International Journal of Sediment Research*, 25(4): 411-422.

Henderson-Sellers, A., Zhang, H., Berz, G., Emanuel, K, Gray, W., Landsea, C., Holland, G., Lighthill, J., Shieh, S-L., Webster, P., and McGuffie, K. (1998). Tropical

cyclones and global climate change: A post-IPCC assessment. *Bulletin of the American Meteorological Society*, 79(1), 19.

Herbert, P.J. and Taylor, J.G. (1975). *Hurricane experience levels of coast county populations – Texas to Maine.* Special Report, NWS Community Preparedness Staff and SR, 153 pp.

Herbert, P. J., Jarrell, J. D., and Mayfield, M. (1996). *The deadliest, costliest, and most intense United States hurricanes of this century*. Technical Memorandum NWS TPC-1 NOAA, National Hurricane Center, Miami, USA.

Herszberg, I., Li, H., Dharmawan, F., Mouritz, A., Nguyen, M., and Bayandor, J. (2005). Damage assessment and monitoring of composite ship joints. *Composite Structures*, 67(2): 205-216.

Hirabayashi Y., Mahendran R., Koirala S., Konoshima L., Yamazaki D., Watanabe S., Kim H., and Kanae S. (2013). Global flood risk under climate change. *Nature Climate Change*, 3(9): 816-821.

Hodapp, D. P., Collette, M. D., and Troesch, A. W. (2015). Stochastic nonlinear fatigue crack growth predictions for simple specimens subject to representative ship structural loading sequences. *International Journal of Fatigue*, 70: 38-50.

Huang, P., Mirmiran, A., Chowdhury, A. G., Abishdid, C., and Wang, T. L. (2009). Performance of roof tiles under simulated hurricane impact. *Journal of Architectural Engineering*, 15(1): 26-34.

Hughes, O.F.(1983). *Ship structural design: a rationally-based, computer-aided, optimization approach*. Wiley-Interscience.

Hunt A. and Watkiss P. (2011). Climate change impacts and adaptation in cities: a review of the literature. *Climatic Change*, 104(1), 13-49.

Hurrell, J. W., Kushnir, Y., Ottersen, G., and Visbeck, M. (2003). An overview of the North Atlantic oscillation. *American Geophysical Union*, 35 pp.

IACWD. (1982). *Guidelines for determining flood flow frequency, Bulletin 17-B.* Technical report, Interagency Committee on Water Data, Hydrology Subcommittee.

ICF International. (2016). *2013-2015 Climate resilience pilot program: Outcomes, lessons learned, and recommendations*. FHWA Publication No: FHWA-HEP-16-079, Washington D.C., USA, 57 pp.

IPCC. (2014a). *Climate change 2014: synthesis report*. Contribution of Working Groups I, II and III to the Fifth Assessment Report of the Intergovernmental Panel on Climate Change, Intergovernmental Panel on Climate Change, Geneva, Switzerland, 151 pp.

IPCC. (2014b). *Climate change 2014: Impacts, adaptation, and vulnerability. Part A: Global and sectoral aspects.* Contribution of Working Group II to the Fifth Assessment Report of the Intergovernmental Panel on Climate Change [Field, C.B., V.R. Barros, D.J. Dokken, K.J. Mach, M.D. Mastrandrea, T.E. Bilir, M. Chatterjee, K.L. Ebi, Y.O. Estrada, R.C. Genova, B. Girma, E.S. Kissel, A.N. Levy, S. MacCracken, P.R. Mastrandrea, and L.L. White (eds.)]. Cambridge University Press, Cambridge, United Kingdom and New York, NY, USA, 1132 pp.

Iphar, C., Napoli, A. and Cyril, R. (2015). Data quality assessment for maritime situation awareness. In *ISSDQ 2015-The 9th International Symposium on Spatial Data Quality*, (2): 291-296.

Irish, J. L., Resio, D. T., and Ratcliff, J. J. (2008). The influence of storm size on hurricane surge. *Journal of Physical Oceanography*, 38(9): 2003-2013.

Jawad, D. and Ozbay, K. (2006). The discount rate in life cycle-cost analysis of transportation projects. In *85th Annual Meeting of the Transportation Research Board*, National Academy of Science, pp. 22-26.

Jensen, J. J., and Dogliani, M. (1996). Wave-induced ship full vibrations in stochastic seaways. *Marine Structures*, 9(3): 353-387.

Jensen, J.J. and Mansour, A.E. *(*2002). Estimation of ship long-term wave-induced bending moment using closed-form expressions. *Royal Institution of Naval Architects. Transactions. Part A. International Journal of Maritime Engineering.*

Jensen, J.J., Mansour, A.E. and Olsen, A.S. (2004). Estimation of ship motions using closed-form expressions. *Ocean Engineering*, 31(1): 61-85.

Jevrejeva, S., Grinsted, A., and Moore, J. C. (2009). Anthropogenic forcing dominates sea level rise since 1850, *Geophysical Research Letters*, 36(20).

Jin, J. and Meng, B. (2011). Computation of wave loads on the superstructures of coastal highway bridges. *Ocean Engineering*, 38(17-18): 2185-2200.

Johnson, P.A. and Niezgoda, S.L. (2004). Risk-based method for selecting bridge scour countermeasures. *Journal of Hydraulic Engineering*, 130(2): 121-128.

Kahma, K., Pettersson, H., and Tuomi, L. (2003). Scatter diagram wave statistics from the northern Baltic Sea. *MERI–Report Series of the Finnish Institute of Marine Research*, 49: 15-32.

Kameshwar, S. and Padgett, J.E. (2014). Multi-hazard risk assessment of highway bridges subjected to earthquake and hurricane hazards. *Engineering Structures*, 78: 154-166.

Kawashima, K., Kosa, K., Takahashi, Y., Akiyama, M., and Nishioka, T. (2012). Damage of bridges due to the 2011 Great East Japan Earthquake. *Journal of Japan Association for Earthquake Engineering*, 12(4): 4319-4338.

Kerenyi, K., Sofu, T. and Guo, J. (2009). *Hydrodynamic forces on inundated bridge decks*, Federal Highway Administration, FHWA-HRT-09-028.

Khalil, A., Wipf, T. J., Greimann, L., Wood, D. L., and Brakke, B. (1998). Retrofit solution for out-of-plane distortion of X-type diaphragm bridges. In *Transportation Conference Proceedings*, Iowa Department of Transportation, 99-102.

Kim, C.H. (2008). *Nonlinear waves and offshore structures* (Vol. 27). World Scientific.

Kim, S. and Frangopol, D.M. (2010). Cost-effective lifetime structural health monitoring based on availability. *Journal of Structural Engineering*, 137(1): 22-33.

Kirshen, P., Ruth, M., and Anderson, W. (2008). Interdependencies of urban climate change impacts and adaptation strategies: a case study of Metropolitan Boston USA. *Climatic Change*, 86(1-2): 105-122.

Knight, J. R., Folland, C. K., and Scaife, A. A. (2006). Climate impacts of the Atlantic multidecadal oscillation. *Geophysical Research Letters*, 33(17).

Knutson, T. R., and Tuleya, R. E. (2004). Impact of CO2-induced warming on simulated hurricane intensity and precipitation: sensitivity to the choice of climate model and convective parameterization. *Journal of Climate*, 17(18): 3477-3495.

Knutson, T. R., McBride, J. L., Chan J., Emanuel K., Holland, G., Landsea, C., Held, I., Kossin, J.P., A. K. Srivastava, and Sugi, M. (2010). Tropical cyclones and climate change. *Nature Geoscience*, (3): 157-163.

Komen, G., Hasselmann, K., and Hasselmann, H. (1984). On the existence of a fully developed wind-sea spectrum. *Journal of Physical Oceanography*, 14(8): 1271-1285.

Kong, J. S., and Frangopol, D. M. (2003). Life-cycle reliability-based maintenance cost optimization of deteriorating structures with emphasis on bridges. *Journal of Structural Engineering*, 129(6): 818-828.

Kroll, C.N. and Vogel, R.M. (2002). Probability distribution of low streamflow series in the United States. *Journal of Hydrologic Engineering*, 7(2): 137-146.

Kulicki, J. M. (2010). Development of the AASHTO guide specifications for bridges vulnerable to coastal storms. In *Proc., 5th International Conference on Bridge Maintenance, Safety and Management, IABMAS 2010*, 2837-2844.

Lagasse, P. F., Clopper, P.E., Zevenbergen, L.W., and Girard, L.G. (2007). *Countermeasures to protect bridge piers from scour*. NCHRP Report 593, Transportation Research Board.

Lagasse, P.F., Ghosn, M., Johnson, P.A., Zevenbergen, L.W. and Clopper, P.E. (2013). *Risk-based approach for bridge scour prediction.* National Cooperative Highway Research Program No. NCHRP 24-34.

Landman, J. (1993). *Regret: The persistence of the possible*. Oxford University Press.

Landsea, C. W., Pielke Jr, R. A., Mestas-Nunez, A. M., and Knaff, J. A. (1999). Atlantic basin hurricanes: Indices of climatic changes. *Climatic Change,* 42(1): 89-129.

Lau, T.L., Lukkunaprasit, P., Inoue, S. and Ohmachi, T. (2011). *Experimental and numerical modeling of tsunami force on bridge decks*. Vienna, Austria: INTECH Open Access Publisher.

Lebbe, M.F.K., Lokuge, W., Setunge, S. and Zhang, K. (2014). Failure mechanisms of bridge infrastructure in an extreme flood event. In *Proceedings of the First International Conference on Infrastructure Failures and Consequences*, Melbourne, Australia, 124-32.

LeBeau, K.H. and Wadia-Fascetti, S.J. (2007). Fault tree analysis of Schoharie Creek Bridge collapse. *Journal of Performance of Constructed Facilities,* 21(4): 320-326.

Lempert, R. J., and Collins, M. T. (2007). Managing the risk of uncertain threshold responses: comparison of robust, optimum, and precautionary approaches. *Risk Analysis*, 27(4): 1009-1026.

Lempert, R.J. and Schlesinger, M.E. (2000). Robust strategies for abating climate change. *Climatic Change,* 45(3): 387-401.

Lempert, R.J., Popper, S.W. and Bankes, S.C. (2010). Robust decision making: coping with uncertainty. *The Futurist*, 44(1): 47.

Lewis, S. and Grogan, T. (2013). A Hundred Years of ENR Cost Indexes. *ENR: Engineering News Record*, 271(13): 22.

Li, Z. X., Chan, T.H.T., and Ko, J.M. (2002). Evaluation of typhoon induced fatigue damage for Tsing Ma Bridge. *Engineering Structures*, 24(8): 1035-1047.

Li, Y., Ahuja, A., and Padgett, J. E. (2012). Review of methods to assess, design for, and mitigate multiple hazards. *Journal of Performance of Constructed Facilities*, 26(1): 104-117.

Lim B, Spanger-Siegfried E, Burton I., Malone E., and Huq S. (2004). *Adaptation policy frameworks for climate change: developing strategies, policies and measures.* Cambridge University Press, Cambridge, UK.

Lindquist K. and Wendt M. (2012). *Climate Change Adaptation and Mitigation: State Transportation, Regional, and International Strategies: Synthesis*. Washington State Department of Transportation, Transportation Synthesis Reports. Washington, USA.

Ling, Y., Shantz, C., Mahadevan, S., and Sankararaman, S. (2011). Stochastic prediction of fatigue loading using real-time monitoring data. *International Journal of Fatigue*, 33(7): 868-879.

Liu, M., and Frangopol, D.M. (2006). Optimizing bridge network maintenance management under uncertainty with conflicting criteria: Life-cycle maintenance, failure, and user costs. *Journal of Structural Engineering*, 132(11): 1835-1845.

Liu, Y. and Nayak, S. (2012). Structural health monitoring: state of the art and perspectives. *JOM*, 64(7): 789-792.

Lohninger, H. (1999). *Teach/me: Data Analysis*. Springer. Berlin-New York-Tokyo.

Loomes, G. and Sugden, R. (1982). Regret theory: An alternative theory of rational choice under uncertainty. *The Economic Journal*, 92(368): 805-824.

Lounis, Z. and Vanier, D.J. (1998). Optimization of bridge maintenance management using Markovian models. In *Proceedings of the International Conference on Short and Medium Span Bridges 1998*, Calgary, Alberta, pp.1045-1053, v.2.

Lwin, M., Yen, W., and Shen, J. (2014). Effects of Hurricane Katrina on the performance of U.S. highway bridges. *Journal of Performance of Constructed Facilities,* 28(1): 40-48.

Lyn, D.A., Cooper, T.J., Condon, C.A. and Gan, L. (2007). *Factors in debris accumulation at bridge piers*. Joint Transportation Research Program, No. FHWA/IN/JTRP-2006/36.

Lynch, J. P., and Loh, K. J. (2006). A Summary review of wireless sensors and sensor networks for structural health monitoring. *Shock and Vibration Digest*, 38(2): 91-130.

Mallela, J. and Sadasivam, S. (2011). *Work Zone Road User Costs - Concepts and Applications.* Federal Highway Administration, United States Department of Transportation, Washington, D.C.

Mann, M. E., Woodruff, J. D., Donnelly, J. P., and Zhang, Z. (2009). Atlantic hurricanes and climate over the past 1,500 years. *Nature*, 460(7257): 880-883.

Mao, W., Ringsberg, J. W., Rychlik, I., and Storhaug, G. (2010). Development of a fatigue model useful in ship routing design. *Journal of Ship Research*, 54(4): 281-293.

MathWorks (2013). [Computer software]. *User's Guide*, The MathWorks Inc., Natick, MA.

McConnell, K., Allsop, W., and Cruickshank, I. (2004). *Piers, Jetties and Related Structures Exposed to Waves - Guidelines for Hydraulic Loading*, Thomas Telford Ltd, London.

McLean, R.F., Tsyban, A., Burkett, V., Codignotto, J.O., Forbes, D.L., Mimura, N., Beamish, R.J. and Ittekkot, V. (2001). Coastal zones and marine ecosystems. *Climate Change*, 343-379.

Melville, B.W. and Coleman, S.E. (2000). *Bridge scour*. Water Resources Publication.

Melville, B. W., and Hadfield, A. C. (1999). Use of sacrificial piles as pier scour countermeasures. *Journal of Hydraulic Engineering*, 125(11): 1221-1224.

Meng, B. and Jin, J. (2007). Uplift wave load on the superstructure of coastal bridges. In *Proceeding of Structures Congress: New Horizons and Better Practice*s, Long Beach, CA, 1-10.

Merz, B., Aerts, J.C.J.H., Arnbjerg-Nielsen, K., Baldi, M., Becker, A., Bichet, A., Blöschl, G., Bouwer, L.M., Brauer, A., Cioffi, F. and Delgado, J.M. (2014). Floods and climate: emerging perspectives for flood risk assessment and management. *Natural Hazards and Earth System Sciences*, 14(7): 1921-1942.

Merz, B., Vorogushyn, S., Uhlemann, S., Delgado, J., and Hundecha, Y. (2012). HESS Opinions: More efforts and scientific rigour are needed to attribute trends in flood time series. *Hydrology and Earth System Sciences*, 16(5): 1379-1387.

Meyer, M. D. (2008). *Design standards for US transportation infrastructure: the implications of climate change*. Transportation Research Board, Washington, D.C.

Meyer, M.D. and Weigel, B., (2010). Climate change and transportation engineering: Preparing for a sustainable future. *Journal of Transportation Engineering*, 137(6): 393-403.

Milly P.C.D., Wetherald R.T., Dunne K.A., and Delworth T.L. (2002). Increasing risk of great floods in a changing climate. *Nature*, 415(6871): 514-517.

Mitchell, J. F., Lowe, J., Wood, R. A., and Vellinga, M. (2006). Extreme events due to human-induced climate change. *Philosophical Transactions of the Royal Society of London A: Mathematical, Physical and Engineering Sciences*, 364(1845): 2117-2133.

Miyamoto, A., Kawamura, K., and Nakamura, H. (2000). Bridge management system and maintenance optimization for existing bridges. *Computer-Aided Civil and Infrastructure Engineering*, 15(1): 45-55.

Mondoro, A., and Frangopol, D.M. (2016). Climate change, hurricanes and the performance of coastal bridges. In: *Proceedings of the Fifth International Symposium on Life-Cycle Civil Engineering, IALCCE2016*, Delft, The Netherlands, October 16-20, 2016; in *Life-Cycle of Engineering Systems:*

Emphasis on Sustainable Civil Infrastructure, J. Bakker, D.M. Frangopol, and K. van Breugel, eds., CRC Press/Balkema, Taylor & Francis Group plc, London, 47, and full paper on USB card, Taylor & Francis Group plc, London, 141-149

Mondoro, A., and Frangopol, D.M. (2017). Risk-based cost-benefit analysis for the retrofit of bridges exposed to extreme hydrologic events considering multiple failure modes. (submitted)

Mondoro, A., and Frangopol, D.M. (2018). Balancing Payoff and Regret: A Bi-Objective Formulation for the Optimal Adaptation of Riverine Bridges under Climate Change. In: *Sixth International Symposium on Life-Cycle Civil Engineering, IALCCE2018.* Ghent, Belgium, October 28-31, 2018 (submitted).

Mondoro, A., Frangopol, D.M., and Soliman, M. (2016a). Risk-based approach for the optimal management of coastal bridges. In: *Proceedings of the Eighth International Conference on Bridge Maintenance, Safety, and Management, IABMAS2016*, Foz do Iguaçu, Brazil, June 26-30, 2016; in *Maintenance, Monitoring, Safety, Risk and Resilience of Bridges and Bridge Networks,* T.N. Bittencourt, D.M. Frangopol, and A.T. Beck, eds., CRC Press/Balkema, Taylor & Francis Group plc, London, 149, and full paper on DVD, Taylor & Francis Group plc, London, 170-177.

Mondoro, A., Soliman, M., and Frangopol, D.M. (2016b). Prediction of structural response of naval vessels based on available structural health monitoring data. *Ocean Engineering*, 125:295-307.

Mondoro, A., Frangopol, D.M., and Liu, L. (2017a). Bridge adaptation and management under climate change uncertainties: A review. *Natural Hazards Review*. (accepted).

Mondoro, A., Frangopol, D.M.., and Liu, L. (2017b). Multi-criteria robust optimization framework for bridge adaptation under climate change. (submitted).

Mondoro, A., Frangopol, D.M., and Soliman, M. (2017c). Optimal risk-based management of coastal bridges vulnerable to hurricanes. *Journal of Infrastructure Systems*, 23(3): 04016046, 1-12.

Mondoro, A., Soliman, M., and Frangopol, D.M. (2017d). Nonlinear prediction surfaces for estimating the structural response of naval vessels. Chapter 3 in *Model Validation and Uncertainty Quantification*, R. Barthorpe, R. Platz, I. Lopez, B. Moaveni, and C. Papadimitriou, eds., Springer, Springer International Publishing, Switzerland,13-20

Mondoro, A., Soliman, M., and Frangopol, D.M. (2017e). Optimum Management of Coastal Bridges under Changing Climate Conditions. In: *12th International Conference on Structural Safety & Reliability, ICOSSAR 2017*, Vienna, Austria; in *Safety, Reliability, Risk, Resilience and Sustainability of Structures and Infrastructure*, Bucher, C., Ellingwood, B.R., and Frangopol, D.M. eds., TU-Verlag Vienna.

Mori, Y. and Ellingwood, B.R. (1994). Maintaining reliability of concrete structures. II: Optimum inspection/repair. *Journal of Structural Engineering*, 120(3): 846-862.

Naess, A., and Moan, T. (2012). *Stochastic dynamics of marine structures*, Cambridge University Press.

Nakicenovic, N. and Swart, R. (2000). *Special report on emissions scenarios*. Cambridge, UK: Cambridge University Press, pp. 612.

Neumann, J.E., Price, J., Chinowsky, P., Wright, L., Ludwig, L., Streeter, R., Jones, R., Smith, J.B., Perkins, W., Jantarasami, L. and Martinich, J. (2015). Climate change risks to US infrastructure: impacts on roads, bridges, coastal development, and urban drainage. *Climatic Change*, 131(1): 97-109.

New Jersey Motor Vehicle Commission (2014). *The New Jersey Driver Manual*, State of New Jersey Motor Vehicle Commission, Trenton, NJ, USA.

National Hurricane Center (NHC) Storm Surge Unit (2015). *Storm Surge Inundation (SLOSH Maximum of Maximums*)." <http://noaa.maps.arcgis.com/apps/StorytellingTextLegend/index.html?appid=b1a20ab5eec149058bafc059635a82ee>, (May 21, 2015).

Niang-Diop, I., Bosch, H., Burton, I., Khan, S. R., Lim, B., North, N., and Spanger-Siegfried, E. (2004). Formulating an adaptation strategy. *Adaptation policy frameworks for climate change: Developing strategies, policies and measures*, 183-204.

Nicholls, R. J., and Cazenave, A. (2010). Sea-level rise and its impact on coastal zones. *Science*, 328(5985): 1517-1520.

Nichols, J.M., Fackler, P.L., Pacifici, K., Murphy, K.D., and Nichols, J.D. (2014). Reducing fatigue damage for ships in transit through structured decision making. *Marine Structures*, 38: 18-43.

NOAA. (2016). *NOAA: global sea level rate and the local vertical land motion*, http://tidesandcurrents.noaa.gov/sltrends/sltrends.html, accessed July 2016.

North Jersey Transportation Planning Authority. (2011). *Monmouth County S-31 Bridge - Scoping Study*. <http://co.monmouth.nj.us/documents/30/2011_Sept_S31_Presentation.pdf>, (May 21, 2015).

Ochi, M.K. (1978). Wave statistics for the design of ships and ocean structures (Paper No. 2). *SNAME Transactions*, 86: 47-76.

Okasha, N. M., and Frangopol, D. M. (2010). Novel approach for multicriteria optimization of life-cycle preventive and essential maintenance of deteriorating structures. *Journal of Structural Engineering*, 136(8): 1009-1022.

Okasha, N. M., Frangopol, D. M., and Decò, A. (2010). Integration of structural health monitoring in life-cycle performance assessment of ship structures under uncertainty. *Marine Structures*, 23(3): 303-321.

Okasha, N.M., Frangopol, D.M., Saydam, D. and Salvino, L.W. (2011). Reliability analysis and damage detection in high-speed naval craft based on structural health monitoring data. *Structural Health Monitoring*, 10(4): 361-379.

Okeil, A. M., and Cai, C. S. (2008). Survey of short-and medium-span bridge damage induced by Hurricane Katrina. *Journal of Bridge Engineering*, 13(4): 377-387.

Osborne, A.R. (2010). *Nonlinear Ocean Waves and the Inverse Scattering Transform.* (Vol. 97). Academic Press.

Padgett J.E., Dennemann K., and Ghosh, J. (2010). Risk-based seismic life-cycle cost–benefit (LCC-B) analysis for bridge retrofit assessment. *Structural Safety*, 32(3): 165-173.

Padgett, J., DesRoches, R., Nielson, B., Yashinsky, M., Kwon, O. S., Burdette, N., and Tavera, E. (2008). Bridge damage and repair costs from Hurricane Katrina. *Journal of Bridge Engineering*, 13(1): 6-14.

Parola, A.C., Apelt, C.J., and Jempson, M.A. (2000). *Debris forces on highway bridges*, NCHRP No. Report 445.

Patidar, V. (2007). *Multi-objective optimization for bridge management systems* (Vol. 67). Transportation Research Board.

Paulsen, C., and Phillips, A. (2011). State Departments of Transportation working to adapt to a changing climate. *Transportation to the Impacts of Climate Change*, 27 pp.

Pearson, D., Jones, J. and Stein, S. (2000). Risk-based design of bridge scour countermeasures. *Transportation Research Record*, 1696(1): 229-235.

Pei, B., Pang, W., Testik, F., and Ravichandran, N. (2013). Joint distributions of hurricane wind and storm surge for the city of Charleston in South Carolina. In *2012 ATC and SEI Conference on Advances in Hurricane Engineering: Learning from our Past*, October 24, 2012 - October 26, American Society of Civil Engineers (ASCE), 703-714.

Peterka, J. A. and Shahid, S. (1998). Design gust wind speeds in the United States. *Journal of Structural Engineering*, 124(2): 207-214.

Phan, T. L., Simiu, E., McInerney, M. A., Taylor, A. A., Glahn, B., and Powell, M. D. (2007). *Methodology for Development of Design Criteria for Joint Hurricane Wind Speed and Storm Surge Events: Proof of Concept*. NIST Technical Note 1482, National Institute of Standards and Technology, Gaithersburg, MD, USA.

Pielke Jr, R. A., and Pielke Sr, R. A. (1997). *Hurricanes: Their nature and impacts on society*. John Wiley and Sons, New York, 279 pp.

Pierson Jr, W. J. and Moskowitz, L. (1963). A Proposed spectral form for fully developed wind seas based on the similarity theory of SA Kitaigorodskii. *Journal of Geophysical Research*, 69(24): 5181-5190.

Posenato, D., Kripakaran, P., Inaudi, D., and Smith, I. F. (2010). Methodologies for model-free data interpretation of civil engineering structures. *Computers and Structures*, 88(7): 467-482.

Prendergast, L. J., and Gavin, K. (2014). A review of bridge scour monitoring techniques. *Journal of Rock Mechanics and Geotechnical Engineering*, 6(2): 138-149.

Rackwitz, R. (2002). Optimization and risk acceptability based on the life quality index. *Structural Safety*, 24(2–4): 297-331.

Reed, T. D., D. V. Rosowsky, and Schiff, S.D. (1997). Uplift capacity of light-frame rafter to top plate connections. *Journal of Architectural Engineering*, 3(4): 156-163.

Reed, H., and Earls, C. (2015). Stochastic identification of the structural damage condition of a ship bow section under model uncertainty. *Ocean Engineering*, 103: 123-143.

Robertson, I. N., Riggs, H. R., Yim, S. C., and Young, Y. L. (2007). Lessons from Hurricane Katrina storm surge on bridges and buildings. *Journal of Waterway, Port, Coastal, and Ocean Engineering*, 133(6): 463-483.

Rootzén, H., and Katz, R. W. (2013). Design life level: quantifying risk in a changing climate. *Water Resources Research*, 49(9): 5964-5972.

Rosenzweig, C., Solecki, W.D., Blake, R., Bowman, M., Faris, C., Gornitz, V., Horton, R., Jacob, K., LeBlanc, A., Leichenko, R. and Linkin, M. (2011). Developing coastal adaptation to climate change in the New York City infrastructure-shed: process, approach, tools, and strategies. *Climatic Change*, 106(1): 93-127.

Rosowsky, D. V., and Cheng, N. (1999). Reliability of light-frame roofs in high-wind regions. I: Wind loads. *Journal of Structural Engineering*, 125(7): 725-733.

Rowan, E., Evans, C., Riley-Gilbert, M., Hyman, R., Kafalenos, R., Beucler, B., Rodehorst, B., Choate, A. and Schultz, P. (2013). Assessing the sensitivity of transportation assets to extreme weather events and climate change. *Transportation Research Record: Journal of the Transportation Research Board*, pp.16-23.

Sabatino, S., Frangopol, D. M., and Dong, Y. (2015). Sustainability-informed maintenance optimization of highway bridges considering multi-attribute utility and risk attitude. *Engineering Structures*, 102: 310-321.

Salvesen, N., Tuck, E.O. and Faltinsen, O., (1970). Ship motions and sea loads. *SNAME Transactions*, 78(8): 250-287.

Santos, A., McGuckin, N., Nakamoto, H. Y., Gray, D., and Liss, S. (2009). *Summary of Travel Trends: 2009 National Household Travel Survey*, No. FHWA-PL-11-022. 2011. Federal Highway Administration, Washington, D.C.

Sawyer, A. D. (2008). Determination of hurricane surge wave forces on bridge superstructures and design/retrofit options to mitigate or sustain these forces. MS thesis, Department of Civil Engineering, Auburn University, Auburn, AL, USA.

Saydam, D., Frangopol, D. M., and Dong, Y. (2013). Risk assessment methodology for bridges based on element condition ratings considering different maintenance strategies. In *11th International Conference on Structural Safety and Reliability, ICOSSAR 2013*, Taylor & Francis - Balkema, 3593-3599.

Schmocker, L. and Hager, (2011). W.H. Probability of drift blockage at bridge decks. *Journal of Hydraulic Engineering*, 137(4): 470-479.

Schwartz Jr, H. G. (2010). Adaptation to the impacts of climate change on transportation. *Bridge*, 40(3): 5-13.

Seneviratne, S.I., Nicholls, N., Easterling, D., Goodess, C.M., Kanae, S., Kossin, J., Luo, Y., Marengo, J., McInnes, K., Rahimi, M. and Reichstein, M. (2012). Changes in climate extremes and their impacts on the natural physical environment. *Managing the risks of extreme events and disasters to advance climate change adaptation*, pp.109-230.

Seville, E. and Metcalfe, J. (2005). *Developing a hazard risk assessment framework for the New Zealand state highway network.* Land Transport New Zealand Research Report No. 276.

Shan, H., Xie, Z., Bojanowski, C., Suaznabar, O., Lottes, S., Shen, J., and Kerenyi, K. (2012). *Submerged flow bridge scour under clear water conditions*, Federal Highway Administration No. FHWA-HRT-12-034.

Shao, W., Xian, S., Keim, B. D., Goidel, K., and Lin, N. (2016). Understanding perceptions of changing hurricane strength along the US Gulf coast. *International Journal of Climatology*, 37(4): 1716-1727.

Shinozuka, M. and Deodatis, G. (1991). Simulation of stochastic processes by spectral representation. *Applied Mechanics Review*, 44(4): 191-204.

Shirole, A. M. and Malik, A. H. (1993). Seismic retrofitting of bridges in New York State. In *Proc. Symposium on Practical Solutions for Bridge Strengthening and Rehabilitation*, Iowa State University, 123-131.

Sielski, R. A. (2012). Ship structural health monitoring research at the Office of Naval Research. *JOM*, 64(7): 823-827.

Sielski, R. A., Nahshon, K., Salvino, L. W., Anderson, K., and Dow, R. (2013). The ONR ship structural reliability program. *Naval Engineers Journal*, 125(4): 61-84.

Sikora, J. P. (1998). Cumulative lifetime loadings for naval ships. *ASME-Publications-AD*, 56: 299-312.

Sikora, J. P., Michaelson, R. W., and Ayyub, B. M. (2002). Assessment of cumulative lifetime seaway loads for ships. *Naval Engineers Journal*, 114(2): 167-180.

Small, D., Islam, S., and Vogel, R. M. (2006). Trends in precipitation and streamflow in the eastern U.S.: Paradox or perception?. *Geophysical Research Letters*, 33(3).

Snyder, L. V. (2006). Facility location under uncertainty: a review. *IIE Transactions*, 38(7): 547-564.

Soliman, M., Barone, G., and Frangopol, D. M. (2015). Fatigue reliability and service life prediction of aluminum naval ship details based on monitoring data. *Structural Health Monitoring*, 14(1): 3-19.

Stanton, E. A., and Ackerman, F. (2007). *Florida and climate change: the costs of inaction. Florida and climate change: the costs of inaction.* Tufts University Global Development and Environment Institute and Stockholm Environment Institute - US Center.

Stein, S. M., Young, G. K., Trent, R. E., and Pearson, D. R. (1999). Prioritizing scour vulnerable bridges using risk. *Journal of Infrastructure Systems*, 5(3): 95-101.

Stewart, M.G. (2016). Climate change impact assessment of metal-clad buildings subject to extreme wind loading in non-cyclonic regions. *Sustainable and Resilient Infrastructure*, 1(1-2): 32-45.

Stewart, M. G. and Rosowsky, D. V. (1998). Time-dependent reliability of deteriorating reinforced concrete bridge decks. *Structural Safety*, 20(1): 91-109.

Stewart M.G., Rosowsky D.V., and Val D.V. (2001). Reliability-based bridge assessment using risk-ranking decision analysis. *Structural Safety*, 23(4): 397-405.

Stewart, M.G., Wang, X., and Nguyen, M.N. (2011). Climate change impact and risks of concrete infrastructure deterioration. *Engineering Structures*, 33(4): 1326-1337.

Stewart, M.G., Val, D.V., Bastidas-Arteaga, E, O'Connor A.J., and Wang, X. (2014). Climate adaptation engineering and risk-based design and management of infrastructure. Frangopol D.M., and Tsompanakis, Y. (Eds.) *Maintenance and Safety of Aging Infrastructure*, pp.641-684, CRC Press.

Su, H.T. and Tung, Y.K. (2012). Flood-damage-reduction project evaluation with explicit consideration of damage cost uncertainty. *Journal of Water Resources Planning and Management*, 139(6): 704-711.

Thoft-Christensen, P. (2009). Life-cycle cost-benefit (LCCB) analysis of bridges from a user and social point of view. *Structures and Infrastructure Engineering*, 5(1): 49-57.

Thoft-Christensen, P. (2012). Infrastructures and life-cycle cost-benefit analysis. *Structure and Infrastructure Engineering*, 8(5): 507-516.

Trenberth, K. E. (2011). Changes in precipitation with climate change. *Climate Research*, 47(1-2): 123-138.

Tuitman, J.T. (2010). Hydro-elastic response of ship structures to slamming induced whipping. Ph.D. thesis, Dept. of Marine and Transport Technology, Delft University of Technology, Delft, Netherlands.

Tveiten, B.W. (1999). *Fatigue assessment of welded aluminium ship details.* Norwegian University of Science and Technology, Faculty of Marine Technology, Department of Marine Structures.

USACE. (1996). *Shoreline protection and beach erosion control study.* IWR Report 96 - PS – 1, U.S. Army Corps of Engineers Shoreline Protection and Beach Erosion Control Task Force.

van der Pol T.D., van Ierland E.C., and Gabbert S.G.M. (2015). Economic analysis of adaptive strategies for flood risk management under climate change. *Mitigation and Adaptation Strategies for Global Change*, 22(2): 267-285.

Vanik, M. W., Beck, J., and Au, S. (2000). Bayesian probabilistic approach to structural health monitoring. *Journal of Engineering Mechanics*, 126(7): 738-745.

Vecchi, G. A., and Knutson, T. R. (2008). On estimates of historical North Atlantic tropical cyclone activity. *Journal of Climate*, 21(14): 3580-3600.

Vickery, P., Skerlj, P., and Twisdale, L. (2000). Simulation of hurricane risk in the U.S. using empirical track model. *Journal of Structural Engineering*, 126(10): 1222-1237.

Vogel, R. M., Yaindl, C., and Walter, M. (2011). Nonstationarity: Flood magnification and recurrence reduction factors in the United States. *Journal of the American Water Resources Association*, 47(3): 464-474.

Vu, K. A. T. and Stewart, M. G. (2000). Structural reliability of concrete bridges including improved chloride-induced corrosion models. *Structural Safety*, 22(4): 313-333.

Walbridge, S., Fernando, D. and Adey, B.T. (2012). Total cost-benefit analysis of alternative corrosion management strategies for a steel roadway bridge. *Journal of Bridge Engineering*, 18(4): 318-327.

Wang, X., Stewart M.G., and Nguyen, M.N. (2012). Impact of climate change on corrosion and damage to concrete infrastructure in Australia. *Climatic Change*, 110(3-4): 941-957.

Wardhana K. and Hadipriono F.C. (2003). Analysis of recent bridge failures in the United States. *Journal of Performance of Constructed Facilities*, 17(3): 144-150.

Webster, P. J., Holland, G. J., Curry, J. A., and Chang, H. R. (2005). Changes in tropical cyclone number, duration, and intensity in a warming environment. *Science*, 309(5742): 1844-1846.

Wiggert, V. and Jarvinen, B. (1995). Hurricane storm surge model: SLOSH. *Proc., Proceedings of the 9th 1995 Conference on Coastal Zone*, July 16, 1995 - July 21, ASCE, 251-252.

Wilby, R. L., and Wigley, T. M. L. (2000). Precipitation predictors for downscaling: observed and general circulation model relationships. *International Journal of Climatology*, 20(6): 641-661.

Wirsching, P. and Shehata, A. M. (1977). Fatigue under wide band random stresses using the rain-flow method. J*ournal of Engineering Materials and Technology*, 99(3): 205-211.

World Meteorological Organization, WMO. (2005). *Hurricane operational plan*, Regional Association IV (North America, Central America and the Caribbean), Secretariat of the World Meteorological Organization.

Wright, L., Chinowsky, P., Strzepek, K., Jones, R., Streeter, R., Smith, J.B., Mayotte, J.M., Powell, A., Jantarasami, L. and Perkins, W. (2012). Estimated effects of

climate change on flood vulnerability of US bridges. *Mitigation and Adaptation Strategies for Global Change*, 17(8): 939-955.

WSDOT. (2016). *Bridge design manual (LRFD)*, Washington State Department of Transportation.

Wu, S. Y., Najjar, R., and Siewert, J. (2009). Potential impacts of sea-level rise on the Mid-and Upper-Atlantic Region of the United States. *Climatic Change*, 95(1-2): 121-138.

Yanmaz, A.M. and Apaydin, M. (2011). Bridge scour risk assessment and countermeasure design. *Journal of Performance of Constructed Facilities*, 26(4): 499-506.

Yim, S.C. (2005). Modeling and simulation of tsunami and storm surge hydrodynamic loads on coastal bridge structures. In *21st US-Japan Bridge Engineering Workshop*, 3-5.

Zárate, B., Caicedo, J., Yu, J., and Ziehl, P. (2012). Probabilistic prognosis of fatigue crack growth using acoustic emission data. *Journal of Engineering Mechanics*, 138(9): 1101-1111.

Zarrati, A. R., Nazariha, M., and Mashahir, M. B. (2006). Reduction of local scour in the vicinity of bridge pier groups using collars and riprap. *Journal of Hydraulic Engineering*, 132(2): 154-162.

Zevenbergen, L.W., Arneson, L.A., Hunt, J.H., and Miller, A.C. (2012). *Hydraulic design of safe bridges*, No. FHWA-HIF-12-018 HDS 7. Federal Highway Administration.

Zhang, W., Cai, C. S., Pan, F., and Zhang, Y. (2014). Fatigue life estimation of existing bridges under vehicle and non-stationary hurricane wind. *Journal of Wind Engineering and Industrial Aerodynamics*, 133 (2014): 135-145.

Zhu, J. (2014). Life cycle fatigue management for high-speed vessel using Bayesian updating approaches. Ph.D. thesis, Dept. of Naval Architecture and Marine Engineering, University of Michigan, Michigan, USA.

Zhu, B. and Frangopol, D. M. (2013). Risk-based approach for optimum maintenance of bridges under traffic and earthquake loads. *Journal of Structural Engineering*, 139(3): 422-434.

Zhu B. and Frangopol D.M. (2016). Time-variant risk assessment of bridges with partially and fully closed lanes due to traffic loading and scour. *Journal of Bridge Engineering*, 21(6): 04016021.

APPENDIX.

LIST OF NOTATIONS

Notations of Chapter 2

A	Fatigue coefficient for the structural detail
A_{LF}, B_{LF}	Fitting coefficients for the low frequency content $S^{+}_{PM_{GEN}}$
A_{HF}, B_{HF}	Fitting coefficients for the high frequency content of $S^{+}_{PM_{GEN}}$
C_b	Block coefficient of a ship
C_{LF}, D_{LF}, E_{LF}	Fitting coefficients for the low frequency content of $S^{+}_{JONSWAP_{GEN}}$
C_{HF}, D_{HF}, E_{HF}	Fitting coefficients for the high frequency content of $S^{+}_{JONSWAP_{GEN}}$
D	Fatigue damage index
g	Gravitational constant (9.81 m/s^2)
g_o	General characteristic of the external field for ships
H_s	Wave height
L	Length of the ship
m	Slope of the S-N line in logarithmic scale for a structural detail
m_n	n^{th} spectral moment of a PSD
N	Number of cycles to failure under S_i.
n_i	Number of stress cycles in i^{th} bin with stress range S_i
n_{ss}	Number of stress range bins in a stress histogram,

p_i	Prediction surface parameters for Ψ^{lin}, Ψ^{nonlin}, $\Psi^{nonlin\text{-}poly}$
$R_A(\omega)$	Response amplitude operator
S	Stress range
$S^+_{PM}(\omega)$	Single sided Pierson-Moskowitz spectrum
$S^+_{JONSWAP}(\omega)$	Single sided JONSWAP spectrum
$S^+_{PM_{GEN}}$	Complete generalized Pierson-Moskowitz function
$S^+_{JONSWAP_{GEN}}$	Complete generalized JONSWAP function
$S_R(\omega)$	Response spectrum
$S_\xi(\omega)$	sea wave spectrum
S_{VBM}	Response spectrum for vertical bending moment
S_{xx}	Single sided spectral density function
T	Draught of the ship
V	Ship speed
α	Constant single sided JONSWAP spectrum, 8.10×10^{-3}
β	Ship heading angle
γ	Peak enhancement factor in the single sided JONSWAP spectrum
k	Wave number
Φ_m	Transfer function for vertical bending moment
Φ_n	Set of uniform random variables from 0 to 1.
Ψ^{lin}	Linear prediction surface for ship response

Ψ^{nonlin}	Nonlinear prediction surface for ship response
$\Psi^{nonlin\text{-}poly}$	Polynomial based, nonlinear prediction surface for ship response
Ω	Wave frequency in ocean wave spectra

Notations of Chapter 3

A	Cross-sectional area of flow
ADT	Average daily traffic
a_{pier}	Width of the pier
A_s	Area of the steel
$BCR_{deck,MSi}$	Benefit-cost ratio for management strategies considering only deck failure
$BCR_{found,MSi}$	Benefit-cost ratio for management strategies considering only foundation failure
BCR_{MSi}	Benefit-cost ratio for management strategies considering bridge failure
$BCR_{pier,MSi}$	Benefit-cost ratio for management strategies considering only pier failure
$Benefit_{MS}$	Benefit for a given management strategy
$BF_{L,deck}$	Buoyancy force
c	Coefficient, 1.00 (for S.I. units)
$C_{D,deck}$	Coefficient of drag on the deck
$C_{D,pier}$	Coefficient of drag on pier
$C_{L,deck}$	Coefficient for lift on the deck

$C_{L,pier}$	Coefficient of lift on pier
$C_{M,deck}$	Coefficient for the overturning deck moment
C_{MS}	Life-cycle costs associated with the management strategy
C_{rem}	Cost of removal per square area
C_{tva}	Value of time per adult
C_{tvtk}	Time value of the truck
C_v	Average running cost for vehicles
D_{50}	Median grain size
$F_{D,deck}$	Drag force on the deck
$F_{L,deck}$	Total lift force on the deck
Fr	Froude number
f_y	Yield strength of the steel
g	Gravitational acceleration
h^*	Inundation ratio
h_b	Height of the low chord of the bridge deck
$HF_{L,deck}$	Hydrodynamic lift force on the deck
h_t	Flow depth above the bottom of the bridge superstructure
h_u	Height of the free surface
h_{ue}	The effective approach flow depth directed under the bridge
h_w	Height of the weir flow overtopping the bridge
K_1	Correction factor for pier nose shape
K_2	Correction factor for angle of attack of flow

K_3	Correction factor for bed condition
K_u	Constant equal to 11.17 ft2/s
k_v	Model uncertainty factor
L	Span length of the bridge
L_d	Length of the detour
l_{pier}	Length of the pier
$M_{CG,deck}$	Overturning moment on bridge deck
$M_{nx,p}$	Moment capacity about x-axis of pile in pile group
$M_{nx,pier}$	Moment capacity about x-axis of pier
$M_{ny,p}$	Moment capacity about y-axis of pile in pile group
$M_{ny,pier}$	Moment capacity about y-axis of pier
$M_{x,p}$	Moment about x-axis on pile in pile group
$M_{x,pier}$	Moment demand about x-axis on pier
$M_{y,p}$	Moment about y-axis on pile in pile group
$M_{y,pier}$	Moment demand about y-axis on pier
n	Manning roughness coefficient
O_{car}	Average car occupancy
O_{trk}	Average truck occupancy
P	Wetted perimeter
$P_{B,i}$	Probability of branch i
$P_{D,pier}$	Drag pressure on pier
P_f	Probability of failure

$P_{f,bridge}$	Probability of bridge failure
$P_{f,deck}$	Probability of deck failure
$P_{f,found}$	Probability of foundation failure
$P_{f,pier}$	Probability of pier failure
$P_{L,pier}$	Lift pressure on pier
$P_{n,p}$	Nominal axial capacity of pile in pile group
P_p	Axial load on pile in pile group
P_{pg}	Axial load on pile group
Q	Discharge
R	Risk
R_{bridge}	Risk of the associated with bridge failure
$R_{bridge,MSi}$	Life-cycle risk associated with the management strategy
$R_{bridge,MSo}$	Life-cycle risk associated with the bridge without retrofit
R_{deck}	Risk only due to deck failure
R_{found}	Risk only due to foundation failure
$R_{pg,c}$	The resistance of pile group to compressive loads
$R_{pg,l}$	Resistance of pile group to lateral loads
R_{pier}	Risk only due to pier failure
s	Deck thickness
S	Channel bed slope
SW	Self-weight of the structure
T_d	Duration of the detour

T_{trk}	Average daily truck traffic
U_C	Uplift capacity
v	Flow velocity
V	Average detour speed
V_{pg}	Lateral load on pile group
V_{ue}	Effective average approach velocity directed under the bridge
W	Width of bridge deck
y_s	Total scour depth
$y_{s,local}$	Submerged flow contraction scour
$y_{s,pc}$	Local scour due to the pile cap
$y_{s,pg}$	Local scour due to the pile group
$y_{s,pier}$	Local scour due to the pier stem
$y_{s,SFCS}$	Submerged flow contraction scour
α	Constant dependent on the ratio between applied axial load, and axial load capacity
γ_w	Specific weight of water
κ	Total, monetarized consequences associated with failure
κ_d	Costs associated with the detour
κ_{reb}	The rebuilding cost of the structure
κ_{rem}	Removal costs
κ_{tl}	Time loss consequence,
μ	Coefficient of friction

ρ	Density of water

Notations of Chapter 4

A	Projected area subjected to the current storm water level
A_c, b_c	Regression parameters obtained based on the environmental conditions
A_r(t)	Residual area of steel reinforcement
$b_0, b_1, \ldots, b_6$	Coefficients based on bridge type for estimating wave loads on deck
C_{cr}	Critical concentration of chlorides at which corrosion begins
C_{life}	Total life-cycle costs
C_o	Surface chloride content
D	Diffusion coefficient
d	Average water depth over the fetch
d_s	Water depth at or near the bridge
F	Fetch length in the direction of the wind from the upwind shore
F_{res}	Restraint forces of the steel tie-downs
F_S	Vertical slamming force
$F_{v\text{-}max}$	Maximum quasi-static vertical force
F_w	Weight of the structure
g	Gravitational constant.
H_i	Hazard i
H_{max}	Maximum probable wave height
i_{corr}	Corrosion rate based on cover and water-cement ratio (normally expressed as μA/mm)

L	Length of the bridge
$M_{c,deck}$	Bending moment capacity of the deck
$M_{c,girder}$	Flexural capacity of the composite girder
$M_{d,deck}$	Moment demand on the deck
$M_{d,girder}$	Flexural demand on deck
m_{ret}	Type of retrofit action measure included in action i
m_{ri}	Type of repair measure included in action i
PV	Present value of future costs
R	Total risk
R_{life}	Maximum life-cycle risk
r	Interest rate
S	Scale factor adjusting for the post-disaster economic status
TAF	Entrapped air coefficient
T_i	Corrosion initiation time
T_p	Period of the wave with the greatest energy exhibited
t_{ret}	Time of retrofit action
t_{ri}	Time of repair action i
U^*_t	Wind stress factor
$V_{c,girder}$	Shear capacity of the composite girder
$V_{d,girder}$	Shear demand on deck
W	Bridge width
α	Shape parameter for the Weibull distribution

γ_w	Unit weight of water
$K_{traffic}$	Consequence of failure for the traffic hazard
$K_{hurricane}$	Consequence of failure for the hurricane hazard
κ_{det}	Detour consequence associated with structural failure
κ_{reb}	Rebuilding cost associated with structural failure
κ_{rem}	Removal costs associated with structural failure
κ_{tl}	Time loss consequence associated with structural failure
κ_{sl}	Social loss consequence associated with structural failure
κ_i	Monetary consequence associated with failure
λ	Wave length
μ	Scale parameter for the Weibull distribution

Notations of Chapter 6

a_a	Type of adaptation action in an adaptation strategy
a_a^*	Optimal adaptation action
B_m	Benefit associated with adaptation strategy m.
B_{mk}	Benefit associated with adaptation strategy m for climate scenario k
BCR_{mk}	Benefit-cost ratio associated with adaptation strategy m for climate scenario k
C_m	Present value of the cost of the adaptation action
C_m'	Cost of the adaptation action at the time that the adaptation action is applied
CCS_k	Climate change scenario k

$D(t)$	Time variant demand.
ES_e	Economic scenario e
FS_f	Future scenario f
G_m	Gain associated with adaptation strategy m
GLR_m	Gain-loss ratio associated with adaptation strategy m
GLR_{mk}	Gain-loss ratio with adaptation strategy m for climate scenario k
L_m	Loss associated with adaptation strategy m
m	Adaptation strategy, composed of a_a and t_a
m^*	Optimal adaptation strategy composed of a_a^* and t_a^*
$P_{f,m}(t)$	Time-variant probability of failure for adaptation strategy m
$R_m(t)$	Time-variant risk associated with adaptation strategy m
Q_{100}	100-year flood discharge under the current climate
Rgt_m	Regret associated with adaptation strategy m
Rgt_{mk}	Regret associated with adaptation strategy m for climate scenario k
RI_m	Robustness index for payoff (generic) for adaptation strategy m
RI_m^{BCR}	Robustness index for BCR for adaptation strategy m
RI_m^{GLR}	Robustness index for GLR for adaptation strategy m
$S(t)$	Time-variant capacity of the structure
S_A	Structural design information for all potential adaptation actions
S_B	Structural design information for the bridge.
T'	Future recurrence period for the 100 year flood under the current climate

T_{ph}	Planning horizon (expected life of the structure, service life, or expected remaining life
t_a	Time the adaptation action is applied to the structure in an adaptation strategy
t_a^*	Time of optimal adaptation action
$\mathbb{C}$	Set of costs for the potential adaptation actions in Φ
$\kappa(t)$	Time variant consequences of failure
μ_{Rm}	Average annual risk
Φ	Set of the potential adaptation actions
Ψ	Set of climate scenarios

VITA

Alysson Mondoro was born in Red Bank, New Jersey, USA in 1989. After graduating from Holmdel High School in 2007, Alysson attended Johns Hopkins University. In 2011, Alysson graduated with General and Departmental Honors with a Bachelor of Science in Civil Engineering. Alysson was awarded the University Fellowship from Lehigh University to support her graduate studies in 2012 and the Gibson Fellowship from the Department of Civil and Environmental Engineering in 2013. She received a P.C. Rossin Doctoral Fellowship in 2015 from the P.C. Rossin College of Engineering, Lehigh University. Alysson was awarded a National Science Foundation East Asia Pacific Summer Institute grant and was the principle investigator of the award. As a result, she was a visiting researcher at Waseda University, Shinjuku, Tokyo, Japan in 2016.